EXTREME MEDICINE

SCIENTIFIC AND PRACTICAL REVIEWED JOURNAL OF FMBA OF RUSSIA

Indexed in Scopus in 2022

Indexed in RSCI. IF 2018: 0,570

Listed in HAC 31.01.2020 (№ 1292)

Open access to archive

Scopus®

e-LIBRARY.RU НАУЧНАЯ ЭЛЕКТРОННАЯ БИБЛИОТЕКА

ВЫСШАЯ АТТЕСТАЦИОННАЯ КОМИССИЯ (ВАК)

CYBERLENINKA

МЕДИЦИНА ЭКСТРЕМАЛЬНЫХ СИТУАЦИЙ

НАУЧНО-ПРАКТИЧЕСКИЙ РЕЦЕНЗИРУЕМЫЙ ЖУРНАЛ ФМБА РОССИИ

Contents
Содержание

MULTIPOTENT MESENCHYMAL STEM CELLS: PROSPECTS FOR USE IN THE TREATMENT OF INJURIES SUSTAINED IN THE FAR NORTH

Volkova MV ✉, Eremin PS, Markov PA

National Medical Research Center for Rehabilitation and Balneology, Moscow, Russia

The review compares promising approaches to treatment of skin and bone tissue injuries sustained under extreme conditions that employ mesenchymal stem cells. The materials have been extracted from Google Scholar and PubMed. We describe key factors of the Arctic region that affect human epidermis and bone tissues, as well as those that complicate their healing in case of injury. The reviewed papers allowed identifying promising products that have a multifaceted effect on the tissue repair processes, which are those employing mesenchymal stem cells, their exosomes, and recombinant growth factors in combination with biomaterials. Medical products developed for treatment of injuries sustained in the Arctic conditions can be used for wounds sustained in other extreme environments.

МУЛЬТИПОТЕНТНЫЕ МЕЗЕНХИМНЫЕ СТВОЛОВЫЕ КЛЕТКИ: ПЕРСПЕКТИВЫ ПРИМЕНЕНИЯ ДЛЯ ЛЕЧЕНИЯ ТРАВМ, ПОЛУЧЕННЫХ НА КРАЙНЕМ СЕВЕРЕ

М. В. Волкова ✉, П. С. Ерёмин, П. А. Марков

Национальный медицинский исследовательский центр реабилитации и курортологии Министерства здравоохранения России, Москва, Россия

В обзоре сделано сравнение перспективных подходов лечения с использованием мезенхимных стволовых клеток повреждений кожи и костной ткани, полученных в экстремальных для организма условиях. Использованы ресурсы поисковых систем Google Scholar и PubMed. Описаны основные факторы Арктического региона, оказывающие влияние на покровные и костные ткани человека, а также затрудняющие их заживление в случае получения травм. С учетом литературных данных выявлены перспективные продукты, оказывающие многогранное влияние на процессы репарации тканей, а именно применение мезенхимных стволовых клеток, их экзосом и рекомбинантных факторов роста в комбинации с биоматериалами. Разрабатываемые медицинские продукты для лечения травм, полученных в условиях Арктики, могут быть использованы при терапии ранений, приобретенных в других воздействующих на организм экстремальных средах.

Skin is a vital organ that prevents penetration of foreign agents into the body and participates in metabolism. In the absence of surgical treatment, deep and extensive skin lesions that accompany serious wounds (burns, frostbite, etc.) heal unevenly in most cases, with subsequent fibrosis, scars, and wound becoming chronic, as well as increased risk of amputation, sepsis, and death of the patient [1].

Bones are an equally complex organ that has protective, shaping, and mechanical support functions in the body as a whole. [2]. Bone tissue is a highly dynamic structure that constantly undergoes remodeling needed to adapt to changing mechanical loads and repair the developing fatigue fractures. Despite the high regenerative capacity thereof, bone loss and its subsequent restoration are important problems in orthopedics and related fields: their clinical and economic impacts are significant, because patients take long time to recover and risk losing ability to work [3]. Bone is a unique tissue that regenerates constantly and is capable of complete regeneration, with healed fractures being the vivid evidence. However, in some cases, damaged tissues require greater regenerative potential than what is normally available in the body. As a rule, such cases involve defects of critical magnitude brought by orthopedic or maxillofacial surgery, injuries, infections, and tumor resections; every such situation requires clinical intervention and endogenous stimulation of bone regeneration [4].

Every year, more than 10 million injuries — from skin damage through bone fractures to damage to internal organs — are registered in the Russian Federation. About 4 million more people have diseases of the skin and subcutaneous tissue, about 5 million suffer from conditions affecting musculoskeletal system and connective tissues [5]. A significant proportion of injuries sustained in the context of domestic, road traffic, and industrial incidents involve skin, muscle, and bone damage. In wartime, these figures increase manyfold and incorporate gunshot, shrapnel, and mine blast wounds.

Currently, the Arctic region, which has global geopolitical significance, is being developed with transport corridors, hydrocarbon production facilities, etc. [6]. These activities in the Far North increase the risks of injury and disability, as the Arctic affects all systems of the body significantly. Difficult working conditions, high risk of injury, and remoteness from inpatient medical institutions underpin the urgency of development of the new methods and materials that stimulate regeneration of hard and soft tissues, including in cases of combined genesis [7].

Preparing this review, we searched relevant papers in Google Scholar and PubMed. The key words cited above were used in the search for publications.

The review aims to compare promising approaches to treatment of skin and bone tissue injuries sustained under extreme conditions that employ mesenchymal stem cells.

The specifics of inflammatory and regenerative processes in the extreme climatic conditions of the Arctic

Climatic and geographical factors of the Arctic have a significant effect on human body, leading to a complex restructuring of the homeostatic systems and activation of all physiological reserves [8]. The so-called polar stress syndrome, which is state of specific physical strain, affects people who have recently arrived in the region and undergo adaptation to the extreme conditions [9].

Low temperatures are one of the key climate-driven factors peculiar to the Far North and the Arctic. They activate mechanisms boosting production of heat and preventing its loss [10]. Normal internal body temperature is 35.6–37.8 °C. When it drops below 35 °C, the person suffers hypothermia. Prolonged or deep hypothermia can translate into irreversible damage, up to loss of motor function and death [11–12].

Hypothermia is not the only dangerous condition risked in the Far North and the Arctic. Extreme weather and climate of the region strain respiratory system excessively and increase the risk of pulmonary pathologies [13]. Cold air causes activation of a number of protective physiological mechanisms, including respiratory rate slowdown and reflexive shallow breathing, with the functional residual lung capacity growing in the background. Upper respiratory tract actively loses moisture and heat necessary to dampen and warm the inhaled air [14]. Changes in the respiratory organs and tissues negatively affect the entire body, with efficiency of oxygen transport and utilization dropping in the first place, which triggers oxidative stress and increased formation of free radicals, including reactive oxygen species (ROS) [15–17]. Excessive accumulation of ROS leads to mitochondrial dysfunction, further exacerbating the effects of the said stress, mediating and accelerating cell apoptosis [18, 19].

Being in the Arctic region boosts development of hypovitaminosis. Insufficient supply of fat-soluble vitamins can cause severe disorders of the functions of various organs and metabolism in general [16]. Vitamin D3 deficiency translates into disruption of bone mineral metabolism: coupled with lack of essential trace elements, it accelerates the said metabolism and raises the risk of osteoporotic fractures [20].

Cold and light stress also alter functioning of the hormonal systems. Almost all cellular functions and physiological systems are synchronized with circadian rhythms, which are governed by external stimuli, light of certain bandwidth and intensity in particular. Seasonal insolation fluctuations and insufficient UV radiation amounts in the Arctic cause light stress that contributes to the development of metabolic, immune and mental diseases, hinders wound healing, and weakens body's detoxification capacities [21].

In the Arctic, people actively interact with various mechanisms and machines. The chemicals used in this context can irritate skin and cause allergies. Low temperatures necessitate use of special, often heavy clothing, worn while doing physical work. These factors are also among those that provoke diseases of the musculoskeletal and connective tissues and make their course severe.

Thus, there is a number of diseases that are considerably more common in the Arctic, given its climatic and geographical conditions, than in the milder belt south thereof [6]. Damage to local vessels makes injured tissues hypoxic, regardless of the external conditions. Consequently, tissue hypoxia and ischemic reperfusion syndrome caused by general hypothermia complicates healing of various skin, soft and hard tissues injuries while raising the risk of frostbite. Accumulation of ROS, causing excessive inflammation, also interferes with the healing process. Lack of oxygen and nutrients, the deficiency of which will be aggravated by hypoxia and hypothermia, significantly hinders the processes of tissue regeneration, i.e., synthesis of collagen and angiogenesis [22].

As a rule, people stay/work in the Far North on a rotational basis, which prevents development of persisting adaptive protection mechanisms [19], since it takes a person over 3 years of continuous stay in a given climatic and geographical region to fully adapt [9]. In addition, prolonged stay in the Far North often causes hypovitaminosis, which adversely affects body's regenerative capacities and, simultaneously, raises the risk of infections.

Long time spent away from residential quarters, subsequent severely abridged personal hygiene routines, and prolonged wearing of special protective clothing create the risk of development of inflammatory and infectious diseases of the skin and subcutaneous tissue [23].

In extreme environmental conditions, changes in the circulatory system of the body in general and longer angiogenesis caused by lack of oxygen in particular play one of the key roles in preventing active tissue repair after injury [11]. In this connection, it is feasible to consider damaged tissue revascularization possibilities and methods when developing respective treatment protocols. Restoration of skin and bone tissue strongly depends on the body's ability to form new blood vessels. Angiogenesis ensures cells receive the necessary nutrients and, accordingly, helps to maintain their viability [4]. Blood supply plays a significant part in bone regeneration, as it is a highly vascularized tissue. Paracrine regulation of osteogenesis depends on blood vessels [24]. Thus, technologies and methods that improve angiogenesis can help to significantly accelerate tissue regeneration [4].

Disruptions of the first (inflammatory) phase of the healing process are another problem. In particular, hypothermia delays the release of proinflammatory cytokines, reduces the amount and function of neutrophils, and disturbs chemotaxis of leukocytes and phagocytes [25]. Immunosuppression is one of the negative consequences of hypothermia, combined with delayed healing, increased risk of sepsis, impaired plasma coagulation and platelet function. The latter two factors, in particular, can delay surgical removal of necrotic tissues, which adversely affects the recovery and survival of patients in general [26].

Developing new treatment approaches, medical professionals should prioritize these two key processes prioritized as the most important. However, extreme climate, low population density, remoteness and problematic access to the areas comprising the region affect the setup of the medical

care system there, which also conditions rescue of people injured in emergency situations [27]. Therefore, new treatment methods should factor in a considerable delay in delivery of the patient to a qualified medical facility.

New therapeutic approaches to hard and soft tissue damage repair using MMSC

Multipotent mesenchymal stem cells (MMSC) participate in all stages of skin and bone regeneration, so employing them for wound treatment is a promising approach. The key therapeutic effect of MMSC stems from the secretory activity, but they can also differentiate into cells of damaged tissue [28]. The cells regulate the duration of the inflammatory phase, participate in the paracrine regulation of scar formation and reorganization at the later stages. Protocols employing MMSC are particularly relevant for chronic wounds and persisting wounds for which traditional therapies have proven ineffective [29]. Populations of MMSC grown on various bioscaffolds are also widely used for bone tissue regeneration [30]. There is evidence that MMSC can improve the outcomes of thermal damage healing due to their immunomodulatory, antioxidant, and angiogenic effects [31, 32]. The results of the pioneer studies investigating administration of MMSC (injections) to treat injuries sustained under simulated hypoxia and hypothermia suggest a significant expansion of the list of indications for cell therapy [33]. In particular, they were shown to be effective against cold injuries. Injections of MMSC have two key therapeutic effects: alleviation of inflammation and improvement of angiogenesis along wound's periphery [34].

Another developing area of cell therapy is employs MMSC exosomes. These extracellular vesicles contain nucleic acids, proteins and lipids. Proteins, enzymes, and microRNAs contained in exosomes are involved in many biochemical and cellular processes, including inflammation and tissue regeneration. This involvement determines their versatility and the ability to interact with several types of cells and trigger the appropriate cellular reactions. In particular, catalytically active enzymes that promote tissue homeostasis are potentially capable of restoring normal tissue function. This is especially important when an injury or a disease alters its microenvironment and, as a result, disrupts homeostasis and tissue functioning. Compared to most other medicines, such preparations offer a lower risk of overdose or dose insufficiency, since the level of activity of the enzyme is controlled directly by the concentration of the substrate. Thus, the therapeutic effect is proportional to the severity of the injury [35, 36].

The secretion of MMSC contains a wide range of biologically active molecules that can be synthesized with the help of recombinant technologies. For example, growth factors have a significant impact on the restoration of damaged tissues. Vascular endothelial growth factor (VEGF) is involved in angiogenesis and neovascularization, and aids, inter alia, migration of endothelial cells [37, 38]. Fibroblast growth factor (FGF) stimulates production of extracellular matrix in many types of cells participating in wound healing [37, 39]. Platelet-derived growth factor (PDGF) supports wound healing, too; it stimulates proliferation of fibroblasts, smooth muscle cells, osteoblasts and other cells [39]. Growth factors can be used both as a drug per se and as a component of cellular products, with particular purposes of their administration bein tissue engineering and/or cellular reprogramming. They offer efficacy proven in cases of treatment of various injuries, and the technologies of production of proteins in yeast are well-established [40].

The specifics of the effect of the Arctic's climate and geography on the human body increase the urgency of designing medicines and biomedical cellular products that treat the lesion in a complex manner, since tissue hypoxia worsens the wound's condition significantly. Another factor is that none of the currently common approaches is a panacea, as all of them have certain peculiarities (Table 1). In addition, the use

Table 1. The specifics of approaches to tissue repair involving cellular and recombinant technologies

	Mesenchymal stem cells	MMSC exosomes	Recombinant growth factors
Type	Biomedical cell product (No.180-FZ of June 23, 2016)		Medicinal product (No.61-FZ of April 12, 2010)
Technological process			
Source	Human donor	Human donor	Genetically engineered producer strain
Duration	7–14 days (2–3 days from the cell bank) on average; the results of some quality control tests (sterility) are available after administration due to the product's short shelf life	+1–2 days from the time of cultivation of MMSC; before development of conservation methods (shelf life increase), product quality control is similar to MMSC	Full cycle — 3–7 days; batch release after total quality control
Variability	Depends on the cultivation conditions; impossible to completely characterize during quality control before use (given the shelf life of less than 7 days)		Minimal, controlled after receiving the batch
Characteristics of finished product			
Storage conditions	Mostly +2...+8 °C, not fully established		Mostly +2...+8 °C
Duration	Up to 8–12 hours (unfrozen, outside the incubator)	1–30 days (depending on the form)	From 10 days to a year (depending on the form)
Dosage	Determined individually	Approximate, a multicomponent system	Determination of the exact amount of protein and dose calculation
Specifics of therapeutic use			
Effect duration (single administration)	Up to 24 hours due to significant cell death	Several hours (the form of exosomes ensures extended release time)	Several hours (not extended release time)
Ease of use	Special skills required, administered only in medical institutions	Pattern of administration is similar to that of other medicines	
Risks	Poor survival and cell death after injection	Idiosyncrasy to auxiliary components after purification	Overdose; scarring

Table 2. Characteristics of bioscaffolds required for tissue restoration, and factors conditioning them

	Soft tissues (skin)	Hard tissues (bones)
Materials (most common)	Collagen, fibrin, gelatin, hyaluronan, chitosan, agarose, cellulose, alginate, polylactide, polycaprolactone, etc.	Collagen, fibrin, gelatin, hyaluronan, starch, chitosan, phosphates, bioactive glass, polymethylmethacrylate, etc.
Scaffold form and dimensions	Small thickness (1 mm or less), often a large area	Small area (depending on type of bone); thickness determined by size of the defect
Use of cells in the scaffold	Optional keratinocytes, fibroblasts (other cells being considered, including MMSC)	Most desirable MMSC, osteoblasts
Biocompatibility and biodegradation	+ Use of temporary wound dressings possible (allow atraumatic removal, which is important)	++ Requires use of fully biodegradable material for complete tissue replacement
Porosity	+ Fibroblast migration, vascularization; water loss prevention and barrier function maintenance required	+ / ++ Cortical bone 5–10%; trabecular bone 50–90%; migration of stem cells and osteoblasts, vascularization
Strength	+ E-modulus 0.002–1.5 MPa	++ E-modulus and compressive strength: cortical bone 15–20 GPa and 100–200 MPa; cortical bone 0.1–2 GPa and 2–20 MPa
Vascularization	+ Restoration of trophism in the dermal layer	++ The most vascularized tissue
Epidermal keratinization	+ Restoration of skin's barrier function	–
Osteoinductivity	–	+ MMSC differentiation and osteoblast development
Complications of injuries requiring compensation	Chronic wound (excessive inflammation), scars	Non-union of bone
Key negative factors of the Far North that affect healing	Comprehensive exposure to cold (entire area of the skin); aggressive chemicals; infections	Hypovitaminosis (mineral metabolism in bone tissue); exposure of limbs to cold; physical exertion

of allogeneic cells, exosomes, or recombinant growth factors suffers several significant limitations, both therapeutic and technological.

In this connection, one of the prioritized task is selection and development of a biological matrix for the used cells, exosomes, or proteins. Currently, autografts or cell-free allografts are the golden standards in bone restoration and skin damage treatment, because scaffoldings used in the respective protocols are fully compatible from the physico-chemical and biochemical viewpoints, they ensure the degree of porosity needed for angiogenesis and offer the required proliferative and osteoinductive capacities. Small area of donor sites and high risks of scarring underpin development of full-size skin equivalents and osteoinductive materials [41–43]. Drugs, surgical methods, and medical devices available today cannot fully substitute for all the functions of damaged tissue or a lost organ [44] because of the importance of extracellular matrix: it provides a physical basis for maintaining the integrity of tissues and organs, and also serves as an inducer of biochemical and biophysical signals. This matrix creates a microenvironment that includes highly complex cellular interactions and molecular genetic processes [45]. Tissue engineering can solve the respective problems.

As a base, the matrix can have both natural materials (preferred solution) and synthetic polymers with finely adjustable physico-chemical properties. Table 2 presents the required characteristics of bioscaffolds.

Collagen, which is the key component of extracellular matrix of most body tissues, remains the preferred choice among natural polymers. Its derivative, gelatin, is also widely used in wound dressings designs. Hyaluronic acid, common in our tissues, is another natural polymer suitable for the development

of scaffolds supporting restoration of bone and soft tissues. The main advantage of these polymers is their affinity to the human extracellular matrix, but the associated high cost, risks of disease transfer, insufficient supply of raw materials, and other factors necessitate search for other polymers [44]. Scaffolds based on fibrin, silk, chitosan, agarose, cellulose, starch, alginate, and synthetic polymers are also being developed for skin restoration purposes. As for bone tissue engineering, osteoinductivity, an important property of the material, limits its potential considerably, while skin tissue engineering does not have such limitations. Nevertheless, not only collagen, fibrin and hyaluronic can underpin bone scaffolds, but also chitosan, which supports attachment and proliferation of osteoblast bone-forming cells and ensures formation of a mineralized bone matrix [46].

The conditions of the Arctic disrupt tissue trophism, which renders body's own reserves insufficient for repair of the related tissue damage. This fact substantiates the need for new, most effective therapy. One of the possible solutions revolves around matrices containing MMSC, exosomes, or recombinant growth factors; such preparations reduce inflammation and enhance angiogenesis in the first place.

CONCLUSION

The effect of the Far North's natural and climatic conditions is multifactorial, but it does not render impossible development of pluripotent therapeutic products and methods based, in particular, on multipotent mesenchymal stem cells. The said products and methods can be used to treat skin and tissue injuries in other climatic zones, and also help repair damage sustained under extreme conditions of different nature, for example, in the context of a spaceflight, high altitude activities, scuba diving.

References

1. Zheng K, Tong Y, Zhang S, He R, Xiao L, Iqbal Z, et al. Flexible bicolorimetric polyacrylamide/chitosan hydrogels for smart real–time monitoring and promotion of wound healing. Advanced Functional Materials. 2021; 31 (34): 2102599.

2. Fourie J, Taute F, du Preez L, De Beer D. Chitosan composite biomaterials for bone tissue engineering — a review. Regenerative Engineering and Translational Medicine. 2022; 1–21.

3. Loi F, Cordova LA, Pajarinen J, Lin T, Yao Z, Goodman SB. Inflammation, fracture and bone repair. Bone. 2016; 86: 119–30.

4. Курбонов Х. Р., Джуракулов Б. И., Хусанов Т. Б. Методы улучшения ангиогенеза в регенерации костной ткани. Journal of Universal Science Research. 2023; 1 (10): 683–92.

5. Zdravoohranenie v Rossii. Stat. sb. Rosstat. M., 2023; 181. Russian.

6. Azarov II, Butakov SS, Zholus BI, Zetkin AYu, Remmer VN. Opyt sohranenija zdorov'ja voennosluzhashhih v Arktike v povsednevnoj dejatel'nosti i chrezvychajnyh situacijah. Morskaja medicina. 2017; 3 (3): 102–11. Russian.

7. Shapovalov KA, Shapovalova PK. Travmatizm plavajushhego sostava morskogo transportnogo flota Cevernogo vodnogo bassejna. Hirurgija. Vostochnaja Evropa. 2019; 8 (3): 469–484. Russian.

8. Pryanichnikov SV. Psihofiziologicheskoe sostojanie organizma v zavisimosti ot dlitel'nosti prebyvanija v vysokih shirotah Arktiki. Jekologija cheloveka. 2020; 12: 4–10. Russian.

9. Zagorodnikov GG, Uhovskij DM. Voenno-professional'naja adaptacija voennosluzhashhih v uslovijah Krajnego Severa. SPb.: VmedA, 2013. Russian.

10. Turk EE. Hypothermia. Forensic science, medicine, and pathology. 2010; 6 (2): 106–15.

11. Moffatt S. E. Hypothermia in trauma. Emergency Medicine Journal. 2013; 30 (12): 989–96.

12. McDonald A, Stubbs R, Lartey P, Kokot S. Environmental injuries: hyperthermia and hypothermia. MacEwan University Student eJournal. 2020; 4 (1).

13. Grishin OV, Ustyuzhaninova NV. Gipometabolizm u severjan v uslovijah dejstvija nizkih temperatur. Sibirskij nauchnyj medicinskij zhurnal. 2010; 3: 12–17. Russian.

14. Shishkin GS, Ustyuzhaninova NV. Funkcional'nye sostojanija vneshnego dyhanija zdorovogo cheloveka. Novosibirsk: Izd-vo SO RAN, 2012; 329 c. Russian.

15. Ermolin SP. Fiziologicheskie reakcii organizma voennosluzhashhih v uslovijah arkticheskoj zony: dis. kand. med. nauk: 03.03.01. Arhangel'sk, 2015: 139. Russian.

16. Ovechkina E, Ovechkin F. Human Pathophysiology in the Conditions of North Russia. Bulletin of Science and Practice. 2021.

17. Liu J, Ding Y, Liu Z, Liang X. Senescence in mesenchymal stem cells: functional alterations, molecular mechanisms, and rejuvenation strategies. Frontiers in Cell and Developmental Biology. 2020; 8: 258.

18. Lv H, Liu Q, Zhou J, Tan G, Deng X, Ci X. Daphnetin-mediated Nrf2 antioxidant signaling pathways ameliorate tert-butyl hydroperoxide (t-BHP)-induced mitochondrial dysfunction and cell death. Free Radical Biology and Medicine. 2017; 106: 38–52.

19. Vorobeva NA, Vorobeva AI, Marusij AA. Risk jendotelial'noj disfunkcii i obshhaja antioksidantnaja sposobnost' u morjakov v uslovijah arkticheskogo rejsa. Zhurnal mediko-biologicheskih issledovanij. 2021; 9 (2): 192–200. Russian.

20. Tyrenko VV, Aganov DS, Toporkov MM, Cygan EN, Bologov SG. Rannjaja diagnostika narushenija mineral'nogo obmena, kak sposob pervichnoj i vtorichnoj profilaktiki perelomov u voennosluzhashhih Arkticheskoj gruppirovki vojsk. Vestnik Rossijskoj voenno-medicinskoj akademii. 2018; 4: 45–51. Russian.

21. Volkova MV, Biryukov SA. Metodicheskie aspekty razrabotki i doklinicheskih issledovanij lekarstvennyh preparatov v interesah Arkticheskoj mediciny. Medicina jekstremal'nyh situacij. 2023; 25 (1): 12–20. Russian.

22. Tamama K, Kerpedjieva SS. Acceleration of wound healing by multiple growth factors and cytokines secreted from multipotential stromal cells/mesenchymal stem cells. Advances in Wound Care. 2012; 1 (4): 177–82.

23. Myznikov IL, Polishhuk YuS. Sostojanie zdorov'ja, zabolevaemost' i travmatizm u vodolazov, prohodjashhih sluzhbu v Kol'skom Zapoljar'e. Gigiena i sanitarija. 2014; 93 (4): 61–66. Russian.

24. Revokatova DP, Zurina IM, Gorkun AA, Saburina IN. Sovremennye podhody k sozdaniju vaskuljarizirovannyh kostnyh biojekvivalentov. Patologicheskaja fiziologija i jeksperimental'naja terapija. 2022; 66 (3): 151–65. Russian.

25. Wood T, Thoresen M. Physiological responses to hypothermia. Seminars in fetal and neonatal medicine. 2015; 20 (2): 87–96.

26. Trupkovic T, Giessler G. Das Verbrennungstrauma–Teil. Der Anaesthesist. 2008; 57 (9): 898–907.

27. Kotenko PK, Shevcov VI. Analiz mediko-social'nyh faktorov, opredeljajushhih perspektivnyj oblik sistemy okazanija medicinskoj pomoshhi postradavshim v chrezvychajnyh situacijah v Arkticheskoj zone Rossijskoj Federacii. Morskaja medicina. 2018; 4 (4): 44–54. Russian.

28. Han Y, Li X, Zhang Y, Han Y, Chang F, Ding J. Mesenchymal stem cells for regenerative medicine. Cells. 2019; 8 (8): 886.

29. Yorukoglu AC, Kiter A, Akkaya S, Satiroglu-Tufan NL, Tufan AC. A concise review on the use of mesenchymal stem cells in cell sheet-based tissue engineering with special emphasis on bone tissue regeneration. Stem cells international. 2017; 2017.

30. Petite H, Viateau V, Bensaid W, Meunier A, de Pollak C, Bourguignon M, et al. Tissue-engineered bone regeneration. Nature biotechnology. 2000; 18 (9): 959–63.

31. Rangatchew F, Vester-Glowinski P, Rasmussen BS, Haastrup E, Munthe-Fog L, Talman ML, et al. Mesenchymal stem cell therapy of acute thermal burns: A systematic review of the effect on inflammation and wound healing. Burns. 2021; 47 (2): 270–94.

32. Chang YW, Wu YC, Huang SH, Wang HMD, Kuo YR, Lee SS. Autologous and not allogeneic adipose-derived stem cells improve acute burn wound healing. PloS one. 2018; 13 (5): e0197744.

33. Volkova MV, Boyarinsev VV, Trofimenko AV, Rybalkin SP, Kovaleva EV, Biryukov SA, i dr. Jeffektivnost' primenenija mezenhimal'nyh stromal'nyh kletok dlja lechenija rvano-ushiblennyh ran v uslovijah gipotermii i gipoksii. Izvestija Rossijskoj Voenno-medicinskoj akademii. 2022; 41 (3): 261–68. Russian.

34. Volkova MV, Boyarintsev VV, Trofimenko AV, Kovaleva EV, Al Othman A, Melerzanov AV, et al. Local injection of bone-marrow derived mesenchymal stromal cells alters a molecular expression profile of a contact frostbite injury wound and improves healing in a rat model. Burns. 2023; 49 (2): 432–43.

35. Lai RC, Yeo RWY, Lim SK. Mesenchymal stem cell exosomes. Seminars in cell & developmental biology. 2015; 40: 82–88.

36. Yin K, Wang S, Zhao RC. Exosomes from mesenchymal stem/stromal cells: a new therapeutic paradigm. Biomarker research. 2019; 7: 1–8.

37. Barrientos S, Brem H, Stojadinovic O, Tomic-Canic M. Clinical application of growth factors and cytokines in wound healing. Wound Repair and Regeneration. 2014; 22 (5): 569–78.

38. El Sadik AO, El Ghamrawy TA, Abd El-Galil TI. The effect of mesenchymal stem cells and chitosan gel on full thickness skin wound healing in albino rats: histological, immunohistochemical and fluorescent study. PloS one. 2015; 10 (9): e0137544.

39. Graves DT, Cochran DL. Mesenchymal cell growth factors. Critical Reviews in Oral Biology & Medicine. 1990; 1 (1): 17–36.

40. Misterova AAV. Optimizacija metoda ochistki rekombinantnogo faktora rosta trombocitov cheloveka RHPDGF-BB, poluchennogo v metiltrofnyh drozhzhah Pichia Pastoris. Prikladnaja biohimija i mikrobiologija. 2023; 59 (4): 383–91. Russian.

41. Muhametov UF, Lyulin SV, Borzunov DYu, Gareev IF, Bejlerli OA. Alloplasticheskie i implantacionnye materialy dlja kostnoj plastiki: obzor literatury. Kreativnaja hirurgija i onkologija. 2021; 4: 343–53. Russian.

42. Böttcher-Haberzeth S, Biedermann T, Reichmann E. Tissue engineering of skin. Burns. 2010; 36 (4): 450–60.

43. Radke D, Chen L, Qi S, Zhao F. Prevascularized stem cell sheet for full-thickness skin wound repair. Vascular Surgery, Neurosurgery, Lower Extremity Ulcers, Antimicrobials, Wound Assessment, Care, Measurement and Repair. 2020: 167–72.

44. Alaribe FN, Manoto SL, Motaung SCKM. Scaffolds from biomaterials: advantages and limitations in bone and tissue

engineering. Biologia. 2016; 71 (4): 353–66. Available from: https://doi.org/10.1515/biolog-2016-0056.

45. Hussey GS, Dziki JL, Badylak SF. Extracellular matrix-based materials for regenerative medicine. Nature Reviews Materials.

2018; 3 (7): 159–73.

46. Levengood SKL, Zhang M. Chitosan-based scaffolds for bone tissue engineering. Journal of Materials Chemistry B. 2014; 2 (21): 3161–84.

Литература

1. Zheng K, Tong Y, Zhang S, He R, Xiao L, Iqbal Z, et al. Flexible bicolorimetric polyacrylamide/chitosan hydrogels for smart real–time monitoring and promotion of wound healing. Advanced Functional Materials. 2021; 31 (34): 2102599.

2. Fourie J, Taute F, du Preez L, De Beer D. Chitosan composite biomaterials for bone tissue engineering — a review. Regenerative Engineering and Translational Medicine. 2022; 1–21.

3. Loi F, Cordova LA, Pajarinen J, Lin T, Yao Z, Goodman SB. Inflammation, fracture and bone repair. Bone. 2016; 86: 119–30.

4. Курбонов Х. Р., Джуракулов Б. И., Хусанов Т. Б. Методы улучшения ангиогенеза в регенерации костной ткани. Journal of Universal Science Research. 2023; 1 (10): 683–92.

5. Здравоохранение в России. Стат. сб. Росстат. М., 2023; 181.

6. Азаров И. И., Бутаков С. С., Жолус Б. И., Зеткин А. Ю., Реммер В. Н. Опыт сохранения здоровья военнослужащих в Арктике в повседневной деятельности и чрезвычайных ситуациях. Морская медицина. 2017; 3 (3): 102–11.

7. Шаповалов К. А., Шаповалова П. К. Травматизм плавающего состава морского транспортного флота Северного водного бассейна. Хирургия. Восточная Европа. 2019; 8 (3): 469–484.

8. Пряничников С. В. Психофизиологическое состояние организма в зависимости от длительности пребывания в высоких широтах Арктики. Экология человека. 2020; 12: 4–10.

9. Загородников Г. Г., Уховский Д. М. Военно-профессиональная адаптация военнослужащих в условиях Крайнего Севера. СПб.: ВмедА, 2013.

10. Turk EE. Hypothermia. Forensic science, medicine, and pathology. 2010; 6 (2): 106–15.

11. Moffatt S. E. Hypothermia in trauma. Emergency Medicine Journal. 2013; 30 (12): 989–96.

12. McDonald A, Stubbs R, Lartey P, Kokot S. Environmental injuries: hyperthermia and hypothermia. MacEwan University Student eJournal. 2020; 4 (1).

13. Гришин О. В., Устюжанинова Н. В. Гипометаболизм у северян в условиях действия низких температур. Сибирский научный медицинский журнал. 2010; 3: 12–17.

14. Шишкин Г. С., Устюжанинова Н. В. Функциональные состояния внешнего дыхания здорового человека. Новосибирск: Изд-во СО РАН, 2012; 329 с.

15. Ермолин С. П. Физиологические реакции организма военнослужащих в условиях арктической зоны: дис. канд. мед. наук: 03.03.01. Архангельск, 2015: 139.

16. Ovechkina E, Ovechkin F. Human Pathophysiology in the Conditions of North Russia. Bulletin of Science and Practice. 2021.

17. Liu J, Ding Y, Liu Z, Liang X. Senescence in mesenchymal stem cells: functional alterations, molecular mechanisms, and rejuvenation strategies. Frontiers in Cell and Developmental Biology. 2020; 8: 258.

18. Lv H, Liu Q, Zhou J, Tan G, Deng X, Ci X. Daphnetin-mediated Nrf2 antioxidant signaling pathways ameliorate tert-butyl hydroperoxide (t-BHP)-induced mitochondrial dysfunction and cell death. Free Radical Biology and Medicine. 2017; 106: 38–52.

19. Воробьева Н. А., Воробьева А. И., Марусий А. А. Риск эндотелиальной дисфункции и общая антиоксидантная способность у моряков в условиях арктического рейса. Журнал медико-биологических исследований. 2021; 9 (2): 192–200.

20. Тыренко В. В., Аганов Д. С., Топорков М. М., Цыган Е. Н., Бологов С. Г. Ранняя диагностика нарушения минерального обмена, как способ первичной и вторичной профилактики переломов у военнослужащих Арктической группировки войск. Вестник Российской военно-медицинской академии. 2018; 4: 45–51.

21. Волкова М. В., Бирюков С. А. Методические аспекты

разработки и доклинических исследований лекарственных препаратов в интересах Арктической медицины. Медицина экстремальных ситуаций. 2023; 25 (1): 12–20.

22. Tamama K, Kerpedjieva SS. Acceleration of wound healing by multiple growth factors and cytokines secreted from multipotential stromal cells/mesenchymal stem cells. Advances in Wound Care. 2012; 1 (4): 177–82.

23. Мызников И. Л., Полищук Ю. С. Состояние здоровья, заболеваемость и травматизм у водолазов, проходящих службу в Кольском Заполярье. Гигиена и санитария. 2014; 93 (4): 61–66.

24. Ревокатова Д. П., Зурина И. М., Горкун А. А., Сабурина И. Н. Современные подходы к созданию васкуляризированных костных биоэквивалентов. Патологическая физиология и экспериментальная терапия. 2022; 66 (3): 151–65.

25. Wood T, Thoresen M. Physiological responses to hypothermia. Seminars in fetal and neonatal medicine. 2015; 20 (2): 87–96.

26. Trupkovic T, Giessler G. Das Verbrennungstrauma–Teil. Der Anaesthesist. 2008; 57 (9): 898–907.

27. Котенко П. К., Шевцов В. И. Анализ медико-социальных факторов, определяющих перспективный облик системы оказания медицинской помощи пострадавшим в чрезвычайных ситуациях в Арктической зоне Российской Федерации. Морская медицина. 2018; 4 (4): 44–54.

28. Han Y, Li X, Zhang Y, Han Y, Chang F, Ding J. Mesenchymal stem cells for regenerative medicine. Cells. 2019; 8 (8): 886.

29. Yorukoglu AC, Kiter A, Akkaya S, Satiroglu-Tufan NL, Tufan AC. A concise review on the use of mesenchymal stem cells in cell sheet-based tissue engineering with special emphasis on bone tissue regeneration. Stem cells international. 2017; 2017.

30. Petite H, Viateau V, Bensaid W, Meunier A, de Pollak C, Bourguignon M, et al. Tissue-engineered bone regeneration. Nature biotechnology. 2000; 18 (9): 959–63.

31. Rangatchew F, Vester-Glowinski P, Rasmussen BS, Haastrup E, Munthe-Fog L, Talman ML, et al. Mesenchymal stem cell therapy of acute thermal burns: A systematic review of the effect on inflammation and wound healing. Burns. 2021; 47 (2): 270–94.

32. Chang YW, Wu YC, Huang SH, Wang HMD, Kuo YR, Lee SS. Autologous and not allogeneic adipose-derived stem cells improve acute burn wound healing. PloS one. 2018; 13 (5): e0197744.

33. Волкова М. В., Бояринцев В. В., Трофименко А. В., Рыбалкин С. П., Ковалева Е. В., Бирюков С. А., и др. Эффективность применения мезенхимальных стромальных клеток для лечения рвано-ушибленных ран в условиях гипотермии и гипоксии. Известия Российской Военно-медицинской академии. 2022; 41 (3): 261–68.

34. Volkova MV, Boyarintsev VV, Trofimenko AV, Kovaleva EV, Al Othman A, Melerzanov AV, et al. Local injection of bone-marrow derived mesenchymal stromal cells alters a molecular expression profile of a contact frostbite injury wound and improves healing in a rat model. Burns. 2023; 49 (2): 432–43.

35. Lai RC, Yeo RWY, Lim SK. Mesenchymal stem cell exosomes. Seminars in cell & developmental biology. 2015; 40: 82–88.

36. Yin K, Wang S, Zhao RC. Exosomes from mesenchymal stem/stromal cells: a new therapeutic paradigm. Biomarker research. 2019; 7: 1–8.

37. Barrientos S, Brem H, Stojadinovic O, Tomic-Canic M. Clinical application of growth factors and cytokines in wound healing. Wound Repair and Regeneration. 2014; 22 (5): 569–78.

38. El Sadik AO, El Ghamrawy TA, Abd El-Galil TI. The effect of mesenchymal stem cells and chitosan gel on full thickness skin wound healing in albino rats: histological, immunohistochemical and fluorescent study. PloS one. 2015; 10 (9): e0137544.

39. Graves DT, Cochran DL. Mesenchymal cell growth factors. Critical

Reviews in Oral Biology & Medicine. 1990; 1 (1): 17–36.

40. Мистерова А. А. В. Оптимизация метода очистки рекомбинантного фактора роста тромбоцитов человека RHPDGF-BB, полученного в метилтрофных дрожжах Pichia Pastoris. Прикладная биохимия и микробиология. 2023; 59 (4): 383–91.

41. Мухаметов У. Ф., Люлин С. В., Борзунов Д. Ю., Гареев И. Ф., Бейлерли О. А. Аллопластические и имплантационные материалы для костной пластики: обзор литературы. Креативная хирургия и онкология. 2021; 4: 343–53.

42. Böttcher-Haberzeth S, Biedermann T, Reichmann E. Tissue engineering of skin. Burns. 2010; 36 (4): 450–60.

43. Radke D, Chen L, Qi S, Zhao F. Prevascularized stem cell sheet for full-thickness skin wound repair. Vascular Surgery, Neurosurgery, Lower Extremity Ulcers, Antimicrobials, Wound Assessment, Care, Measurement and Repair. 2020: 167–72.

44. Alaribe FN, Manoto SL, Motaung SCKM. Scaffolds from biomaterials: advantages and limitations in bone and tissue engineering. Biologia. 2016; 71 (4): 353–66. Available from: https://doi.org/10.1515/biolog-2016-0056.

45. Hussey GS, Dziki JL, Badylak SF. Extracellular matrix-based materials for regenerative medicine. Nature Reviews Materials. 2018; 3 (7): 159–73.

46. Levengood SKL, Zhang M. Chitosan-based scaffolds for bone tissue engineering. Journal of Materials Chemistry B. 2014; 2 (21): 3161–84.

MORPHOLOGICAL CHARACTERISTICS OF TOXIC BRAIN DAMAGE

Gaikova ON[1], Kozlov AA[1], Katretskaya GG[1], Melnikova MV[1], Melekhova AS[1], Bondarenko AA[1], Sokolova YuO[1], Bazhanova ED[1,2] ✉

[1] Golikov Research Clinical Center of Toxicology of the Federal Medical Biological Agency, Saint-Petersburg, Russia

[2] Sechenov Institute of Evolutionary Physiology and Biochemistry of the Russian Academy of Sciences, Saint-Petersburg, Russia

The effects of various toxicants on the body tissues cause tissue abnormalities resulting in dystrophic changes and necrosis. The nervous system is the most vulnerable to the effects of exogenous substances, both chemical and biological, due to high metabolic activity and the cells' incapability of self-renewal. Neurotoxicants lead to disturbances of cellular nutrition and eventually to neurodegeneration. Neurons can die due to both apoptosis and necrosis.

✉ **Correspondence should be addressed:** Elena D. Bazhanova
Bekhtereva, 1, Saint-Petersburg, Russia; 192019; bazhanovae@mail.ru

МОРФОЛОГИЧЕСКИЕ ХАРАКТЕРИСТИКИ ТОКСИЧЕСКОГО ПОРАЖЕНИЯ ГОЛОВНОГО МОЗГА

О. Н. Гайкова[1], А. А. Козлов[1], Г. Г. Катрецкая[1], М. В. Мельникова[1], А. С. Мелехова[1], А. А. Бондаренко[1], Ю. О. Соколова[1], Е. Д. Бажанова[1,2] ✉

[1] Научно-клинический центр токсикологии имени С. Н. Голикова Федерального медико-биологического агентства, Санкт-Петербург, Россия

[2] Институт эволюционной физиологии и биохимии имени И. М. Сеченова Российской академии наук, Санкт-Петербург, Россия

Воздействие различных токсикантов на ткани организма вызывает в них патологические изменения, в итоге приводящие к дистрофическим и некротическим изменениям. Из-за высокой метаболической активности и неспособности клеток к самовозобновлению нервная система наиболее уязвима к влиянию экзогенных веществ как химической, так и биологической природы. Нейротоксиканты приводят к нарушению питания клеток и в итоге к нейродегенерации. Нейроны могут погибать как вследствие апоптоза, так и некроза.

✉ **Для корреспонденции:** Елена Давыдовна Бажанова
ул. Бехтерева, д. 1, г. Санкт-Петербург, Россия; 192019; bazhanovae@mail.ru

Normal brain functioning depends on the complex interactions between neurotransmitters, hormones, enzymes, and electrolytes. Many chemically complex substances can intervene in these interactions and disrupt them. Today, there are more than 100,000 chemical compounds, of those 25% can damage the brain [1]. Apparently, there are still many unrecognized neurotoxins in the environment. The central nervous system (CNS) is to some extent protected against toxic effects by the blood-brain barrier, however, some compounds can easily cross the barrier (for example, non-polar fat-soluble substances). Neurons are vulnerable to toxic effects due to high lipid content and high metabolism [2].

The neurotoxin exposure can cause a number of symptoms, all of which are non-specific. Acute toxic encephalopathies are often manifested by the symptoms of confusion, attention deficit, seizure, and coma. It is believed that most of these symptoms are associated with damage to the CNS capillaries, hypoxy, and cerebral edema. Neurological symptoms can vanish completely in case of correct and timely treatment. However, even a single toxic exposure can leave consequences. In cases if chronic negligible exposure to minor toxin doses, the symptoms can show up slowly and remain undetected for some time. The symptoms usually include mood changes, fatigue, memory problems, and congnitive impairment. The toxin elimination can be followed by improvement, but neurological deficit can persist over a long time in cases of severe encephalopathy or long-term exposure. Achieving the peak of recovery from chronic encephalopathy caused by toxins can take from months to years [3].

Toxic exposure is especially dangerous during the period of brain development. The available data suggest that the exposure to ubiquitous toxicants, such as fine particulate matter, manganese, and many phthalates, is associated with alterations of the development trajectory, physical and mental health throughout life [4]. Laboratory and clinical studies have shown that the developing brain demonstrates unique sensitivity to toxic agents [5].

Until recently, toxic neuropathy and brain damage were considered to be rare; these were caused mostly by alcohol intoxication or side effects of chemotherapy agents. These came to the fore due to the development of new treatment methods for neoplasms, improved diagnosis, and the increase in their share in the overall morbidity. Introduction of immunotherapy have led to the increase in the number of toxic

neuropathy cases and the need to develop the diagnosis and treatment methods for toxic neuropathy [6].

The other problem is the use of anesthesia. There is growing concern that the brain, both young and elderly, can be vulnerable to harmful effects of many modern anesthetics. Animal studies have yielded strong evidence of the fact that the exposure to sedatives and anesthesia causes morphological damage to the brain cells and neurocognitive impairment. However, these data can be hardly extrapolated to humans. Anesthetics can cause apoptosis of neurons and glial cells. The mechanisms underlying their toxic effects include excitatory neurotransmission, loss of calcium homeostasis, neuroinflammation induction, and trophic factor modulation [7].

Major characteristics of toxic damage to nervous system

Toxic damage to the nervous system, the same as that to the whole body, is characterized by activation of dystrophic and necrotic processes.

Due to the nervous system morphological features and high vulnerability to adverse factors, the disease processes in the nervous system, expecially in the brain, are significantly different from that observed in other human organs and systems. The body's exposure to new or poorly understood chemical compounds, as well as previously unknown infections, poses the challenges of the diagnosis and treatment of such disorders to pathologists, forensic experts, and occupational therapists. The development and use of the technology for diagnosis, treatment, and prevention of health problems associated with the adverse effects of hazardous chemical and biological factors is one of the challenges of state policy in the field of ensuring chemical and biological safety of the Russian Federation. The brain and nervous system in general represent the most vulnerable targets of both chemical and biological pathological agents. At the same time, even the general pathological processes that take place in the nervous tissue, i.e. the possibility to differentiate between normal and disease, are definitely underrepresented in the literature, especially domestic. Sporadic monographs are focused on

specific issues of the diagnosis of nervous system tumors [8], vascular diseases [9, 10].

At the same time, the general pathological processes, such as damage, atrophy, circulation disorders, inflammation showing some specifics in the nervous system, are discussed only in sporadic monographs [11]. Neurohistologists pay attention only to certain components of brain tissue, most often to neurons [12], and they describe such types of pathology and in such a variety that can only confuse the pathologist. There is no detailed description of pathology of the other nervous system components: glial cells, neuropil, myelin, cerebral blood vessels.

Damage has various morphological manifestations at the cellular and tissue levels. Injuries can be superficial and reversible or deep and irreversible. One can distinguish damage to the single cell or tissue; this process can be represented by dystrophy or necrosis at the tissue level.

Among cellular dystrophies, pigment dystrophy manifested by the lipofuscin pigment buildup normally occurring with age and developing under exposure to toxicants, alcohol, and drugs, is considered to be the most common in the nervous system. In the majority of observations lipofuscin accumulates in neurons (Fig. 1), however, in drug addiction, its accumulation in the choroid plexus epithelium, where it does not occur either normally or in other disorders under the age of 30 years, is pathognomonic (Fig. 2). Furthermore, this pigment is sometimes detected in astrocytes, oligodendrocytes, and pericytes. Lipofuscin represents a glycolipoprotein found in the form of golden or brown granules, depending on the stain used. These graniles show different electron density when examined by electron microscopy [13, 14].

Lipofuscin consists of lipids, metals, and abnormally folded proteins; it has the property of autofluorescence. In addition to the nervous system, it can be found in cardiomyocytes and the skin. In the CNS, lipofuscin accumulates in the form of aggregates, shaping a specific ageing pattern associated with both physiological and pathological conditions, changing the neuronal cytoskeleton, cell transport and metabolism. It is also associated with the loss of neurons, proliferation and activation of glial cells. Historically, the lipofuscin buildup was
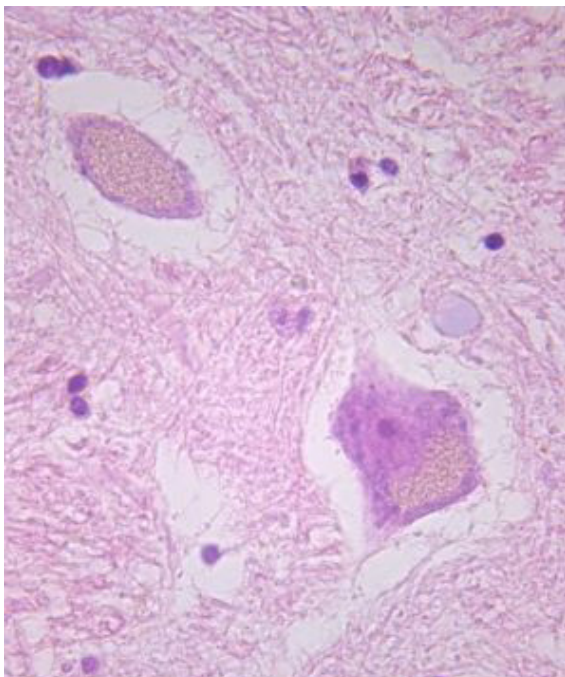
Fig. 1. Lipofuscin in the cytoplasm of neurons, multiple light-yellow granules, sectional material. Hematoxylin and eosin staining, ×630
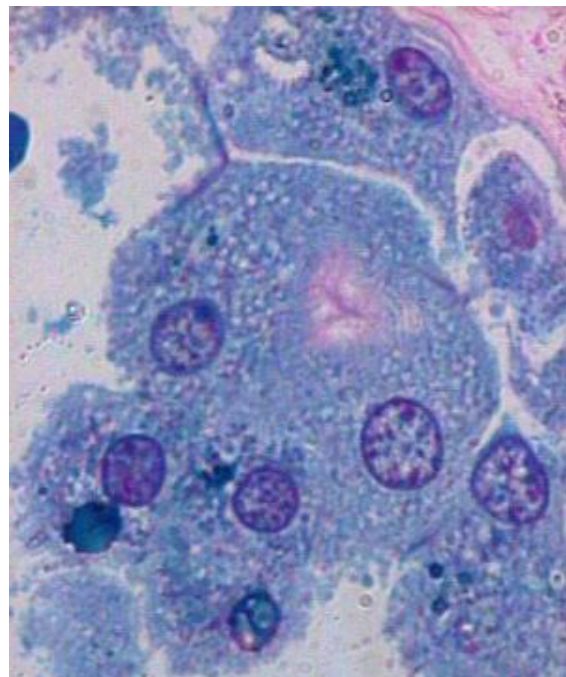
Fig. 2. Lipofuscin in the epithelium of the vascular plexus, blue-green granules in the cytoplasm, sectional material. Staining with alcian blue, ×1000
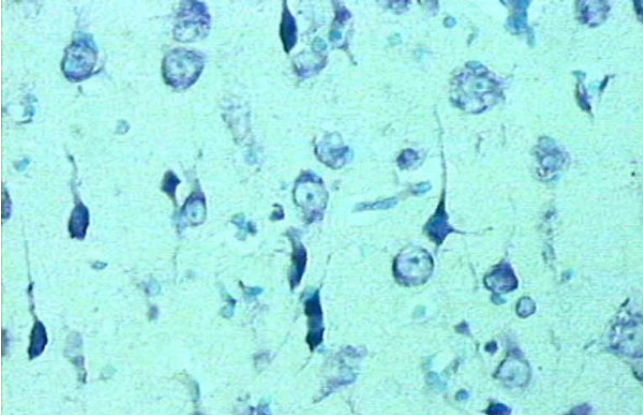
Fig. 3. Temporal lobe cortex acute swelling of neurons, shadow cells, dark, shriveled neurons, biopsy material. Nissl staining, ×400

considered to be secondary to ageing associated with various neurodegenerative disorders. However, the new data suggest that lipofuscin aggregates play an active role in ageing and neurodegeneration [15].

The other dystrophy type typical for the nervous system, hydropic dystrophy, is manifested by swelling of neurons in response to toxic damage. Acute swelling is reversible; it is associated with excess liquid accumulation in the cell. During this process the neuron becomes round, the cytoplasm and nucleus become lighter, and the tigroid is lost. Such dystrophy can be caused by hypoxy, intoxication, and other factors resulting in the cell damage and increased osmolality of the cytoplasm.

A rapid decrease in plasma osmolality causes rapid water absorption by astrocytes, but not neurons, while cells of both types swell due to ischemia. However, these abnormalities are fundamentally different at the cellular level. Astrocytes swell osmotically or shrink, since functional water channels, aquaporins, are expressed in these cells, while neurons have no functional aquaporins, so the volume of neurons is preserved. Nevertheless, both neurons and astrocytes swell slowly, when blood supply to the brain is impaired after the onset of stroke, sudden cardiac arrest or traumatic brain injury. In each situation swelling of neurons results directly from the spreading depolarization (SD) associated with the impaired function of the ATP-dependent sodium/potassium ATPase (Na^+/K^+ pump). Despite the fact that these mechanisms are poorly understood, they refute the dogma that states that swelling of neurons is associated with the absoption of water regulated by osmotic gradient with aquaporins as a vehicle [16].

When the toxicant effect is over, the neuron can return to normal again, taking a triangular shape. However, when damage is too severe and irreversible, the neuron transforms into the shadow cell. Such changes are typical for acute carbon monoxide poisoning [17, 18] and neurotoxic sequelae of poisoning with the substances exerting convulsive effects [19].

The emergence of dark neurons can represent one more variant of dystrophy. When examined by light microscopy, these seem to decrease in size and are usually rod-shaped, sharply stained with hematoxylin or thionin; it is almost impossible to see the nuclei of these neurons. These cells looking the same when examined by light microscopy can be divided into two types when examined with the electron microscope: the first represent precursors of necrosis followed by pyknosis and rhexis of the nucleus and cytoplasm, while the second (more common) represent the state of stress of the neuron, its increased activity with accumulation of organelles. Only one type of changes predominates in some cortical areas, most often acute swelling, however, the combination of acute

swelling with the dark schriveled neurons can be found in some fields of view (Fig. 3).

Such neurons also do not necessarily die. In the experiments involving the rat model of septoplasty, the emergence of dark and p53-positive neurons in the hippocampus can be considered as the typical nervous system response to stress. The peak p53 protein expression growth in the cytoplasm of the neurons in the CA1 and CA2 fields was observed on days 2–4 after surgery; the number of such neurons decreased on day 6. Presumably p53 protein can not only trigger activation of damaged neurons in the hippocampus, but also plays a neuroprotective role [20].

Different dystrophic changes are typical for various cortical areas. However, these can be combined somewhere, and both swollen and dark schriveled cells are seen in the field of view.

The presence of myelin sheaths around the axonal processes of neurons, which are also prone to atrophy, is a characteristic feature of the nervous system. Little attention is paid to myelinopathy variants in the literarute, both domestic [11] and foreign [21, 22, 23]. Only demyelination processes are discussed, which are considered to result primarily from the death of oligodendrogliocytes [22, 24]. There are no detailed classifications of damage to myelin sheath, as well as no widely accepted classification. The same is typical for axonal pathology. Toxic peripheral neuropathies represent an important form of acquired polyneuropathy caused by various zenobiotics and toxicants. Primary damage occurs in the most distal parts of the nerves, particularly in the axons with the thickest myelin sheath and large diameter having the highest metabolism. Primary lesion is represented by edema and color change (pale or more intense color), which transform into fragmentation of the axon with time. The surrounding myelin sheath is disrupted due to secondary reaction. The main lesion is represented by segmental demyelination. The remains of the nerve fibers are decomposed by Schwann cells capable of functioning as phagocytes, or penetrating macrophages [25].

Among alterations of myelin sheaths at the microscopic level revealed by light and electron microscopy, the following are distinguished: dissociation, delamination, granular disintegration, homogenization, and demyelination. The axon that has lost myelin is prone to swelling and axial cylinder destruction.

Myelinopathy

1. Delamination — disrupted regularity of the myelin sheath layers fitted tightly around each other with the formation of dilated areas with significant hollows between individual lamellae.

2. Dissociation — disruption of the myelin sheath configuration — the type of myelin deformation associated with mismatch in the circle's circumference values of the axial cylinder and the covering myelin sheath, due to which protrusions of lamella folds, both outward and inward of the fiber, are formed.

3. Granular disintegration — type of myelin sheath local destruction, when the strict order of myelin layers is replaced with granular fragmentation of membranes.

4. Myelin homogenization — type of myelin sheath local or total destruction characterized by enzymatic degradation of membranes to the state of dispersion with varying electron density.

The combinations of the delamination and dissociation or granular disintegration and myelin homogenization are rather common (Fig. 4A, B).

5. Demyelination — myelin sheath thinning due to rapid decrease in the number of lamellae constituting it structure or total lack of myelin sheath.

6. Remyelination — restoration of the thinned myelin sheath.

7. Hypermyelination — excess increase in the number of
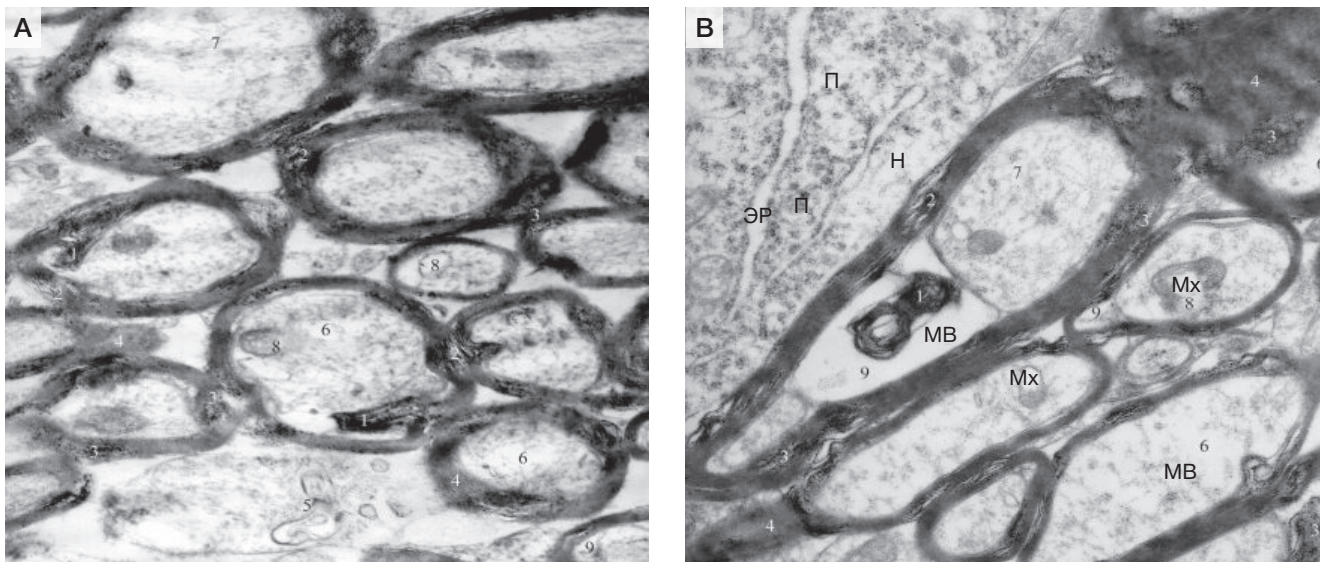
Fig. 4. Changes in myelinated fibers of the white matter Fig. 4A — ×20,000.; Fig. 4B — ×16000. MF — myelin fiber; N — neuron; ER — endoplasmic reticulum; P —polysomes; Mch — mitochondrion; 1 — Disruption of myelin sheath configuration; 2 — delamination; 3 — granular disintegration; 4 — homogenization; 5 — demyelination; 6 — brightening of the axial cylinder matrix; 7— disorientation of neurofilaments; 8 — destruction of mitochondria; 9 — periaxonal edema, experimental material (rats). Electronograms

lamellae in the myelin sheath resulting in significant constriction of the axial cylinder [11].

Demyelination is often found in many disorders. However, the role of demyelination is poorly understood and is not considered to be leading.

There is a term "leukoaraiosis" in radiation diagnosis. Comparison of postmortem MRI scans and morphological data has shown that neuropil rarefaction associated with demyelination is among visible equivalents of this MRI phenomenon.

Necrosis is the death of cells or tissues in the living organism. Single cells can die due to both necrosis and apoptosis (programmed cell death). Pathologists are familiar with the term "necrosis", while the term "apoptosis" is rather new, and the diagnosis of apoptosis can cause some difficulties, since this is cell damage without inflammation or cell lysis.

Apoptosis

Light microscopy allows one to suspect apoptosis. Chromatin condensation in the cell nucleus that later becomes fragmented, is a typical sign of the apoptosis onset. Each fragment is surrounded by the cytoplasm, and the apoptotic body is formed that are ingested by macrophages. Electron microscopy, immunohistochemical methods, and the TUNEL apoptosis detection method are used to diagnose apoptosis. Programmed cell death was determined in the majority of chronic disorders and cases of toxic damage to the nervous system. Immunohistochemical studies of the human brain showed that cortical neurons responded positively to the p53 tumor suppressor controlling the state of DNA in the cell and triggering the cell death (apoptosis) program in case of DNA damage and impossibility of repair (Fig. 5, 6).

Necrosis of cells, particularly neurons, can go in two ways: through cytolysis and cytorhexis. For the neuron, cytolysis is a continuation of acute swelling, when it proceeds to the irreversible stage of the shadow cell, while cytorhexis is developed after shriveling of neurons with subsequent fragmentation of the nucleus.

Direct (traumatic and toxic damage) and indirect necrosis most often associated with circulation disorders represent the clinical and
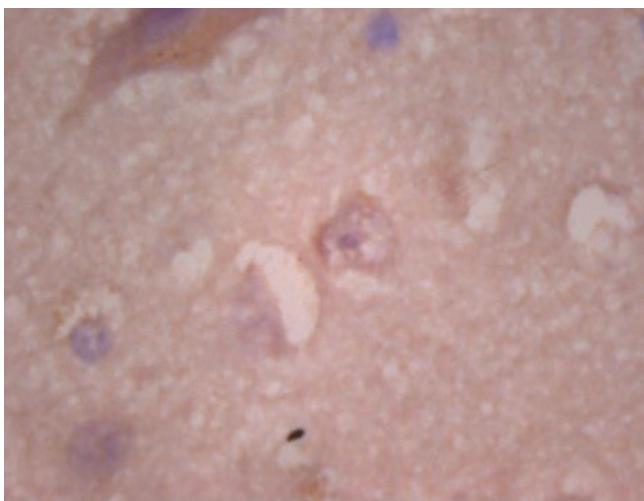
Fig. 5. Oncosuppressor gene is determined in the nucleus of the "dementia neuron". The cytoplasm of a large neuron of typical structure has a large amount of lipofuscin (sectional material). Immunohistochemical reaction of p53, ×1000
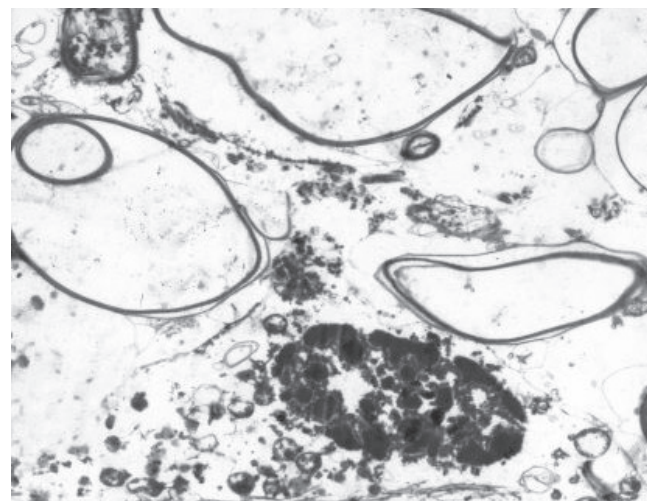
Fig. 6. Sections of white matter. Filamentous myelin fibers with transparent axial cylinders. Near oligodendrocyte with signs of apoptosis (sectional material). Electronogram, ×5000
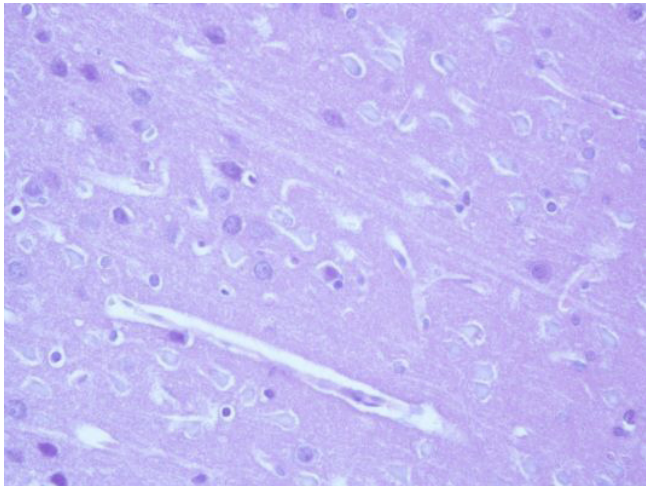
Fig. 7. Cerebral cortex. The perivascular spaces are dilated. Most neurons are "shadow cells", single neurons with neuronophagy phenomena. Foci of neuron loss, experimental material (rats). Hematoxylin and eosin staining, ×400

Fig. 8. Brain, subcortical nuclei. The perivascular spaces are significantly enlarged. Most neurons are unchanged, marked rarefaction of the neuropil of the conducting pathways, experimental material (rats). Hematoxylin and eosin staining, ×400

morphological forms of the brain necrosis. Small foci of necrosis that are often elective, where only some components of the tissue are damaged, while other components are preserved (Fig. 7, 8), are most typical for toxic brain tissue damage. Such foci show up as neuropil rarefaction and gliopenia [11].

CONCLUSION

Thus, common disease mechanisms, such as neuroinflammation, atrophy and dystrophy, damage to neurons and glial component that can result in the death of cells occurring in different ways,

including apoptosis and necrosis, underlie toxic damage to the brain, regardless of the cause (toxic or medicinal substances, bacteria, protozoa or viruses, endogenous toxicants, drugs, alcohol, traumatic brain injury, etc.).

The changes in cell morphology can be both reversible and irreversible; these can to varying degrees and in different ways manifest themselves in the brain regions. Today, such changes are poorly understood due to non-specific nature, despite the fact that these data are essential for selection of optimal treatment and reduction of dangerous sequelae of the number of medical procedures.

References

1. Katamanova EV, Rukavishnikov VS, Lahman OL, Shevchenko OI, Denisova IA. Kognitivnye narushenija pri toksicheskom porazhenii mozga. Zhurnal nevrologii i psihiatrii. 2015; 2: 11–15. Russian.
2. Dobbs RM. Toxic encephalopathy. Semin Neurol. 2011; 31 (2): 184–93.
3. Eicher T, Avery E. Toxic encephalopathies. Neurol Clin. 2005; 23 (2): 353–76.
4. Wylie AC, Short SJ. Environmental Toxicants and the Developing Brain. Biol Psychiatry. 2023; b93 (10): b921–33.
5. Gagnon-Chauvin A, Bastien K, Saint-Amour D. Environmental toxic agents: The impact of heavy metals and organochlorides on brain development. Handb Clin Neurol. 2020; 173: 423–42.
6. McNeish BL, Kolb N. Toxic Neuropathies. Continuum (Minneap Minn). 2023; 29 (5): 1444–68.
7. Brambrink AM, Orfanakis A, Kirsch JR. Anesthetic neurotoxicity. Anesthesiol Clin. 2012; 30 (2): 207–28.
8. Macko DE, Korshunov AG. Atlas opuholej central'noj nervnoj sistemy. SPb.: Izd. RNHI im. prof. A. L. Polenova, 1998; 200 s. Russian.
9. Gulevskaja TS, Morgunov VA. Patologicheskaja anatomija narushenij mozgovogo krovoobrashhenija pri ateroskleroze i arterial'noj gipertenzii. M.: Medicina, 2009; 294 s. Russian.
10. Medvedev YuA, Zabrodskaja YuM. Novaja koncepcija proishozhdenija bifurkacionnyh anevrizm arterij osnovanija golovnogo mozga. SPb.: Jeskulap, 2000; 168 s. Russian.
11. Gaikova ON, Ananeva NI, Zabrodskaja YuM. Morfologicheskie projavlenija obshhepatologicheskih processov v nervnoj sisteme. SPb.: Ves', 2015; 158 s. Russian.
12. Ermohin PN. Gistopatologija central'noj nervnoj sistemy. M.: Medicina, 1969; 244 s. Russian.
13. Litvincev BS. Nevrologicheskie narushenija pri narkomanii: principy diagnostiki i terapii. Voenno-medicinskaja akademija imeni S. M. Kirova. SPb.: VmedA, 2018; 167 s. Russian.
14. Litvincev BS. Porazhenija nervnoj sistemy pri narkomanii. Voenno-medicinskaja akademija imeni S. M. Kirova. SPb.: VMedA, 2018; 160 s. Russian.
15. Moreno-García A, Kun A, Calero O, Medina M, Calero M. An Overview of the Role of Lipofuscin in Age-Related Neurodegeneration. Front Neurosci. 2018; 12: 464.
16. Hellas JA, Andrew RD. Neuronal Swelling: A Non-osmotic Consequence of Spreading Depolarization. Neurocrit Care. 2021; 35 (2): 112–34.
17. Kim AA, Indiaminov SI, Assatulaev AF. Osobennosti porazhenija struktury golovnogo mozga pri otravlenii ugarnym gazom na fone termicheskoj travmy i alkogol'noj intoksikacii. Zhurnal biomediciny i praktiki. 2021; 6 (4): 247–54. Russian.
18. Petrov LV, Salova IYu. Harakteristika ochagovyh izmenenij golovnogo mozga pri ostrom otravlenii okis'ju ugleroda. Uchenye zapiski SPbGMU im. akad. I. P. Pavlova. 2012; XIX (2): 61–64. Russian.
19. Petrov AN, Vojcehovich KO, Melehova AS, Lisickij DS, Belskaja AV, Mihajlova MV, i dr. Problemy diagnostiki nejrotoksicheskih narushenij — posledstvij otravlenij veshhestvami sudorozhnogo dejstvija. Vestnik Rossijskoj voenno-medicinskoj akademii. 2017; 3 (59): 211–17. Russian.
20. Torshin VI, Kastyro IV, Reshetov IV, Kostyaeva MG, Popadyuk VI. The Relationship between p53-Positive Neurons and Dark Neurons in the Hippocampus of Rats after Surgical Interventions on the Nasal Septum. Dokl Biochem Biophys. 2022; 502 (1): 30–35.
21. Blümcke I, Thom M, Aronica E, et al. The clinic-pathologic spectrum of focal cortical dysplasias: a consensus classification proposed by an ad hoc Task Force of the ILAE Diagnostic Methods Commission. Epilepsia. 2011; 52 (1): 158–74.
22. Hu X, Wang JY, Gu R, Qu H, Li M, Chen L, et al. The relationship between the occurrence of intractable epilepsy with glial cells and

myelin sheath — an experimental study. Eur Rev Med Pharmacol Sci. 2016; 20 (21): 4516–24. PMID: 27874947.

23. Lapato AS, Szu JI, Hasselmann JPC, et al. Chronic demyelination-induced seizures. Neuroscience. 2017; 27 (346): 409–22.

24. Kim SH, Choi J. Pathological Classification of Focal Cortical Dysplasia (FCD): personal comments for well understanding FCD classification. J Korean Neurosurg Soc. 2019; 62 (3): 288–95.

25. Lanigan LG, Russell DS, Woolard KD, Pardo ID, Godfrey V, Jortner BS, et al. Comparative Pathology of the Peripheral Nervous System. Vet Pathol. 2021; 58 (1): 10–33.

Литература

1. Катаманова Е. В., Рукавишников В. С., Лахман О. Л., Шевченко О. И., Денисова И. А. Когнитивные нарушения при токсическом поражении мозга. Журнал неврологии и психиатрии. 2015; 2: 11–15.

2. Dobbs RM. Toxic encephalopathy. Semin Neurol. 2011; 31 (2): 184–93.

3. Eicher T, Avery E. Toxic encephalopathies. Neurol Clin. 2005; 23 (2): 353–76.

4. Wylie AC, Short SJ. Environmental Toxicants and the Developing Brain. Biol Psychiatry. 2023; b93 (10): b921–33.

5. Gagnon-Chauvin A, Bastien K, Saint-Amour D. Environmental toxic agents: The impact of heavy metals and organochlorides on brain development. Handb Clin Neurol. 2020; 173: 423–42.

6. McNeish BL, Kolb N. Toxic Neuropathies. Continuum (Minneap Minn). 2023; 29 (5): 1444–68.

7. Brambrink AM, Orfanakis A, Kirsch JR. Anesthetic neurotoxicity. Anesthesiol Clin. 2012; 30 (2): 207–28.

8. Мацко Д. Е., Коршунов А. Г. Атлас опухолей центральной нервной системы. СПб.: Изд. РНХИ им. проф. А. Л. Поленова, 1998; 200 с.

9. Гулевская Т. С., Моргунов В. А. Патологическая анатомия нарушений мозгового кровообращения при атеросклерозе и артериальной гипертензии. М.: Медицина, 2009; 294 с.

10. Медведев Ю. А., Забродская Ю. М. Новая концепция происхождения бифуркационных аневризм артерий основания головного мозга. СПб.: Эскулап, 2000; 168 с.

11. Гайкова О. Н., Ананьева Н. И., Забродская Ю. М. Морфологические проявления общепатологических процессов в нервной системе. СПб.: Весь, 2015; 158 с.

12. Ермохин П. Н. Гистопатология центральной нервной системы. М.: Медицина, 1969; 244 с.

13. Литвинцев Б.С. Неврологические нарушения при наркомании: принципы диагностики и терапии. Военно-медицинская академия имени С. М. Кирова. СПб.: ВмедА, 2018; 167 с.

14. Литвинцев Б. С. Поражения нервной системы при наркомании. Военно-медицинская академия имени С. М. Кирова. СПб.: ВМедА, 2018; 160 с.

15. Moreno-García A, Kun A, Calero O, Medina M, Calero M. An Overview of the Role of Lipofuscin in Age-Related Neurodegeneration. Front Neurosci. 2018; 12: 464.

16. Hellas JA, Andrew RD. Neuronal Swelling: A Non-osmotic Consequence of Spreading Depolarization. Neurocrit Care. 2021; 35 (2): 112–34.

17. Ким А. А., Индиаминов С. И., Ассатулаев А. Ф. Особенности поражения структуры головного мозга при отравлении угарным газом на фоне термической травмы и алкогольной интоксикации. Журнал биомедицины и практики. 2021; 6 (4): 247–54.

18. Петров Л. В., Салова И. Ю. Характеристика очаговых изменений головного мозга при остром отравлении окисью углерода. Ученые записки СПбГМУ им. акад. И. П. Павлова. 2012; XIX (2): 61–64.

19. Петров А. Н., Войцехович К. О., Мелехова А. С., Лисицкий Д. С., Бельская А. В., Михайлова М. В., и др. Проблемы диагностики нейротоксических нарушений — последствий отравлений веществами судорожного действия. Вестник Российской военно-медицинской академии. 2017; 3 (59): 211–17.

20. Torshin VI, Kastyro IV, Reshetov IV, Kostyaeva MG, Popadyuk VI. The Relationship between p53-Positive Neurons and Dark Neurons in the Hippocampus of Rats after Surgical Interventions on the Nasal Septum. Dokl Biochem Biophys. 2022; 502 (1): 30–35.

21. Blümcke I, Thom M, Aronica E, et al. The clinic-pathologic spectrum of focal cortical dysplasias: a consensus classification proposed by an ad hoc Task Force of the ILAE Diagnostic Methods Commission. Epilepsia. 2011; 52 (1): 158–74.

22. Hu X, Wang JY, Gu R, Qu H, Li M, Chen L, et al. The relationship between the occurrence of intractable epilepsy with glial cells and myelin sheath — an experimental study. Eur Rev Med Pharmacol Sci. 2016; 20 (21): 4516–24. PMID: 27874947.

23. Lapato AS, Szu JI, Hasselmann JPC, et al. Chronic demyelination-induced seizures. Neuroscience. 2017; 27 (346): 409–22.

24. Kim SH, Choi J. Pathological Classification of Focal Cortical Dysplasia (FCD): personal comments for well understanding FCD classification. J Korean Neurosurg Soc. 2019; 62 (3): 288–95.

25. Lanigan LG, Russell DS, Woolard KD, Pardo ID, Godfrey V, Jortner BS, et al. Comparative Pathology of the Peripheral Nervous System. Vet Pathol. 2021; 58 (1): 10–33.

STRUCTURAL AND FUNCTIONAL CHANGES IN THE BRAIN OF COSMONAUTS UNDER THE INFLUENCE OF MICROGRAVITY

Latartsev KV[1,2] ✉, Demina PN[1], Yashina VA[1,2], Kaspranskiy RR[1]

[1] Federal Research and Clinical Center of Space Medicine of Federal Medical Biological Agency, Moscow, Russia

[2] Lomonosov Moscow State University, Moscow, Russia

During a space flight, cosmonauts have to adapt to new unique environmental conditions. As a result, they accumulate changes to their bodily systems that can eventually cause undesirable consequences potentially detrimental to the success of the mission. The review examines research papers investigating functional and structural changes occurring in the brain in the context of a spaceflight. Microgravity is believed to be the main factor behind the said changes: it causes redistribution of fluid in the body and conditions adaptive neural rearrangements at the microstructural level. Other elements peculiar to a spaceflight that can have this or that effect on the brain are also considered. In addition, this review scopes publications that allow assumptions about the specific causes of the registered morphofunctional alterations in the brain of cosmonauts.

Author contribution: Latartsev KV — analysis of source materials, article authoring and editing; Demina PN — search for source materials, analysis thereof; Yashina VA — search for source materials, analysis thereof; Kaspransky RR — study conceptualization, search for source materials, manuscript editing.

✉ **Correspondence should be addressed:** Konstantin V. Latartsev
Shchukinskaya, 5, st. 2, Moscow, 123182, Russia; k.latartsev@gmail.com

СТРУКТУРНЫЕ И ФУНКЦИОНАЛЬНЫЕ ИЗМЕНЕНИЯ В ГОЛОВНОМ МОЗГЕ КОСМОНАВТОВ ПОД ВЛИЯНИЕМ МИКРОГРАВИТАЦИИ

К. В. Латарцев[1,2] ✉, П. Н. Демина[1], В. А. Яшина[1,2], Р. Р. Каспранский[1]

[1] Федеральный научно-клинический центр космической медицины Федерального медико-биологического агентства, Москва, Россия

[2] Московский государственный университет имени М. В. Ломоносова, Москва, Россия

Во время космического полета космонавты вынуждены приспосабливаться к новым специфическим условиям окружающей среды. Это приводит к накоплению изменений в организме, которые в конечном счете могут вызывать нежелательные последствия, способные оказывать негативное влияние на успех проводимой миссии. В обзоре рассмотрены публикации, посвященные функциональным и структурным изменениям головного мозга, происходящим во время космического полета. Основным фактором, вызывающим описываемые изменения, считается микрогравитация, приводящая к перераспределению жидкости в организме, а также обуславливающая адаптационные нейронные перестройки на микроструктурном уровне. Помимо этого, затрагиваются и другие факторы космического полета, способные оказывать влияние на головной мозг. Рассмотрены также публикации, на основе которых можно выдвигать предположения о конкретных причинах наблюдаемых морфофункциональных перестроек в головном мозге космонавтов.

Вклад авторов: К. В. Латарцев — анализ источников, написание текста, редактирование; П. Н. Демина — поиск источников, анализ источников; В. А. Яшина — поиск источников, анализ источников; Р. Р. Каспранский — разработка концепции, поиск источников, редактирование рукописи.

✉ **Для корреспонденции:** Константин Владимирович Латарцев
ул. Щукинская, д. 5, ст. 2, г. Москва, 123182, Россия; k.latartsev@gmail.com

During a spaceflight, a number of factors specific thereto cause structural and functional rearrangements in the brain, same as in other organs and tissues of the body [1]. Presently, such attributes of a space mission as microgravity, prolonged isolation, radiation, disruption of sleep patterns and circadian rhythms are known to affect human psychophysiology by disturbing operation of various parts of the brain [2–4]. In microgravity, gravitational pull of the nearest space object is extremely small, and physical items seem weightless; the associated stable background acceleration is of the order of 1×10^{-6} g. To date, there has been accumulated a large amount of information yielded by the studies designed to investigate the effect of microgravity on physiology of the brain. The respective papers describe both structural and functional changes occurring in the brain under the influence of this spaceflight factor: disorders of the vestibular function, neuroplastic adaptation, redistribution of fluid in the body (shifts to the upper part of the body, subsequently elevates intracranial pressure (ICP) and triggers many concomitant effects). Changes in the functioning of the brain that result from adaptation to the conditions of spaceflight can become a problem during deep space missions, therefore, studying the effect of microgravity as a phenomenon integral to spaceflights, is an important task.

The effect of microgravity on the volumetric characteristics of brain structures

Redistribution of fluid in the body is one of the main problems associated with a spaceflight. Earth gravity gradients hydrostatic pressure in a human being: its value gradually increases from the head to the lower extremities. In microgravity, there is no force to effect this gradient, and weaker forces (surface tension, etc.) gain control over the behavior of fluid in the body, eventually redistributing it. Apparently, the upper body's vascular network, spinal membranes, interstitial tissues, and possibly the lymphatic system receive and store most of the redistributed fluid [5]. This entails various changes, including those in the central nervous system, like the previously registered narrowing of the cerebrospinal spaces around central and calcarine sulci and upward displacement of the brain inside the skull [6]. At the same time, post-flight examinations and observations revealed expansion of the cerebrospinal fluid spaces along ventral surface of brain and ventricles, gray matter contraction in the orbitofrontal and temporal cortices with the total volume of gray and white matter remaining unchanged [7, 8], and growth of the volume of free water in the frontal, temporal and occipital lobes [9]. Moreover, it was found that long-term spaceflight (LTSF) boosts the dynamics of cerebrospinal fluid (CSF) in cerebral aqueduct, causes its volume to grow and brain to expand. Previous research revealed LTSF to be associated with a progressive increase in mean and pulse ICP, conditioned by the mentioned greater volumes of the CSF and brain matter, and reported white matter expansion and pituitary deformity in 6 out of 11 crew members after a long-term space mission [10]. One study sought to assess volume and morphology of periventricular white matter (PWM), and found that it increased in first-time cosmonauts, whereas no such phenomenon was registered in their experienced counterparts [11]. Other studies, which established a link between spaceflight duration and the degree of enlargement of cerebral cavities, confirm these findings [12].

However, fluid redistribution is not the only reason for changes in the volumetric characteristics of the brain. There are also microstructural changes, which will be discussed in the following sections.

The effect of microgravity on the sensorimotor system

Prolonged stay in microgravity impairs human cognitive abilities, causes asthenia, and disrupts spatial orientation. In addition, as shown by post-flight and simulation studies, LTSF adversely affects performance and learning ability, both dependent on the higher mental functions [13, 14]. It is clear that an abrupt change in gravitation can have negative consequences for a human being's sensorimotor control, since it developed in the conditions of Earth. Researchers have set up experiments to investigate the effect of hypergravity (simulated) and microgravity (simulated and real), and learned that both have a negative impact on the accuracy and speed of hand movements, with more noticeable changes registered for upward arm movements than for downward movements. Shoulder girdle's muscles have been shown to work differently, too, the respective alteration conditioned by the degree of parallelism between the gravity vector and the direction of application of force exerted by these muscles. For example, pectoral muscle worked perpendicularly to gravity, and in the experiment, gravitational changes affected it the least [15, 16]. These findings found confirmation in subsequent studies. Presumably, altered gravitation could have forced the sensorimotor system to perceive weight changes as an increase or decrease of the mass of the held object, as well as that of the hand itself, when these parameters have in fact remained unchanged. Microgravity made hand movements slower and lasting longer, hypergravity — less accurate and lasting longer; the latter effect is probably conditioned by a more concentrated conscious cognitive control effort. The increased feedback seems to have helped compensate for the decreased accuracy [17]. These experiments show that in microgravity, there is a need for additional cognitive control of movements, which, apparently, gives rise to a deficit of neural resources due to sensorimotor adaptation to microgravity. This process, in turn, degrades the ability to simultaneously perform cognitive and motor tasks when in space [18]. Terrestrial experiments simulating individual effects weightlessness also show rearrangements in sensorimotor and spatial working memory that hinder the ability to solve complex tasks and cause psychoemotional shifts [19, 20].

The effect of microgravity on structural changes in the brain

Adaption to the peculiarities of movements and performing various tasks in microgravity is accompanied by structural changes in the brain departments and pathways that are mainly associated with motor activity. Functional MRI has revealed that prolonged exposure to weightlessness promotes rearrangements in the vestibular and motor regions of the brain, with alterations registered predominantly in the cerebellum, cortical sensorimotor and somatosensory regions, as well as vestibular pathways, accompanied by the changes in the number of synapses and axonal degeneration [21, 22]. It was also found that microgravity causes microstructural changes in the brain in general and sensorimotor tracts in particular [23]. In 2016, scientists noted a decrease in the amount of gray matter in the frontal and temporal lobes, in the orbitofrontal cortex, as well as in the bilateral medial sections of the middle cerebellar peduncles, and changes in some regions of the brain were significantly more pronounced after LTSF [24]. As for white matter, changes therein were detected in the right superior and inferior longitudinal fascicles, corticospinal tract and cerebellar peduncles [9]. In 2022, significant microstructural changes were identified in the corpus callosum, arcual fascicle, corticospinal, corticostriar and cerebellar tracts [23]. These discoveries point to adaptive neuroplasticity mechanisms that are activated when a person's environmental conditions alter. A greater volume of white matter in the cerebellum registered after spaceflight also clearly confirms activation of these mechanisms [25]. Russian scientists have also demonstrated adaptive neuroplasticity in Russian cosmonauts [26].

At the same time, brain rearrangements occurring in the context of an LTSF reduce the individual's adaptability to the conditions of Earth gravity. Post-flight examinations of cosmonauts have revealed hindered operation of the precentral and postcentral gyri, responsible for voluntary movements and proprioception, respectively, and maloperation of the cerebellum, which governs movement coordination. Damage to these areas of the brain leads to somatosensory disorders, problems with the accuracy and speed of voluntary movements, and obstructs movement synchronization [27]. Observations of cosmonauts show that on the day of landing they experience ataxia, manifested in impaired coordination of movements and pose maintenance, which indicates dysfunction of the vestibular system and impaired proprioception. Impaired coordination of movements is recorded three days after the flight, too, but

without dizziness [2]. The post-spaceflight changes in human sensorimotor characteristics, including degraded motor activity, balance and fine motor skills, are well-documented [18]. Investigation of the adverse effects of microgravity associated with alterations in somatosensory and vestibular signals revealed significant changes in the volume of gray matter. Antiorthostatic hypokinesia triggered growth of its volume in the postparietal and shrinkage thereof in the frontal regions of the brain. These structures govern control and coordination of voluntary movements, sensorimotor coordination, and processing of sensory information. In addition, functional mobility and the ability to maintain balance while standing have been observed to deteriorate. Such changes are associated with a greater amount of gray matter in the region that includes quader, precentral and postcentral gyri, which are responsible for sensory perception, motor control, and orientation in space and time [28].

The effect of microgravity on functional changes in the brain

The listed adaptive mechanisms condition functional connectivity of the brain regions after exposure to microgravity. For example, structural connectivity of white matter changes in areas involved in visual-spatial data processing, vestibular function, and motion control, suggesting that the processes requiring prefrontal multimodal integration of sensory signals may be at risk during spaceflight [9]. Immediately after the LTSF and 8 months later, there has been registered a persisting deterioration of connectivity in the posterior cingulate cortex and thalamus, with the respective indicator increasing in the right angular gyrus. Connectivity in the bilateral insular cortex decreased after spaceflight, but returned to normal by the time of the next examination. The study shows that the altered gravitational environment affects functional connectivity longitudinally in multimodal brain centers, reflecting adaptation to unfamiliar and contradictory sensory information peculiar to microgravity [26]. Another study detected deteriorating connectivity in the right insular lobe associated with afferents of otolith organs and semicircular canals, as well as between the cerebellum's left hemisphere and the motor cortex's right zone. The conclusions that the motor cortex is less connected during rest and gets more activated in the context of an active task can be considered a compensatory adaptive response to microgravity, as well as a mechanism of adaptation triggered in the early post-landing period [27]. In one study, scientists sought to determine correlations between changes in the brain and changes in the performance of spatial working memory (SWM) before and after flight; they did not register any significant impact of LTSF on the performance of SWM or brain activity, but observed significant changes in brain connections. Thus, superior occipital gyrus was found to communicate with the rest of the brain less effectively. Testing of SWM also revealed poorer connection between left middle occipital gyrus and left parahippocampal gyrus, as well as left cerebellum and left lateral occipital cortex [29]. In addition, another study recorded intra- and interhemispheric anti-correlations between temporoparietal junction and supramarginal gyri, which indicate a change in both vestibular functions and functions associated with consciousness [30]. Prolonged stay in antiorthostatic hypokinesia led to a deterioration of balance and motor activity, as well as significant changes in the functional connectivity of the motor, somatosensory and vestibular regions of the brain [31]. Moreover, some of these changes were largely associated with rearrangements in the sensorimotor and spatial working

memory, which suggests that neuroplasticity mechanisms may contribute to adaptation to simulated microgravity [20]. For cosmonauts, one of the most important problems associated with impaired sensorimotor and cognitive functions is space motion sickness, which occurs when a person undergoes acute adaptation to microgravity. Examinations of the brain during nausea caused by two different types of stimuli have revealed dipoles in the area of cerebral cortex (lower part of the frontal gyrus) measuring 2–3 cm in diameter, which signals of activation of neurons. Severe nausea meant more dipoles than milder nausea. Thus, nausea caused by the vestibular system affects the prefrontal areas of the brain that are associated with autonomic regulation of emotions, which implies that motion sickness can have an effect on those prefrontal areas and disrupt autonomic mechanisms [32]. Clearly, transformation of the pathways participating in cognition and processing of sensory information can negatively affect the ability to pilot and dock a spacecraft or perform other operations that also require spatial memory. In 2020, there have been designed studies to determine the effect of microgravity on higher cognitive functions. However, they yielded contradictory results: some reported deterioration thereof, others — improvement, yet others — lack of changes [33]. A year earlier, there was conducted a study that observed twin astronauts before, during, and after a one-year mission to the International Space Station (ISS). This study has shown that cognitive tasks proved to be significantly more difficult to solve only after the flight, but the earlier periods of the experiment the ability of the participants to tackle them remained unchanged [34].

Causes and mechanisms of microstructural changes in the brain

Based on the analysis of the literature, it can be concluded that adaptive neuroplasticity and fluid redistribution are considered to be the two main microgravity-associated factors that drive microstructural changes in the brain. Presumably, neuroplastic adaptations mainly occur in the systems that govern motor activity. Based on the already existing theory of how cerebellum processes information, it can be assumed why microgravity triggers certain changes.

The cerebellum of a mammalian combines information from a variety of sensory systems with motor commands and sends projections to the motor and premotor regions of the cerebral cortex, as well as to the nuclei of the brain stem and spinal cord. Many areas of the cerebellum receive inputs directly from vestibular afferents and vestibular nuclei. Presumably, cerebellum generates an internal model that predicts somatosensory consequences of the movements performed, after which the predicted and actual consequences of motor behavior are compared. Currently, it is believed that the cerebellum calculates differences and generates an error signal that controls recalibration of motor centers [35]. On Earth, the body is constantly exposed to gravity, which leads to continuous stimulation of otolith organs and proprioceptors. Studies show that some of the Purkinje cells in the cerebellum encode head positions and their changes relative to the direction of gravity. Apparently, orientation in space factors in constant gravity, so researchers believe that the internal model of motion calculated inside the cerebellum also accounts for this force [35]. However, spaceflights imply microgravity, which translates into a discrepancy between sensory consequences of movements modeled by the brain and the real sensations. Consequently, this triggers rearrangements in the vestibular signal processing system that enable adaptation to the new

environmental conditions. In this connection, a study reported an increase in the mass of otoliths and the number of hair cells in the first weeks of spaceflight, a short-term increase in the sensitivity of the vestibular pathways (returned to normal over time), and changes in the morphology of the Purkinje cell dendrites and synaptic organization of afferent mossy fibers [36].

From a molecular point of view, microstructural rearrangements occur under the influence of various signaling protein molecules. One of the key protein factors that play a part in the mechanisms of neuroplasticity is the brain0derived neurotrophic factor (BDNF), different isoforms of which positively and negatively contribute to the maintenance of brain homeostasis. For example, pro-BDNF stimulates apoptosis and negatively affects remodeling of neurons, eliminating an excessive number of maturing or damaged cells and ineffective neural connections, while m-BDNF (m — mature) supports neuro- and gliogenesis, branching of dendrites and development of the dendritic processes. Multidirectional influence of these isoforms allows precise control of dynamic balance, which is necessary to maintain brain homeostasis [37]. In an animal experiment (rats), it was shown that learning boosts expression level of BDNF isoforms, as well as tyrosine kinase receptor B (TrkB), which mainly acts as a BDNF receptor [38].

Regular physical exercises by cosmonauts should also be taken into account. Some data indicate that physical exertion has a positive effect on neuroplasticity, increasing expression of certain proteins; in particular, high-intensity short workouts boost production of BDNF, TrkB, and pCREB [39]. Phosphorylated transcription factor CREB activates transcription of the BDNF gene and acts as a marker of LIM kinase 1 (LIMK1) activity, which blocks actin depolymerization, with subsequent restructuring of dendrite spikes and supported neural plasticity [40]. Other studies have shown that regular exercising enhances neuroplasticity by increasing the expression of insulin-like growth factor 1 (IGF 1), which is important for the development and maintenance of brain functions, as well as BDNF protein and the positively correlated vascular endothelial growth factor (VEGF), which mediates angiogenesis in the brain. Moreover, it was found that smaller BDNF expression has a similar effect on the VEGF, with ultimate slowdown of angiogenesis [41].

The described changes lead to enhanced neuro-, angio- and synaptogenesis and, apparently, cause structural and functional rearrangements in the brain, including growth of the volume of gray matter in the cerebellum, hippocampus, basal ganglia and some parts of the cortex, and changes in the volume of white matter [42].

In addition to molecular effects, it is necessary to note the general physiological effects mediating microstructural changes in the brain. For example, a simulated microgravity experiment (dry immersion) has shown a slowdown of blood flow in 32 cortical and subcortical regions after 5 days [43]. Presumably, this effect may be the result of the narrowing of cerebral arteries caused by displacement of brain fluid: in the early days of a spaceflight, cerebral blood flow increases along with intracranial pressure, which leads to chronic vasoconstriction of the arteries and subsequent hypertrophy. Prolonged vasoconstriction, combined with histological changes, is probably responsible for stronger vascular resistance and weaker total blood flow in the brain [43]. Moreover, there is evidence of plasma volume decreasing in microgravity, which also contributes to a decrease of cerebral blood flow [44]. In addition to the general blood flow decrease, there is a redistribution of blood supply in various parts of the brain. Inter alia, regional blood flow in the basal ganglia was registered decreasing, a phenomenon explained

by intensification of operation of these areas due to their central role in information processing; however, there are assumptions of a potential modification of neurotransmitter metabolism, which is largely unexplored in the context of microgravity [43]. Such changes in the nature of blood supply are presumably closely related to the structural changes in the brain. It has been shown that transformations in the primary sensorimotor cortex, basal ganglia and cerebellum do not entail changes in the proportion of free fluid, which shows the importance of further research efforts designed to fully clarify the exact nature of the effects of spaceflight on brain structures [21]. There are other factors that affect the brain of the cosmonaut, and they need to be taken into account, too. Thus, it was shown that one of the conditions of spaceflight — prolonged isolation — decreases the volume of the hippocampus and brings down the correlated concentration of BDNF [45]. Moreover, a decrease in the volume of the dentate gyrus of the hippocampus was also associated with deteriorating cognitive performance as shown by spatial processing and selective attention tests [45]. In addition, it is known that ISS crew members often complain of headaches, visual and cognitive impairments that correlate with CO_2 levels, and, judging by the existing studies, the redistribution of fluids in microgravity in combination with an increased CO_2 content in the atmosphere affects nervous functions and cognitive performance [46]. In this regard, it should be mentioned that cosmonauts on the ISS have increased expression of hypoxia-induced factor alpha-1 (HIF-1a), which, in turn, pushes up the concentration of VEGF-1, a protein the expression of which correlates with BDNF [47]. All these phenomena indicate wide network interactions of molecular genetic effects resulting from the complex of various factors of spaceflight that are to be investigated.

CONCLUSION

Thus, we can assume that the functional and structural transformations observed in cosmonauts' brains are consequences of molecular, genetic, and other intracellular changes, which, in turn, are caused by living conditions altered by spaceflight. The most influential factor is microgravity, which causes the redistribution of fluid in the body and neuroplastic adaptation of sensorimotor systems to changed conditions. There are, however, other factors of spaceflight that also affect cosmonauts. For example, prolonged isolation translates into weaker expression of BDNF, and hypoxia occurring in stagnant zones of the ISS, where the level of CO_2 is increased, leads to greater concentrations of VEGF-1, which is associated with BDNF. Clearly, other conditions cause their own molecular effects, which are interconnected. There is a complex interaction following the pattern of an extensive network, where each external factor adds its contribution. Determining the specific roles of each of the factors of spaceflight is an extremely labor-intensive task that is yet to be tackled. Solving this task would allow a more accurate and detailed study of the influence of spaceflight factors on the human central nervous system, which is necessary, first of all, to develop preventive measures aimed at minimizing the negative consequences of such flight. Investigation of these issues is of special interest, since it is the improvement of health and efficiency of crew members that largely determines the success and safety of future mission, including flights to deep space, Mars, and asteroids, which are the immediate goals defined in the strategy and concept of the development of the Russian space industry.

References

1. Rabin R, et al. Effects of spaceflight on the musculoskeletal system: NIH and NASA future directions. FASEB journal: official publication of the Federation of American Societies for Experimental Biology. 1993; 7 (5): 396–8.

2. Demertzi A, et al. Cortical reorganization in an astronaut's brain after long-duration spaceflight. Brain Structure and function. 2016; 221: 2873–6.

3. Ryumin OO. Some issues of the psychological support to piloted interplanetary missions. Aviakosmicheskaya i Ekologicheskaya Meditsina. 2017; 51 (4): 15. Russian.

4. Nasrini J, et al. Cognitive performance in long-duration Mars simulations at the Hawaii space exploration analog and simulation (HI-SEAS). NASA Human Research Program Investigators' Workshop. 2017; 1–2.

5. Nelson ES, Mulugeta L, Myers JG. Microgravity-induced fluid shift and ophthalmic changes. Life. 2014; 4 (4): 621–65.

6. Roberts DR, et al. Effects of spaceflight on astronaut brain structure as indicated on MRI. New England Journal of Medicine. 2017; 377 (18): 1746–53.

7. Van Ombergen A, et al. Brain tissue–volume changes in cosmonauts. New England Journal of Medicine. 2018; 379 (17): 1678–80.

8. Van Ombergen A, et al. Brain ventricular volume changes induced by long-duration spaceflight. Proceedings of the National Academy of Sciences. 2019; 116 (21): 10531–6.

9. Lee JK, et al. Spaceflight-associated brain white matter microstructural changes and intracranial fluid redistribution. JAMA neurology. 2019; 76 (4): 412–9.

10. Kramer LA, et al. Intracranial effects of microgravity: a prospective longitudinal MRI study. Radiology. 2020; 295 (3): 640–8.

11. Hupfeld KE, et al. Longitudinal MRI-visible perivascular space (PVS) changes with long-duration spaceflight. Scientific Reports. 2022; 12 (1): 7238.

12. McGregor HR, et al. Impacts of spaceflight experience on human brain structure. Scientific Reports. 2023; 13 (1): 7878.

13. Karpenko MP, Davydov DG, Chmykhova EV. Crew training in the course of long-duration space missions as a way to maintain cosmonauts' socialization and cognitive abilities. Aviakosmicheskaya i Ekologicheskaya Meditsina. 2018; 52 (6): 19–25. Russian.

14. Kanas N, et al. Psychology and culture during long-duration space missions. Springer Berlin Heidelberg. 2013; 153–84.

15. Jamšek M, et al. Effects of simulated microgravity and hypergravity conditions on arm movements in normogravity. Frontiers in Neural Circuits. 2021; 15: 750176.

16. Seidler RD, et al. Future research directions to identify risks and mitigation strategies for neurostructural, ocular, and behavioral changes induced by human spaceflight: A NASA-ESA expert group consensus report. Frontiers in Neural Circuits. 2022; 16: 876789.

17. Kunavar T, et al. Effects of local gravity compensation on motor control during altered environmental gravity. Frontiers in Neural Circuits. 2021; 15: 750267.

18. Tays GD, et al. The effects of long duration spaceflight on sensorimotor control and cognition. Frontiers in neural circuits. 2021; 15: 723504.

19. Strangman GE, Sipes W, Beven G. Human cognitive performance in spaceflight and analogue environments. Aviation, space, and environmental medicine. 2014; 85 (10): 1033–48.

20. Cassady K, et al. Effects of a spaceflight analog environment on brain connectivity and behavior. Neuroimage. 2016; 141: 18–30.

21. Stella AB, et al. Neurophysiological adaptations to spaceflight and simulated microgravity. Clinical Neurophysiology. 2021; 132 (2): 498–504.

22. Koppelmans V, et al. Study protocol to examine the effects of spaceflight and a spaceflight analog on neurocognitive performance: extent, longevity, and neural bases. BMC neurology. 2013; 13: 1–15.

23. Doroshin A, et al. Brain connectometry changes in space travelers after long-duration spaceflight. Frontiers in neural circuits. 2022; 16: 6.

24. Koppelmans V, et al. Brain structural plasticity with spaceflight. npj Microgravity. 2016; 2 (1): 2.

25. Jillings S, et al. Macro-and microstructural changes in cosmonauts' brains after long-duration spaceflight. Science advances. 2020; 6

26. Jillings S, et al. Prolonged microgravity induces reversible and persistent changes on human cerebral connectivity. Communications Biology. 2023; 6 (1): 46.

27. Pechenkova E, et al. Alterations of functional brain connectivity after long-duration spaceflight as revealed by fMRI. Frontiers in Physiology. 2019; 10: 761.

28. Li K, et al. Effect of simulated microgravity on human brain gray matter and white matter–evidence from MRI. PloS one. 2015; 10 (8): e0135835.

29. Salazar AP, et al. Changes in working memory brain activity and task-based connectivity after long-duration spaceflight. Cerebral Cortex. 2023; 33 (6): 2641–54.

30. Van Ombergen A, et al. Intrinsic functional connectivity reduces after first-time exposure to short-term gravitational alterations induced by parabolic flight. Scientific Reports. 2017; 7 (1): 3061.

31. Koppelmans V, et al. Brain plasticity and sensorimotor deterioration as a function of 70 days head down tilt bed rest. PloS one. 2017; 12 (8): e0182236.

32. Miller AD, et al. Human Cortical Activity during Vestibular-and Drug-Induced Nausea Detected Using MSI a. Annals of the New York Academy of Sciences. 1996; 781 (1): 670–2.

33. Mammarella N. The effect of microgravity-like conditions on high-level cognition: a review. Frontiers in Astronomy and Space Sciences. 2020; 7: 6.

34. Garrett-Bakelman FE, et al. The NASA Twins Study: A multidimensional analysis of a year-long human spaceflight. Science. 2019; 364 (6436): eaau8650.

35. Cullen KE. Vestibular processing during natural self-motion: implications for perception and action. Nature Reviews Neuroscience. 2019; 20 (6): 346–63.

36. Carriot J, Mackrous I, Cullen KE. Challenges to the vestibular system in space: how the brain responds and adapts to microgravity. Frontiers in neural circuits. 2021; 15: 760313.

37. Kowiański P, et al. BDNF: a key factor with multipotent impact on brain signaling and synaptic plasticity. Cellular and molecular neurobiology. 2018; 38: 579–93.

38. Silhol M, et al. Spatial memory training modifies the expression of brain-derived neurotrophic factor tyrosine kinase receptors in young and aged rats. Neuroscience. 2007; 146 (3): 962–73.

39. Okamoto M, et al. High-intensity intermittent training enhances spatial memory and hippocampal neurogenesis associated with BDNF signaling in rats. Cerebral Cortex. 2021; 31 (9): 4386–97.

40. Kaminskaya AN, et al. Influence of limk1 Gene Polymorphism on Learning Acquisition and Memory Formation with pCREB Distribution and Aggregate Formationin Neuromuscular Junctions in Drosophila melanogaster. Russian J. Genetics. 2015; 51 (6): 685. Russian.

41. Lin CY, et al. Brain-derived neurotrophic factor increases vascular endothelial growth factor expression and enhances angiogenesis in human chondrosarcoma cells. Biochemical pharmacology. 2014; 91 (4): 522–33.

42. El-Sayes J, et al. Exercise-induced neuroplasticity: a mechanistic model and prospects for promoting plasticity. The Neuroscientist. 2019; 25 (1): 65–85.

43. Guillon L, et al. Reduced Regional Cerebral Blood Flow Measured by 99mTc-Hexamethyl Propylene Amine Oxime Single-Photon Emission Computed Tomography in Microgravity Simulated by 5-Day Dry Immersion. Frontiers in Physiology. 2021; 12: 789298.

44. Ogoh S, et al. Internal carotid, external carotid and vertebral artery blood flow responses to 3 days of head-out dry immersion. Experimental Physiology. 2017; 102 (10): 1278–87.

45. Stahn AC, et al. Brain changes in response to long Antarctic expeditions. New England Journal of Medicine. 2019; 381 (23): 2273-5.

46. Mahadevan AD, et al. Head-down-tilt bed rest with elevated CO2: effects of a pilot spaceflight analog on neural function and performance during a cognitive-motor dual task. Frontiers in Physiology. 2021; 12: 654906.

47. Luxton JJ, et al. Telomere length dynamics and DNA damage responses associated with long-duration spaceflight. Cell Reports. 2020; 33 (10): 108457.

Литература

1. Rabin R, et al. Effects of spaceflight on the musculoskeletal system: NIH and NASA future directions. FASEB journal: official publication of the Federation of American Societies for Experimental Biology. 1993; 7 (5): 396–8.

2. Demertzi A, et al. Cortical reorganization in an astronaut's brain after long-duration spaceflight. Brain Structure and function. 2016; 221: 2873–6.

3. Рюмин О. О. Вопросы психологического обеспечения пилотируемых межпланетных полетов. Авиакосм. и экол. мед. 2017; 51 (4): 15.

4. Nasrini J, et al. Cognitive performance in long-duration Mars simulations at the Hawaii space exploration analog and simulation (HI-SEAS). NASA Human Research Program Investigators' Workshop. 2017; 1–2.

5. Nelson ES, Mulugeta L, Myers JG. Microgravity-induced fluid shift and ophthalmic changes. Life. 2014; 4 (4): 621–65.

6. Roberts DR, et al. Effects of spaceflight on astronaut brain structure as indicated on MRI. New England Journal of Medicine. 2017; 377 (18): 1746–53.

7. Van Ombergen A, et al. Brain tissue–volume changes in cosmonauts. New England Journal of Medicine. 2018; 379 (17): 1678–80.

8. Van Ombergen A, et al. Brain ventricular volume changes induced by long-duration spaceflight. Proceedings of the National Academy of Sciences. 2019; 116 (21): 10531–6.

9. Lee JK, et al. Spaceflight-associated brain white matter microstructural changes and intracranial fluid redistribution. JAMA neurology. 2019; 76 (4): 412–9.

10. Kramer LA, et al. Intracranial effects of microgravity: a prospective longitudinal MRI study. Radiology. 2020; 295 (3): 640–8.

11. Hupfeld KE, et al. Longitudinal MRI-visible perivascular space (PVS) changes with long-duration spaceflight. Scientific Reports. 2022; 12 (1): 7238.

12. McGregor HR, et al. Impacts of spaceflight experience on human brain structure. Scientific Reports. 2023; 13 (1): 7878.

13. Карпенко М. П., Давыдов Д. Г., Чмыхова Е. В. Обучение экипажей в ходе длительных космических полетов как средство поддержания социализации и когнитивных способностей космонавтов. Авиакосмическая и экологическая медицина. 2018; 52 (6): 19–25.

14. Kanas N, et al. Psychology and culture during long-duration space missions. Springer Berlin Heidelberg. 2013; 153–84.

15. Jamšek M, et al. Effects of simulated microgravity and hypergravity conditions on arm movements in normogravity. Frontiers in Neural Circuits. 2021; 15: 750176.

16. Seidler RD, et al. Future research directions to identify risks and mitigation strategies for neurostructural, ocular, and behavioral changes induced by human spaceflight: A NASA-ESA expert group consensus report. Frontiers in Neural Circuits. 2022; 16: 876789.

17. Kunavar T, et al. Effects of local gravity compensation on motor control during altered environmental gravity. Frontiers in Neural Circuits. 2021; 15: 750267.

18. Tays GD, et al. The effects of long duration spaceflight on sensorimotor control and cognition. Frontiers in neural circuits. 2021; 15: 723504.

19. Strangman GE, Sipes W, Beven G. Human cognitive performance in spaceflight and analogue environments. Aviation, space, and environmental medicine. 2014; 85 (10): 1033–48.

20. Cassady K, et al. Effects of a spaceflight analog environment on brain connectivity and behavior. Neuroimage. 2016; 141: 18–30.

21. Stella AB, et al. Neurophysiological adaptations to spaceflight and simulated microgravity. Clinical Neurophysiology. 2021; 132 (2): 498–504.

22. Koppelmans V, et al. Study protocol to examine the effects of spaceflight and a spaceflight analog on neurocognitive performance: extent, longevity, and neural bases. BMC neurology. 2013; 13: 1–15.

23. Doroshin A, et al. Brain connectometry changes in space travelers after long-duration spaceflight. Frontiers in neural circuits. 2022; 16: 6.

24. Koppelmans V, et al. Brain structural plasticity with spaceflight. npj Microgravity. 2016; 2 (1): 2.

25. Jillings S, et al. Macro-and microstructural changes in cosmonauts' brains after long-duration spaceflight. Science advances. 2020; 6 (36): eaaz9488.

26. Jillings S, et al. Prolonged microgravity induces reversible and persistent changes on human cerebral connectivity. Communications Biology. 2023; 6 (1): 46.

27. Pechenkova E, et al. Alterations of functional brain connectivity after long-duration spaceflight as revealed by fMRI. Frontiers in Physiology. 2019; 10: 761.

28. Li K, et al. Effect of simulated microgravity on human brain gray matter and white matter–evidence from MRI. PloS one. 2015; 10 (8): e0135835.

29. Salazar AP, et al. Changes in working memory brain activity and task-based connectivity after long-duration spaceflight. Cerebral Cortex. 2023; 33 (6): 2641–54.

30. Van Ombergen A, et al. Intrinsic functional connectivity reduces after first-time exposure to short-term gravitational alterations induced by parabolic flight. Scientific Reports. 2017; 7 (1): 3061.

31. Koppelmans V, et al. Brain plasticity and sensorimotor deterioration as a function of 70 days head down tilt bed rest. PloS one. 2017; 12 (8): e0182236.

32. Miller AD, et al. Human Cortical Activity during Vestibular-and Drug-Induced Nausea Detected Using MSI a. Annals of the New York Academy of Sciences. 1996; 781 (1): 670–2.

33. Mammarella N. The effect of microgravity-like conditions on high-level cognition: a review. Frontiers in Astronomy and Space Sciences. 2020; 7: 6.

34. Garrett-Bakelman FE, et al. The NASA Twins Study: A multidimensional analysis of a year-long human spaceflight. Science. 2019; 364 (6436): eaau8650.

35. Cullen KE. Vestibular processing during natural self-motion: implications for perception and action. Nature Reviews Neuroscience. 2019; 20 (6): 346–63.

36. Carriot J, Mackrous I, Cullen KE. Challenges to the vestibular system in space: how the brain responds and adapts to microgravity. Frontiers in neural circuits. 2021; 15: 760313.

37. Kowiański P, et al. BDNF: a key factor with multipotent impact on brain signaling and synaptic plasticity. Cellular and molecular neurobiology. 2018; 38: 579–93.

38. Silhol M, et al. Spatial memory training modifies the expression of brain-derived neurotrophic factor tyrosine kinase receptors in young and aged rats. Neuroscience. 2007; 146 (3): 962–73.

39. Okamoto M, et al. High-intensity intermittent training enhances spatial memory and hippocampal neurogenesis associated with BDNF signaling in rats. Cerebral Cortex. 2021; 31 (9): 4386–97.

40. Каминская А. Н. и др. Обучение и формирование памяти в сопоставлении с распределением pCREB и белковых агрегатов в нейромышечных контактах у Drosophila melanogaster при полиморфизме limk1. Генетика. 2015; 51 (6): 685.

41. Lin CY, et al. Brain-derived neurotrophic factor increases vascular endothelial growth factor expression and enhances angiogenesis in human chondrosarcoma cells. Biochemical pharmacology. 2014; 91 (4): 522–33.

42. El-Sayes J, et al. Exercise-induced neuroplasticity: a mechanistic model and prospects for promoting plasticity. The Neuroscientist. 2019; 25 (1): 65–85.

43. Guillon L, et al. Reduced Regional Cerebral Blood Flow Measured by 99mTc-Hexamethyl Propylene Amine Oxime Single-Photon Emission Computed Tomography in Microgravity Simulated by 5-Day Dry Immersion. Frontiers in Physiology. 2021; 12: 789298.

44. Ogoh S, et al. Internal carotid, external carotid and vertebral artery blood flow responses to 3 days of head-out dry immersion. Experimental Physiology. 2017; 102 (10): 1278–87.

45. Stahn AC, et al. Brain changes in response to long Antarctic expeditions. New England Journal of Medicine. 2019; 381 (23): 2273-5.

46. Mahadevan AD, et al. Head-down-tilt bed rest with elevated CO_2: effects of a pilot spaceflight analog on neural function and performance during a cognitive-motor dual task. Frontiers in Physiology. 2021; 12: 654906.

47. Luxton JJ, et al. Telomere length dynamics and DNA damage responses associated with long-duration spaceflight. Cell Reports. 2020; 33 (10): 108457.

EFFECT OF SODIUM BICARBONATE OR HYDROCHLORIC ACID INTRAGASTRIC ADMINISTRATION ON GUT-DERIVED ENDOTOXEMIA IN RATS RECEIVING CYCLOPHOSPHAMIDE MYELOABLATIVE CONDITIONING

Vakunenkova OA[1], Zolotoverkhaya EA[1], Pechurina TB[2] ✉, Schäfer TV[2], Ivnitsky JuJu[1]

[1] Golikov Research Clinical Center of Toxicology of the Federal Medical Biological Agency, Saint-Petersburg, Russia

[2] State Research and Testing Institute of Military Medicine of the Ministry of Defense of the Russian Federation, Saint-Petersburg, Russia

Toxic effects of the myeloablative cyclophosphamide (CP) doses include damage to the gastrointestinal tract. This is manifested by gastrointestinal stasis, cytostatic drug-induced damage to the small intestinal mucosa, and acute gut-derived endotoxemia. The study was aimed to identify causal relationships between gastrointestinal stasis, enterocytopenia, and acute gut-derived endotoxemia in the rat model of the CP myeloablative conditioning. We assessed the effects of the intragastrically administered 0.48 M sodium bicarbonate (NaHCO$_3$) solution or the 0.1 M hydrochloric acid (HCl) solution on the indicators of gastrointestinal stasis, enterocytopenia, portal blood levels of endotoxin, ammonia, urea, and urinary indican excretion. The stomach overfilled with chyme, decreased alkaline phosphatase and cholinesterase activity in the small intestinal tissues, 4.4-fold increased endotoxin levels, 4.6-fold increased urea levels, twofold increased portal blood plasma creatinine levels, and twofold increased urinary indican excretion were observed three days after intravenous administration of CP in a dose of 390 mg/kg. Intragastric administration of NaHCO$_3$ or HCl partially prevented gastric stasis, but not acute gut-derived endotoxemia. Administration of NaHCO$_3$, not HCl, prevented enterocytopenia in the duodenum. Acute gut-derived endotoxemia resulted mainly from the more intense release of the cecal microflora waste products into blood. Testing the use of sodium bicarbonate intragastric administration combined with the enteral detoxification and/or options for suppression of colonic microflora vegetation for prevention of the myeloablative cytostatic therapy complications is promising.

Keywords: gastric stasis, sodium bicarbonate, myeloablation, hydrochloric acid, cyclophosphamide, endotoxemia, enterocytopenia

ВЛИЯНИЕ ВНУТРИЖЕЛУДОЧНОГО ВВЕДЕНИЯ ГИДРОКАРБОНАТА НАТРИЯ ИЛИ СОЛЯНОЙ КИСЛОТЫ НА КИШЕЧНУЮ ЭНДОТОКСЕМИЮ У КРЫС ПРИ МИЕЛОАБЛЯЦИИ ЦИКЛОФОСФАМИДОМ

О. А. Вакуненкова[1], Е. А. Золотоверхая[1], Т. Б. Печурина[2] ✉, Т. В. Шефер[2], Ю. Ю. Ивницкий[1]

[1] Научно-клинический центр токсикологии имени С. Н. Голикова Федерального медико-биологического агентства, Санкт-Петербург, Россия

[2] Государственный научно-исследовательский испытательный институт военной медицины Министерства обороны Российской Федерации, Санкт-Петербург, Россия

К токсическим эффектам циклофосфамида (ЦФ) в миелоабляционных дозах относится повреждение желудочно-кишечного тракта. Оно проявляется желудочно-кишечным стазом, цитостатическим повреждением слизистой оболочки тонкой кишки и острой кишечной эндотоксемией. Целью работы было выявить причинно-следственные связи между желудочно-кишечным стазом, энтероцитопенией и острой кишечной эндотоксемией при моделировании на крысах миелоабляционной терапии ЦФ. Изучали влияние вводимого в желудок 0,48 М раствора гидрокарбоната натрия (NaHCO$_3$) или 0,1 М раствора соляной кислоты (HCl) на показатели желудочно-кишечного стаза, энтероцитопении, содержание в портальной крови эндотоксина, аммиака, мочевины и экскрецию индикана с мочой. Через трое суток после внутривенного введения ЦФ в дозе 390 мг/кг наблюдали переполнение химусом желудка, снижение активности щелочной фосфатазы и холинэстеразы в тканях тонкой кишки, повышение содержания эндотоксина в 4,0 раза и мочевины в 4,6 раза при двукратном повышении уровня креатинина в плазме портальной крови, двукратное повышение экскреции индикана с мочой. Введение в желудок NaHCO$_3$ или HCl частично предупреждало гастростаз, но не острую кишечную эндотоксемию. Введение NaHCO$_3$, но не HCl, предупреждало энтероцитопению в двенадцатиперстной кишке. Острая кишечная эндотоксемия была обусловлена преимущественно интенсификацией поступления в кровь продуктов жизнедеятельности микрофлоры слепой кишки. Перспективна апробация внутрижелудочного введения гидрокарбоната натрия в сочетании с энтеральной детоксикацией и (или) применением средств подавления вегетации толстокишечной микрофлоры для профилактики желудочно-кишечных осложнений миелоабляционной цитостатической терапии.

Ключевые слова: гастростаз, гидрокарбонат натрия, миелоабляция, соляная кислота, циклофосфамид, эндотоксемия, энтероцитопения

In supralethal doses, cyclophosphamide (CP) is used for myeloablation with the aim of preparing recipients to hematopoietic stem cell transplantation. Side effects of such treatment include inhibition of gastrointestinal motility, cytostatic damage to the small intestine's epithelium, and endotoxemia. These complications disrupt enteral nutrition, reduce the effectiveness of orally administered drugs, and increase the likelihood of death of patients before transplantation. Gastrostasis and acute small intestinal mucositis, prevented by introduction of sodium bicarbonate solution (NaHCO3) into the stomach, were observed in rats after administration of a myeloablation dose of CP [1]. The currently unclear matters are the nature of the relationship between gastrointestinal stasis, enterocytopenia, and endotoxemia, and how $NaHCO_3$ or hydrochloric acid (agents that change the pH of gastric chyme) affect them. This study aimed to identify the relationship between gastrointestinal stasis, damage to the mucous membrane of the small intestine, and acute intestinal endotoxemia in the context of modeling myeloablation cytostatic therapy in rats.

METHODS

We used male albino Wistar rats weighing 161–190 g (branch of the Kurchatov Institute – PNPI – Rappolovo Laboratory Animal Nursery; Russia). The animals received standard rat feed and drinking water *ad libitum*. We randomized the animals into four groups: 1) intact animals; 2) those who received CP only; 3) those who received CP and NaHCO3; 4) rats that received CP and HCl. Twenty-four hours after administration of CP, rats were placed in cages with a lattice floor that prevented coprophagia and eating of litter, with access only to water. Myeloablation was triggered by a single injection (into the tail's lateral vein) of a freshly prepared aqueous solution of Endoxan, a CP drug (Baxter Oncology GMBH; Germany). The dose was 390 mg /kg ($\approx$ 1.7 $LD_{99/30\ days}$), the volume — 10 ml/kg. This dose of CP was 1.7 $LD_{99/30\ days}$, which allowed the rats to survive for at least 3 days after administration. Twice, 30 minutes before and immediately after administration of CP, the animals received intragastric injections of 0.48 M $NaHCO_3$ solution (pH = 8.34) in a volume of 15 ml/kg, or 0.1 M HCl solution (pH = 1) in the same volume. The animals were examined 72 hours after administration of CP.

The rats were put under halothane anesthesia for blood sampling from *v. portae* and organ extraction. To gage the gastrointestinal tract's (GIT) propulsive function, we measured the relative mass of gastric and intestinal chyme, which was calculated as the difference (in grams) between the mass of a chyme-filled and an empty organ (*gaster*, *caecum*), related to body weight (in kilograms). In parallel, we measured the relative mass of the spleen in order to assess the selectivity of action of $NaHCO_3$ or HCl.

To assess the severity of enterocytopenia in the small intestine's tissues, we assessed the activity of enterocyte markers: alkaline phosphatase, alkaline phosphatase (AP) [2], and cholinesterase (CE) [3]. Cranial segments of duodenum, caudal segments of jejunum and ilum (length — 4 cm each) were homogenized in a 15-fold volume of tris-HCl buffer (50 mM, pH = 7.4) and frozen at –20 °C. After 15 hours, the homogenates were thawed at 4 °C and centrifuged at 2000 g for 10 minutes. In the supernatant, we established the activity of AP with the help of the kinetic optimized method and using a set of reagents (Olvex Diagnosticum; Russia), and assessed the activity of CE using Ellman's assay, substrate of acetylthiocholine iodide (Sigma-Aldrich; USA), and ChemWell 2910 biochemical analyzer (Awareness Tech.; USA). Another determined parameter

was protein content, which we quantified using the Bradford method.

The assessment of intestinal endotoxemia was based on the content of endotoxin and ammonia in portal blood plasma, and urea, which is the product of neutralization of ammonia by the liver. Endotoxin was detected with a LAL reagent in the gel-thrombus test modification, the process enabled by the ALPYR Test reagent kit (Algimed Techno LLC; Russia). To increase sensitivity, we incubated the samples at 70 °C for 15 minutes before diluting them and mixing with the LAL reagent, thus unbinding the endotoxin from albumin [4]. Ammonia concentration was determined spectrophotometrically using the Ammonium Ultra reagent kit (Sentinel Diagnostics; Italy). Concentration of urea was established after its hydrolysis to ammonia, with the help of the Urea UV reagent kit (Biosystems; Spain). Concurrently, we measured blood plasma concentrations of creatinine (reaction with picric acid), albumin (reaction with bromocresol green), and total protein (reaction with acid blue 90).

Urinary excretion of indican was used as an indicator of excessive bacterial growth [5]; for this purpose, we collected urine while the animals were in metabolic chambers from 48th to 72nd hour after administration of CP. Indican was quantified with Obermayer reagent [6], and excretion was expressed in micrograms per kilogram of body weight per hour.

The results were given as a mean and an error of mean ($M \pm m$). We applied ANOVA to assess the effect of the administered substances on the studied quantitative indicators. When the models reached significance, the means between groups were compared through Tukey's honest significant difference test [7]. The differences were considered significant at $p = 0.05$.

RESULTS

After two days of fasting, chyme was concentrated only in gaster and caecum. Animals that received CP had the relative mass of gastric chyme 10.5 times greater than intact animals, while the mass index of the caecal chyme did not differ significantly between the groups. Both $NaHCO_3$ and HCl partially prevented the overfilling of stomach with chyme, but did not change the volume of content of caecum (Fig. 1).

Administration of CP led to enterocytopenia. The activity of AP decreased 1.6–4.9 times in all parts of the small intestine, most significantly in the ileum; the activity of ACE was reduced only in the ileum. $NaHCO_3$ partially prevented the decrease of activity of AP in duodenum (Fig. 2). Neither $NaHCO_3$ nor HCl influenced the systemic cytopenic effect of CP, which made the spleen's relative weight 57% smaller (Fig. 1).

In intact rats, the portal blood plasma ammonia content was 0.88 mM, three times higher in plasma after decapitation [8]. Administration of CP did not change the blood ammonia level significantly, but content of urea has grown 4.6 times. $NaHCO_3$, administered by gavage, made the level of urea increase further, and HCl halved it, but the said level still remained higher than in the control group. After administration of CP, the portal blood endotoxin content was 4 times higher than in intact animals, with $NaHCO_3$ or HCl having little effect on this parameter. The concentration of creatinine in blood of rats that received CP was twice as high as in intact animals, and remained largely the same after administration of $NaHCO_3$ or HCl. There were no significant intergroup differences in the content of total protein or albumin in blood plasma (Figure 3). Administration of CP intensified urinary excretion of indican two-fold, with HCl unable to change the respective dynamics.
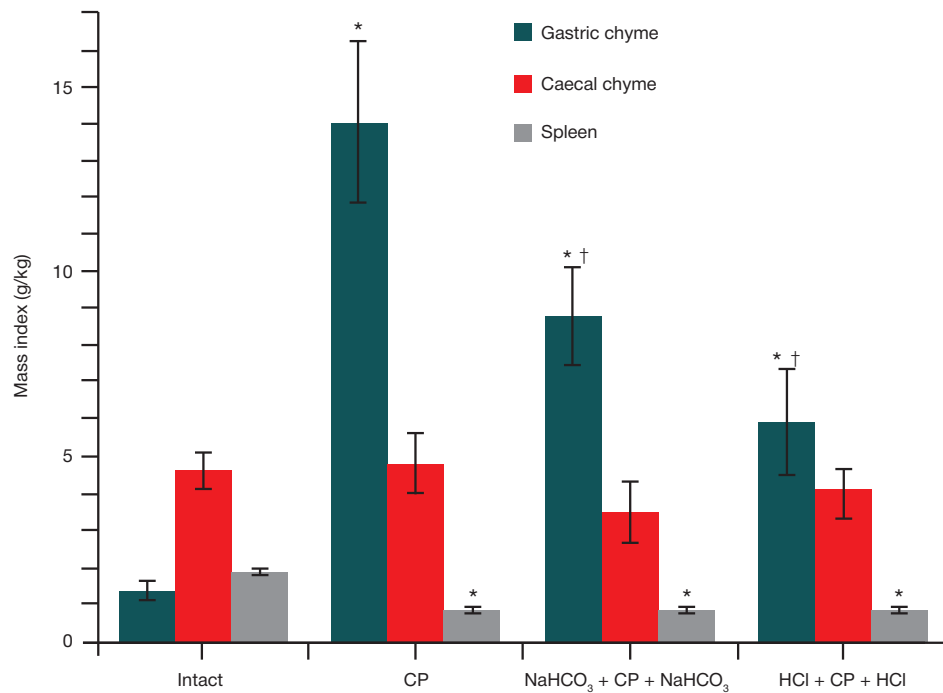
Fig. 1. Mass indexes of gastric, caecal chyme, and spleen in rats 72 hours after intravenous administration of cyclophosphamide (M ± *m*; *n* = 8). Intact — rats that received no medicines; CP — rats that received only cyclophosphamide; NaHCO$_3$ + CP + NaHCO$_3$ — intragastric administration of 0.48 M of sodium bicarbonate 30 minutes before and immediately after cyclophosphamide; HCl + CP + HCl — intragastric administration of 0.1 M of hydrochloric acid 30 minutes before and immediately after cyclophosphamide. Significant difference, *p* < 0.05: * — with intact group; † — with the CP group

Intragastric injection of NaHCO$_3$ induced hyperindicanuria as a trend (Fig. 4).

DISCUSSION

After the animals are deprived of food, the mass of their gastric contents is determined by the propulsive function of the stomach. Therefore, the overfilling of stomach with chyme after administration of CP, which we registered in this and the previous study [1], reflected the development of gastrostasis. If the change in gastrointestinal motility were limited to gastrostasis, then the flow of chyme into the cecum would have happened after its emptying, and the relative mass of chyme therein would have been decreasing. However, against the background of administration of CP, the mass of the caecal chyme did not change significantly (Fig. 1). This means that CP inhibited the propulsive function not only in the stomach, but also in the colon.

It can be assumed that gastrostasis was a protective response aimed at preventing chyme from injuring the small intestine, the part of the gastrointestinal tract most sensitive to CP. The damage thereto manifested as enterocytopenia, as indicated by the decreasing content of enterocyte markers in the small intestine's tissues (Fig. 2). Another consequence of gastrostasis could be restricted delivery of substrates to bacteria vegetating in the lumen of the colon. In its chyme, the specific content of bacteria is eight orders of magnitude higher than in the chyme of the stomach [9], which makes colonic microflora the source of endotoxemia. Given the division frequency of 3 h^{-1} (the mean for *Escherichia coli* at 37 °C), it is theoretically possible that the amount of bacteria increases eightfold within an hour after colon loses the propulsive function. Substrate limitations stemming from gastrostasis could restrain such a rapid growth of colonic microflora, as well as production of ammonia thereby. However, gastrointestinal
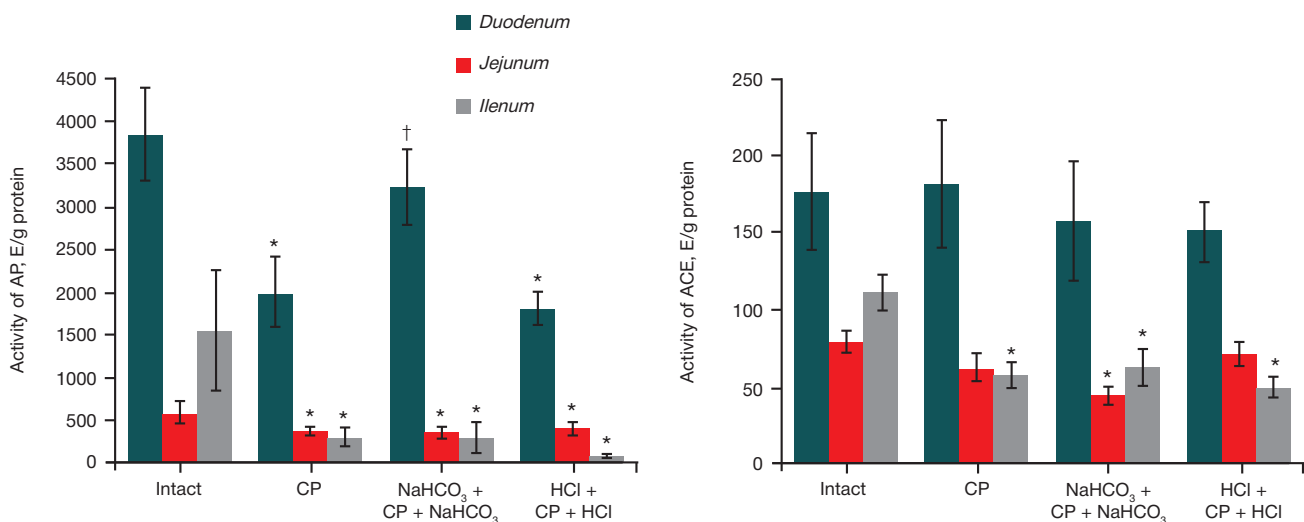
Fig. 2. Activity of alkaline phosphatase (left) and cholinesterase (right) in rats' small intestine tissues 72 hours after administration of cyclophosphamide (M ± *m*; *n* = 8). Significant difference, *p* < 0.05: * — with intact group; † — with the CP group
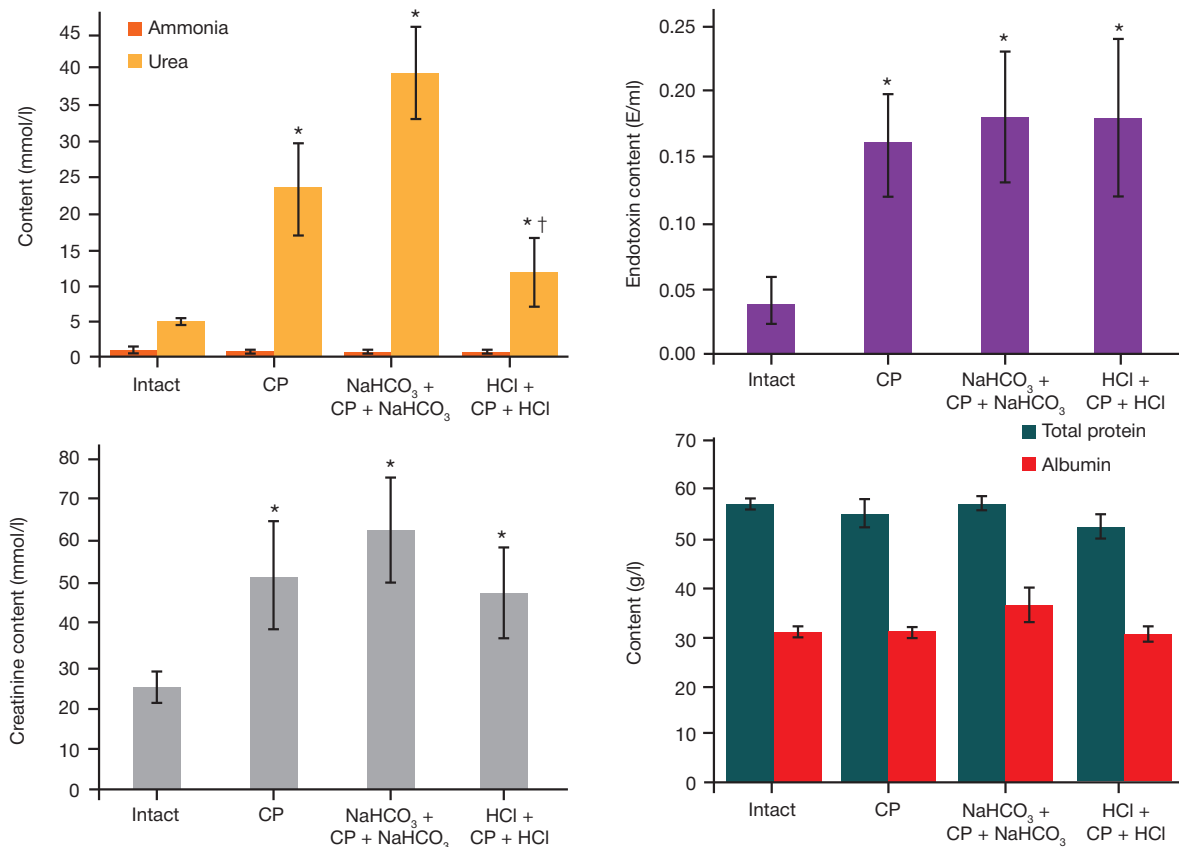
Fig. 3. Content of ammonia, urea, endotoxin, creatinine, albumin, and total protein in blood plasma sampled from rats' portal veins 72 hours after administration of cyclophosphamide (M ± m; n = 8). Significant difference, $p < 0.05$: * — with intact group; † — with the CP group

stasis could not suppress ammonia-producing wall microflora, the substrates for which are substances diffusing to the luminal surface of the gastrointestinal mucosa from the blood. Colon stasis, which prevented discharge of the ammonia-producing microflora from the body, could have promoted production of ammonia in the caecum. Ammonia produced by the intestinal microflora becomes part of urea in the liver. Its content in the blood of animals that received CP increased fourfold three days after administration (Fig. 3), which means that production of ammonia in the intestine was intensified earlier. This hypothesis is supported by an almost twofold spike of the level of blood ammonia 3 hours after administration of myeloablation dose of CP [8]. Partially, uremia could also have been associated with a delay in the excretion of urea from the body, as backed by a twofold increase of the blood level of creatinine, a marker of renal insufficiency. Therefore, the increase in blood urea levels registered in this study 3 days after administration of CP was a marker of acute intestinal endotoxemia of a mixed type, productive and retention.

In the animals that received CP, gram-negative bacteria, which are the source of endotoxin, could be concentrated in the stomach and caecum, since other parts of the gastrointestinal tract were free of chyme. The content of endotoxin in the colonic chyme is close to 2.5 g/l [10], and its release from bacteria could have been intensified by their death due to substrate limitations imposed by gastrostasis. Colonic stasis increased the duration of endotoxin contact with the sorbing surface of the mucous membrane, therefore portal endotoxinemia after administration of CP (Fig. 3) could have been both productive and redistributive. The lack of effect of CP on the blood plasma protein level indicates that the content of endotoxin in biologically active free form increased in proportion to its total plasma content.

Indican is the end product of metabolism of indole, the only source of which in the experimental conditions was a reaction catalyzed by tryptophanase of the intestinal microflora. Hyperindicanuria is a valid indicator of excessive growth of indole-producing bacteria in the gastrointestinal tract [5]. Urinary excretion of indican intensified (Fig. 4) despite the impairments of the renal excretory function, which were confirmed by the increased blood level of creatinine (Figure 3). In the CP group, this indicates the predominance of productive and (or) redistributive component of intestinal endotoxemia over the retention component.

Both NaHCO₃ and HCl partially prevented gastric overfilling in rats (Fig. 1), and only NaHCO₃ could stop enterocytopenia to a certain degree. The alkalizing effect of NaHCO₃ was predominantly local, since it prevented enterocytopenia only in the duodenum, but not in the caudal parts of the small intestine and not in the spleen (Fig. 2). This supports the hypothesis [1] that has lower cytostatic damage to the mucous membrane's epithelium a probable mechanism of prevention of gastrostasis (induced by CP) by NaHCO₃. Administration of HCl partially prevented gastric overfilling, which could have been the result of the boost it gave to pepsin [11], and accelerated digestion of feed consumed by the animals in the next 24 hours. This explanation is supported by data on the depressing effect of CP on gastric secretion [12].

The severity of intestinal endotoxemia depends on the intensity of release of toxicants by the intestinal microflora, permeability of the enterohematic barrier, and the rate of their excretion from the body. Rats that received CP had the cytostatic damage most pronounced in the small intestine [13], while the intestinal microflora was concentrated in the stomach and caecum, where mucosal epithelium is more resistant to cytostatics. Therefore, cytostatic damage to the small intestine
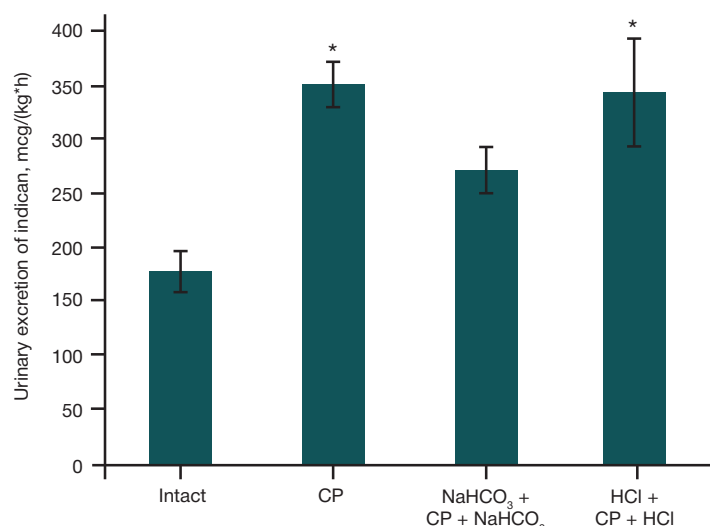
Fig. 4. Urinary excretion of indican, 48th to 72nd hours after administration of cyclophosphamide (M ± m; n = 8). * — significant difference with the intact group, p < 0.05

could not directly affect the appearance of intestinal toxicants in blood. This is further evidenced by the lack of a significant effect of $NaHCO_3$, which reduced the severity of enterocytopenia, on the portal blood level of endotoxin (Fig. 3) and severity of indicanuria (Fig. 4) in rats that received CP. The difference in the effect of $NaHCO_3$ and HCl on the portal blood level urea, product of neutralization of ammonia (Fig. 2), could have been conditioned by ammonia becoming NH_3 in the alkaline medium, a free form that easily diffuses through biomembranes [14], while in the acidic medium ammonia was in its ionized form $NH4^+$, which can hardly penetrate enterohematic barrier.

Thus, in a rat model of myeloablative cytostatic therapy, prevention of gastrostasis or cytostatic damage to the small intestine — complications of the said therapy — does not suppress acute intestinal endotoxemia. It is feasible to consider intragastric administration of $NaHCO_3$ in combination with agents suppressing vegetation of the colonic microflora when developing measures to prevent complications of myeloablation cytostatic therapy. These measures can be supplemented by enteric detoxification (enterosorption, intestinal lavage) aimed at removing endogenous toxicants from the sites of their secretion [15].

CONCLUSIONS

Intravenous administration of a myeloablation dose of cyclophosphamide to rats causes gastrointestinal stasis, cytostatic damage to the mucous membrane of the small intestine, and development of a mixed-type acute gut-derived endotoxemia. The latter, in a rat model of myeloablative cytostatic therapy, was predominantly caused by penetration into blood of waste products of the caecum microflora. Intragastric administration of weak solutions of sodium bicarbonate or hydrochloric acid helps prevent gastrostasis triggered in rats by the myeloablative effect of cyclophosphamide, but these solutions do not stop acute intestinal endotoxemia. Intragastric administration of weak solutions of sodium bicarbonate prevents enterocytopenia triggered in rats by the myeloablative effect of cyclophosphamide, but it cannot halt the development of acute intestinal endotoxemia. For the measures designed to counter gastrointestinal toxicity of cyclophosphamide in the context of myeloablative cytostatic therapy, it is feasible to consider administration of sodium bicarbonate in combination with agents for enteric detoxification and suppression of vegetation of the colonic microflora.

References

1. Vakunenkova OA, Ivnitsky JJ, Gaykova ON, Kozlov AA, Schäfer TV. Effect of sodium bicarbonate on the development of gastric stasis in the rat model of myeloablative chemotherapy with cyclophosphamide. Extreme Medicine. 2023; (2): 91–7.
2. Lallès J-P. Recent advances in intestinal alkaline phosphatase, inflammation, and nutrition. Nutrit Rev. 2019; 77 (10): 710–24.
3. Sine JP. Acetylcholinesterase and butyrylcholinesterase in the gut mucosal cells of various mammal species: distribution along the intestine and molecular forms. Compar Biochem Physiol. C Comp Pharmacol Toxicol. 1988; 91 (2): 597–602.
4. Dawson ME. A wealth of options. Choosing an LAL test method. Associates of Cape Cod, Inc., Woods Hole, Massachusetts. LAL Update. 1995; 13 (3): 1–6.
5. Martynov VL, Semenov AG, Tulupov AA, Chesnokov AA, Kurilov VA, Kazarina NV. Urine indican and hydrogen breath test as methods of screening diagnosis of bacterial overgrowth syndrome in the small intestine. Med. Almanakh. 2017; 2 (47): 117–21. Russian.
6. Balakhovskiy SD, Balakhovskiy IS. Methods of chemical blood analysis. 3-rd ed. Moscow.: Medgiz, 1953; 746 p. Russian.
7. Zar JH. Biostatistical Analysis. 5th ed. Prentice-Hall/Pearson: Upper Saddle River, 2010; 944 p.
8. Ivnitsky JuJu, Schäfer TV, Tyaptin AA, Rejniuk VL. Changes in the chemical composition of the blood and brain of rats under the conditions of modeling the myeloablation regimen of cyclophosphamide administration. Toxicologicheskiy vestnik. 2019; 156 (3): 13–8. Russian.
9. Sender R, Fuchs S. Revised estimates for the number of human and bacteria cells in the body. PLoS Biol. 2016; 14 (8): e1002533.
10. Bested AC, Logan AC, Selhub EM. Intestinal microbiota, probiotics and mental health: from Metchnikoff to modern advances: Part II – contemporary contextual research. Gut Pathog. 2013; 5 (1): 3.
11. Heda R, Toro F, Tombazzi CR. Physiology, pepsin. In: StatPearls. StatPearls Publishing: 2024. Available from: https://www.ncbi.nlm.nih.gov/books/NBK537005/.
12. Visnovsky P. The effect of cyclophosphamide and methotrexate on gastric emptying and secretion in rats. Bratisl Lek Listy. 1992; 93 (2): 90–2.
13. Dahlgren D, Sjöblom M, Hellström P, Lennernäs H. Chemotherapeutics-induced intestinal mucositis: pathophysiology

and potential treatment strategies. Front Pharmacol. 2021; 12 (Art. 681417): 1–12.

14. Ott P, Vilstrup H. Cerebral effects of ammonia in liver disease: current hypotheses. Metab Brain Dis. 2014; 29 (4): 901–11.

15. Khubutiya MSh, Kabanova SA, Goldfarb YuS, Matkevich VA, Bogopolskiy PM, Badalyan AV. Prognosis of the development of clinical toxicology in Russia. Zhurnal im. N.V. Sklifosovskogo «Neotlozhnaya meditsinskaya pomoshch». 2016; (3): 26–31. Russian.

Литература

1. Вакуненкова О. А., Ивницкий Ю. Ю., Гайкова О. Н., Козлов А. А., Шефер Т. В. Влияние гидрокарбоната натрия на формирование гастростаза у крыс при моделировании миелоабляционной химиотерапии циклофосфаном. Медицина экстремальных ситуаций. 2023; (2): 98–104.

2. Lallès J-P. Recent advances in intestinal alkaline phosphatase, inflammation, and nutrition. Nutrit Rev. 2019; 77 (10): 710–24.

3. Sine JP. Acetylcholinesterase and butyrylcholinesterase in the gut mucosal cells of various mammal species: distribution along the intestine and molecular forms. Compar Biochem Physiol. C Comp Pharmacol Toxicol. 1988; 91 (2): 597–602.

4. Dawson ME. A wealth of options. Choosing an LAL test method. Associates of Cape Cod, Inc., Woods Hole, Massachusetts. LAL Update. 1995; 13 (3): 1–6.

5. Мартынов В. Л., Семенов А. Г., Тулупов А. А., Чесноков А. А., Курилов В. А., Казарина Н. В. Индикан мочи и водородный дыхательный тест как методы скрининг-диагностики синдрома избыточного бактериального роста в тонкой кишке. Мед. Альманах. 2017; 2 (47): 117–21.

6. Балаховский С. Д., Балаховский И. С. Методы химического анализа крови. 3-е изд. М.: Медгиз, 1953; 746 с.

7. Zar JH. Biostatistical Analysis. 5th ed. Prentice-Hall/Pearson: Upper Saddle River, 2010; 944 р.

8. Ивницкий Ю. Ю., Шефер Т. В., Тяптин А. А., Рейнюк В. Л. Изменения химического состава крови и головного мозга крыс при моделировании миелоабляционного режима применения циклофосфана. Токсикол. вестник. 2019; 156 (3): 13–18.

9. Sender R, Fuchs S. Revised estimates for the number of human and bacteria cells in the body. PLoS Biol. 2016; 14 (8): e1002533.

10. Bested AC, Logan AC, Selhub EM. Intestinal microbiota, probiotics and mental health: from Metchnikoff to modern advances: Part II – contemporary contextual research. Gut Pathog. 2013; 5 (1): 3.

11. Heda R, Toro F, Tombazzi CR. Physiology, pepsin. In: StatPearls. StatPearls Publishing: 2024. Available from: https://www.ncbi.nlm.nih.gov/books/NBK537005/.

12. Visnovsky P. The effect of cyclophosphamide and methotrexate on gastric emptying and secretion in rats. Bratisl Lek Listy. 1992; 93 (2): 90–2.

13. Dahlgren D, Sjöblom M, Hellström P, Lennemäs H. Chemotherapeutics-induced intestinal mucositis: pathophysiology and potential treatment strategies. Front Pharmacol. 2021; 12 (Art. 681417): 1–12.

14. Ott P, Vilstrup H. Cerebral effects of ammonia in liver disease: current hypotheses. Metab Brain Dis. 2014; 29 (4): 901–11.

15. Хубутия М. Ш., Кабанова С. А., Гольдфарб Ю. С., Маткевич В. А., Богопольский П. М., Бадалян А. В.. Прогноз развития клинической токсикологии в России. Журнал им. Н. В. Склифосовского «Неотложная медицинская помощь». 2016; (3): 26–31.

COMPARATIVE ASSESSMENT OF TOXIC PULMONARY EDEMA CAUSED BY POISONING WITH CARBONYL CHLORIDE AND FLUOROPLASTIC THERMAL DEGRADATION PRODUCTS

Yaroshenko DM[1]✉, Lopat'ko VS[1], Tolkach PG[1], Vengerovich NG[2], Basharin VA[1]

[1] Kirov Military Medical Academy of the Ministry of Defense of the Russian Federation, Saint-Petersburg, Russia

[2] State Research and Testing Institute of Military Medicine of the Ministry of Defense of the Russian Federation, Saint-Petersburg, Russia

Poisoning with acylating pulmonary toxicants results in toxic pulmonary edema (TPE), the approaches to treatment of which are limited. The lung injury similar to poisoning with acylating pulmonary toxicants can be simulation through body's exposure to the fluoroplastic thermal degradation products containing perfluoroisobutylene. The study was aimed to compare toxic pulmonary edema manifestations in the laboratory animals poisoned with an acylating pulmonary toxicant (carbonyl chloride) and fluoroplastic thermal degradation products. Animals (male rats, $n = 78$) were divided into three groups: controls; Poisoning 1, where the animals were exposed to carbonyl chloride; Poisoning 2, where the animals were exposed to the fluoroplastic thermal degradation products. The animals' lung/body ratio was determined and the partial pressure of arterial oxygen (PaO_2) and carbon dioxide ($PaCO_2$) was assesed 10 min, 1, 3, 6, 24, and 48 h after the exposure. Histological examination of lung tissue was performed 3 and 6 h after the exposure. The increase in the lung/body ratio, decrease in PaO_2, and increase in $PaCO_2$ relative to controls were revealed 3, 6, 24, and 48 h after the exposure to carbonyl chloride and fluoroplastic thermal degradation products. The signs of the interstitial toxic pulmonary edema phase were detected 3 h after the exposure to the studied toxicants, and the signs of alveolar phase were revealed after 6 h. Similar changes were identified in animals of the experimental groups. The findings have shown that the exposure to carbonyl chloride and the fluoroplastic thermal degradation products containing perfluoroisobutylene lead to similar changes in the early post-intoxication period.

Keywords: carbonyl chloride, perfluoroisobutylene, toxic pulmonary edema, fluoroplastic, combustion products, acylating agents

СРАВНИТЕЛЬНАЯ ОЦЕНКА ТОКСИЧЕСКОГО ОТЕКА ЛЕГКИХ, ВЫЗВАННОГО ИНТОКСИКАЦИЕЙ КАРБОНИЛХЛОРИДОМ И ПРОДУКТАМИ ТЕРМИЧЕСКОГО РАЗЛОЖЕНИЯ ФТОРОПЛАСТА

Д. М. Ярошенко[1]✉, В. С. Лопатько[1], П. Г. Толкач[1], Н. Г. Венгерович[2], В. А. Башарин[1]

[1] Военно-медицинская академия имени С. М. Кирова Министерства обороны Российской Федерации, Санкт-Петербург, Россия

[2] Государственный научно-исследовательский испытательный институт военной медицины Министерства обороны Российской Федерации, Санкт-Петербург, Россия

Интоксикация ацилирующими пульмонотоксикантами приводит к формированию токсического отека легких (ТОЛ), подходы к лечению которого ограничены. Поражение легких, сходное с интоксикацией ацилирующими пульмонотоксикантами, может быть смоделировано посредством воздействия на организм продуктов термодеструкции фторопластов, содержащих перфторизобутилен. Целью исследования было сравнить проявления токсического отека легких у лабораторных животных при интоксикации ацилирующим пульмонотоксикантом (карбонилхлорид) и продуктами термического разложения фторопласта. Животных (крыс-самцов, $n = 78$) разделили на три группы: контроль; «интоксикация 1», где животных подвергали воздействию карбонилхлорида; «интоксикация 2», где их подвергали воздействию продуктов термического разложения фторопласта. Через 10 мин, 1, 3, 6, 24 и 48 ч после воздействия у животных определяли легочный коэффициент, анализировали парциальное давление кислорода (PaO_2) и диоксида углерода ($PaCO_2$) в артериальной крови. Через 3 и 6 ч после воздействия проводили гистологическое исследование тканей легких. Через 3, 6, 24 и 48 ч после воздействия карбонилхлорида и продуктов термодеструкции фторопласта были обнаружены увеличение легочного коэффициента, снижение PaO_2 и нарастание $PaCO_2$ по сравнению с контролем. Через 3 ч после воздействия исследуемых токсикантов были выявлены признаки интерстициальной, а через 6 ч после воздействия — альвеолярной фазы токсического отека легких. Выявленные изменения были схожи у животных экспериментальных групп. Результаты исследования показали, что воздействие карбонилхлорида и продуктов термодеструкции фторопласта, содержащих перфторизобутилен, приводят к сходным изменениям в раннем постинтоксикационном периоде.

Ключевые слова: карбонилхлорид, перфторизобутилен, токсический отек легких, фторопласт, продукты термодеструкции, ацилирующие агенты

The range on substances capable of causing toxic pulmonary edema (TPE) when inhaled is extremely diverse. Pulmonary toxicants with the acylating mechanism of action, carbonyl chloride and perfluoroisobutylene, should be treated as a separate group [1, 2].

Carbonyl chloride and perfluoroisobutylene are used in various sectors of industry. Thus, carbonyl chloride is used as a source component for synthesis of pesticides, plastics, dyes, isocyanates, etc. About 12 million tons of carbonyl chloride is produced annually for the needs of industry [3, 4]. Perfluoroisobutylene is used for synthesis of various fluoroplastic types. Furtermore, it is produced by thermal degradation of various fluoropolymers [2, 4]. The most likely situations associated with the carbonyl chloride and perfluoroisobutylene poisoning can arise during accidents at appropriate chemically hazardous objects [1, 3, 5], including in cases of terrorist acts and sabotage attacks on such objects [6].

Inhalation poisoning with carbonyl chloride and perfluoroisobutylene leads to toxic pulmonary edema, the mechanism underlying the development of which is currently poorly understood [1, 2]; there are no effective approaches to treatment of toxic pulmonary edema [1, 2, 7]. According to the literature, pathological changes observed in the laboratory animals poisoned with carbonyl chloride and perfluoroisobutylene have much in common, which suggests that these toxicants have common mechanisms of action [4].

Today, the literature reports approaches to simulation of toxic pulmonary edema caused by the exposure to the chemically pure carbonyl chloride and perfluoroisobutylene [1, 4, 8]. It is well known that thermal degradation of fluoroplastic yields perfluoroisobutylene [2] that represents a primary cause of toxicity of the resulting thermal degradation products [9]. Given the fact that fluoroplastic itself does not require any specific storage conditions and the fluoroplastic thermal degradation products can be obtained *ex tempore*, the model of toxic lung edema caused by the exposure to the fluoroplastic thermal degradation products can be used to search for agents for etiotropic and pathogenetic therapy of poisoning with the acylating pulmonary toxicants.

The study was aimed to compare manidestations of toxic pulmonary edema in the laboratory animals poisoned with an acylating pulmonary toxicant (carbonyl chloride) and the fluoroplastic thermal degradation products containing perfluoroisobutylene.

METHODS

The experiments involved mature outbred male rats with the body weight of 180–200 g obtained from the Rappolovo breeding nursery ($n = 78$). Animals were divided into groups (six animals per group): controls; Poisoning 1, where rats were exposed to carbonyl chloride; Poisoning 2, where rats were exposed to the fluoroplastic thermal degradation products. Sedation, analgesia and withdrawal of animals from the experiment were accomplished by using appropriate doses of the tiletamine–zolazepam solution (Zoletil 100, Virbak; France).

Static inhalation carbonyl chloride poisoning of the rats was accomplished in the chamber with the volume of 0.25 m³. The rats' exposure to the products of thermal degradation of the heat-treated granular fluoroplastic-4 (hereinafter, fluoroplastic) was simulated in the original unit [10]. The temperature of thermal degradation was 320–650 °C, and the thermal exposure duration was 3 min.

Static inhalation poisoning of the rats with carbonyl chloride and the fluoroplastic thermal degradation products in the

average lethal concentrations was simulated; the exposure time was 15 min. The carbonyl chloride concentration in the inhalation chamber was determined using the PortaSens II gas analyzer (ATI; USA). Qualitative assessment of perfluoroisobutylene in the gas/air mixture was performed by gas-liquid chromatography–mass spectrometry (Agilent 7890B chromatography system with the Agilent 240 MS mass selective detector (Agilent; USA)). The concentrations of carbon monoxide (CO), carbon dioxide (CO_2), and oxygen (O_2) in the inhalation chamber were determined using the Avtotrest-02.02 gas analyzer (Meta; Russia).

Laboratory animals were withdrawn from the experiment 10 min, 1, 3, 6, 24 and 48 h after the exposure. The lung/body ratio was determined; partial pressure of oxygen (PaO_2), partial pressure of carbon dioxide ($PaCO_2$), and the arterial blood pH were estimated using the i-STAT biochemical analyzer (Abbott; USA). The ribbon lung sections were cut with the PFM Slide 2003 sliding microtome (PFM Medical GmbH; Germany). The resulting slides were stained with hemotoxylin and eosin and placed on the glass slides. Histological examination was performed using the Leica DM2000 microscope (Leica Microsystems; Germany). Images were captured using the Olympus LC35 camera (Olympus Scientific Solutions; Japan).

The experimental data obtained were expressed as the median, first and third quartiles (Me [Q_1; Q_3]). The Kruskal–Wallis test was used to compare two or more independent groups; the Newman–Keuls method was used for multiple pairwise comparisons. The intergroup differences were considered to be significant at $p < 0.05$.

RESULTS

When simulating poisoning of animals with carbonyl chloride and the fluoroplastic thermal degradation products, the analysis of the gas/air mixture in the inhalation chamber was performed. The concentration of carbonyl chloride was 68 ppm, the concentration of carbon dioxide was 472 ppm, and the oxygen concentration was 20.8%. Perfluoroisobutylene, carbon monoxide (780 ppm), carbon dioxide (1120 ppm), and oxygen (concentration 20.4%) were determined in the inhalation chamber after the end of thermal degradation.

No signs of the irritant effect were revealed when simulating poisoning of animals with carbonyl chloride and the fluoroplastic thermal degradation products. The condition of the animals after retrieval from the inhalation chamber was the same as that of the control group.

The dynamic changes in the rats' lung/body ratio are provided in Fig. 1. The lung/body ratio of the experimental group animals measured 10 min and 1 h after the exposure did not differ from the values of the control group animals. A significant increase ($p < 0.05$) in the lung/body ratio relative to controls was determined 3, 6, 24, and 48 h after the exposure in the experimental group animals, however, there were no significant differences between animals of the experimental groups (Fig. 1).

Histological examination revealed no abnormalities in the rat lungs obtained 1 h after the exposure to the studied toxicants. The increase in the lung/body ratio 3 h after the exposure was accompanied by the emergence of microscopic changes in the lung tissues (Fig. 2). Thickening of the interalveolar septa, impregnation of those with neutrophils and erythrocytes, vascular congestion, and the emergence of single erythrocytes in the alveolar cavity were revealed in the histology slides 3 h after the exposure to carbonyl chloride and the fluoroplastic thermal degradation products. Alternation of the
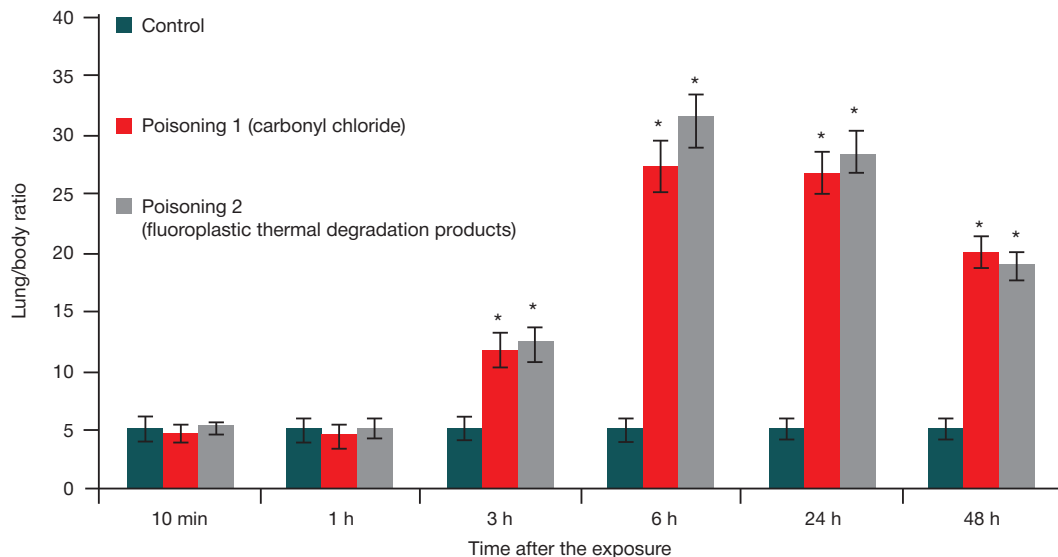
Fig. 1. Dynamic changes in the rat lung/body ratio after the exposure to carbonyl chloride and fluoroplastic thermal degradation products (relative units (Me [Q_1; Q_3]). * — significant differences from controls; six animals per group

emphysematous dilated areas and edematous alveoli filled with the effusion containing fibrin threads, segmented neutrophils, and single erythrocytes was determined in the slides 6 h after the exposure. Some alveoli were enlarged, the alveolar septa were thinned or sometimes absent. Bronchial lumens contained desquamated epithelium. Lymphoid infiltration was visible in the perivascular and peribronchial tissue. The histological alterations identified suggest the development of toxic pulmonary edema (Fig. 2).

The arterial blood gas analysis was conducted for indirect estimation of gas exchange in the lungs. A significant decrease in PaO_2 ($p < 0.05$) and a significant increase in $PaCO_2$ ($p < 0.05$) were reported as early as 1 h after the exposure to the studied toxicants. Significant hypoxemia (decreased PaO_2) and hypercapnia (elevated $PaCO_2$) were observed in blood of the rats poisoned

with both carbonyl chloride and the fluoroplastic thermal degradation products 3, 6, 24, and 48 h after the exposure (Fig. 3). Accumulation of carbon dioxide in the rat blood resulted in the pH decrease. Thus, blood pH dropped to 7.22 [7.19; 7.29] and 7.18 [7.11; 7.23] (Poisoning 1 and Poisoning 2 groups, respectively) 6 h after the exposure.

The changes in the arterial blood gas composition of the rats poisoned with carbonyl chloride and the fluoroplastic thermal degradation products identified during the studied period were similar (Fig. 3).

DISCUSSION

Perfluoroisobutylene, which is primarily responsible for toxicity of the resulting gas/air mixture, was determined in the inhalation
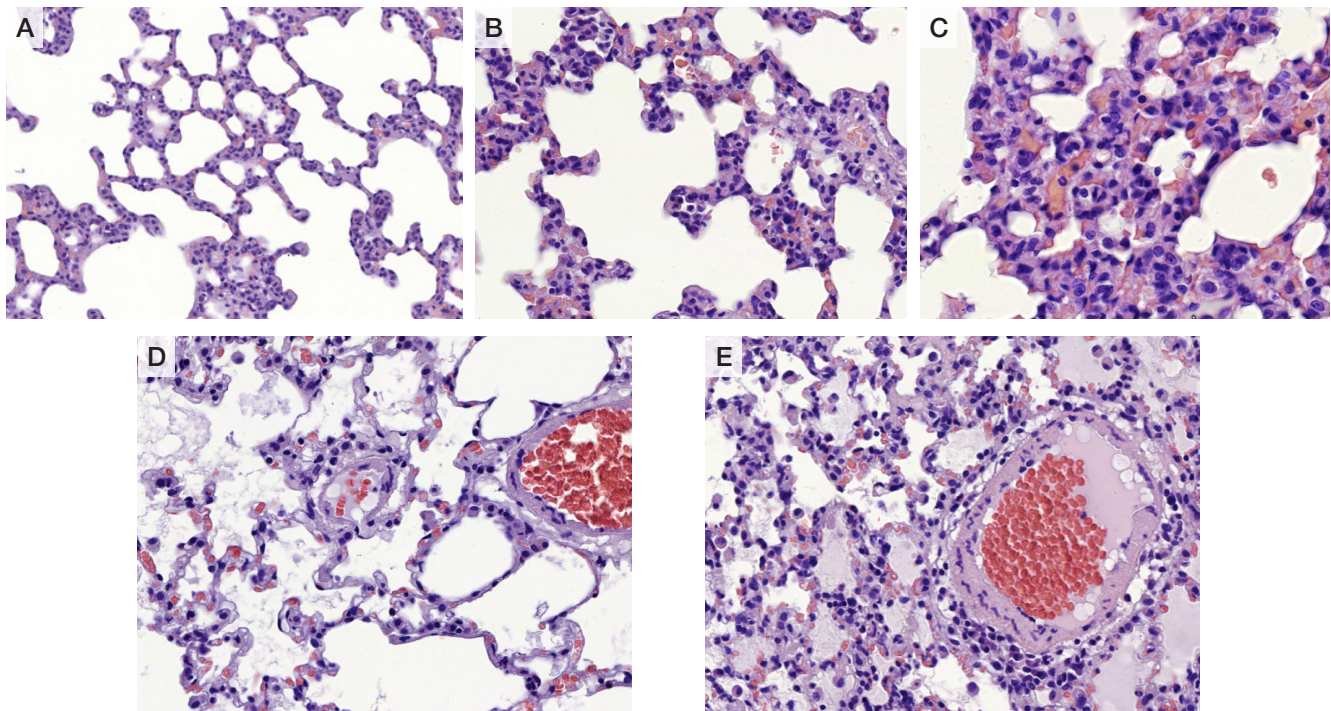
Fig. 2. Histological changes in the rat lung tissues 3 and 6 h after the exposure to carbonyl chloride and fluoroplastic thermal degradation products (hematoxylin and eosin, 50× magnification). **A**. Control. **B**. Poisoning 1 (carbonyl chloride), 3 h. **C**. Poisoning 2 (fluoroplastic thermal degradation products), 3 h. **D**. Poisoning 1 (carbonyl chloride), 6 h. **E**. Poisoning 2 (fluoroplastic thermal degradation products), 6 h
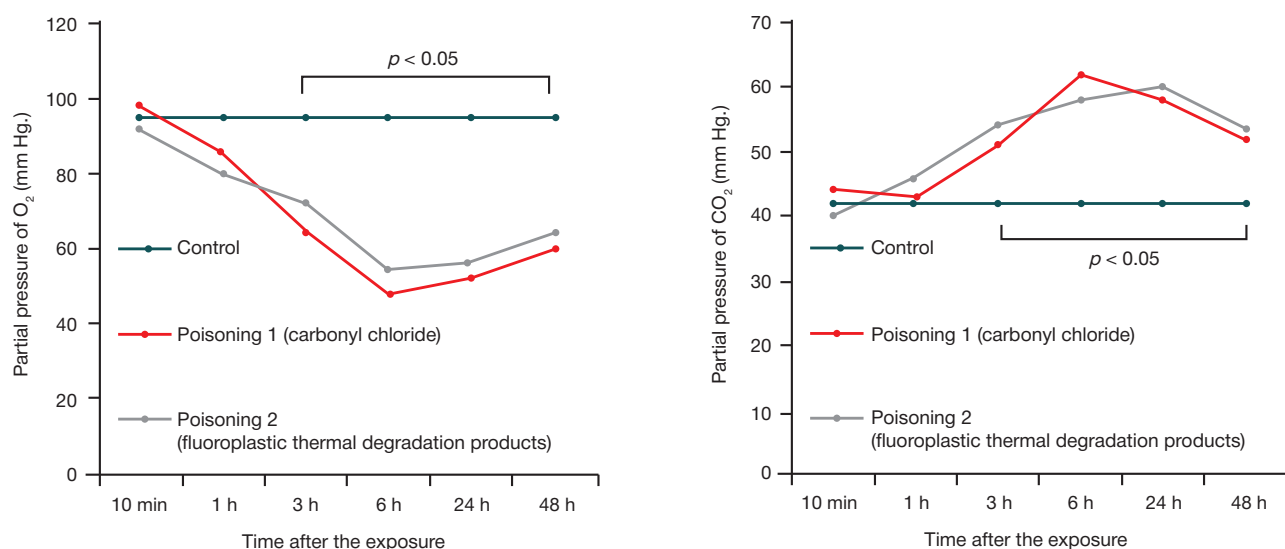
Fig. 3. Dynamic changes in the rat arterial blood partial pressure of oxygen (left) and carbon dioxide (right) at different times after the exposure to carbonyl chloride and fluoroplastic thermal degradation products (mm Hg (Me)). $p < 0.05$ — significant differences from the groups Poisoning 1 (carbonyl chloride) and Poisoning 2 (fluoroplastic thermal degradation products)

chamber during thermal degradation of fluoroplastic [9]. The carbon monoxide concentration in the inhalation chamber corresponded to 0.1 LC_{50} (for rats exposed for 15 min) [11]. The oxygen concentration did not drop below 20.4%. Thus, the animals' condition severity cannot be associated with hypoxic and/or hemic hypoxia.

In our study, lesions in the lung tissues of the rats exposed to the studied toxicants were detected 3 h after the end of exposure. The increase in the lung/body ratio was revealed, which indirectly indicated accumulation of extravascular lung water [12]. As toxic pulmonary edema manifestation progressed (6 h after the exposure), an even higher lung/body ratio was determined, which remained elevated 24 and 48 h after the exposure. The lung/body ratio increase was accompanied by the emergence of mixroscopic changes in lung tissues. The signs of the interstitial toxic pulmonary edema phase were detected 3 h after the exposure to the studied toxicants, and the signs of alveolar phase were revealed after 6 h.

Disruption of the blood-air barrier structure was accompanied by disturbed gas exchange. Thus, the most prominent decrease in PaO_2 and increase in $PaCO_2$ of arterial blood were determined 6 h after the exposure. Such changes are associated with abnormal gas diffusion caused by thickening of the blood-air barrier due to extravascular fluid accumulation [12]. Accumulation of carbon dioxide in arterial blood and disturbance of the aerobic oxidation processes associated with arterial hypoxemia resulted in the altered acid-base condition of blood manifested by mixed acidosis.

The experimental data obtained suggest that severity of the condition of the laboratory animals poisoned with carbonyl chloride and the fluoroplastic thermal degradation products results from respiratory hypoxia. Among respiratory hypoxia manifestations, arterial hypoxemia and altered acid-base condition caused by disruption of the blood-air barrier and disturbed gas exchange in the lungs were reported. It is important to note that in the studied period manifestations of toxic pulmonary edema were similar in rats exposed to both carbonyl chloride and the fluoroplastic thermal degradation products containing perfluoroisobutylene.

CONCLUSIONS

Manifestations of toxic pulmonary edema (arterial hypoxemia and hypercapnia, morphological changes in the lung tissues, lung/body ratio) caused by the rat exposure to the fluoroplastic thermal degradation products containing perfluoroisobutylene were similar to that observed under exposure to the chemically pure carbonyl chloride in the early post-intoxication period. Given the fact that fluoroplastic is chemically, physically, and biologically inert and does not require specific storage conditions [9], the fluoroplastic thermal degradation products obtained ex tempore can be used for modeling toxic pulmonary edema in animals, as demonstrated in our study. Thus, the model reported allows one to adequately simulate toxic pulmonary edema in rats, similar to that resulting with poisoning with the acylating pulmonary toxicants. This makes it possible to conduct experimental studies focused on further investigation of the development mechanism and the search for treatment options for toxic pulmonary edema.

References

1. Cao C, Zhang L, Shen J. Phosgene-induced acute lung injury: approaches for mechanism-based treatment strategies. Front Immunol. 2022; (13): 917395.
2. Patocka J. Perfluoroisobutene: poisonous choking gas. Mil Med Sci Lett (Voj Zdrav Listy). 2019; 883): 98–105.
3. Lu Q, Huang S, Meng X, Zhang J, Yu S, Li J, et al. Mechanism of phosgene-induced acute lung injury and treatment strategy. Int J Mol Sci. 2021; 22 (20): 10933.
4. Muir B, Cooper DB, Carrick WA, Timperley CM, Slater BJ,

Quick S. Analysis of chemical warfare agents III. Use of bis-nucleophiles in the trace level determination of phosgene and perfluoroisobutylene. J Chromatogr A. 2005; 1098 (1-2): 156–65.
5. Marzec J, Nadadur S. Countermeasures against pulmonary threat agents. J Pharmacol Exp Ther. 2024; 388 (2): 560–7.
6. Bezmakova AL, Potapova AV, Judin MA, Chepur SV, Shefer TV. Iz istorii ispol'zovanija himicheskogo oruzhija kak instrumenta diversifikacii voenno-politicheskogo vlijanija. Voenno-medicinskij zhurnal. 2023; 344 (11): 68–74. Russian.

7. Mistry S, Scott TE, Jugg B, Perrott R, Saffaran S, Bates DG. An in-silico porcine model of phosgene-induced lung injury predicts clinically relevant benefits from application of continuous positive airway pressure up to 8 h post exposure. Toxicol Lett. 2024; (391): 45–54.
8. Zhang XD, Yu WH, Liu MM, Liu R, Wu H, Wang Z, et al. Pentoxifylline inhibits phosgene-induced lung injury via improving hypoxia. Drug Chem Toxicol. 2023; 46 (6): 1100–7.
9. Panshin JuA, Malkevich SG, Dunaevskaja CS. Ftoroplasty. L.: Himija, 1978. 232 p. Russian.
10. Tolkach PG, Basharin VA, Sizova DT, Chajkina MA, Lopatko VS. Kamera termookislitel'noj destrukcii dlja ocenki pokazatelja toksichnosti produktov gorenija. Patent RU2791221C1. 3.06.2023.
11. Zobnin JuV, redaktor. Otravlenie monooksidom ugleroda (ugarnym gazom). SPb.: Taktik-Studio, 2011; 86 p. Russian.
12. Moroz VV, Golubev AM, Kuzovlev AN. Otek legkih: klassifikacija, mehanizmy razvitija, diagnostika. Obshhaja reanimatologija. 2009; (1): 83–8. Russian.

Литература

1. Cao C, Zhang L, Shen J. Phosgene-induced acute lung injury: approaches for mechanism-based treatment strategies. Front Immunol. 2022; (13): 917395.
2. Patocka J. Perfluoroisobutene: poisonous choking gas. Mil Med Sci Lett (Voj Zdrav Listy). 2019; 883): 98–105.
3. Lu Q, Huang S, Meng X, Zhang J, Yu S, Li J, et al. Mechanism of phosgene-induced acute lung injury and treatment strategy. Int J Mol Sci. 2021; 22 (20): 10933.
4. Muir B, Cooper DB, Carrick WA, Timperley CM, Slater BJ, Quick S. Analysis of chemical warfare agents III. Use of bis-nucleophiles in the trace level determination of phosgene and perfluoroisobutylene. J Chromatogr A. 2005; 1098 (1-2): 156–65.
5. Marzec J, Nadadur S. Countermeasures against pulmonary threat agents. J Pharmacol Exp Ther. 2024; 388 (2): 560–7.
6. Безмакова А. Л., Потапова А. В., Юдин М. А., Чепур С. В., Шефер Т. В. Из истории использования химического оружия как инструмента диверсификации военно-политического влияния. Военно-медицинский журнал. 2023; 344 (11): 68–74.
7. Mistry S, Scott TE, Jugg B, Perrott R, Saffaran S, Bates DG. An in-silico porcine model of phosgene-induced lung injury predicts clinically relevant benefits from application of continuous positive airway pressure up to 8 h post exposure. Toxicol Lett. 2024; (391): 45–54.
8. Zhang XD, Yu WH, Liu MM, Liu R, Wu H, Wang Z, et al. Pentoxifylline inhibits phosgene-induced lung injury via improving hypoxia. Drug Chem Toxicol. 2023; 46 (6): 1100–7.
9. Паншин Ю. А., Малкевич С. Г., Дунаевская Ц. С. Фторопласты. Л.: Химия, 1978; 232 с.
10. Толкач П. Г., Башарин В. А., Сизова Д. Т., Чайкина М. А., Лопатько В. С. Камера термоокислительной деструкции для оценки показателя токсичности продуктов горения. Патент RU2791221C1. 3.06.2023.
11. Зобнин Ю. В., редактор. Отравление монооксидом углерода (угарным газом). СПб.: Тактик-Студио, 2011; 86 с.
12. Мороз В. В., Голубев А. М., Кузовлев А. Н. Отек легких: классификация, механизмы развития, диагностика. Общая реаниматология. 2009; (1): 83–8.

COMPUTATIONAL PHANTOM FOR THE DOSIMETRY OF THE RED BONE MARROW OF A 10-YEAR-OLD CHILD DUE TO INCORPORATED BETA-EMITTERS

Sharagin PA[1]✉, Tolstykh EI[1], Shishkina EA[1,2]

[1] Urals Research Center for Radiation Medicine of the Federal Medical-Biological Agency, Chelyabinsk, Russia

[2] Chelyabinsk State University, Chelyabinsk, Russia

Bone-seeking radionuclides, in particular ^{89,90}Sr, could get into the environment in the course of various anthropogenic radiation incidents. From there they enter a human body with food and water. This leads to red bone marrow (RBM) internal exposure. These elements were present in the composition of radioactive releases into the Techa River in 1950s, and are the major source of RBM exposure for the residents of the riverside settlements. RBM dose estimation relies on dosimetric modeling which comprises the development of 3D computational phantoms of the skeleton parts. By imitating the energy transfer in these phantoms, the conversion coefficients from the radionuclide activity in a bone to the dose rate in RBM are evaluated. The given study is yet another step in the research aimed at the elaboration of a set of computational phantoms of the skeleton for people of various age. The objective is to develop a computational phantom of a skeleton of a 10-year-old child to estimate dose to RBM due to incorporated beta-emitters. Original SPSD (stochastic parametric skeletal dosimetry) approach was used to create the phantoms. According to this method the skeleton sites containing RBM were divided into smaller segment of simple geometric shape, for which voxel phantoms were generated. The parameters for phantom generation were based on published research data. They included linear dimensions of bones, thickness of the cortical layer, characteristics/properties of the bone micro-architecture, density and chemical composition of the modelled media and the percentage of RBM content in bones. Generated computational phantom of the skeleton sites with active hematopoiesis of a 10-year-old child consists of 38 phantom-segments. Linear dimensions of the segments were from 3 to 88 mm, cortical layer thickness: 0.2–2.2 mm.

Keywords: trabecular bone, cortical bone, bone marrow dosimetry, computational phantoms, Sr

✉ **Correspondence should be addressed:** Pavel A. Sharagin
Vorovskogo, 68-a, Chelyabinsk, 454141, Russia; sharagin@urcrm.ru

ВЫЧИСЛИТЕЛЬНЫЙ ФАНТОМ ДЛЯ ДОЗИМЕТРИИ КРАСНОГО КОСТНОГО МОЗГА ДЕСЯТИЛЕТНЕГО РЕБЕНКА ОТ ИНКОРПОРИРОВАННЫХ БЕТА-ИЗЛУЧАТЕЛЕЙ

П. А. Шарагин[1]✉, Е. И. Толстых[1], Е. А. Шишкина[1,2]

[1] Уральский научно-практический центр радиационной медицины Федерального медико-биологического агентства России, Челябинск, Россия

[2] Челябинский государственный университет, Челябинск, Россия

Остеотропные радионуклиды, в частности ^{89,90}Sr, могут попадать в окружающую среду при различных техногенных радиационных инцидентах, оттуда с пищей и водой они поступают в организм человека, что приводит к внутреннему облучению красного костного мозга (ККМ). Эти элементы были в составе радиоактивных сбросов в реку Теча в 1950-е гг., и являются основным источником облучения ККМ жителей прибрежных территорий. Оценка доз на ККМ опирается на дозиметрическое моделирование, которое включает разработку трехмерных вычислительных фантомов частей скелета. На основе имитации переноса энергии в этих фантомах оценивают коэффициенты перехода от активности радионуклида в кости к мощности дозы в ККМ. Целью исследования было разработать вычислительный фантом скелета десятилетнего ребенка для оценки доз на ККМ от инкорпорированных бета-излучателей. Для создания фантомов использовали оригинальный SPSD (от англ. stochastic parametric skeletal dosimetry) подход. Согласно данной методике, участки скелета, содержащие ККМ, разбивались на меньшие сегменты простой геометрической формы, для которых генерировались воксельные фантомы. Параметры для генерации фантомов основаны на опубликованных данных, они включали: линейные размеры костей, толщину кортикального слоя, характеристики костной микроархитектуры, плотность и химический состав моделируемых сред и долю содержания ККМ в костях. Сгенерированный вычислительный фантом участков скелета с активным гемопоэзом десятилетнего ребенка состоит из 38 фантомов-сегментов. Линейные размеры сегментов были 3–88 мм, толщина кортикального слоя — 0,2–2,2 мм.

Ключевые слова: трабекулярная кость, кортикальная кость, дозиметрия костного мозга, вычислительные фантомы, Sr

✉ **Для корреспонденции:** Павел Алексеевич Шарагин
ул. Воровского, д. 68-а, г. Челябинск, 454141, Россия; sharagin@urcrm.ru

Internal exposure of the red bone marrow (RBM) due to bone-seeking radionuclides may lead to serious health effects for a human body. The most dangerous and wide-spread bone-seeking radionuclides are ^{89,90}Sr. These elements could be found in the composition of the global radioactive fallouts as a result of the nuclear weapon testing. They also got into the environment due to some other radiation incidents [1]. For example, strontium isotopes were present in the composition

of the radioactive releases into the Techa River in 1950s leading to their accumulation in the bodies of the residents of territories along the river [2–5]. It was ^{89,90}Sr that were the main sources of the RBM exposure for the members of the Techa River Cohort. Estimation of doses from these radionuclides is a challenging task. It involves biokinetic modeling of the radionuclide turnover to evaluate its concentration in a bone (source-tissue) [6], as well as dosimetric modeling which allows assessing the dose conversion factors (DF) from the radionuclide activity in a bone to the absorbed dose rate in RBM. Dosimetric models imitate the location of the source-tissue and target-tissue relative each other. At present computational phantoms (3D models of the skeleton and RBM) serve the function of such models. The radiation transfer is imitated inside these phantoms. Modern skeletal phantoms to estimate RBM doses are based on the analysis of the computer tomography (CT) images of the skeletons of very few deceased people [7–13].

Limited amount of biopsy material does not allow assessing the uncertainties associated with the variability of the size and micro-architecture of the skeleton within the population. As an alternative URCRM has developed an original parametric method of stochastic modeling of bone structures — SPSD-modeling (Stochastic parametric skeletal dosimetry) [14, 15]. Within the framework of this approach, it is suggested that numerous published measurement results of morphometric and hystomorphometric studies of the bones should be used as model parameters. High degree of statistical significance of the published measurement results makes it possible to estimate uncertainties associated with the individual variability of the skeletal parameters.

SPSD-phantom of a skeleton as a whole is a set of small phantom segments. These are the digital models of simple geometric shape filled with trabecular bone with RBM located in the inter-trabecular cavities. Some part of the phantom surfaces is covered with the layer of solid cortical bone. Thus, SPSD-phantoms contain two source-tissues: trabecular and cortical bone and one target-tissue — RBM. This model suits perfectly the internal dosimetry of bone-seeking beta-emitters [14, 15]. Model adequacy is supported by good agreement of the calculated energy dependences for the SPSD-phantoms and similar dependences described in some published research [14, 16, 17].

In case of population exposure, the radionuclides may enter a body of a person of various age. For example, radioactive contamination of the Techa River led to the exposure of residents in the age-range from newborns to elderly people [2–4, 18]. To estimate doses to RBM for all age groups we have previously developed SPSD-phantoms representing the skeleton of a new-born [19], one-year-old [20], and five-year-old child [21]. The objective of the current study is to develop computational phantoms representing the skeleton of a ten-year-old child to estimate RBM doses from beta-emitting radionuclides incorporated in a bone. The study is yet another step in the work aimed at the development of a set of computational phantoms of a standard man for different age groups.

METHODS

Computational phantom of a ten-year-old child was generated within the framework of SPSD method similarly to the phantoms for younger age groups [14]. The method consists of the following steps:

1) evaluation of the RBM distribution within the skeleton, identification of the modeled sites of the skeleton with active hematopoiesis (hematopoietic sites);

2) measuring linear dimensions and micro-structure parameters of the modeled bones based on the published data;

3) hematopoietic site segmentation;

4) voxel phantom generation for every segment.

Bone marrow distribution within the skeleton of 10-years-old child was evaluated using ICRP-data [13], which based on results of MRI-research [22].

In total the analysis included 11,927 measurement results of the bone samples [23, 24]. To measure the morphometric parameters of the phantoms of a ten-year-old child, manuscripts published in peer-reviewed journals, atlases, manuals, monographs, and dissertations were studied as well as digital resources containing collections of x-ray images. The measurement results of individuals/samples that the authors considered to be healthy and having no disorders resulting in bone deformities were used for the analysis. Ethnicity: Caucasians and Mongoloids, since these groups are typical of the Urals region. The subjects' age was 8–12 years.

Histomorphometry and micro-CT data were used to estimate the parameters of trabecular bone (*Tb. Th*., *Tb. Sp*., *BV/TV*) and cortical layer thickness. The following properties of the bone micro-architecture were evaluated: trabecular thickness (*Tb. Th*.), trabecular separation (*Tb. Sp*.), bone volume to total spongiosa volume relation (*BV/TV*). The data of the linear dimension measurement results of the skeletal bones were examined with the help of various techniques: micrometers, osteometric boards, ultrasound scans and radiography, as well as computed tomography (CT).

Within each skeletal site with active hematopoiesis the bones are subdivided into relatively small segments. The so-called Bone Phantom Segments (BPS) was modeled for every segment [25, 26]. Each segment should have relatively homogeneous microarchitecture and cortical layer thickness. Segments should be described by simple geometric shapes (cylinder, rectangular parallelepiped, etc.). Such subdivision allows taking into account the micro-architecture heterogeneity inside a bone. Moreover, relatively small size of the segments makes it possible to generate the phantoms imitating them with rather high resolution.

Averaged estimates of bone characteristics were taken as computational phantom parameters. If the published data on individual measurements were available, they were combined to calculate the means and standard deviations (SD). When the measurement results of groups of people were averaged, a weighting factor (W_N) which took account of the number of subjects (N) was introduced for each group: $W_N = 1$, when $N \geq 25$; $W_N = N/25$, when $N < 25$. Methods to select and assess the published data were previously described in detail in [23].

Linear dimensions and parameters of the bone micro-architecture influence the geometry of source and target tissue in BPS. They were determined for each segment separately. In addition to these parameters, the chemical composition and density of the modeled media were determined based on the published research data [27, 28] and were used for all the BPS of a ten-year-old child.

A voxel BPS was generated for each segment using the original Trabecula software [29]. Every voxel in a BPS imitates either mineralized bone, or bone marrow (BM), depending on the voxel center position in a phantom.

Trabecular (TB) and cortical bone (CB) were considered as source tissues, while bone marrow (BM) was viewed as target tissue. BM was uniformly distributed across the trabeculae in the BPS. Voxel size was selected individually for each phantom. It did not exceed 70% of trabecular thickness and varied in the
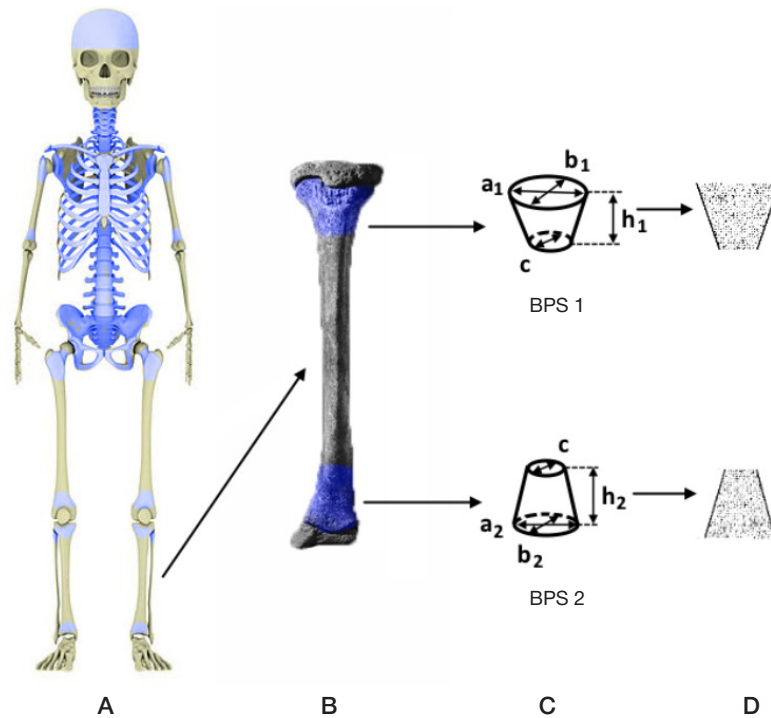
Fig. 1. Segmentation of the skeletal hematopoietic sites of a ten-year-old child using the example of the tibia. **A**. Skeleton of a ten-year-old child (modeled skeletal sites with active hematopoiesis are highlighted in *blue*). **B**. Tibia (modeled skeletal sites with active hematopoiesis are highlighted in *blue*). **C**. Scheme of bone division into BPS and BPS linear dimensions. **D**. BPS of the tibia — voxel representation, cross section (voxels simulating bone tissue are highlighted in *black*, those simulating RBM are highlighted in *white*)

range 50–200 μm [29, 30]. The modeled media volumes were calculated for each BPS using the Trabecula software package.

Hematopoietic sites of a ten-year-old child, segmentation process and generated BPS are given in Fig. 1 (exemplified by the tibia).

SPSD method allows simulating the population variability of the micro-structure sizesand characteristics for every BPS. With this objective in view, 12 Supplementary Phantom Segments (SPS) were created for every BPS with the bone micro- and macro-structure parameters randomly selected within the range of their individual variability (within the limits of minimum and maximum measured values).

RESULTS

Skeletal sites with active hematopoiesis of the skeleton of a ten-year-old child and RBM mass fraction in these sites have

been determined based on the ICRP data [22] and are provided in Table 1.

As it can be seen from Table 1, the skeleton of a ten-year-old child has 13 hematopoietic sites. RBM mass fraction in these sites varies from 0.9% to 18.1% of the total RBM content in the skeleton. In addition, distribution of RBM within each hematopoietic site was determined based on the published MRI data [31–36].

Chemical composition of the modeled media was obtained based on the ICRP data for adults (Table 2) [25].

The density of mineral bone tissue has been estimated based on the measurement results of the cortical bone thickness in children aged 10 and is equal to 1.85 g/cm³ [26]. It has been assumed that RBM density is equal to that of water (1 g/cm³) [25].

Bone micro-structure characteristics were evaluated based on the published research data. A detailed description of their

Table 1. Mass fraction of RBM (% of the total mass of RBM in the skeleton) in the main hematopoietic sites of a ten-year-old child's skeleton [13, 22]

№	Hematopoietic site	RBM mass fraction, %
1	Femur	15.7
2	Humerus	4.1
3	Sacrum	6.8
4	Tibia bones	5.6
5	Pelvic bones	15.8
6	Skull	12.8
7	Clavicle	0.9
8	Scapula	2.9
9	Sternum	1.8
10	Ribs	11
11	Cervical vertebrae	2.7
12	Thoracic vertebrae	11
13	Lumbar vertebrae	8.5

Table 2. Chemical composition of simulated media adopted for all BPS

Chemical composition, rel. units		
Chemical element	Bone	Active marrow
H	0.035	0.105
C	0.16	0.414
N	0.042	0.034
O	0.445	0.439
Na	0.003	0.001
Mg	0.002	0.002
P	0.095	0.002
S	0.003	0.002
Ca	0.215	–

analysis and calculation of the population-average were given in [23]. Micro-architecture parameter values for the BPS of a ten-year-old child are provided in Table 3.

Linear dimensions and values of cortical layer thickness assumed for the BPS of a ten-year-old child are given in Table 4.

As it is shown in Table 4 the phantom of hematopoietic sites of a ten-year-old child skeleton consists of 38 BPS. The number of BPS within a hematopoietic site depended on its shape and varied from 1 (ribs) to 9 (pelvic bones).

Most of the BPSs of a ten-year-old child were represented by cylinders and rectangular parallelepipeds. Their linear dimensions were within the range from 3 to 88 mm. The minimum *Ct. Th*. value was reported for the BPSs of the vertebra (0.2 mm). It differed tenfold from the maximum value assumed for the proximal end of the femora (2.2 mm). Bone micro-architecture parameters also varied widely. *BV/TV* value in BPS varies in the range 14-52%, *Tb. Th* — from 0.12 mm to 0.29 mm, *Tb. Sp.* — from 0.46 mm to 1 mm (Table 3).

On the average, individual variability of the BPS linear dimensions made up 12%. The greatest variability was reported for the iliac bone (30%), the least — for the lateral border of scapula. The cortical layer thickness of the bone varied within the range from 7% (cervical vertebra) to 62% (sternum). On the average, it made up 24%. The variability of the micro-structure parameters was within the range 6–42%, and on the average it was 19%. The obtained values of the variability parameters of the phantoms were used to model SPS. The volume of the SPS

could differ from the volume of the BPS more than 3 times both upwards or downwards. Calculation of the DF for the BPSs and SPSs will make it possible to evaluate DF population variability as a mean-square deviation of the DF values calculated for SPS from those calculated for the BPS.

DISCUSSION

The phantom of a skeleton of a ten-year-old child has less BPSs than that of a five-year-old child. It could be explained by the fact that RBM has been substituted by yellow bone marrow in the tubular bone diaphyses, therefore these skeletal sites were not modeled. At the age of 10 the greatest RBM fraction is located in the pelvic bones and femora as compared to the younger age groups when the greatest amount of RBM is reported for the cranial bones. Also, at this age 29% of the total RBM is reported for the segments of the spine and sacrum. Micro-structure parameters of the BPS change little as compared to the phantom of a five-year-old child. There is a tendency to a decrease in *BV/TV* and *Tb.Th*, and an increase in *Tb. Sp*. Over a 5-year period, i.e. by the age of 10, the cortical layer thickness has increased by 20% in any given BPS. The age-dependent changes in the characteristics of the phantoms could be demonstrated by comparing the volumes of the simulated media. Table 5 shows the comparison of the volume of the skeletal sites of five- and ten-year old child on the example of the distal end of the femur, clavicle, cervical and lumbar vertebra.

Table 3. Micro-architecture parameters assumed for BPS of a ten-year-old-child [11, 34–56] (coefficient of variation (CV) is given in parentheses, %)

Hematopoietic site	BV/TV, %	Tb. Th, mm	Tb. Sp, mm
Femur (proximal part)	35 (22–53)	0.24 (22)	0.54 (14)
Femur (distal part)	26 (17–40)		
Humerus	22 (13–37)	0.21 (13)	0.58 (32)
Ribs	20 (10–37)	0.23 (34)	0.5 (14)
Tibia bones*	25 (20–31)	0.21 (13)	0.74 (11)
Pelvic bones (ilium)	25 (20–31)	0.16 (10)	0.46 (15)
Other pelvic bones	25 (20–31)	0.16 (10)	0.6 (12)
Skull*	52 (41–65)	0.29 (32)	0.57 (35)
Clavicle (central part)	15 (10–23)	0.2 (32)	0.8 (25)
Clavicle (end's)	29 (15–46)	0.15 (13)	0.8 (25)
Scapula*	22 (6–38)	0.24 (42)	0.96 (23)
Sternum*	15 (7–23)	0.15 (27)	1.0 (6)
Cervical vertebrae	21 (12–35)	0.14 (14)	0.65 (24)
Thoracic vertebrae + lumbar vertebrae + sacrum	14 (7–26)	0.12 (17)	0.65 (24)

Note: * — micro-architecture parameters were calculated based on the measurement results of similar bones or based on the data for other age groups; the calculation method was reported previously in [23].

Table 4. Linear dimensions and cortical layer thickness assumed for the BPS representing a ten-year-old child

Hematopoietic site	Segment	Shape[1]	Phantom parameters, mm (CV is given in parentheses, %)[2]						Data sources
			h	*a*	*b*	*c*	*d*	*Ct.Th.*	
Бедро	Proximal end (upper part)	c	30	25 (7)	25 (7)			1.8 (17)	[56–64]
	Proximal end (lower part)	c	30	25 (7)	25 (7)			2.2 (12)	
	Distal end	dc	69 (5)	78 (7)	33 (10)	21 (9)	21 (9)	1.1 (14)	
Humerus	Proximal end	dc	27 (4)	39 (4)	33 (5)	18 (4)	18 (4)	1.1 (16)	[57–61, 65]
	Distal end	dc	27 (4)	54 (9)	18 (4)	18 (4)	18 (4)	0.8 (10)	
Ribs	Ribs[4]	p	10 (16)	30	5 (10)			0.7 (20)	[66, 67]
Sacrum	Body of the 1st vertebra	p	22 (20)	88 (20)	26 (10)			0.9 (34)	[68–73]
	Body of the 2nd vertebra	p	20 (20)	70 (20)	15 (10)			0.9 (34)	
	Body of the 3rd vertebra	p	18 (20)	62 (20)	10 (10)			0.9 (34)	
	Body of the 4th vertebra	p	13 (20)	53 (20)	7.7 (10)			0.9 (34)	
	Body of the 5th vertebra	p	13 (20)	44 (20)	7.7 (10)			0.9 (34)	
Tibia bones	Fibula proximal end[4]	c	30	11 (6)	11 (6)			1.7 (12)	[58, 70, 72]
	Tibia proximal end	dc	49 (6)	63 (7)	32 (20)	21 (6)	21 (6)	0.7 (11)	[57, 58, 74–77]
	Tibia distal end	dc	48 (6)	35 (12)	35 (12)	21 (6)	21 (6)	0.7 (11)	
Pelvic bones	Ilium part 1	p	8 (22)	30	30			1.7 (33) 0.9 (19)[3]	[78–85]
	Ilium part 2	p	8 (22)	30	30			0.9 (19)	
	Acetabular part of the ilium	dc	26 (7)	44 (7)	20 (22)	37 (3)	28 (30)	0.9 (17)	
	Acetabular part of the pubis	dc	9.8 (15)	28 (9)	21 (10)	16 (9)	11 (10)	0.5 (30)	
	Pubis bone (superior ramus)	c	39 (15)	16 (9)	11 (10)			0.5 (30)	
	Pubis bone (inferior ramus)	c	32 (15)	11 (10)	11 (10)			0.5 (30)	
	Acetabular part of the ischium	pr	29 (15)	28 (7)	29 (15)	28 (7)		0.5 (30)	
	Ischial tuberosity	c	34 (15)	19 (15)	19 (15)			0.5 (30)	
	Inferior ramus of the ischium	c	32 (15)	11 (10)	11 (10)			0.5 (30)	
Skull	Flat bones[4]	p	4.6 (18)	30	30			1.2 (18)	[86, 87]
Clavicle	Body[4]	c	30	11 (12)	8.3 (10)			1.8 (26)	[88–90]
	Sternal end	dc	17 (7)	22 (11)	20 (11)	11 (12)	8.3 (10)	0.8 (26)	
	Acromial end	dc	17 (7)	19 (11)	11 (23)	11 (12)	8.3 (10)	0.8 (26)	
Scapula	Glenoid	c	15 (5)	28 (5)	20 (7)			0.9 (28)	[91–93]
	Acromion	p	8.2 (18)	27 (8)	21 (8)			0.8 (13)	
	Lateral border	p	30	3.5 (3)	10 (12)			0.8 (13)	
Sternum	Sternum	p	8.5 (15)	30	30			0.7 (62)	[39, 94, 95]
Cervical vertebrae	Vertebral body	c	9.4 (12)	14 (7)	19 (13)			0.2 (7)	[79, 96, 97]
Thoracic vertebrae	Vertebral body	c	14 (17)	22 (21)	27 (24)			0.2 (25)	[98–101]
	Transverse process	p	8.6 (21)	13 (21)	7.3 (21)			0.2 (25)	
	Spinous process	p	7.2 (21)	25 (21)	4.1 (21)			0.2 (25)	
Lumbar vertebrae	Vertebral body	c	19 (18)	27 (21)	36 (21)			0.2 (25)	[73, 98, 99, 102]
	Transverse process	p	8.6 (20)	16 (20)	5.2 (20)			0.2 (25)	
	Spinous process	p	17 (20)	27 (20)	5.2 (20)			0.2 (25)	

Note: [1] — phantom shape was designated as follows: c — cylinder, dc — deformed cylinder, p — rectangular parallelepiped, [2] pr – prism with triangle base — BPS dimensions were designated as follows: *h* — height; *a* — major axis (c), major axis for a larger base (dc) or side a (p); *b* — minor axis (c), minor axis for a large base (dc) or side b (p); *c* — major axis for a small base (dc); *d* — minor axis for a small base (dc); for prism (pr): *a*, *b*, *c* — the sides of the prism base; [3] — cortical layer thickness was considered to be different for the inner (medial) and outer (gluteal) surfaces of this segment of the ilium; [4] — BPS imitated only a part of the simulated bone segment, when the bone segment dimensions significantly exceeded 30 mm, since in such cases it makes no sense to simulate the entire bone fragment in terms of dosimetry [15, 24].

It has been shown in Table 5 that the volume of the modeled media of a ten-year-old child exceeds that for a five-year-old one, which reflects the growth of the skeletal bones. The source-tissue volume increased on the average 1.96 times for TB, and 1.48 times for the CB. The total volume of the BPS increased 1.6 times over a 5-year period (from the age of 5 till 10). Over the same period of time the total volume of the CB increased only 1.3 times. It is due to the cessation of the hematopoiesis in skeletal sites with high *Ct.Th*. (the middle of the diaphyses of the long tubular bones). We expect that such

age-dependent dynamics of the phantom characteristics will result in the decrease of the DF from Sr incorporated in the cortical bone.

In the course of the future studies the phantom parameters (Table 3, 4) provided in this manuscript will be integrated into the Trabecula software package to generate voxel phantom. The simulation of the energy transfer in these phantoms will allow estimating he DF for the bone-seeking beta-emitters, which gives an opportunity to estimate the RBM absorbed dose rate.

Table 5. Comparison of BPS volumes of five- and ten-year-old children

BPS	Simulated medium	Modeled structure volume, cm³		
		5 years	10 years	10/5 years
Distal end of the femur	BM	22.9	49.94	2.18
	TB	7.56	17.49	2.31
	CB	5.21	8.97	1.72
	Entire BPS	35.67	76.4	2.14
Sternal end of the clavicle	BM	0.89	1.8	2.02
	TB	0.36	0.73	2.03
	CB	0.22	0.58	2.64
	Entire BPS	1.47	2.53	1.72
Body of the lumbar vertebra	BM	8.51	12.42	1.46
	TB	1.34	1.97	1.47
	CB	0.3	0.38	1.27
	Entire BPS	10.15	14.77	1.46
Body of the cervical vertebra	BM	0.89	1.43	1.61
	TB	0.24	0.38	1.58
	CB	0.05	0.07	1.4
	Entire BPS	1.18	1.88	1.59

CONCLUSIONS

As a result of the conducted study computational phantoms of the main skeletal sites with active hematopoiesis have been developed for a ten-year-old child. These phantoms were elaborated based on the SPSD method similar to the phantoms developed for other age groups. The obtained phantoms imitate the structure of the bone tissue. These sets demonstrate the population variability of the dimensions of the structure of certain skeletal bones. The provided phantom representing a ten-year-old child will further be used to calculate DF for ^{89,90}Sr, which

in their turn are necessary for the assessment of the improved coefficients linking the individual radionuclide intake to dose to RBM. It will enable the dose estimates improvement for the residents of the Urals region. For the future studies we plan to develop SPSD-phantoms of the skeleton of men and women aged 15, and for adults. The given phantoms could be used for the dosimetry of incorporated bone-seeking beta-emitters in the population, in case of the contamination of the environment with radionuclides, and for the dosimetry of other beta-emitting radionuclides including those used in radionuclide therapy, such as ^{89}Sr, ^{32}P, ^{186}Re, ^{188}Re, ^{117}mSn.

References

1. Sources and effects of ionizing radiation. UNSCEAR 2000 Report to the General Assembly, with Scientific Annexes/ United Nations. New York, 2000; 1229 c.
2. Degteva MO, Shagina NB, Vorobiova MI, Shishkina EA, Tolstykh EI, Akleyev AV. Contemporary Understanding of Radioactive Contamination of the Techa River in 1949–1956. Radiats Biol Radioecol. 2016; 56 (5): 523–34. PMID: 30703313.
3. Krestinina LY, Epifanova S, Silkin S, Mikryukova L, Degteva M, Shagina N, et al. Chronic low-dose exposure in the Techa River Cohort: risk of mortality from circulatory diseases. Radiat Environ Biophys. 2013; 52 (1): 47–57. DOI: 10.1007/s00411-012-0438-5. Epub 2012 Nov 4.
4. Akleev AV. Hronicheskij luchevoj sindrom u zhitelej pribrezhnyh sel reki Techa. Cheljabinsk: Kniga, 2012; 464 s. Russian.
5. Preston DL, Sokolnikov ME, Krestinina LY, Stram DO. Estimates of Radiation Effects on Cancer Risks in the Mayak Worker, Techa River and Atomic Bomb Survivor Studies. Radiat Prot Dosimetry. 2017; 173 (1–3): 26–31. DOI: 10.1093/rpd/ncw316.
6. Degteva MO, Napier BA, Tolstykh EI, et al. Enhancements in the Techa River Dosimetry System: TRDS-2016D Code for Reconstruction of Deterministic Estimates of Dose From Environmental Exposures. Health Phys. 2019; 117 (4): 378–87. DOI: 10.1097/HP.0000000000001067.
7. Spiers FW, Beddoe AH, Whitwell JR. Mean skeletal dose factors for beta-particle emitters in human bone. Part I: volume-seeking radionuclides. The British journal of radiology. 1978; 51 (608): 622–7.
8. O'Reilly SE, DeWeese LS, Maynard MR, Rajon DA, Wayson MB, Marshall EL, et al. An 13 image-based skeletal dosimetry model for the ICRP reference adult female-internal electron 14 sources.

Phys Med Biol. 2016; 61 (24): 8794–24. Epub 2016 Nov 29.
9. Xu XG, Chao TC, Bozkurt A. VIP-Man: an image-based whole-body adult male model constructed from color photographs of the Visible Human Project for multi-particle Monte Carlo calculations. Health Phys. 2000; 78 (5): 476–86. DOI: 10.1097/00004032-200005000-00003. PMID: 10772019.
10. Shah AP, Bolch WE, Rajon DA, Patton PW, Jokisch DW. A paired-image radiation transport model for skeletal dosimetry. J Nucl Med. 2005; 46 (2): 344–53. PMID: 15695796.
11. Pafundi D. Image-based skeletal tissues and electron dosimetry models for the ICRP reference pediatric age series. A dissertation presented to the graduate schools of the University of Florida in partial fulfillment of the requirements for the degree of doctor of the philosophy. University of Florida. 2009.
12. Hough M, Johnson P, Rajon D, Jokisch D, Lee C, Bolch W. An image-based skeletal dosimetry model for the ICRP reference adult male–internal electron sources. Phys Med Biol. 2011; 56 (8): 2309–46. DOI: 10.1088/0031-9155/56/8/001. Epub 2011 Mar 22.
13. Bolch WE, Eckerman K, Endo A, et al. ICRP Publication 143: Paediatric Reference Computational Phantoms. Ann ICRP. 2020; 49 (1): 5–297. DOI: 10.1177/0146645320915031.
14. Degteva MO, Tolstykh EI, Shishkina EA, Sharagin PA, Zalyapin VI, Volchkova AY, et al. Stochastic parametric skeletal dosimetry model for humans: General approach and application to active marrow exposure from bone-seeking beta-particle emitters. PLoS ONE. 2021; 16 (10): e0257605. Available from: https://doi.org/10.1371/journal.pone.0257605.
15. Djogteva MO, Shishkina EA, Tolstyh EI, Zaljapin VI, Sharagin PA, Smit MA,

i dr. Metodologicheskij podhod k razrabotke dozimetricheskih modelej skeleta cheloveka dlja beta-izluchajushhih radionuklidov. Radiacionnaja gigiena. 2019; 12 (2). DOI: 10.21514/1998-426X-2019-12-2-66-75. Russian.

16. Volchkova AYu, Sharagin PA, Shishkina EA. Internal bone marrow dosimetry: the effect of the exposure due to 90Sr incorporated in the adjacent bone segments. Bulletin of the South Ural State University. Ser. Mathematical Modelling, Programming & Computer Software. 2022; 15 (4): 44–58. DOI: 10.14529/mmp220404.

17. Shishkina EA, Sharagin PA, Volchkova AYu. Analiticheskoe opisanie dozoobrazovanija v kostnom mozge ot 90Sr, inkorporirovannogo v kal'cificirovannyh tkanjah. Voprosy radiacionnoj bezopasnosti. 2021; 3: 72–82. Russian.

18. Silkin SS, Krestinina LYu, Starcev NV, Akleev AV. Ural'skaja kogorta avarijno-obluchennogo naselenija. Medicina jekstremal'nyh situacij. 2019; 21 (3): 393–402. Russian.

19. Sharagin PA, Shishkina EA, Tolstykh EI. Computational phantom for red bone marrow dosimetry from incorporated beta emitters in a newborn baby. Extreme Medicine. 2022; 4: 74–82. DOI: 10.47183/mes.2022.045. Russian.

20. Sharagin PA, Shishkina EA, Tolstykh EI. Computational red bone marrow dosimetry phantom of a one-year-old child enabling assessment of exposure due to incorporated beta emitters. Extreme Medicine. 2023; 3: 44–55. DOI: 10.47183/mes.2023.030. Russian.

21. Sharagin PA, Tolstykh EI, Shishkina EA. Computational phantom for a 5-year-old child red bone marrow dosimetry due to incorporated beta emitters. Extreme Medicine. 2023; (4): 79–90. DOI: 10.47183/mes.2023.061. Russian.

22. Cristy M. Active bone marrow distribution as a function of age in humans. Phys Med Biol. 1981; 26 (3): 389–400. 1981.

23. Tolstyh EI, Sharagin PA, Shishkina EA, Volchkova AYu, Degteva MO. Anatomo-morfologicheskij bazis dlja dozimetricheskogo modelirovanija trabekuljarnoj kosti cheloveka s ispol'zovaniem stohasticheskogo parametricheskogo podhoda. Klinicheskij vestnik GNC FMBC im. A. I. Burnazjana. 2022; 3: 25–40. Russian.

24. Tolstyh EI, Sharagin PA, Shishkina EA, Degteva MO. Formirovanie doz obluchenija krasnogo kostnogo mozga cheloveka ot 89,90Sr, ocenka parametrov trabekuljarnoj kosti dlja dozimetricheskogo modelirovanija. V sbornike: Materialy mezhdunarodnoj nauchnoj konferencii «Sovremennye problemy radiobiologii». Belarus', Gomel', 23–24 sentjabrja 2021. 2021; s. 176–179. Russian.

25. Sharagin PA, Tolstyh EI, Shishkina EA, Degteva MO. Dozimetricheskoe modelirovanie kosti dlja osteotropnyh beta-izluchajushhih radionuklidov: razmernye parametry i segmentacija. V sbornike: Materialy mezhdunarodnoj nauchnoj konferencii «Sovremennye problemy radiobiologii». Belarus', Gomel', 23–24 sentjabrja 2021. 2021; s. 200–204. Russian.

26. Sharagin PA, Shishkina EA, Tolstykh EI, Volchkova AYu, Smith MA, Degteva MO. Segmentation of hematopoietic sites of human skeleton for calculations of dose to active marrow exposed to bone-seeking radionuclides. In: RAD Conference Proceedings. 2018; (3): 154–58. DOI: 10.21175/RadProc.2018.33.

27. Valentin J. Basic anatomical and physiological data for use in radiological protection: reference values. Annals of the ICRP. Annals of the ICRP. 2002; 32 (3–4): 1–277.

28. Woodard HQ and White DR. The composition of body tissues. Br J Ru&ol. 1986; 59: 1209–18.

29. Shishkina EA, Timofeev YS, Volchkova AY, Sharagin PA, Zalyapin VI, Degteva MO, et al. Trabecula: A Random Generator of Computational Phantoms for Bone Marrow Dosimetry. Health Phys. 2020; 118 (1): 53–59. DOI: 10.1097/HP.0000000000001127.

30. Zalyapin VI, Timofeev YuS, Shishkina EA. A parametric stochastic model of bone geometry. Bulletin of Southern Urals State University, Issue «Mathematical Modelling. Programming & Computer Software» (SUSU MMCS) 2018; 11 (2): 44–57. DOI: 10.14529/mmp180204.

31. Robinson RA. Chemical analysis and electron microscopy of bone. In: Bone as a tissue, ed. by Rodahl K, Nicholson JT, Brown EM. New York: McGraw-Hill, 1960; p. 186–250.

32. Vogler JB 3rd, Murphy WA. Bone marrow imaging. Radiology. 1988; 168 (3): 679–93.

33. Vande Berg BC, Malghem J, Lecouvet FE, Maldague B. Magnetic resonance imaging of the normal bone marrow. Skeletal Radiology. 1998; 27: 471–83.

34. Vande Berg BC, Malghem J, Lecouvet FE, Maldague B. Magnetic resonance imaging of normal bone marrow. Eur Radiol. 1998; 8 (8): 1327–34.

35. Taccone A, Oddone M, Dell'Acqua AD, Occhi M, Ciccone MA. MRI "road-map" of normal age-related bone marrow. II. Thorax, pelvis and extremities. Pediatr Radiol. 1995; 25 (8): 596–606. PubMed PMID: 8570312.

36. Taccone A, Oddone M, Occhi M, Dell'Acqua AD, Ciccone MA. MRI "road-map" of normal age-related bone marrow. I. Cranial bone and spine. Pediatr Radiol. 1995; 25 (8): 588–95. PubMed PMID: 8570311.

37. Milovanovic P, Djonic D, Hahn M, Amling M, Busse B, Djuric M. Region-dependent patterns of trabecular bone growth in the human proximal femur: A study of 3D bone microarchitecture from early postnatal to late childhood period. Am J Phys Anthropol. 2017; 164 (2): 281–91. DOI: 10.1002/ajpa.23268. Epub 2017 Jun 20.

38. Ryan TM, Krovitz GE. Trabecular bone ontogeny in the human proximal femur. J Hum Evol. 2006; 51 (6): 591–602.

39. Cunningham C, Scheuer L, Black S. Developmental Juvenile Osteology. Second Edition. Elsevier Academic Press. 2016.

40. man JH, Ketcham RA. Patterns in ontogeny of human trabecular bone from SunWatch Village in the Prehistoric Ohio Valley: general features of microarchitectural change. Am J Phys Anthropol. 2009; 138 (3): 318–32. DOI: 10.1002/ajpa.20931. PubMed PMID: 18785633.

41. Glorieux FH, Travers R, Taylor A, Bowen JR, Rauch F, Norman M, Parfitt AM. Normative data for iliac bone histomorphometry in growing children. Bone. 2000; 26 (2): 103–9.

42. Gao S, Ren L, Qui R, Wu Z, Li C, Li J. Electron absorbed fractions in an image-based microscopic skeletal dosimetry model of chinese adult male. Radiat Prot Dosimetry. 2017; 175 (4): 450–59.

43. Pafundi D. Image-based skeletal tissues and electron dosimetry models for the ICRP reference pediatric age series. A dissertation presented to the graduate schools of the University of Florida in partial fulfillment of the requirements for the degree of doctor of the philosophy University of Florida. 2009.

44. Ryan TM, Raichlen DA, Gosman JH. Structural and Mechanical Changes in Trabecular Bone during Early Development in the Human Femur and Humerus. Chapter 12. In: Building Bones: Bone Formation and Development in Anthropology. Cambridge University Press 2017; 281–302. Available from: https://doi.org/10.1017/9781316388907.013.

45. Milenković P. Age Estimation Based on Analyses of Sternal End of Clavicle and the First Costal Cartilage Doctoral Dissertation. University OF Belgrade School of Medicine. Belgrade, 2013.

46. Kirmani S, Christen D, van Lenthe GH, Fischer PR, Bouxsein ML, McCready LK, Melton LJ 3rd, Riggs BL, Amin S, Müller R, Khosla S. Bone structure at the distal radius during adolescent growth. J Bone Miner Res. 2009; 24 (6): 1033–42. DOI: 10.1359/jbmr.081255.

47. Mitchell DM, Caksa S, Yuan A, Bouxsein ML, Misra M, Burnett-Bowie SM. Trabecular Bone Morphology Correlates Wwith Skeletal Maturity and Body Composition in Healthy Adolescent Girls. J Clin Endocrinol Metab. 2018; 103 (1): 336–45. DOI: 10.1210/jc.2017-01785.

48. Li X, Williams P, Curry EJ, Choi D, Craig EV, Warren RF, et al. Trabecular Bone Microarchitecture and Characteristics in Different Regions of the Glenoid. Orthopedics. 2015; 38 (3): 163–68.

49. Knowles NK, G Langohr GD, Faieghi M, Nelson A, Ferreira LM. Development of a validated glenoid trabecular density-modulus relationship. J Mech Behav Biomed Mater. 2019; 90: 140–45. DOI: 10.1016/j.jmbbm.2018.10.013.

50. Jun BJ, Vasanji A, Ricchetti ET, Rodriguez E, Subhas N, Li ZM, Iannotti JP.Quantification of regional variations in glenoid trabecular bone architecture and mineralization using clinical computed tomography images. J Orthop Res. 2018; 36 (1): 85–96. DOI: 10.1002/jor.23620.

51. Frich LH, Odgaard A, Dalstra M. Glenoid bone architecture J Shoulder Elbow Surg. 1998; 7 (4): 356–61.

52. Kneissel M, Roschger P, Steiner W, et al. Cancellous bone structure in the growing and aging lumbar spine in a historic Nubian population. Calcif Tissue Int. 1997; 61 (2): 95–100. DOI:

10.1007/s002239900302.

53. Arbabi A. A quantitative analysis of the structure of human sternum. J Med Phys. 2009; 34 (2): 80–86.

54. Bartl R, Frisch B. Biopsy of bone in internal medicine — an atlas and sourcebook. Kluwer Academic Publishers, Dordrecht. London, 1993.

55. Baur-Melnyk A. Magnetic Resonance Imaging of the Bone Marrow. Springer Science & Business Media, 2012.

56. Byers S, Moore AJ, Byard RW, Fazzalari NL. Quantitative histomorphometric analysis of the human growth plate from birth to adolescence. Bone. 2000; 27 (4): 495–501.

57. Florence JL. Linear and cortical bone dimensions as indicators of health status in subadults from the Milwaukee County Poor Farm Cemetery. M.A., University of Colorado at Denver, 2007.

58. Maresh MM. Measurements from roentgenograms. In: R.W. McCammon, editor. Human Growth and Development. Springfield, IL: Charles C. Thomas, 1970; 157–200.

59. Singh SP, Malhotra P, Sidhu LS, Singh PP. Skeletal Frame Size of Spitian Children. Journal of Human Ecology. 2007; 21 (3): 227–30.

60. Zivicnjak M, Smolej Narancić N, Szirovicza L, Franke D, Hrenović J, Bisof V, Tomas Z, Skarić-Jurić T. Gender-specific growth patterns of transversal body dimensions in Croatian children and youth (2 to 18 years of age). Coll Antropol. 2008; 32 (2): 419–31. PubMed PMID: 18756891.

61. Svadovskij BS. Vozrastnaja perestrojka kostnoj tkani. O roste i razvitii diafizov plechevoj i bedrennoj kostej. M.: Izd-vo akad. ped. nauk RSFSR, 1961; 110 s.

62. Miles AEW. Growth Curves of Immature Bones from a Scottish Island Population of Sixteenth to mid-Nineteenth Century: Limb-bone Diaphyses and Some Bones of the Hand and Foot. International Journal of Osteoarcheology. 1994; 4: 121–36.

63. Gosman JH, Ketcham RA. Patterns in ontogeny of human trabecular bone from SunWatch Village in the Prehistoric Ohio Valley: general features of microarchitectural change. Am J Phys Anthropol. 2009; 138 (3): 318–32. DOI:10.1002/ajpa.20931. PubMed PMID: 18785633.

64. Petit MA, McKay HA, MacKelvie KJ, Heinonen A, Khan KM, Beck TJ. A randomized school-based jumping intervention confers site and maturity-specific benefits on bone structural properties in girls: a hip structural analysis study. J Bone Miner Res. 2002; 17 (3): 363–72. PubMed PMID: 11874228.

65. Danforth ME, Wrobel GD, Armstrong CW, Swanson D. Juvenile age estimation using diaphyseal long bone lengths among ancient Maya populations. Latin American Antiquity. 2017; 20 (1): 3–13.

66. Beresheim AC, Pfeiffer S, Grynpas M. Ontogenetic changes to bone microstructure in an archaeologically derived sample of human ribs. J Anat. 2019. DOI: 10.1111/joa.13116.

67. Pfeiffer S. Cortical Bone Histology in Juveniles. Available from: https://www.researchgate.net/publication/303179375_Cortical_bone_histology_in_Juveniles

68. Hresko AM, Hinchcliff EM, Deckey DG, Hresko MT. Developmental sacral morphology: MR study from infancy to skeletal maturity. Eur Spine J. 2020; Available from: https://doi.org/10.1007/s00586-020-06350-6.

69. Kuznecov LE. Perelomy taza u detej (morfologija, biomehanika, diagnostika). Moskva: Folium, 1994; 192 s. Russian.

70. Bernert Zs, Évinger S, Hajdu T. New data on the biological age estimation of children using bone measurements based on historical populations from the Carpathian Basin. Annales Historico-Naturales Musei Nationalis Hungarici. 2007; 99: 199–206.

71. Sadofyeva VI. Normal X-ray anatomy of the bone-joint system of children. Leningrad "Medicine" Leningrad branch 1990. Russian.

72. White TD, Black MT, Folkens PA. Human osteology: Third edition. Human Osteology: Third Edition. 2011; 1–662.

73. Mavrych V, Bolgova O, Ganguly P and Kashchenko S. Age-Related Changes of Lumbar Vertebral Body Morphometry. Austin J Anat. 2014; 1 (3): 7.

74. Kindler JM, Pollock NK, Laing EM, et al. Insulin Resistance and the IGF-I-Cortical Bone Relationship in Children Ages 9 to 13 Years. J Bone Miner Res. 2017; 32 (7): 1537–1545. DOI: 10.1002/jbmr.3132.

75. Farr JN, Khosla S. Skeletal changes through the lifespan–from growth to senescence. Nat Rev Endocrinol. 2015; 11 (9): 513–21. DOI: 10.1038/nrendo. 2015.89. Epub 2015 Jun 2. Review. PubMed PMID: 26032105; PubMed Central PMCID: PMC4822419.

76. Gindhart PS. Growth Standards for the Tibia and Radius in Children Aged One Month through Eighteen Years. Am J Phys Anthrop. 1973; 39: 41–48.

77. Lopez-Costas O, Rissech C, Trancho G, Turbón D. Postnatal ontogenesis of the tibia. Implications for age and sex estimation. Forensic Sci Int. 2012; 214 (1–3): 207.e1–11. DOI: 10.1016/j.forsciint.2011.07.038. Epub 2011. PubMed PMID: 21862250.

78. Blake KAS. An investigation of sex determination from the subadult pelvis: A morphometric analysis. Doctoral Dissertation, University of Pittsburgh, 2011.

79. Cunningham CA, Black SM. Iliac cortical thickness in the neonate — the gradient effect. J Anat. 2009a Sep; 215 (3): 364–70. DOI: 10.1111/j.1469-7580.2009.01112.x.

80. Cunningham CA, Black SM. Anticipating bipedalism: trabecular organization in the newborn ilium. J Anat. 2009b Jun; 214 (6): 817–29. DOI: 10.1111/j.1469-7580.2009.01073.x

81. Rissech C, García M, Malgosa A. Sex and age diagnosis by ischium morphometric analysis. Forensic Science International. 2003; 135: 188–96.

82. Rissech C, Malgosa A. Pubis growth study: Applicability in sexual and age diagnostic. Forensic Science International. 2007; 173: 137–45.

83. Corron L, Marchal F, Condemi S, Chaumoître K, Adalian P. A New Approach of Juvenile Age Estimation using Measurements of the Ilium and Multivariate Adaptive Regression Splines (MARS) Models for Better Age Prediction. Forensic Sci. 2017; 62 (1): 18–29. DOI: 10.1111/1556-4029.13224.

84. Parfitt AM, Travers R, Rauch F, Glorieux FH. Structural and cellular changes during bone growth in healthy children. Bone. 2000; 27 (4): 487–94. PMID: 11033443.

85. Schnitzler CM, Mesquita JM, Pettifor JM. Cortical bone development in black and white South African children: iliac crest histomorphometry. Bone. 2009; 44 (4): 603–11. DOI: 10.1016/j.bone.2008.12.009.

86. De Boer HH, Van der Merwe AE, Soerdjbalie-Maikoe VV. Human cranial vault thickness in a contemporary sample of 1097 autopsy cases: relation to body weight, stature, age, sex and ancestry. Int J Legal Med. 2016; 130 (5): 1371–7. DOI: 10.1007/s00414-016-1324-5.

87. Margulies S, Coats B. Experimental Injury Biomechanics of the Pediatric Head and Brain. Chapter 4 in: Pediatric Injury Biomechanics Springer Science + Business Media New York. 2013; 157–90.

88. McGraw MA, Mehlman CT, Lindsell CJ, Kirby CL. Postnatal growth of the clavicle: birth to eighteen years of age. Journal of Pediatric Orthopedics. 2009; 29: 937

89. Bernat A, Huysmans T, Van Glabbeek F, Sijbers J, Gielen J, Van Tongel A. The anatomy of the clavicle: a three-dimensional cadaveric study. Clin Anat. 2014; 27 (5): 712–23

90. Corron L. Juvenile age estimation in physical anthropology: A critical review of existing methods and the application of two standardised methodological approaches. Biological anthropology. Aix-Marseille Universite. English, 2016.

91. Saunders S, Hoppa R, Southern R. Diaphyseal growth in a nineteenth-century skeletal sample of subadults from St Thomas' Church, Belleville, Ontario. International Journal of Osteoarchaeology. 1993; 3: 265–81.

92. Badr El Dine F, Hassan H. Ontogenetic study of the scapula among some Egyptians: Forensic implications in age and sex estimation using Multidetector Computed Tomography, Egyptian Journal of Forensic Sciences. 2015; 6 (2): 56–77.

93. Rissech C, Black S. Scapular development from neonatal period to skeletal maturity. A preliminary study. Int J Osteoarchaeol. 2007; 17: 451–64.

94. Bayaroğullan H, Yengil E, Davran R, Ağlagül E, Karazincir S, Balcı A. Evaluation of the postnatal development of the sternum and sternal variations using multidetector CT. Diagn Interv Radiol. 2014; 20 (1): 82–9.

95. Weaver AA, Schoell SL, Nguyen CM, Lynch SK, Stitzel JD. Morphometric analysis of variation in the sternum with sex and age. J Morphol. 2014; 275 (11): 1284–99.

96. Johnson KT, Al-Holou WN, Anderson RC, Wilson TJ, Karnati T, et al. Morphometric analysis of the developing pediatric cervical spine. J Neurosurg Pediatr. 2016; 18 (3): 377–89. DOI: 10.3171/2016.3.PEDS1612. Epub 2016 May 27. PubMed PMID: 27231821.

97. Caldas Md P, Ambrosano GM, Haiter Neto F. New formula to objectively evaluate skeletal maturation using lateral cephalometric radiographs. Braz Oral Res. 2007; 21 (4): 330–5. PubMed PMID: 18060260

98. Peters JR, Chandrasekaran C, Robinson LF, Servaes SE, Campbell RM Jr, Balasubramanian S. Age- and gender-related changes in pediatric thoracic vertebral morphology. Spine J. 2015; 15 (5): 1000–1020. DOI: 10.1016/j.spinee.2015.01.016.

99. Peters JR, Servaes SE, Cahill PJ, Balasubramanian S. Morphology and growth of the pediatric lumbar vertebrae. Spine J. 2021; 21 (4): 682–97. DOI: 10.1016/j.spinee.2020.10.029.

100. Newman SL, Gowland RL. The use of non-adult vertebral dimensions as indicators of growth disruption and non-specific health stress in skeletal populations. American journal of physical anthropology. 2015; 158 (1): 155–64.

101. Comeau A. Age-related Changes in Geometric Characteristics of the Pediatric Thoracic Cage and Comparison of Thorax Shape with a Pediatric CPR Manikin. PhD thesis. 2010

102. Knirsch W, Kurtz C, Häffner N, Langer M, Kececioglu D. Normal values of the sagittal diameter of the lumbar spine (vertebral body and dural sac) in children measured by MRI. Pediatr Radiol. 2005; 35: 419–24. Available from: https://doi.org/10.1007/s00247-004-1382-6.

Литература

1. Sources and effects of ionizing radiation. UNSCEAR 2000 Report to the General Assembly, with Scientific Annexes/ United Nations. New York, 2000; 1229 с.

2. Degteva MO, Shagina NB, Vorobiova MI, Shishkina EA, Tolstykh EI, Akleyev AV. Contemporary Understanding of Radioactive Contamination of the Techa River in 1949–1956. Radiats Biol Radioecol. 2016; 56 (5): 523–34. PMID: 30703313.

3. Krestinina LY, Epifanova S, Silkin S, Mikryukova L, Degteva M, Shagina N, et al. Chronic low-dose exposure in the Techa River Cohort: risk of mortality from circulatory diseases. Radiat Environ Biophys. 2013; 52 (1): 47–57. DOI: 10.1007/s00411-012-0438-5. Epub 2012 Nov 4.

4. Аклеев А. В. Хронический лучевой синдром у жителей прибрежных сел реки Теча. Челябинск: Книга, 2012; 464 с.

5. Preston DL, Sokolnikov ME, Krestinina LY, Stram DO. Estimates of Radiation Effects on Cancer Risks in the Mayak Worker, Techa River and Atomic Bomb Survivor Studies. Radiat Prot Dosimetry. 2017; 173 (1–3): 26–31. DOI: 10.1093/rpd/ncw316.

6. Degteva MO, Napier BA, Tolstykh EI, et al. Enhancements in the Techa River Dosimetry System: TRDS-2016D Code for Reconstruction of Deterministic Estimates of Dose From Environmental Exposures. Health Phys. 2019; 117 (4): 378–87. DOI: 10.1097/HP.0000000000001067.

7. Spiers FW, Beddoe AH, Whitwell JR. Mean skeletal dose factors for beta-particle emitters in human bone. Part I: volume-seeking radionuclides. The British journal of radiology. 1978; 51 (608): 622–7.

8. O'Reilly SE, DeWeese LS, Maynard MR, Rajon DA, Wayson MB, Marshall EL, et al. An 13 image-based skeletal dosimetry model for the ICRP reference adult female-internal electron 14 sources. Phys Med Biol. 2016; 61 (24): 8794–24. Epub 2016 Nov 29.

9. Xu XG, Chao TC, Bozkurt A. VIP-Man: an image-based whole-body adult male model constructed from color photographs of the Visible Human Project for multi-particle Monte Carlo calculations. Health Phys. 2000; 78 (5): 476–86. DOI: 10.1097/00004032-200005000-00003. PMID: 10772019.

10. Shah AP, Bolch WE, Rajon DA, Patton PW, Jokisch DW. A paired-image radiation transport model for skeletal dosimetry. J Nucl Med. 2005; 46 (2): 344–53. PMID: 15695796.

11. Pafundi D. Image-based skeletal tissues and electron dosimetry models for the ICRP reference pediatric age series. A dissertation presented to the graduate schools of the University of Florida in partial fulfillment of the requirements for the degree of doctor of the philosophy. University of Florida. 2009.

12. Hough M, Johnson P, Rajon D, Jokisch D, Lee C, Bolch W. An image-based skeletal dosimetry model for the ICRP reference adult male–internal electron sources. Phys Med Biol. 2011; 56 (8): 2309–46. DOI: 10.1088/0031-9155/56/8/001. Epub 2011 Mar 22.

13. Bolch WE, Eckerman K, Endo A, et al. ICRP Publication 143: Paediatric Reference Computational Phantoms. Ann ICRP. 2020; 49 (1): 5–297. DOI: 10.1177/0146645320915031.

14. Degteva MO, Tolstykh EI, Shishkina EA, Sharagin PA, Zalyapin VI, Volchkova AY, et al. Stochastic parametric skeletal dosimetry model for humans: General approach and application to active marrow exposure from bone-seeking beta-particle emitters. PLoS ONE. 2021; 16 (10): e0257605. Available from: https://doi.org/10.1371/journal.pone.0257605.

15. Дёгтева М. О., Шишкина Е. И., Толстых Е. И., Заляпин В. И., Шарагин П. А., Смит М. А., и др. Методологический подход к разработке дозиметрических моделей скелета человека для бета-излучающих радионуклидов. Радиационная гигиена. 2019; 12 (2). DOI: 10.21514/1998-426X-2019-12-2-66-75.

16. Volchkova AYu, Sharagin PA, Shishkina EA. Internal bone marrow dosimetry: the effect of the exposure due to 90Sr incorporated in the adjacent bone segments. Bulletin of the South Ural State University. Ser. Mathematical Modelling, Programming & Computer Software. 2022; 15 (4): 44–58. DOI: 10.14529/mmp220404.

17. Шишкина Е. А., Шарагин П. А., Волчкова А. Ю. Аналитическое описание дозообразования в костном мозге от 90Sr, инкорпорированного в кальцифицированных тканях. Вопросы радиационной безопасности. 2021; 3: 72–82.

18. Силкин С. С., Крестинина Л. Ю., Старцев Н. В., Аклеев А. В. Уральская когорта аварийно-облученного населения. Медицина экстремальных ситуаций. 2019; 21 (3): 393–402.

19. Шарагин П. А., Шишкина Е. А., Толстых Е. И. Вычислительный фантом для дозиметрии красного костного мозга новорожденного ребенка от инкорпорированных бета-излучателей. Медицина экстремальных ситуаций. 2022; (4): 74–82. DOI: 10.47183/mes.2022.045.

20. Шарагин, П. А., Шишкина, Е. А., Толстых, Е. И. Вычислительный фантом для дозиметрии красного костного мозга годовалого ребенка от инкорпорированных бета-излучателей. Медицина экстремальных ситуаций. 2023, (3): 44 –55. DOI: 10.47183/mes.2023.030.

21. Шарагин П. А., Толстых Е. И., Шишкина Е. А. Вычислительный фантом для дозиметрии красного костного мозга пятилетнего ребенка от инкорпорированных бета-излучателей. Медицина экстремальных ситуаций. 2023; (4): 86–97. DOI: 10.47183/mes.2023.061.

22. Cristy M. Active bone marrow distribution as a function of age in humans. Phys Med Biol. 1981; 26 (3): 389–400. 1981.

23. Толстых Е. И., Шарагин П. А., Шишкина Е. А., Волчкова А. Ю. Дегтева М. О. Анатомо-морфологический базис для дозиметрического моделирования трабекулярной кости человека с использованием стохастического параметрического подхода. Клинический вестник ГНЦ ФМБЦ им. А. И. Бурназяна. 2022; 3: 25–40.

24. Толстых Е. И., Шарагин П. А., Шишкина Е. А., Дегтева М. О. Формирование доз облучения красного костного мозга человека от ^{89,90}Sr, оценка параметров трабекулярной кости для дозиметрического моделирования. В сборнике: Материалы международной научной конференции «Современные проблемы радиобиологии». Беларусь, Гомель, 23–24 сентября 2021. 2021; с. 176–179.

25. Шарагин П. А., Толстых Е. И., Шишкина Е. А., Дегтева М. О. Дозиметрическое моделирование кости для остеотропных бета-излучающих радионуклидов: размерные параметры и сегментация. В сборнике: Материалы международной научной конференции «Современные проблемы радиобиологии». Беларусь, Гомель, 23–24 сентября 2021. 2021; с. 200–204.

26. Sharagin PA, Shishkina EA, Tolstykh EI, Volchkova AYu, Smith MA, Degteva MO. Segmentation of hematopoietic sites of human skeleton for calculations of dose to active marrow exposed to bone-seeking radionuclides. In: RAD Conference Proceedings. 2018; (3): 154–58. DOI: 10.21175/RadProc.2018.33.

27. Valentin J. Basic anatomical and physiological data for use in

radiological protection: reference values. Annals of the ICRP. Annals of the ICRP. 2002; 32 (3–4): 1–277.

28. Woodard HQ and White DR. The composition of body tissues. Br J Ru&ol. 1986; 59: 1209–18.

29. Shishkina EA, Timofeev YS, Volchkova AY, Sharagin PA, Zalyapin VI, Degteva MO, et al. Trabecula: A Random Generator of Computational Phantoms for Bone Marrow Dosimetry. Health Phys. 2020; 118 (1): 53–59. DOI: 10.1097/HP.0000000000001127.

30. Zalyapin VI, Timofeev YuS, Shishkina EA. A parametric stochastic model of bone geometry. Bulletin of Southern Urals State University, Issue «Mathematical Modelling. Programming & Computer Software» (SUSU MMCS) 2018; 11 (2): 44–57. DOI: 10.14529/mmp180204.

31. Robinson RA. Chemical analysis and electron microscopy of bone. In: Bone as a tissue, ed. by Rodahl K, Nicholson JT, Brown EM. New York: McGraw-Hill, 1960; p. 186–250.

32. Vogler JB 3rd, Murphy WA. Bone marrow imaging. Radiology. 1988; 168 (3): 679–93.

33. Vande Berg BC, Malghem J, Lecouvet FE, Maldague B. Magnetic resonance imaging of the normal bone marrow. Skeletal Radiology. 1998; 27: 471–83.

34. Vande Berg BC, Malghem J, Lecouvet FE, Maldague B. Magnetic resonance imaging of normal bone marrow. Eur Radiol. 1998; 8 (8): 1327–34.

35. Taccone A, Oddone M, Dell'Acqua AD, Occhi M, Ciccone MA. MRI "road-map" of normal age-related bone marrow. II. Thorax, pelvis and extremities. Pediatr Radiol. 1995; 25 (8): 596–606. PubMed PMID: 8570312.

36. Taccone A, Oddone M, Occhi M, Dell'Acqua AD, Ciccone MA. MRI "road-map" of normal age-related bone marrow. I. Cranial bone and spine. Pediatr Radiol. 1995; 25 (8): 588–95. PubMed PMID: 8570311.

37. Milovanovic P, Djonic D, Hahn M, Amling M, Busse B, Djuric M. Region-dependent patterns of trabecular bone growth in the human proximal femur: A study of 3D bone microarchitecture from early postnatal to late childhood period. Am J Phys Anthropol. 2017; 164 (2): 281–91. DOI: 10.1002/ajpa.23268. Epub 2017 Jun 20.

38. Ryan TM, Krovitz GE. Trabecular bone ontogeny in the human proximal femur. J Hum Evol. 2006; 51 (6): 591–602.

39. Cunningham C, Scheuer L, Black S. Developmental Juvenile Osteology. Second Edition. Elsevier Academic Press. 2016.

40. man JH, Ketcham RA. Patterns in ontogeny of human trabecular bone from SunWatch Village in the Prehistoric Ohio Valley: general features of microarchitectural change. Am J Phys Anthropol. 2009; 138 (3): 318–32. DOI: 10.1002/ajpa.20931. PubMed PMID: 18785633.

41. Glorieux FH, Travers R, Taylor A, Bowen JR, Rauch F, Norman M, Parfitt AM. Normative data for iliac bone histomorphometry in growing children. Bone. 2000; 26 (2): 103–9.

42. Gao S, Ren L, Qui R, Wu Z, Li C, Li J. Electron absorbed fractions in an image-based microscopic skeletal dosimetry model of chinese adult male. Radiat Prot Dosimetry. 2017; 175 (4): 450–59.

43. Pafundi D. Image-based skeletal tissues and electron dosimetry models for the ICRP reference pediatric age series. A dissertation presented to the graduate schools of the University of Florida in partial fulfillment of the requirements for the degree of doctor of the philosophy University of Florida. 2009.

44. Ryan TM, Raichlen DA, Gosman JH. Structural and Mechanical Changes in Trabecular Bone during Early Development in the Human Femur and Humerus. Chapter 12. In: Building Bones: Bone Formation and Development in Anthropology. Cambridge University Press 2017; 281–302. Available from: https://doi.org/10.1017/9781316388907.013.

45. Milenković P. Age Estimation Based on Analyses of Sternal End of Clavicle and the First Costal Cartilage Doctoral Dissertation. University OF Belgrade School of Medicine. Belgrade, 2013.

46. Kirmani S, Christen D, van Lenthe GH, Fischer PR, Bouxsein ML, McCready LK, Melton LJ 3rd, Riggs BL, Amin S, Müller R, Khosla S. Bone structure at the distal radius during adolescent growth. J Bone Miner Res. 2009; 24 (6): 1033–42. DOI: 10.1359/jbmr.081255.

47. Mitchell DM, Caksa S, Yuan A, Bouxsein ML, Misra M, Burnett-Bowie SM. Trabecular Bone Morphology Correlates Wwith Skeletal Maturity and Body Composition in Healthy Adolescent Girls. J Clin Endocrinol Metab. 2018; 103 (1): 336–45. DOI: 10.1210/jc.2017-01785.

48. Li X, Williams P, Curry EJ, Choi D, Craig EV, Warren RF, et al. Trabecular Bone Microarchitecture and Characteristics in Different Regions of the Glenoid. Orthopedics. 2015; 38 (3): 163–68.

49. Knowles NK, G Langohr GD, Faieghi M, Nelson A, Ferreira LM. Development of a validated glenoid trabecular density-modulus relationship. J Mech Behav Biomed Mater. 2019; 90: 140–45. DOI: 10.1016/j.jmbbm.2018.10.013.

50. Jun BJ, Vasanji A, Ricchetti ET, Rodriguez E, Subhas N, Li ZM, Iannotti JP.Quantification of regional variations in glenoid trabecular bone architecture and mineralization using clinical computed tomography images. J Orthop Res. 2018; 36 (1): 85–96. DOI: 10.1002/jor.23620.

51. Frich LH, Odgaard A, Dalstra M. Glenoid bone architecture J Shoulder Elbow Surg. 1998; 7 (4): 356–61.

52. Kneissel M, Roschger P, Steiner W, et al. Cancellous bone structure in the growing and aging lumbar spine in a historic Nubian population. Calcif Tissue Int. 1997; 61 (2): 95–100. DOI: 10.1007/s002239900302.

53. Arbabi A. A quantitative analysis of the structure of human sternum. J Med Phys. 2009; 34 (2): 80–86.

54. Bartl R, Frisch B. Biopsy of bone in internal medicine — an atlas and sourcebook. Kluwer Academic Publishers, Dordrecht. London, 1993.

55. Baur-Melnyk A. Magnetic Resonance Imaging of the Bone Marrow. Springer Science & Business Media, 2012.

56. Byers S, Moore AJ, Byard RW, Fazzalari NL. Quantitative histomorphometric analysis of the human growth plate from birth to adolescence. Bone. 2000; 27 (4): 495–501.

57. Florence JL. Linear and cortical bone dimensions as indicators of health status in subadults from the Milwaukee County Poor Farm Cemetery. M.A., University of Colorado at Denver, 2007.

58. Maresh MM. Measurements from roentgenograms. In: R.W. McCammon, editor. Human Growth and Development. Springfield, IL: Charles C. Thomas, 1970; 157–200.

59. Singh SP, Malhotra P, Sidhu LS, Singh PP. Skeletal Frame Size of Spitian Children. Journal of Human Ecology. 2007; 21 (3): 227–30.

60. Zivicnjak M, Smolej Narancić N, Szirovicza L, Franke D, Hrenović J, Bisof V, Tomas Z, Skarić-Jurić T. Gender-specific growth patterns of transversal body dimensions in Croatian children and youth (2 to 18 years of age). Coll Antropol. 2008; 32 (2): 419–31. PubMed PMID: 18756891.

61. Свадовский Б. С. Возрастная перестройка костной ткани. О росте и развитии диафизов плечевой и бедренной костей. М.: Изд-во акад. пед. наук РСФСР, 1961; 110 с.

62. Miles AEW. Growth Curves of Immature Bones from a Scottish Island Population of Sixteenth to mid-Nineteenth Century: Limb-bone Diaphyses and Some Bones of the Hand and Foot. International Journal of Osteoarcheology. 1994; 4: 121–36.

63. Gosman JH, Ketcham RA. Patterns in ontogeny of human trabecular bone from SunWatch Village in the Prehistoric Ohio Valley: general features of microarchitectural change. Am J Phys Anthropol. 2009; 138 (3): 318–32. DOI:10.1002/ajpa.20931. PubMed PMID: 18785633.

64. Petit MA, McKay HA, MacKelvie KJ, Heinonen A, Khan KM, Beck TJ. A randomized school-based jumping intervention confers site and maturity-specific benefits on bone structural properties in girls: a hip structural analysis study. J Bone Miner Res. 2002; 17 (3): 363–72. PubMed PMID: 11874228.

65. Danforth ME, Wrobel GD, Armstrong CW, Swanson D. Juvenile age estimation using diaphyseal long bone lengths among ancient Maya populations. Latin American Antiquity. 2017; 20 (1): 3–13.

66. Beresheim AC, Pfeiffer S, Grynpas M. Ontogenetic changes to bone microstructure in an archaeologically derived sample of human ribs. J Anat. 2019. DOI: 10.1111/joa.13116.

67. Pfeiffer S. Cortical Bone Histology in Juveniles. Available from: https://www.researchgate.net/publication/303179375_Cortical_bone_histology_in_Juveniles

68. Hresko AM, Hinchcliff EM, Deckey DG, Hresko MT. Developmental sacral morphology: MR study from infancy to skeletal maturity. Eur Spine J. 2020; Available from: https://doi.org/10.1007/s00586-020-06350-6.

69. Кузнецов Л. Е. Переломы таза у детей (морфология, биомеханика, диагностика). Москва: Фолиум, 1994; 192 с.

70. Bernert Zs, Évinger S, Hajdu T. New data on the biological

age estimation of children using bone measurements based on historical populations from the Carpathian Basin. Annales Historico-Naturales Musei Nationalis Hungarici. 2007; 99: 199–206.

71. Sadofyeva VI. Normal X-ray anatomy of the bone-joint system of children. Leningrad "Medicine" Leningrad branch 1990. Russian

72. White TD, Black MT, Folkens PA. Human osteology: Third edition. Human Osteology: Third Edition. 2011; 1–662.

73. Mavrych V, Bolgova O, Ganguly P and Kashchenko S. Age-Related Changes of Lumbar Vertebral Body Morphometry. Austin J Anat. 2014; 1 (3): 7.

74. Kindler JM, Pollock NK, Laing EM, et al. Insulin Resistance and the IGF-I-Cortical Bone Relationship in Children Ages 9 to 13 Years. J Bone Miner Res. 2017; 32 (7): 1537–1545. DOI: 10.1002/jbmr.3132.

75. Farr JN, Khosla S. Skeletal changes through the lifespan–from growth to senescence. Nat Rev Endocrinol. 2015; 11 (9): 513–21. DOI: 10.1038/nrendo. 2015.89. Epub 2015 Jun 2. Review. PubMed PMID: 26032105; PubMed Central PMCID: PMC4822419.

76. Gindhart PS. Growth Standards for the Tibia and Radius in Children Aged One Month through Eighteen Years. Am J Phys Anthrop. 1973; 39: 41–48.

77. Lopez-Costas O, Rissech C, Trancho G, Turbón D. Postnatal ontogenesis of the tibia. Implications for age and sex estimation. Forensic Sci Int. 2012; 214 (1–3): 207.e1–11. DOI: 10.1016/j.forsciint.2011.07.038. Epub 2011. PubMed PMID: 21862250.

78. Blake KAS. An investigation of sex determination from the subadult pelvis: A morphometric analysis. Doctoral Dissertation, University of Pittsburgh, 2011.

79. Cunningham CA, Black SM. Iliac cortical thickness in the neonate — the gradient effect. J Anat. 2009a Sep; 215 (3): 364–70. DOI: 10.1111/j.1469-7580.2009.01112.x.

80. Cunningham CA, Black SM. Anticipating bipedalism: trabecular organization in the newborn ilium. J Anat. 2009b Jun; 214 (6): 817–29. DOI: 10.1111/j.1469-7580.2009.01073.x

81. Rissech C, Garcıa M, Malgosa A. Sex and age diagnosis by ischium morphometric analysis. Forensic Science International. 2003; 135: 188–96.

82. Rissech C, Malgosa A. Pubis growth study: Applicability in sexual and age diagnostic. Forensic Science International. 2007; 173: 137–45.

83. Corron L, Marchal F, Condemi S, Chaumoître K, Adalian P. A New Approach of Juvenile Age Estimation using Measurements of the Ilium and Multivariate Adaptive Regression Splines (MARS) Models for Better Age Prediction. Forensic Sci. 2017; 62 (1): 18–29. DOI: 10.1111/1556-4029.13224.

84. Parfitt AM, Travers R, Rauch F, Glorieux FH. Structural and cellular changes during bone growth in healthy children. Bone. 2000; 27 (4): 487–94. PMID: 11033443.

85. Schnitzler CM, Mesquita JM, Pettifor JM. Cortical bone development in black and white South African children: iliac crest histomorphometry. Bone. 2009; 44 (4): 603–11. DOI: 10.1016/j.bone.2008.12.009.

86. De Boer HH, Van der Merwe AE, Soerdjbalie-Maikoe VV. Human cranial vault thickness in a contemporary sample of 1097 autopsy cases: relation to body weight, stature, age, sex and ancestry. Int J Legal Med. 2016; 130 (5): 1371–7. DOI: 10.1007/s00414-016-1324-5.

87. Margulies S, Coats B. Experimental Injury Biomechanics of the Pediatric Head and Brain. Chapter 4 in: Pediatric Injury Biomechanics Springer Science + Business Media New York. 2013; 157–90.

88. McGraw MA, Mehlman CT, Lindsell CJ, Kirby CL. Postnatal growth of the clavicle: birth to eighteen years of age. Journal of Pediatric Orthopedics. 2009; 29: 937

89. Bernat A, Huysmans T, Van Glabbeek F, Sijbers J, Gielen J, Van Tongel A. The anatomy of the clavicle: a three-dimensional cadaveric study. Clin Anat. 2014; 27 (5): 712–23

90. Corron L. Juvenile age estimation in physical anthropology: A critical review of existing methods and the application of two standardised methodological approaches. Biological anthropology. Aix-Marseille Universite. English, 2016.

91. Saunders S, Hoppa R, Southern R. Diaphyseal growth in a nineteenth-century skeletal sample of subadults from St Thomas' Church, Belleville, Ontario. International Journal of Osteoarchaeology. 1993; 3: 265–81.

92. Badr El Dine F, Hassan H. Ontogenetic study of the scapula among some Egyptians: Forensic implications in age and sex estimation using Multidetector Computed Tomography, Egyptian Journal of Forensic Sciences. 2015; 6 (2): 56–77.

93. Rissech C, Black S. Scapular development from neonatal period to skeletal maturity. A preliminary study. Int J Osteoarchaeol. 2007; 17: 451–64.

94. Bayaroğulları H, Yengil E, Davran R, Ağlagül E, Karazincir S, Balcı A. Evaluation of the postnatal development of the sternum and sternal variations using multidetector CT. Diagn Interv Radiol. 2014; 20 (1): 82–9.

95. Weaver AA, Schoell SL, Nguyen CM, Lynch SK, Stitzel JD. Morphometric analysis of variation in the sternum with sex and age. J Morphol. 2014; 275 (11): 1284–99.

96. Johnson KT, Al-Holou WN, Anderson RC, Wilson TJ, Karnati T, et al. Morphometric analysis of the developing pediatric cervical spine. J Neurosurg Pediatr. 2016; 18 (3): 377–89. DOI: 10.3171/2016.3.PEDS1612. Epub 2016 May 27. PubMed PMID: 27231821.

97. Caldas Md P, Ambrosano GM, Haiter Neto F. New formula to objectively evaluate skeletal maturation using lateral cephalometric radiographs. Braz Oral Res. 2007; 21 (4): 330–5. PubMed PMID: 18060260

98. Peters JR, Chandrasekaran C, Robinson LF, Servaes SE, Campbell RM Jr, Balasubramanian S. Age- and gender-related changes in pediatric thoracic vertebral morphology. Spine J. 2015; 15 (5): 1000–1020. DOI: 10.1016/j.spinee.2015.01.016.

99. Peters JR, Servaes SE, Cahill PJ, Balasubramanian S. Morphology and growth of the pediatric lumbar vertebrae. Spine J. 2021; 21 (4): 682–97. DOI: 10.1016/j.spinee.2020.10.029.

100. Newman SL, Gowland RL. The use of non-adult vertebral dimensions as indicators of growth disruption and non-specific health stress in skeletal populations. American journal of physical anthropology. 2015; 158 (1): 155–64.

101. Comeau A. Age-related Changes in Geometric Characteristics of the Pediatric Thoracic Cage and Comparison of Thorax Shape with a Pediatric CPR Manikin. PhD thesis. 2010

102. Knirsch W, Kurtz C, Häffner N, Langer M, Kececioglu D. Normal values of the sagittal diameter of the lumbar spine (vertebral body and dural sac) in children measured by MRI. Pediatr Radiol. 2005; 35: 419–24. Available from: https://doi.org/10.1007/s00247-004-1382-6.

THE IMPACT OF POLYMORPHISMS IN ANTIOXIDANT GENES ON THE RISK OF MALIGNANT NEOPLASM DEVELOPMENT IN EXPOSED INDIVIDUALS

Blinova EA ✉, Korechenkova AV, Yanishevskaya MA, Akleyev AV

Urals Research Center for Radiation Medicine of the Federal Medical Biological Agency, Chelyabinsk, Russia

In the context of additional radiation exposure, single nucleotide polymorphisms in the genes encoding the antioxidant system enzymes can contribute to the oxidative stress enhancement, damage to DNA, and therefore lead to the increase in the risk of malignant neoplasm (MN) development. The study was aimed to determine the association of the *CYBA* (rs4673), *GPX1* (rs1050450), *MPO* (rs2333227), *CAT* (rs7943316), *SOD2* (rs4880) polymorphic loci with the risk of MN development in individuals affected by low dose rate chronic radiation exposure considering intergenic interactions and the radiation dose. Two groups of individuals were included in the study: exposed individuals with no MNs — 384 people with the mean accumulated dose to the red bone marrow (RBM) of 796.95 ± 35.97 mGy; exposed individuals with the history of MNs — 227 people with the mean accumulated dose to RBM of 520.06 ± 38.72 mGy. Amplification of the rs4880, rs2333227, rs7943316, rs4673, rs1050450 polymorphic loci was performed with real time PCR. Compliance with the Hardy–Weinberg equilibrium was reported for all gene polymorphisms. It has been found that the rs4880*C (SOD2) and rs1050450*T (*GPX1*) alleles are associated with the risk of MN development in accordance with the dominant (OR = 1.49 (1.02–2.18), $p = 0.04$) and recessive (OR = 2.00 (1.11–3.62), $p = 0.02$) inheritance modes, respectively. An interfactor interaction model with the 100% reproducibility and 66% accuracy ($p = 0.001$) has been obtained that includes the *SOD2* (rs4880), *CYBA* (rs4673) polymorphisms and the factor of accumulated dose to RBM. Thus, polymorphic loci of the genes regulating the oxidative status of the cells are associated with the increased risk of MN development in individuals, who have experienced chronic radiation exposure with predominant exposure of RBM.

Keywords: single nucleotide polymorphism, chronic radiation exposure, Techa River, antioxidant system, malignant neoplasm

✉ **Correspondence should be addressed:** Eugenia A. Blinova
Vorovsky, 68-A, Chelyabinsk, 454141, Russia; blinova@urcrm.ru

ВЛИЯНИЕ ПОЛИМОРФИЗМА В ГЕНАХ АНТИОКСИДАНТОВ НА РИСК РАЗВИТИЯ ЗЛОКАЧЕСТВЕННЫХ НОВООБРАЗОВАНИЙ У ОБЛУЧЕННЫХ ЛЮДЕЙ

Е. А. Блинова ✉, А. В. Кореченкова, М. А. Янишевская, А. В. Аклеев

Уральский научно-практический центр радиационной медицины Федерального медико-биологического агентства, Челябинск, Россия

На фоне дополнительного радиационного воздействия однонуклеотидные полиморфизмы в генах, кодирующих ферменты антиоксидантной системы, могут способствовать усилению окислительного стресса, возникновению повреждений ДНК и, как следствие, приводить к повышению риска развития злокачественных новообразований (ЗНО). Целью работы было установить связи полиморфных локусов *CYBA* (rs4673), *GPX1* (rs1050450), *MPO* (rs2333227), *CAT* (rs7943316), *SOD2* (rs4880) с риском развития ЗНО у лиц, подвергшихся хроническому низкоинтенсивному радиационному воздействию, с учетом межгенных взаимодействий и дозы радиационного облучения. В исследование были включены две группы людей: облученные лица без ЗНО — 384 человека со средней накопленной дозой облучения красного костного мозга (ККМ) 796,95 ± 35,97 мГр; облученные лица с ЗНО в анамнезе — 227 человек со средней накопленной дозой облучения ККМ 520,06 ± 38,72 мГр. Амплификацию полиморфных локусов rs4880, rs2333227, rs7943316, rs4673, rs1050450 проводили методом ПЦР в реальном времени. Для всех полиморфных участков генов выявлено соответствие равновесию Харди–Вайнберга. Обнаружено, что аллели rs4880*C (SOD2) и rs1050450*T (GPX1) ассоциированы с повышенным риском развития ЗНО согласно доминантной (ОШ = 1,49 (1,02–2,18), $p = 0,04$) и рецессивной (ОШ = 2,00 (1,11–3,62), $p = 0,02$) моделям наследования соответственно. Получена модель межфакторных взаимодействий со 100%-й воспроизводимостью и точностью 66% ($p = 0,001$), включающая в себя полиморфизмы *SOD2* (rs4880), *CYBA* (rs4673) и фактор накопленной дозы облучения ККМ. Таким образом, полиморфные локусы генов, регулирующих оксидантный статус клеток, связаны с повышенным риском развития ЗНО у лиц, подвергшихся хроническому радиационному воздействию с преимущественным облучением ККМ.

Ключевые слова: однонуклеотидный полиморфизм, хроническое облучение, река Теча, антиоксидантная система, злокачественное новообразование

✉ **Для корреспонденции:** Евгения Андреевна Блинова
ул. Воровского, д. 68, корп. А, г. Челябинск, 454141, Россия; blinova@urcrm.ru

The mechanisms underlying the damaging effects of ionizing radiation are closely related to the oxidative stress enhancement in exposed cells [1]. The increase in the levels of reactive oxygen species (ROS) contributes to damage to macromolecules, including proteins, nucleic acids, and lipids, which results in DNA dysfunction and damage, as well as in the apoptotic cell death [2]. The main role in antioxidant defense is played by glutathione peroxidase (*GPX* gene), catalase (*CAT* gene), manganese-dependent superoxide dismutase (*SOD2* gene), myeloperoxidase (*MPO* gene), and cytochrome b-245 (*CYBA* gene). Single nucleotide polymorphisms (SNPs) in the genes encoding antioxidant enzymes can contribute to alteration of the enzyme activity and enzyme function impairment [3]. In particular, alteration of superoxide dismutase and glutathione peroxidase activity and the decrease in their ability to neutralize free radicals is observed in individuals having unfavorable alleles in *SOD2* (rs4880) and *GPX1* (rs1050450) polymorphic loci, respectively [4]. Catalase is an important endogenous antioxidant enzyme that catalyzes decomposition of hydrogen peroxide into oxygen and water, thereby neutralizing the ROS harmful effects. The rs7943316 polymorphic locus in the promoter region of the *CAT* gene can modify the transcription factor binding affinity. Due to the presence of mutant allele T, abnormal transcription factor binding can result in the promoter activity, gene expression alteration, and the decrease in the enzyme catalyst activity [5]. The decrease in the catalyst activity of antioxidant enzymes, in its turn, increases susceptibility to oxidative stress. The rs2333227 polymorphic locus located in the promoter region of the gene encoding myeloperoxidase downregulates the *MPO* gene, thereby disrupting the SP1 transcription factor binding site. It has been found that substitution of the G base with A base is associated with the decreased expression of the *MPO* gene mRNA and the decrease in the amount of enzyme, while the G allele, in contrast, is associated with the increased MPO production [6]. A number of polymorphisms in the *CYBA* promoter and exon regions affect the gene expression and the NADPH oxidase activation, which results in the increased production of free radicals along with the detected antioxidant deficiency [7]. All of these testify to the fact that the presence of SNP in the genes encoding the antioxidant system enzymes can have an effect on both quantitative and functional characteristics of the enzyme, as well as modify the radiation effects in case of ionizing radiation exposure.

The study was aimed to determine the association of the *CYBA* (rs4673), *GPX1* (rs1050450), *MPO* (rs2333227), *CAT* (rs7943316), *SOD2* (rs4880) polymorphic loci with the risk of malignant neoplasm (MN) development in individuals with chronic low dose rate exposure considering intergenic interactions and the radiation dose.

METHODS

Genotyping based on the *CYBA* (rs4673), *GPX1* (rs1050450), *MPO* (rs2333227), *CAT* (rs7943316), *SOD2* (rs4880) polymorphic markers was performed in individuals, who lived in the radioactively contaminated areas along the Techa River and were affected by chronic low dose rate exposure in the low to medium dose range [8]. All the patients enrolled were admitted to the Clinical department of the Urals Research Center for Radiation Medicine of FMBA of Russia (URCRM) in 2003–2023; blood samples collected from these patients were stored in the URCRM tissue bank. The inclusion criteria for all the examined individuals were as follows: residence in one of 41 villages located in the territory adjacent to the Techa River at any time between 1 January 1950 and 31 December 1960; availability of the individual accumulated dose to the red bone marrow (RBM) calculated using the Techa River Dosimetry System-2016 (TRDS-2016) [9]. The exclusion criteria for all the examined individuals were as follows: hematological disorders and the lack of information about the past medical history.

The examined individuals (611 people) were divided into two groups: those, who were chronically exposed on the Techa River and had no MNs, — 384 individuals; those, who were chronically exposed on the Techa River and had a history of MNs of various localization, — 227 individuals. The detailed characteristics of the studied groups are provided in Table 1.

The accumulated dose to RBM of the examined individuals was within the range of 0.85–3 715.72 mGy, and the mean dose did not exceed 659 mGy. No significant differences in the accumulated dose to RBM between the groups of exposed individuals with and without MNs were revealed ($p > 0.05$). The studied groups were matched by sex, ethnicity, and age.

The exposed residents of the Techa riverside villages had the following solid cancers: MNs of the digestive system — 49 individuals (ICD-10 codes: C00, C02, C04, C15, C16, C18.4, C19, C22.7, C25.9, C26), respiratory system — 28 individuals (ICD-10 codes: C30, C32.9, C34), skin — 44 individuals (ICD-10 codes: C43.9, C44), female reproductive system — 70 individuals (ICD-10 codes: C50, C53, C54, C56), male reproductive system — eight individuals (ICD-10 codes: C61, C63), urinary system — 16 individuals (ICD-10 codes: C64, C67), endocrine system — 13 individuals (ICD-10 code: C73). Furthermore, MNs of bone and articular cartilage — one individual (ICD-10 code: C40), brain and nervous system — two individuals (ICD-10 code: C71, C72), eye and adnexa — two individuals (ICD-10 code: C69), MNs without specification of site — four individuals (ICD-10 code: C80), carcinoma *in situ* unspecified — three individuals (ICD-10 code: D09), and MNs of uncertain or unknown behavior of other and unspecified

Table 1. Characteristics of the studied groups

Parameter		Individuals exposed on the Techa River with no MNs (*n* = 384)	Individuals exposed on the Techa River with the history of MNs (*n* = 227)
Sex, *n* (%)	Male Female	124 (32.29) 260 (67.71)	83 (36.56) 144 (63.44)
Ethnicity, *n* (%)	Slavs Turkic people	138 (35.94) 246 (64.06)	104 (45.81) 123 (54.19)
Age at the time of examination, years; mean ± SD (min–max)		73.91 ± 9.04 (43.00–97.00)	73.42 ± 8.82 (47.00–95.00)
Accumulated dose to RBM, mGy; mean ± SE (min–max)		796.95 ± 35.97 (1.69–3715.72)	520.06 ± 38.72 (0.85–3507.07)

Note: mean ± SD (min–max) — mean ± standard deviation (min–max); mean ± SE (min–max) — mean ± standard error of the mean (min–max).

Fig. 1. Distribution of MNs in the group of exposed individuals depending on the cancer localization

sites — three individuals (ICD-10 code: D48) were reported in the studied cohort. The distribution of MNs in the group of exposed individuals is presented in Fig. 1.

Peripheral blood for testing was collected to the 9 mL Vacuette test tubes (Greiner Bio-One; Austria) covered with the K3-EDTA blood anticoagulant. Genomic DNA was isolated on the spin columns using the ExtractDNA Blood & Cells kit (Evrogen; Russia) in accordance with the manufacturer's protocol.

SNPs of the candidate genes were selected for the study based on the location of the polymorphic locus in the gene, as well as the association with MN revealed by analysis of the HapMap (URL: hapmap.ncbi.nlm.nih.gov), NCBI (URL: https://www.ncbi.nlm.nih.gov/), SNPedia (URL: https://snpedia.com/) databases. Table 2 provides characteristics of the studied gene polymorphic regions.

Amplification of the studied polymorphic loci was performed by real-time PCR on the StepOnePlus Real-Time PCR System (Applied Biosystems; USA) using the reagent kits synthesized by TestGen OOO (Russia) in accordance with the manufacturer's protocol.

Deviation of the frequency distribution for genotypes of the studied polymorphisms from the expected Hardy–Weinberg equilibrium distribution was estimated using the chi-squared test (χ^2) in the Gene Calc online calculator (URL: https://gene-calc.pl/hardy-weinberg-page). The odds ratio (OR) with the 95% confidence interval was calculated to estimate the relationship of alleles in the polymorphic loci with the risk of MN development. The relationship was considered significant at $p < 0.05$.

Non-parametric Multifactor Dimensionality Reduction method (MDR software package v. 3.0.2, available at http://sourceforge.net/projects/mdr) [10] was used to estimate intergenic interactions and radiation doses. During such analysis the multilocus genotypes and factors are combined into groups with the increased and decreased risk of the disease development to reduce dimensionality of the number of parameters calculated. Thus, the optimal factor interaction model allowing one to predict susceptibility/no susceptibility to certain disorders is selected among all the proposed variants of models constructed based on the entered primary data through repeated verification [11]. Optimality of the resulting models was assessed based on their reproducibility based on the findings of the cross validation consistency (CVC) and the testing balanced accuracy (TBA). The model should be reproduced at least 9 times out of 10 and the model accuracy should exceed 55%. P-value for the testing balanced accuracy

Table 2. Characteristics of polymorphic regions

Gene	SNP	Alleles	Minor allele	Position	Location
SOD2	rs4880	T/C	C	chr6:159692840	Missense variant
MPO	rs2333227	C/T	T	chr17:58281401	2KB Upstream Variant
CAT	rs7943316	A/T	T	chr11:34438925	2KB Upstream Variant
CYBA	rs4673	C/T	C	chr16:88646828	Missense variant
GPX1	rs1050450	C/T	T	chr3:49357401	Missense variant

Note: 2KB Upstream Variant — a sequence variant located within 2KB 5' of a gene.

Table 3. Abundance of the studied SNP genotypes in exposed individuals

Gene/SNP	Genotype	Exposed individuals without MNs				Exposed individuals with MNs			
		Number (%)	Ho	He	p	Number (%)	Ho	He	p
SOD2/rs4880	C/C C/T T/T	70 (19) 174 (47) 125 (34)	0.47	0.49	0.5	41 (20) 110 (54) 52 (26)	0.54	0.5	0.2
MPO/rs2333227	C/C C/T T/T	276 (72) 101 (27) 4 (1)	0.27	0.25	0.1	122 (74) 42 (25) 1 (1)	0.26	0.23	0.2
CAT/rs7943316	A/A A/T T/T	60 (16) 179 (48) 134 (36)	0.48	0.48	0.9	25 (13) 89 (46) 75 (39)	0.47	0.47	0.8
CYBA/rs4673	C/C C/T T/T	201 (54) 139 (37) 34 (9)	0.37	0.4	0.2	96 (49) 78 (40) 21 (11)	0.4	0.43	0.4
GPX1/rs1050450	C/C C/T T/T	182 (49) 162 (44) 28 (8)	0.44	0.41	0.3	73 (46) 62 (40) 22 (14)	0.4	0.45	0.1

Note: Ho — observed heterozygosity; He — expected heterozygosity; p — value for the Hardy–Weinberg test.

was determined using a 1000-fold permutation test. The differences were considered significant at $p < 0.05$. The factor interaction analysis results were visualized using the graphs plotted using the Fruchterman–Rheingold force-directed layout algorithm. The contribution of each factor and/or interaction of factors is measured using the enthropy value (H) expressed in %. Thus, the factor with the 100% enthropy unambiguously determines the class the individual belongs to (healthy/ unhealthy individuals); therefore, the factor with 0% plays no role in susceptibility to the disease. To evaluate the effect of the dose the examined individuals were subdivided into three dose subgroups: 1 — 0.85–99 mGy; 2 — 100–999 mGy; 3 — ≥ 1000 mGy.

RESULTS

The results of assessing the distribution of SNP of the antioxidant system genes in the chronically exposed individuals are provided in Table 3.

No deviation from Hardy–Weinberg equilibrium was observed for all SNPs of the genes. Furthermore, the observed and expected heterozygosity values were similar for all SNPs, which indicated the random nature of the sample.

In the next phase of the study we performed analysis of the relationship of each gene polymorphism with the risk of MN development based on the recessive and dominant inheritance modes (Table 4).

The analysis showed that the rs4880*C and rs1050450*T alleles were associated with the increased risk of MNs (OR = 1.49 (1.02–2.18), $p = 0.04$) and OR = 2.00 (1.11–3.62), p = 0.02, respectively). Considering the fact that the complex cascade of interactions between the antioxidant system gene products and the contribution of the radiation exposure factor to the risk of MN development are not taken into account when assessing the associations of single alleles and genotypes, we performed the analysis of intergenic interactions with the accumulated dose yielding the 1n-, 2n-, 3n-, and n-factor models (Table 5). Simultaneous testing of all five SNPs and the

Table 4. Association of SNPs with the risk of MN development

Gene/SNP	Mode	Genotype		OR (95% CI)	p
		Exposed individuals without MNs	Exposed individuals with MNs		
SOD2/rs4880	Dominant	T/T (125) C/T-C/C (244)	T/T (52) C/T-C/C (151)	1.00 1.49 (1.02–2.18)	0.04
	Recessive	T/T-C/T (299) C/C (70)	T/T-C/T (162) C/C (41)	1.00 1.08 (0.70–1.66)	0.72
MPO/rs2333227	Dominant	C/C (276) C/T-T/T (105)	C/C (122) C/T-T/T (43)	1.00 0.93 (0.61–1.40)	0.72
	Recessive	C/C-C/T (377) T/T (4)	C/C-C/T (164) T/T (1)	1.00 0.57 (0.06–5.18)	0.6
CAT/rs7943316	Dominant	T/T (134) A/T-A/A(239)	T/T (75) A/T-A/A (114)	1.00 0.85 (0.59–1.22)	0.38
	Recessive	T/T-A/T (313) A/A (60)	T/T-A/T (164) A/A (25)	1.00 0.80 (0.48–1.32)	0.37
CYBA/rs4673	Dominant	C/C (201) C/T-T/T (173)	C/C (96) C/T-T/T (99)	1.00 1.20 (0.85–1.69)	0.31
	Recessive	C/C-C/T (340) T/T (34)	C/C-C/T (174) T/T (21)	1.00 1.21 (0.68–2.14)	0.52
GPX1/rs1050450	Dominant	C/C (182) C/T-T/T (190)	C/C (73) C/T-T/T (84)	1.00 1.10 (0.76–1.60)	0.61
	Recessive	C/C-C/T (344) T/T(28)	C/C-C/T (135) T/T(22)	1.00 2.00 (1.11–3.62)	0.02

Note: OR (95% CI) — odds ratio with the 95% confidence interval.

Table 5. Models of intergenic interactions with the accumulated dose in chronically exposed individuals

Model	Testing balanced accuracy	Cross validation consistency	p	Se	Sp
Dose to RBM	0.53	5/10	0.275	0.304	0.827
SOD2 rs4880, dose to RBM	0.55	6/10	0.162	0.761	0.454
SOD2 rs4880, dose to RBM, *CYBA* rs4673	0.66	10/10	0.001	0.75	0.601
SOD2 rs4880, dose to RBM, *CYBA* rs4673, *GPX1* rs1050450	0.57	10/10	0.062	0.837	0.578

Note: *p* — value for the testing balanced accuracy obtained in the 1000-fold permutation test; Se — sensitivity; Sp — specificity.

factor of accumulated dose to RBM was carried out. Table 5 presents the four best combinations of factors based on the modeling results. Further increase in the number of parameters significantly reduced the accuracy of the models presented.

Among all the models revealed, the 3-factor model including the *SOD2* (rs4880), *CYBA* (rs4673) polymorphisms and the accumulated dose to RBM was the most accurate (66%) and had 100% reproducibility (*p* = 0.001). The rs4880*C (genotypes C/C and C/T) and rs4673*T (genotypes T/T and T/C) alleles were reported as the ones associated with the increased risk of MN development. The *GPX1* (rs1050450) polymorphism was included in the 4n-factor model. However, specificity of such model decreased with increasing sensitivity, which affected accuracy. Other polymorphisms were considered insufficiently informative. The graph of interaction between the elements of the 3-factor model is provided in Fig. 2.

The *SOD2* (rs4880) polymorphism explaining 0.96% of phenotypic entropy (uncertainty) and the factor of the absorbed dose to RBM are of the highest informational value (1.24%). The *CYBA* (rs4673) informational contribution of 0.06% is the least, which is likely to play no significant role in the risk of MN development. However, it is worth considering interactions between all elements of the model that are of synergistic nature. Thus, the pair of rs4880 and rs4673 account for 0.61% of entropy; rs4673 and the accumulated dose to RBM account for 0.83%; rs4880 and the accumulated dose to RBM account for 0.21%.

DISCUSSION

ROS being the products of normal cell metabolism play an important role in stimulation of the intracellular signaling pathway in response to changes in the intra- and extracellular environment. The majority of ROS are generated in the mitochondrial respiratory chain [12]. However, imbalance between the free radical and reactive metabolite formation and elimination by means of the antioxidant system enzymes results in the development of oxidative stress. The factors contributing to oxidative stress are diverse: from lifestyle (smoking, alcohol consumption) to environmental exposures (chemical and radiation exposure). Furthermore, chronic diseases and inflammation can also be associated with oxidative stress. Eventually, oxidative stress results in damage to the important biomolecules and cell structures with potential consequences for the whole body [13]. In case of persistent oxidative stress, ROS are produced for a long time. This is how a significant impairment of the cell structure and functions can occur, which may lead to somatic mutations and neoplastic transformation [14]. The ability of antioxidants to neutralize the effects of free radicals may constitute an important component of the body's antitumor defense. The antioxidant system effectiveness is genetically determined. Overexpression or decreased activity of the antioxidant enzymes can modify the effects of radiation exposure [15].

Our study has shown that the *SOD2* rs4880*C and *GPX1* rs1050450*T alleles are associated with the increased risk of MN development in the individuals, who had chronic radiation exposure in a wide dose range, which is generally in line with the data reported for non-exposed people. According to the genomic assessment of oncogenicity based on the regBase prognostic model, rs4880 is considered to be likely pathogenic. According to the published data, rs4880 is associated with the increased risk of prostate cancer [16]. Furthermore, in individuals with the *SOD2* (rs4880) C/T and T/T genotypes, the measured *SOD2* enzyme activity was 33% lower than in carriers of the C/C genotype [17]. However, the study [18], in contrast, showed a decrease in the enzyme activity in individuals with the T variants in the codon 16 resulting in the oxidative stress enhancement, which is a probable cause of damage to the cell structures. A number of studies have shown the association of the *GPX1* (rs1050450) genetic variant with the susceptibility to MNs in non-exposed individuals [19]. The complex meta-analysis including 31 published papers has demonstrated that rs1050450 can contribute to the susceptibility to MN development due to disrupted antioxidant balance. Carriers of the T allele variant have the increased risk of developing various types of MNs, especially in Asian subgroups, based on the dominant genetic model [20]. The decrease in the gene functional activity can be a possible mechanism underlying such effects. For example, according to the ClinVar data, rs1050450 is associated with glutathione peroxidase deficiency.

With due account of the fact that many factors, including intergenic interactions and environmental factors, influence the malignant transformation of the cell, we have analyzed the role of intergenic interactions of SNPs and the dose to RBM in the development of MNs in exposed individuals. As a result of the analysis a 3-factor model having the highest accuracy (66% (*p* = 0.001)) and 100% reproducibility was identified. According
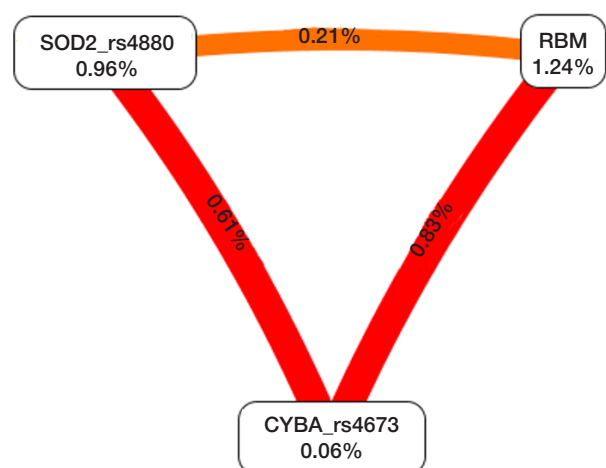
Fig. 2. Graph of interaction between the elements of the 3-factor model

to this model, increased risk of MN development was registered for the combination of the *SOD2* C*rs4880 allele, *CYBA* T*rs4673, and the accumulated dose to RBM. It should be noted that the most accurate model includes the *SOD2* (rs4880) polymorphic variant. Its association with the risk of MN development has been identified in our study. At the same time, the *GPX1* (rs1050450) polymorphism also associated with the risk of MN development was not included in the model: *CYBA* (rs4673) was identified instead of it based on the testing results. However, considering its insignificant contribution (0.06%), it is difficult to unambiguously determine its role at this phase of our research. The research results [21] show that rs4673 is associated with the increased risk of breast cancer. Individuals with the rs4673 C/T and T/T genotype have 1.42 times higher risk of breast cancer, than individuals with the C/C genotype.

Apparently, the increased production of ROS due to radiation exposure against the background of reduced superoxide dismutase activity could possibly contribute to the oxidative stress enhancement, damage to the cells components and DNA, and therefore lead to an increase in the risk of MN development.

CONCLUSIONS

The study has shown that polymorphic loci of the genes regulating the oxidative status of the cells, such as the *SOD2* rs4880*C (OR = 1.49; 95% CI = 1.02–2.18; p = 0.039) and *GPX1* rs1050450*T (OR = 2.00; 95% CI = 1.11–3.62; p = 0.024) alleles, are associated with the increased risk of MN development in the chronically exposed individuals. The model of interfactor interactions has also made it possible to determine the increased risk of MN development in carriers of the rs4880*C, rs4673*T minor alleles and the dose to RBM. Further research is required to reveal the modifying effect of exposure in individuals with unfavorable alleles in SNPs of the antioxidant system genes.

References

1. Buonanno M, de Toledo SM, Pain D, Azzam EI. Long-term consequences of radiation-induced bystander effects depend on radiation quality and dose and correlate with oxidative stress. Radiat Res. 2011; 175 (4): 405–15. DOI: 10.1667/RR2461.1.

2. Sage E, Shikazono N. Radiation-induced clustered DNA lesions: repair and mutagenesis. Free Radic Biol Med. 2017; (107): 125–35. DOI: 10.1016/j.freeradbiomed.2016.12.008.

3. Abd El Azeem RA, Zedan MM, Saad EA, Mutawi TM, Attia ZR. Single-nucleotide polymorphisms (SNPs) of antioxidant enzymes SOD2 and GSTP1 genes and SLE risk and severity in an Egyptian pediatric population. Clin Biochem. 2021; (88): 37–42. DOI: 10.1016/j.clinbiochem.2020.11.010.

4. Nikic P, Dragicevic D, Jerotic D, Savic S, Djukic T, Stankovic B, et al. Polymorphisms of antioxidant enzymes SOD2 (rs4880) and GPX1 (rs1050450) are associated with bladder cancer risk or its aggressiveness. Medicina (Kaunas). 2023; 59 (1): 131. DOI: 10.3390/medicina59010131.

5. Nawab SN, Zehra S, Fawwad A, Azhar A. A study on catalase gene promoter polymorphism-21 A/T (rs7943316) in healthy Pakistani population. Pak J Med Sci. 2017; 33 (6): 1521–4. DOI: 10.12669/pjms.336.13188.

6. Taioli E, Benhamou S, Bouchardy C, Cascorbi I, Cajas-Salazar N, Dally H, et al. Myeloperoxidase G-463A polymorphism and lung cancer: a HuGE genetic susceptibility to environmental carcinogens pooled analysis. Genet Med. 2007; 9 (2): 67–73. DOI: 10.1097/gim.0b013e31803068b1.

7. Kumar R, Kohli S, Ali Z, Duhan K, Ram R, Gupta M, et al. CYBA (p22phox) variants associate with blood pressure and oxidative stress markers in hypertension: a replication study in populations of diverse altitudes. Hypertens Res. 2015; 38 (7): 498–506. DOI: 10.1038/hr.2015.31.

8. Akleev AV, Kiselev MF, redaktory. Mediko-biologicheskie i jekologicheskie posledstvija radioaktivnogo zagrjaznenija reki Techa. M.: Vtoraja tipografija FU "Medbiojekstrem", 2001; 531 p. Russian.

9. Degteva MO, Nape BA, Tolstyh EI, Shishkina EA, Bugrov NG, Krestinina LJu, et al. Raspredelenie individual'nyh doz v kogorte ljudej, obluchennyh v rezul'tate radioaktivnogo zagrjaznenija reki Techi. Medicinskaja radiologija i radiacionnaja bezopasnost'. 2019; 64 (3): 46–53. DOI: 10.12737/article_5cf2364cb49523.98590475. Russian.

10. Hahn LW, Ritchie MD, Moore JH. Multifactor dimensionality reduction software for detecting gene-gene and gene-environment interactions. Bioinformatics. 2003; 19 (3): 376–82. DOI: 10.1093/bioinformatics/btf869.

11. Burmistrova AL, redaktor. Metaorganizm. Stress i adaptacija. Cheljabinsk: Cheljabinskij gosudarstvennyj universitet, 2019; 239 p. Russian.

12. Ďuračková Z. Some current insights into oxidative stress. Physiol Res. 2010; 59 (4): 459–69. DOI: 10.33549/physiolres.931844.

13. Reuter S, Gupta SC, Chaturvedi MM, Aggarwal BB. Oxidative stress, inflammation, and cancer: how are they linked? Free Radic Biol Med. 2010; 49 (11): 1603–16. DOI: 10.1016/j.freeradbiomed.2010.09.006.

14. Khandrika L, Kumar B, Koul S, Maroni P, Koul HK. Oxidative stress in prostate cancer. Cancer Lett. 2009; 282 (2): 125–36. DOI: 10.1016/j.canlet.2008.12.011.

15. Córdoba EE, Abba MC, Lacunza E, Fernánde E, Güerci AM. Polymorphic variants in oxidative stress genes and acute toxicity in breast cancer patients receiving radiotherapy. Cancer Res Treat. 2016; 48 (3): 948–54. DOI: 10.4143/crt.2015.360.

16. Burri RJ, Stock RG, Cesaretti JA, Atencio DP, Peters S, Peters CA, et al. Association of single nucleotide polymorphisms in SOD2, XRCC1 and XRCC3 with susceptibility for the development of adverse effects resulting from radiotherapy for prostate cancer. Radiat Res. 2008; 170 (1): 49–59. DOI: 10.1667/RR1219.1.

17. Bastaki M, Huen K, Manzanillo P, Chande N, Chen C, Balmes JR, et al. Genotype-activity relationship for Mn-superoxide dismutase, glutathione peroxidase 1 and catalase in humans. Pharmacogenet Genomics. 2006; 16 (4): 279–86. DOI: 10.1097/01.fpc.0000199498.08725.9c.

18. Sutton A, Imbert A, Igoudjil A, Descatoire V, Cazanave S, Pessayre D, et al. The manganese superoxide dismutase Ala16Val dimorphism modulates both mitochondrial import and mRNA stability. Pharmacogenet Genomics. 2005; 15 (5): 311–9. DOI: 10.1097/01213011-200505000-00006.

19. Zhao Y, Wang H, Zhou J, Shao Q. Glutathione peroxidase GPX1 and its dichotomous roles in cancer. Cancers (Basel). 2022; 14 (10): 2560. DOI: 10.3390/cancers14102560.

20. Chen J, Cao Q, Qin C, Shao P, Wu Y, Wang M, et al. GPx-1 polymorphism (rs1050450) contributes to tumor susceptibility: evidence from meta-analysis. J Cancer Res Clin Oncol. 2011; 137 (10): 1553–61. DOI: 10.1007/s00432-011-1033-x.

21. Tupurani MA, Padala C, Puranam K, Galimudi RK, Kupsal K, Shyamala N, et al. Association of CYBA gene (-930 A/G and 242 C/T) polymorphisms with oxidative stress in breast cancer: a case-control study. PeerJ. 2018; (6): e5509. DOI: 10.7717/peerj.5509.

Литература

1. Buonanno M, de Toledo SM, Pain D, Azzam EI. Long-term consequences of radiation-induced bystander effects depend on radiation quality and dose and correlate with oxidative stress. Radiat Res. 2011; 175 (4): 405–15. DOI: 10.1667/RR2461.1.

2. Sage E, Shikazono N. Radiation-induced clustered DNA lesions: repair and mutagenesis. Free Radic Biol Med. 2017; (107): 125–35. DOI: 10.1016/j.freeradbiomed.2016.12.008.

3. Abd El Azeem RA, Zedan MM, Saad EA, Mutawi TM, Attia ZR. Single-nucleotide polymorphisms (SNPs) of antioxidant enzymes SOD2 and GSTP1 genes and SLE risk and severity in an Egyptian pediatric population. Clin Biochem. 2021; (88): 37–42. DOI: 10.1016/j.clinbiochem.2020.11.010.

4. Nikic P, Dragicevic D, Jerotic D, Savic S, Djukic T, Stankovic B, et al. Polymorphisms of antioxidant enzymes SOD2 (rs4880) and GPX1 (rs1050450) are associated with bladder cancer risk or its aggressiveness. Medicina (Kaunas). 2023; 59 (1): 131. DOI: 10.3390/medicina59010131.

5. Nawab SN, Zehra S, Fawwad A, Azhar A. A study on catalase gene promoter polymorphism-21 A/T (rs7943316) in healthy Pakistani population. Pak J Med Sci. 2017; 33 (6): 1521–4. DOI: 10.12669/pjms.336.13188.

6. Taioli E, Benhamou S, Bouchardy C, Cascorbi I, Cajas-Salazar N, Dally H, et al. Myeloperoxidase G-463A polymorphism and lung cancer: a HuGE genetic susceptibility to environmental carcinogens pooled analysis. Genet Med. 2007; 9 (2): 67–73. DOI: 10.1097/gim.0b013e31803068b1.

7. Kumar R, Kohli S, Ali Z, Duhan K, Ram R, Gupta M, et al. CYBA (p22phox) variants associate with blood pressure and oxidative stress markers in hypertension: a replication study in populations of diverse altitudes. Hypertens Res. 2015; 38 (7): 498–506. DOI: 10.1038/hr.2015.31.

8. Аклеев А. В., Киселев М. Ф., редакторы. Медико-биологические и экологические последствия радиоактивного загрязнения реки Теча. М.: Вторая типография ФУ «Медбиоэкстрем», 2001; 531 с.

9. Дегтева М. О., Напье Б. А., Толстых Е. И., Шишкина Е. А., Бугров Н. Г., Крестинина Л. Ю. и др. Распределение индивидуальных доз в когорте людей, облученных в результате радиоактивного загрязнения реки Течи. Медицинская радиология и радиационная безопасность. 2019; 64 (3): 46–53. DOI: 10.12737/article_5cf2364cb49523.98590475.

10. Hahn LW, Ritchie MD, Moore JH. Multifactor dimensionality reduction software for detecting gene-gene and gene-environment interactions. Bioinformatics. 2003; 19 (3): 376–82. DOI: 10.1093/bioinformatics/btf869.

11. Бурмистрова А. Л., редактор. Метаорганизм. Стресс и адаптация. Челябинск: Челябинский государственный университет, 2019; 239 с.

12. Ďuračková Z. Some current insights into oxidative stress. Physiol Res. 2010; 59 (4): 459–69. DOI: 10.33549/physiolres.931844.

13. Reuter S, Gupta SC, Chaturvedi MM, Aggarwal BB. Oxidative stress, inflammation, and cancer: how are they linked? Free Radic Biol Med. 2010; 49 (11): 1603–16. DOI: 10.1016/j.freeradbiomed.2010.09.006.

14. Khandrika L, Kumar B, Koul S, Maroni P, Koul HK. Oxidative stress in prostate cancer. Cancer Lett. 2009; 282 (2): 125–36. DOI: 10.1016/j.canlet.2008.12.011.

15. Córdoba EE, Abba MC, Lacunza E, Fernánde E, Güerci AM. Polymorphic variants in oxidative stress genes and acute toxicity in breast cancer patients receiving radiotherapy. Cancer Res Treat. 2016; 48 (3): 948–54. DOI: 10.4143/crt.2015.360.

16. Burri RJ, Stock RG, Cesaretti JA, Atencio DP, Peters S, Peters CA, et al. Association of single nucleotide polymorphisms in SOD2, XRCC1 and XRCC3 with susceptibility for the development of adverse effects resulting from radiotherapy for prostate cancer. Radiat Res. 2008; 170 (1): 49–59. DOI: 10.1667/RR1219.1.

17. Bastaki M, Huen K, Manzanillo P, Chande N, Chen C, Balmes JR, et al. Genotype-activity relationship for Mn-superoxide dismutase, glutathione peroxidase 1 and catalase in humans. Pharmacogenet Genomics. 2006; 16 (4): 279–86. DOI: 10.1097/01.fpc.0000199498.08725.9c.

18. Sutton A, Imbert A, Igoudjil A, Descatoire V, Cazanave S, Pessayre D, et al. The manganese superoxide dismutase Ala16Val dimorphism modulates both mitochondrial import and mRNA stability. Pharmacogenet Genomics. 2005; 15 (5): 311–9. DOI: 10.1097/01213011-200505000-00006.

19. Zhao Y, Wang H, Zhou J, Shao Q. Glutathione peroxidase GPX1 and its dichotomous roles in cancer. Cancers (Basel). 2022; 14 (10): 2560. DOI: 10.3390/cancers14102560.

20. Chen J, Cao Q, Qin C, Shao P, Wu Y, Wang M, et al. GPx-1 polymorphism (rs1050450) contributes to tumor susceptibility: evidence from meta-analysis. J Cancer Res Clin Oncol. 2011; 137 (10): 1553–61. DOI: 10.1007/s00432-011-1033-x.

21. Tupurani MA, Padala C, Puranam K, Galimudi RK, Kupsal K, Shyamala N, et al. Association of CYBA gene (-930 A/G and 242 C/T) polymorphisms with oxidative stress in breast cancer: a case-control study. PeerJ. 2018; (6): e5509. DOI: 10.7717/peerj.5509.

THE EFFECT OF CHRONIC EXPOSURE ON THE PARAMETERS OF CYTOGENETIC MARKERS OF SENESCENCE IN THE RESIDENTS OF THE TECHA RIVERSIDE SETTLEMENTS

Akhmadullina YuR[1,2] ✉, Vozilova AV[1], Krivoshchapova YV[1]

[1] Urals Research Center for Radiation Medicine of the Federal Medical Biological Agency, Chelyabinsk, Russia

[2] Chelyabinsk State University, Chelyabinsk, Russia

The understanding of the exposure effects on the human health could be improved by analyzing the influence of the chronic low dose rate exposure on the senescence of the immune system cells. It will also help to develop the measures aimed at the mitigation of the adverse effects. The objective of the study is to investigate the influence of the chronic low dose rate exposure on the senescence of the immune system cells using the cytogenetic markers. In the course of the research the authors evaluated the cellular senescence markers — genome instability and telomere depletion — in T-lymphocytes of the individuals exposed in the Southern Urals (exposure doses were 0.001 Gy — 4.7 Gy, the age of examined people was 40–89 years). The data analysis has demonstrated that the effect of chronic exposure on the T-cell senescence was indirect. Unstable chromosome aberrations occurred statistically significantly more frequently in exposed people aged 40–59 years ($p = 0.012$). Frequency of lymphocytes with micronuclei in exposed individuals differed in men and women ($p = 0.001$). Statistically significant decrease in the telomere length was revealed (for the chromosome arms 1q, 3p, 3q, 20p, 20q, 13q, 15p, 22q ($p < 0.05$); 19p, 21q ($p < 0.01$)).

✉ **Correspondence should be addressed:** Yulia Rafisovna Akhmadullina
Vorovskogo, 68A, Chelyabinsk, 454141, Russia; akhmadullina.yul@yandex.ru

ВЛИЯНИЕ ХРОНИЧЕСКОГО ОБЛУЧЕНИЯ НА ПОКАЗАТЕЛИ ЦИТОГЕНЕТИЧЕСКИХ МАРКЕРОВ СТАРЕНИЯ У ЖИТЕЛЕЙ ПРИБРЕЖНЫХ СЕЛ РЕКИ ТЕЧА

Ю. Р. Ахмадуллина[1,2] ✉, А. В. Возилова[1], Я. В. Кривощапова[1]

[1] Уральский научно-практический центр радиационной медицины Федерального медико-биологического агентства, Челябинск, Россия

[2] Челябинский государственный университет, Челябинск, Россия

Исследование влияния хронического низкоинтенсивного облучения на старение клеток иммунной системы имеет важное значение для понимания последствий воздействия облучения на здоровье человека и разработки мер минимизации негативных эффектов. Целью работы было исследовать влияние хронического низкоинтенсивного облучения человека на старение клеток иммунной системы с использованием цитогенетических маркеров. В работе оценили маркеры старения — нестабильность генома и истощение теломер в Т-лимфоцитах у облученных людей на Южном Урале (дозы облучения от 0,001 до 4,7 Гр, возраст — от 40 лет до 89 лет). Анализ данных показал, что хроническое воздействие повлияло на старение Т-клеток опосредованно. Частота нестабильных хромосомных аберраций у облученных лиц была статистически выше в 40–59 лет ($p = 0,012$). Частота лимфоцитов с микроядрами у облученных лиц наиболее различалась у мужчин и женщин ($p = 0,001$). Выявили статистически значимое снижение показателей длины теломер у облученных лиц (для хромосомных плеч 1q, 3p, 3q, 20p, 20q, 13q, 15p, 22q ($p < 0,05$); 19p, 21q ($p < 0,01$)).

✉ **Для корреспонденции:** Юлия Рафисовна Ахмадуллина
ул. Воровского, д. 68А, г. Челябинск, 454141, Россия; akhmadullina.yul@yandex.ru

For more than 60 years people chronically exposed as a result of the releases of liquid radioactive waste (LRW) of the "Mayak" PA into the Techa River in the Southern Urals have been undergoing medical examinations at the URCRM. The specific feature of this exposure situation is the combination of internal exposure due to the intake and accumulation of ^{89,90}Sr radionuclides in the body, and external γ-exposure due to the river water. The critical organ was the red bone marrow (RBM), where the hematopoietic precursor-cells were exposed at a wide dose range. Since the LRW started to be released into the Techa River in 1948, the maximum dose rates were recorded in 1951–1952, and exposure doses were formed by 1960. However, chronic internal low dose exposure proceeds up to date. As the youngest of the exposed people are ≥60 years old, therefore, it is possible to study the effect of ionizing radiation on the ageing of a human being [1].

Human body is a complex system with multiple levels. It has its own ontogenesis program. Its implementation is regulated by a group of genes and multiple pathways of interaction and interdependence of their products. An important stage in ontogenesis is the ageing of the body. Nowadays the proportion of the elderly people (aged 60+) in the world population is increasing drastically. That is why, scientists and physicians are interested in studying the mechanisms of the natural ageing of a human being, factors that cause premature ageing, and mechanisms that can postpone or delay in time its development [2].

No doubt, in addition to the natural processes the environmental conditions also influence the ageing of a body. Active application of ionizing radiation (IR) sources for medical and diagnostic purposes leads to a question whether radiation can affect the premature ageing [3, 4].

Investigation of any process is based on the identification of the markers that have qualitative or quantitative attributes. Generally accepted markers of ageing include the following: genomic instability, telomere depletion, epigenetic genome damage, changes in the proteostatus of the cells, changes in the regulation of nutrients, mitochondrial dysfunctions, depletion of the stem cell pool, impaired intracellular interaction [3, 5].

In our study we assess the chromatin status of the nuclear DNA in PHA-stimulated peripheral blood T-lymphocytes of the exposed individuals. The parameters that we have selected are indicative of the two above-mentioned markers of ageing — genomic instability (frequency of unstable chromosome aberrations and cells with micronuclei) and telomere depletion (assessment of the chromosome telomere length).

Unstable chromosome aberrations (UCA) include such rearrangements as dicentrics, ring chromosomes, acentric rings. Numerous studies confirmed the UCA dependence on the age of a person, as the number of errors in repair increases with age and so does the number of cells with UCA [6–9].

The analysis of the cytokinesis-blocked T-lymphocytes with micronuclei is an additional tool for a secondary assessment of the chromosome abnormalities. It is used in case of the exposure to various genotoxic environmental factors. Micronucleus (MN) is the structure that contains chromatin formed out of either unrepaired DNA breaks or as a result of the incorrect segregation of the sister chromatid of a single or several chromosomes. Some studies demonstrate that spontaneous MNs occur more frequently with age [10].

The length of the telomere regions of the chromosomes or "biological clock" of a cell is another marker of the cellular senescence. Daughter cells lose their capacity to divide and die due to gradual depletion of the chromosome telomeres in cell line division (Hayflick limit). The phenomenon of the telomere shortening in the cells of the body with the age of

a person formed the basis of the method of biological age determination [11–12].

Thus, to evaluate the effect of chronic exposure on the DNA ageing of the PHA-stimulated human T-lymphocytes we have chosen cytogenetic methods that allow assessing the status of the chromosome DNA of the immune system cells, the precursors of which started to be exposed already in the RBM more than 50 years ago, and this exposure is still going on.

The objective of the study is to investigate the effect of chronic low dose rate human exposure on the immune cell ageing using cytogenetic markers.

METHODS

The study design: to form comparable subgroups of people of different age among exposed and unexposed individuals; to analyze the parameters of the genomic instability in each age subgroup and to compare the values between themselves. To evaluate the time-dependent changes in chromosome aberrations in age subgroups of exposed and unexposed people (assessment of the nuclear DNA instability).

Characteristics of the studied individuals

People affected by chronic combined exposure in the Southern Urals (hereinafter referred to as 'donors") were chosen as the object of the research. Nuclear chromatin of the PHA-stimulated peripheral blood T-lymphocytes were the subject of the research.

The study comprised the individuals born before 1959 inclusively, with the total RBM external and internal doses from 0.001 to 4.7 Gy calculated with the TRDS-2016 [13]. These were people of both sexes, mainly of three ethnicities — Russians, Tartars, and Bashkirs.

The study also involved people living in similar social and economic conditions in the Southern Urals who were not affected by accidental exposure ("comparison group"). The comparison group for the study of the telomere length consisted of the TRC members whose dose to RBM did not exceed 0.01Gy.

The following cytogenetic criteria were used to select the donors: people who had autoimmune diseases or cancers in past medical history, or chronic inflammatory diseases in the exacerbation phase, or people taking cytostatic drugs or antibiotics were excluded from the study.

Information on the health status of the exposed people has been provided by the department "Database "MAN". Individual exposure doses were calculated at the Biophysics laboratory. The data on the oncopathology in the past medical history of the examined people were provided by the Epidemiology laboratory (Urals Research Center for Radiation Medicine).

In accordance with the existing International Norms and Regulations (Declaration of Helsinki, 1964) and with the approval of the Ethics Committee of the URCRM all the donors provided informed consent to blood sampling and further study.

The study of the UCA frequency

Two groups of donors were formed to assess the frequency of UCA. The comparison group consisted of 83 people. The study group included 570 individuals with RBM doses 0.001–4 Gy. The age of the studied individuals varied in the range 40–89 years. The studied group of exposed people was subdivided into two subgroups. The 1st subgroup comprised the individuals with doses 0.001–0.2 Gy inclusive. The 2nd subgroup included

Table 1. Characteristics of the examined individuals and results of the evaluation of UCA frequency in the studied groups (median, 25% and 75%)

Age sub-groups, years	Comparison group	Exposed individuals		
		0.001–4 Gy	0.001–0.2 Gy	0.3–4 Gy
40–59	0 $n = 17$	0 0–0.27 $p = 0.012$ $n = 100$	0 0–0.4 $p = 0.002$ $n = 39$	0 $p = 0.04$ $n = 61$
60–69	0 $p_1 = 0.064$ n = 44	0 0–0.26 $n = 285$	0 0–0.133 $n = 58$	0 0–0.2 $n = 227$
70–89	0 0–0.62 $p_2 = 0.023$ $n = 22$	0 0–0.22 $n = 185$	0 0–0.18 $n = 43$	0 0–0.255 $n = 142$
Total	0 n = 83	0 0–0.20 $p = 0.04$ $n = 570$		

Note: p — statistically significant differences with the comparison group in one and the same age-group; p_1 — statistically significant differences between age-groups 40–59 years and 60–69 years; p_2 — statistically significant differences between age-groups 40–59 years and 70–89 years.

persons with doses 0.3–4 Gy. The exposed and unexposed individuals were ranked according to their age at the time of examination. Three age-groups were distinguished: 40–59 years, 60–69 years, and the oldest group 70–89 years (Table 1). In our previous studies no dependence of the UCA frequency on sex of the studied individuals was registered. That is why the groups were mixed in terms of sex, most of the studied individuals were women (up to 70%).

The study of the frequency of cells with MN

Characteristics of the studied individuals are given in Table 2.

In total the comparison group included 113 women and 44 men. The age of the studied individuals ranged from 52 to 82 years. Women predominated in all the age-groups. The group of exposed individuals consisted of 573 persons (354 women and 219 men). The age of the studied individuals was 50–89 years. Cumulative doses to the RBM ranged from 0.001 to 4 Gy.

We have also conducted a pilot study with a view to find out whether the X-chromosome chromatin into the micronucleus. It involved 6 exposed women aged 73–82 with RBM doses 0.73–1.93 Gy (study group), and two unexposed women aged 63 and 65 years (comparison group).

Assessment of the telomere length

Two groups of donors were formed to measure the telomere length. The comparison group consisted of 27 people with RBM doses 0–0.01 Gy. Out of these people 23 persons had doses

0.0001–0.01 Gy, and four individuals did not have accidental exposure at all. The group of exposed individuals included 26 people with RBM doses 0.6–4.7 Gy. The age of the examined individuals was 61–84 years. Characteristics of the examined donors are given in Table 3.

To analyze the effect of sex on the telomere length the groups were matched in terms of the number of examined people and their age. The group "Women" consisted of 11 donors aged 61–73 with RBM dose 0–1.4 Gy. The group "Men" included 11 donors aged 61–72 with RBM dose 0–1.4 Gy.

Assuming that the non-radiation factor "sex" could affect the relative telomere length, to estimate the exposure effect on the relative length of the telomere regions two groups of female donors were formed. The comparison group consisted of 20 people with RBM doses 0–0.01 Gy, out of comparison group members 18 women had the dose 0.0001–0.01 Gy, and 2 women did not have accidental exposure at all. The donors' age was 62–80 years. The group of exposed women included 22 individuals with RBM doses 0.6–4.7 Gy. Their age at examination was 70–84 years.

Preparing the chromosome metaphase slides

Preparing and staining of the slides

Cytogenetic slides from the PHA-stimulated peripheral blood T-lymphocytes of the donors were prepared according to the protocol that includes four consecutive steps: cell culturing to

Table 2. Characteristics of the persons examined using the MN assay

Age groups, years	Female		Male	
	Comparison group	Exposed individuals	Comparison group	Exposed individuals
	Age, years number of person	Age, years number of person, RBM dose, Gy	Age, years number of person	Age, years number of persons, RBM dose, Gy
50–59	57 $n = 23$	57 $n = 45$ 0.002–2.9	56 $n = 8$	56 $n = 22$ 0.007–1.0
60–69	65 $n = 45$	65 $n = 177$ 0.004–3.7	65 $n = 20$	65 $n = 125$ 0.004–2.2
70–89	74 $n = 45$	75 $n = 132$ 0.001–4.0	75 $n = 16$	73 $n = 72$ 0.02–2.1

Table 3. Characteristics of the donors with measured telomere length

Age, years	Female		Male	
	Comparison group	Exposed individuals	Comparison group	Exposed individuals
	Age, years number of persons, RBM dose, Gy	Age, years number of persons, RBM dose, Gy	Age, years number of persons, RBM dose, Gy	Age, years number of persons, RBM dose, Gy
61–84	62–80 $n = 20$ 0–0.01	70–84 $n = 22$ 0.6–4.7	61–72 $n = 7$ 0–0.01	71–76 $n = 4$ 0.6–1.35

the metaphase (for 52 hours, colcemid in the final concentration 0.1 mg/ml was added 3 hours before the end of the culturing), hypotonic treatment of the metaphase cells (one hour prior to fixation); metaphase cells fixation (3 parts of ethanol, 1 part glacial acetic acid), and then obtaining the chromosome preparations. Metaphase chromosomes were stained with 2% Gimza solution for 10 min. Then the slides were washed to remove the stain and dried at room temperature [14].

The preparations were analyzed under light microscopy without caryotyping using the AxioImager A2, Z2 microscope. The analysis included cells with 46 chromosomes, with no overlapping or with 1–2 overlappings maximum. Dicentrics, ring chromosomes, acentric rings were the focus of the attention of the researchers. From 100 to 500 cells were analyzed per each studied individual.

Obtaining the preparations of binucleated lymphocytes to detect micronuclei

The protocol of the micronuclei test consists of several steps: culturing the PHA-stimulated peripheral blood lymphocytes, cytokinesis block, hypotonic treatment, fixation of suspension cells, preparation of cytogenetic slides [15]. Preparations were stained with 1% Gimza solution for 20 min. The preparations were analyzed under light microscopy using the AxioImager A2 microscope. 1000 binucleated cells were analyzed per donor.

The chromosomes of the micronuclei were studied with locus-specific fluorescence *in situ* hybridization. Fluorescent probes for centromeric region of X-chromosome (cenX) (Metasystems, Germany) were used. Fluorescent staining was performed in accordance with the manufacturer's protocol which requires DNA denaturation of the preparation and the probe, hybridization for 24 hours at 37 °C, post-hybridization wash-out of the unbound probes. For counter-staining of the chromatin 15 μl of the DAPI antifade (Metasystems, Germany) were applied onto each slide. Then slides were covered with the coverslip and stored at –20 °C.

The analysis of FISH-stained preparations was performed with fluorescent microscope AxioImager Z2 (Zeiss; Germany) with fluorescent filters and Isis Metasystems software module to process fluorescent images. The analysis of centromere signals of X-chromosome was focused on the presence and amount of the signals in a micronucleus. Micronuclei with one or more centromere signals were considered centromere-positive (cen X+). Micronuclei without centromere signals were considered centromere-negative (cen X–).

Detection of the telomere regions of the metaphase chromosomes

Slides with metaphase cells were prepared in accordance to the protocol described for the assessment of the UCA. To perform fluorescent staining with Q-FISH slides were cleared from cytoplasm, the DNA of the probe and preparation was denaturated. Hybridization was preformed according to the manufacturer's protocol with genuine solutions. To estimate the length of the chromosome telomere DAKO probes

(Denmark) were used. Centromere signal of the chromosome #2 (Metasystems, Germany) was used as a reference one.

Fluorescently stained preparations were analyzed on AxioImager Z2 fluorescent microscope (Zeiss, Germany) with DAPI and SpO (spectrum orange) filters. Thirty cells were studied per person. The telomeres were measured with the telomere module of the Isis software. The measurement results were expressed in percentage ratio of the telomere signal length (T) to that of the centromere signal (C) – (%T/C). The method of the telomere length measurement is described in detail in [16].

The telomere lengths for the metacentric (#1, #3, #19, #20) and acrocentric (#13, #14, #15, #21, #22) chromosomes are given in the Results section.

The main focus of the research was on the relative telomere length in metacentric and acrocentric chromosomes as the most diverse ones in terms of the coefficient of the chromosome arms ratio and in terms of the chromosome length on the whole. The chromosomes of various size were also compared within the groups of metacentric and acrocentric chromosomes. Among metacentric chromosomes, chromosome #1 is the largest. It contains approximately 8% of the whole DNA-material of the cell. The smallest metacentric chromosome is #20. It has about 2.5% of the cell DNA. The group of acrocentrics includes chromosomes #13, #14, #15. Each of them contains about 3.5–4% of the cell DNA, while the smallest acrocentrics — chromosomes #21, #22 — have 1.5–2% [17].

Methods of the statistical processing of data

The normality of data distribution was checked with Kolmogorov-Smirnov test. Common methods of variation statistics with the calculation of the median, 25th and 75th percentile were used for the statistical processing of the obtained results. The values in the groups were compared with Mann–Whitney U test.

The relationship between the frequency of UCA, age and dose were determined using the linear regression equations.

Spearman correlation coefficient was used to determine the relationship between the frequency of lymphocytes with micronuclei and age. To assess the effect of a set of factors on the frequency of lymphocytes with micronuclei in the studied individuals a univariant general linear model was applied. The frequency of micronuclei with centromere signals of the X-chromosome was calculated as a percentage of all the micronuclei. The analysis was performed with the help of the chi-square criterion. The differences were considered statistically significant at $p < 0.05$. Statistical processing of the obtained results was performed with the software package Sigmaplot (SYSTAT Software; USA), STATISTICA, version 10.0 (USA) and PAST, version 4.03

RESULTS

The study of the frequency of UCA

The comparison of the parameter values revealed that exposed people have statistically significantly more exchange

Table 4. Frequency of lymphocytes with micronuclei in groups of exposed women of every studied age (median, 25–75%, min-max)

Age groups	Comparison group	Exposed individuals		
		0.001–4 Gy	0.001–0.2 Gy	0.3–4 Gy
50–59	15 9–21 (5–65)	15 11–20 (6–36)	12 10–18 (6–24)	16 14–24 (7–36)
60–69	17 12–26 (4–48)	16 12–22 (2–55)	15 11–19 (2–42)	16 12–25 (3–55)
70–79	16 10–22 (0–40)	18 13–23 (3–47)	19 15 – 25 4–42	17 12–23 (3–47)
80–89	15 11–21 (10–24)	20 17–25 (4–44)	20 18–27 (16–39)	20 15–23 (4–44)

aberrations than unexposed individuals, $p = 0.04$ (Table 1). Weak linear correlation of the studied parameters with the bone marrow dose was observed in the combined group of exposed individuals ($R = 0.125$, $p = 0.005$).

In the comparison group the studied parameter increases slightly with age (mean — 0, 0.18, and 0.30 per 100 cells, respectively). The frequency of CA in unexposed individuals in the age subgroups "60–69 years" and "70–79 years", is increased relative to the subgroup "40–59 years" ($p_1 = 0.06$, $p_2 = 0.02$). Despite the increase in the frequency of exchanges in the subgroup "70–79 years", the differences with the subgroup "60-69 years" are statistically insignificant.

As for the exposed individuals, then there was no increase in the studied parameter with age. On the contrary, UCA in all the age subgroups occurred with equal frequency ($p_1 = 0.69$, $p_2 = 0.37$). It was proved once again by the absence of linear correlation ($R = 0.0002$, $p = 0.76$).

When we compared the frequency of exchange aberrations in the control subgroups and subgroups of exposed people, we revealed a statistically significant increase of the parameters only in the subgroup of exposed individuals aged 40–59 years ($p = 0.038$). The parameter values in exposed individuals from the age subgroup "60-69 years" exceeded those in the respective control group but the differences were statistically insignificant. As for the older age, then the frequency of cells with CA in these groups was similar.

The construction of the linear regression allowed noticing weak dependence of the UCA frequency on age for the comparison group (equation 1). For the group of exposed individuals there was no linear dependence of the UCA frequency on age (equation 2). Weak dependence of the UCA frequency on RBM dose (equation 3) was revealed, and it agrees with the published data [1,18].

$$UCA = 0.013\,A – 0.670 \quad (R = 0.242\ p = 0.04) \tag{1}$$
$$UCA = 1.56 \times 10^{–6}\,A + 0.241 \quad (R = 0.0002\ p = 0.76) \tag{2}$$
$$UCA = 0.109\,D + 0.152 \quad (R = 0.126\ P = 0.005) \tag{3}$$

where UCA — frequency % of exchange aberrations A — age at last birthday, D — dose to RBM, Gy.

Study of the frequency of cells with micronuclei

According to the data presented in Table 4 it is clear that the frequency of lymphocytes with micronuclei is 15‰, 17%, 16‰ and 15‰ in exposed women aged 50–59, 60–69, 70–79, and 80–89, respectively. No statistically significant differences were noted.

No statistically significant differences in the frequency of lymphocytes with micronuclei were observed between the groups of exposed women and comparison groups, and between the groups of exposed women themselves.

It is clear from Table 5 that the frequency of lymphocytes with micronuclei in exposed men aged 50–59 is 11‰, in those aged 60–69 it makes up 12‰. As for men aged 70–79 the frequency of lymphocytes with micronuclei is 15‰. This value does not differ from that in the group of unexposed men. The study of the frequency of lymphocytes with micronuclei in the dose groups of exposed men revealed no statistically significant differences with the comparison group and between the groups of exposed men themselves.

The study of the dependence of the frequency of lymphocytes with micronuclei on sex revealed that in the groups of exposed individuals the studied parameter was statistically significantly higher in women relative to men (18‰ (13–25‰) vs 13‰ (10–19‰), $p = 0.001$).

In the course of the analysis of the differences in the frequency of lymphocytes with micronuclei between men and women in various age subgroups it was noted that parameter values differed statistically significantly in the age subgroups 60–69 and 70–79 ($p = 0.0001$ and $p = 0.033$, respectively). In the age period 50–59 years the differences between men and women followed the trend ($p = 0.119$).

Multivariate analysis was used to study the influence of the combination of radiation and non-radiation factors. The results

Table 5. Frequency of lymphocytes with micronuclei in groups of exposed men of every studied age (median, 25–75%, min-max)

Age groups	Comparison group	Exposed individuals		
		0.001–4 Gy	0.001–0.2 Gy	0.3–4 Gy
50–59	15 8–20 (3–21)	11 9–18 (5–41)	11 8–20 (5–29)	12 10–22 (5–41)
60–69	13 11–19 (5–37)	12 8–19 (2–38)	15 11–22 (3–34)	12 8–18 (2–38)
70–79	15 10–18 (3–21)	15 11–19 (4–41)	16 11–19 (8–28)	15 11–19 (4–41)

Table 6. The effect of radiation exposure, age and sex on the frequency of lymphocytes with micronuclei

Factor	Parameters of the model
adjusted model	$F = 9.5$ $p = 0.0001$
age	$F = 3.75$ $p = 0.053$
RBM dose	$F = 0.3$ $p = 0.599$
sex	$F = 22.24$ $p = 0.0001$

of the analysis are given in Table 6. As it can be seen from the table, the sex of the studied individuals had the greatest effect on the frequency of lymphocytes with micronuclei. No dependence of the frequency of lymphocytes with micronuclei on the RBM dose was observed, $p = 0.599$. The dependence of the frequency of lymphocytes with micronuclei on age was similar to the trend, $p = 0.053$.

Table 7 presents the frequency of micronuclei containing centromeres of the X-chromosome.

It is seen from table 7 that in the group of exposed individuals 46.6% of micronuclei contained centromere-positive chromatin of the X-chromosome. This value was statistically significantly higher than that in the comparison group — 31%, $\chi^2 = 4.78$, $p = 0.04$. Inter-individual variability of the values in exposed women was observed. The frequency of micronuclei with X-chromosome centromere signal varies from 22.8% to 59%.

Individual variability was also observed in the frequency of micronuclei containing different number of centromeres. For instance, in the group of exposed people there was one donor whose centromere-positive micronuclei contained predominately one centromere; three donors who mainly had 2 signals in centromere-positive micronuclei. In the donors from the comparison group centromere-positive micronuclei contained predominately one centromere. These findings show that there has been anaphase X-chromosome nondisjunction or lagging, which is likely to result in chromosome elimination to the micronucleus.

The study of the length of the chromosome telomere regions

The length of the telomere regions of the metacentric and acrocentric chromosomes in men and women is given in Table 8.

It can be seen from table 8 that the relative length of the telomere regions was statistically significantly higher in men than that in women for metacentric chromosomes (#1, #3, #19, #20) and acrocentric chromosomes (#13, #14, #15, #21, #22), differences with $p < 0.05$ were observed for the chromosome arms 1q, 3p, 20q, 13q, 15q, 21q.

Table 9 presents the median of the telomere lengths for metacentric (#1, #3, #19, #20) and acrocentric (#13, #14,

#15, #21, #22) chromosomes in the comparison group and chronically exposed women.

It is clear from Table 9 that on the whole the telomeres of the metacentric chromosome were shorter in chronically exposed women than those in the cells of the people from the comparison group. Statistically significant differences were observed for the 1q, 3p, 3q, 19p, 20p, 20q arms of the metacentric chromosomes, and for the 13q, 15p, 21q, 22q arms of the acrocentric chromosomes.

DISCUSSION

More than 100 thousand residents of the riverside settlements were affected by combined chronic exposure due to the releases of LRW into the Techa River.

Since nowadays a natural decline in the size of the cohort is registered, and at the same time rather big amount of cytogenetic data has been collected it is important to evaluate how chronic exposure influenced the cellular ageing processes. We have used several different cytogenetic methods in the study. They all reflect the status of the chromosome DNA in peripheral blood T-cells. To reach the set objective it was of utmost importance to characterize the status of chromatin at various levels of its structure organization and its behavior in the cellular cycle.

The analysis of data provided in table 1 demonstrates that UCA — are the events that occur occasionally in stimulated T-cells of the residents of the Southern Urals. For example, 60% of the examined individuals in the comparison group in three age periods (the age-range is 40–89) did not have cells with UCA except for the chromosome-exchanges aberrations in members of the oldest age-group. It should also be noted that according to the protocols of the cytogenetic study the exchange aberrations in members of the comparison group were represented mainly by dicentrics without paired fragments which proved that cells had undergone the first mitosis *in vivo*. Only older donors had ring chromosomes and acentric fragments. Similar situation for the dicentrics without paired fragments was observed in exposed individuals. It is known that unstable chromosomes that developed due to the exposure of

Table 7. Frequency of micronuclei with X-chromosome centromere signals, %

No. of the Donor	Cells	Number of MN	Cen X+, %	1 signal, %	2 signals, %	3 signals, %	4 signals, %	Cen X-, %
1	2683	134	59	25.3	68.3	5.1	1.3	41
2	2234	70	40	28.6	71.4	–	–	60
3	1941	27	22.2	66.7	33.3	–	–	77.8
4	633	22	54.5	50	41.7	–	8.3	45.5
5	3191	55	49	37	55.6	7.4	–	51
6	1000	35	22.9	12.5	87.5	–	–	77.1
Total "Exposed persons"		343	46.6	30.6	64.3	3.75	1.25	53.4
7	1667	46	32.6	73.4	13.3	–	13.3	67.4
8	3000	127	30.7	66.7	30.7	–	2.6	69.3
Total "Comparison group"		173	31.2	68.5	26	–	5.5	68.8

Table 8. Dependence of the telomere region length (%T/C) in metacentric and acrocentric chromosomes on sex (median, 25% and 75%)

No. of the chromosome	Chromosome arm	Male, n = 11			Female, n = 11		
		Median	Percentile		Median	Percentile	
			25%	75%		25%	75%
1	p	21.7	11.1	44.3	19.1	10.1	37.6
	q	23.1*	9.8	42	16	8.8	33.6
3	p	21.4*	10.3	46.2	16.8	9.7	30.8
	q	16.4	8.2	40.8	14.8	7.6	29.4
19	p	13.7	7.7	34.1	12.7	6.6	24.7
	q	12.8	6.7	33.2	11.3	6.4	26
20	p	18.3	8.8	33	16.3	9.5	29.2
	q	15.4*	8.5	32.9	11.9	5.9	20.1
13	p	19	9.5	43.4	18.7	10.9	33.3
	q	19.3*	8.5	40.8	14	7.7	29.1
14	p	16.1	8.9	37.6	16.1	9.3	32.6
	q	17.6	8.5	35.3	14.5	7.1	30
15	p	15.3	8.3	32.3	18.1	9.1	35.1
	q	15.5*	6.9	31	11.9	6.4	23.4
21	p	15.1	7.6	39	16.7	8.5	36.1
	q	12.5*	6.5	32.2	11	5.1	27.1
22	p	16.7	8.4	41	15	7.8	32
	q	13.3	6	32.4	12.3	5.9	26

Note: * — statistically significant sex-dependent difference of the values, $p < 0.05$.

the hematopoietic stem cells (HSC) in the bone marrow are eliminated eventually together with the cells that contain them. However, the UCA frequency in exposed individuals exceeds that in the comparison group in the long-term after the onset of radiation exposure. Evidently, the majority of aberrant cells registered in the long-term period after the onset of radiation exposure were exposed in the bone marrow (their precursors),

entered the blood flow, underwent differentiation in the thymus, and remained in quiescent state until the PHA-stimulation *in vitro*.

Micronuclei can be formed as a result of the damage associated with both unrepaired chromosome DNA breaks, and during chromosome segregation impairment which is predetermined by changes in the cytosine methylation in centromeric regions of the chromosome, impairment in the

Table 9. The median of the telomere regions (%T/C) in metacentric and acrocentric chromosomes in women from the comparison group and from the group of chronically exposed people (median, 25% and 75%)

No. of the chromosome	Chromosome arm	Comparison group, n = 20			Exposed persons, n = 22		
		Median	Percentile		Median	Percentile	
			25%	75%		25%	75%
1	p	17.3	7.2	36.6	16	7	35.7
	q	14.6**	6.3	31.2	13.3	5.9	28.8
3	p	16.0*	6.7	31.3	14	6	30.3
	q	12.7**	5.5	26.8	12.2	5.2	24.5
19	p	11.7**	4.7	24	10.5	4.4	22
	q	10.8	5	24.5	9.4	4.5	21.2
20	p	14.4*	7.6	27.6	13.6	7.6	25.8
	q	10.0*	4.7	22.7	9.9	4.5	19.9
13	p	16.7	7.9	32.5	16.6	8	31.1
	q	13.4*	5.5	30.2	12.5	5.2	27.6
14	p	17.1	8.7	32.1	15.5	8.3	30
	q	13.3	5.4	29.4	12	4.8	26.6
15	p	16.6*	7.6	31	15.7	7.5	28.9
	q	11.3	4.8	24	10.4	4.2	21
21	p	16	7.1	32.8	15.2	7	30.1
	q	10.1**	4.5	22.9	9.2	4	30.1
22	p	15	6.9	4.7	13.5	6.1	27.1
	q	10.6*	4.7	24.9	10.1	4.5	21.3

construction of the kinetochore protein and microtubes, and with many other events [19]. In the study [20], having performed the analysis of the age-dependent frequency of cells with micronuclei in unexposed residents of the Southern Urals, we have revealed monotonous increase in the parameter values in men and women aged ≤ 69 years. After the age of 70 this value remains stable or slightly decreases. Similar results concerning the frequency of cells with micronuclei in the age group 60–69 years have been obtained by other researchers. They showed that at the age of 50–69 the frequency of micronuclei reaches its maximum, and then levels off [21–23].

In the current research the age of the examined exposed individuals was 50–89 years. It is the age when micronuclei frequency reaches the plateau. That is why, the frequency of lymphocytes with micronuclei in exposed people is not associated with the increase in age in this age range either.

The study of the sex effect on the frequency of lymphocytes with micronuclei demonstrated that this value is statistically significantly higher in women than in men, $p = 0.001$. When we compared the frequency of lymphocytes with micronuclei between men and women in different age groups it turned out that there were statistically significant differences in the groups of exposed individuals aged 60–69 and 70–79. Thus, it can be said that the differences in the frequency of micronuclei between men and women are more pronounced in the group of exposed individuals, than in the group of unexposed ones. The studies show that the differences in the ratio "frequency of micronuclei in men/women" become more pronounced in people aged 40 and older [21]. However, the mechanisms that lead to such age-dependent increase is not completely clear. In the published papers there are some data stating that sex chromosomes are eliminated to the micronuclei with age. In our study we have noted that micronuclei with X-chromosome are rather frequent and make up 22–59% of the total number of micronuclei. Moreover, micronuclei contain X-chromosomes both with single and several centromeres. It is indicative of the chromosome nondisjunction in the mitotic anaphase. Probably, in our case radiation can have certain impact even without linear dependence of micronuclei frequency on the RBM dose.

In the study [24] the chromosome composition of the micronuclei in exposed women was analyzed using mFISH technique. The study has also demonstrated that X-chromosome is often observed in micronuclei composition. On the average in the group of exposed women the micronuclei are composed of bigger number of chromosomes relative to the comparison group. The amount of chromosome signals per micronucleus in exposed women doubles that in the control group ($p = 0.001$). At the same time mean frequency of micronuclei per 1000 estimated binucleated lymphocytes does not differ in women of these two groups. These results point indirectly at increased frequency of chromosome damages and their elimination from the nuclear genome to micronuclei. The mechanisms of micronucleus formation are similar in the group of exposed women and in the comparison group. Nevertheless, exposed women have some specific features of mono- and multicolored micronuclei formation. Thus, we can assume that there are mechanisms of the segregation impairment of the sex chromosomes and chromosomes with aberrations.

In accordance with the obtained data the relative telomere length in each donor varies within a wide range. Telomeres differ in length both within one cell, and within one chromosome pair. These data agree with the findings of the previous studies [16, 25] and published research data [26–28]. Our findings have demonstrated that the telomere length does not depend on a chromosome or arm where it is located [16]. In the course

of the study we revealed the dependence of the chromosome telomere length on sex: the telomeres were statistically significantly longer in the studied groups of chromosomes in men than those in women.

In the present study in the course of the analysis a statistically significant decrease in the thelomere signals in metacentric and acrocentric chromosomes of exposed women was noted relative to the comparison group. Statistically significant differences were observed for the chromosome arms 1q, 3p, 3q, 20p, 20q, 13q, 15p, 22q ($p < 0.05$); 19p, 21q ($p < 0.01$). These data are in line with the published research data that show that low dose exposure shortens the telomeres. These changes persist even in 20–70 years after the exposure [29, 30]. It is of interest to note that the effect of ionizing radiation exposure on the telomere length is dubious. Some studies demonstrate that the telomeres lengthen in exposed people, which is associated with the elevated expression of the telomerase (the authors associate it with the increased risk of malignant neoplasms development). If the telomeres are short, then it is associated with the replicative ageing of the cells [31, 32]. Moreover, the results we have obtained could be the evidence of the fact that ionizing radiation induced immune cell death in the period of maximum exposure. It resulted in compensatory proliferation of cell differons in hematopoietic organs, and thus, in telomere shortening.

The analysis of the obtained data allows us to draw a conclusion that chronic radiation exposure that occurred in the Southern Urals influences T-cell aging indirectly, as one of the numerous factors. Perhaps, the selection criteria of donors for the cytogenetic study, which could contribute to the selection of the most radio-resistant donors to the group of exposed individuals, influenced the results. For instance, according to the selection criteria, only people without cancer, autoimmune disease, and diabetes in past medical history could be included into the study. Taking into account the fact that the above-mentioned diseases start manifestating more frequently in elderly and old age, then it is rather probable that radiosensitive individuals among the exposed ones could have bigger chance to develop the radiation exposure effects, and therefore, when the groups of donors were being formed, these people did not meet the study inclusion criteria [20–33].

CONCLUSIONS

Based on the conducted cytogenetic study it can be said that chronic radiation exposure that have occurred in the Southern Urals is just one of the factors that influence indirectly the cellular senescence of the peripheral blood T-lymphocytes. The frequency of unstable chromosome aberrations in exposed individuals was statistically significantly higher in the age group 40–59 years ($p = 0.012$). There was a weak linear correlation of the studied parameters and the dose to the bone marrow in the pooled group of the exposed individuals ($R = 0.125$, $p = 0.005$). The frequency of lymphocytes with micronuclei in exposed individuals was similar to that in the comparison group. The frequency of lymphocytes with micronuclei differed in exposed men and women ($p = 0.001$). In 22-59% of the exposed women micronuclei contained X-chromosome. No dependence of the frequency of lymphocytes with micronuclei on the dose to the bone marrow was observed. Statistically significant decrease in the telomere length was found in the exposed individuals (for the chromosome arms 1q, 3p, 3q, 20p, 20q, 13q, 15p, 22q ($p < 0.05$); for chromosome arms 19p, 21q ($p < 0.01$)). In the studied groups the value of the relative length of the telomere regions was statistically significantly higher in men than that in

women (for chromosome arms 1q, 3p, 20q, 13q, 15q, 21q). We cannot exclude the fact that the selection criteria of the elderly donors for the cytogenetic study that is performed many years after the onset of exposure could promote the inclusion into the study group the most radio-resistant exposed people, and it can have counterintuitive results.

References

1. Akleev AV, editor. Posledstviya radioaktivnogo zagryazneniya reki Techa. Chelyabinsk: Kniga, 2016; p. 400. Russian.
2. Aunan J, Watson MM, Hagland HR, et al. Molecular and biological hallmarks of ageing. British Journal of Surgery. 2016; 103 (2): 29–46.
3. Richardson R. Ionizing radiation and aging: rejuvenating an old idea. Aging. 2009; 1 (11): 887–902.
4. Little MP, Brenner AV, Grant E J, et al. Age effects on radiation response: summary of a recent symposium and future perspectives. International Journal of Radiation Biology. 2022; 2: 1–11.
5. López-Otín C, Blasco MA, Partridge L. The hallmarks of aging. Cell. 2013; 153 (6); 1194–217.
6. Bauchinger M. Quantification of low-level radiation exposure by conventional chromosome aberration analysis. Mutation Research. 1995; 339: 177–89.
7. Lyubimova NE, Vorobtsova IE. The Effect of Age and Low-Dose Irradiation on the Chromosomal Aberration Frequency in Human Lymphocytes. Radiation Biology. Radioecology. 2007; 47 (1): 80–5. Russian.
8. Sevankaev AV, Khvostunov IK, Snigiryova GP, et al. Comparative Analysis of Cytogenetic Examination of Control Groups of Subjects Carried out in Different Russian Laboratories. Radiation Biology. Radioecology. 2013; 53 (1): 5–24. Russian.
9. Sigurdson A, Hauptmann M, Bhatti P, et al. International study of factors affecting human chromosome translocations. Mutation Research. 2008; 652 (2): 112–21.
10. Fenech M, Bonassi S. The effect of age, gender, diet and lifestyle on DNA damage measured using micronucleus frequency in human peripheral blood lymphocytes. Mutagenesis. 2011; 26 (1): 43–9.
11. Olovnikov AM. Starenie est' rezul'tat ukorocheniya «differoteny» v telomere iz-za kontsevoy nedoreplikatsii i nedoreparatsii DNK. Izvestiya AN SSSR, Ser. biol. 1992; 4: 641–3. Russian.
12. Aubert G, Lansdorp PM. Telomeres and aging. Physiological Reviews. 2008; 88 (2): 557–79.
13. Degteva MO, Napier BA, Tolstykh EI, et al. Enhancements in the Techa River Dosimetry System: TRDS-2016 D code for reconstruction of deterministic estimates of dose from environmental exposures. Health Physics. 2019; 117 (4): 378–87.
14. IAEA. Cytogenetic dosimetry: applications in preparedness for and response to radiation emergencies. Vienna, Austria: IAEA, 2011; p. 229.
15. Fenech M. Cytokinesis-block micronucleus cytome assay. Nat Protoc. 2007; 2 (5): 1084–104.
16. Krivoshchapova YaV, Vozilova AV. The study of the telomere length of the chromosomes in T-lymphocytes of the exposed individuals. Radiation Safety Problems. 2022; 3 (107): 71–9. Russian.
17. King RC, Stansfield WD, Mulligan PK. A Dictionary of genetics. 7th ed. Oxford University Press, 2006; p. 608.
18. Pilinskaya MA. Tsitogeneticheskie effekty v somaticheskikh kletkakh lits, postradavshikh vsledstvie Chernobyl'skoy katastrofy, kak biomarker deystviya ioniziruyushchikh izlucheniy v malykh dozakh. Mezhdunarodnyy zhurnal radiatsionnoy meditsiny. 1999; 2: 60–6. Russian.
19. Fenech M, Kirsch-Volders M, Natarajan A, et al. Molecular mechanisms of micronucleus, nucleoplasmic bridge and nuclear bud formation in mammalian and human cells. Mutagenesis. 2011; 26 (1): 125–32.
20. Akhmadullina YuR. Study of the age dependence of the spontaneous frequency of lymphocytes with micronuclei in residents of the South Urals. Environment and Human: Ecological Studies. 2021; 11 (2): 230–45. Russian.
21. Fenech M, Neville S, Rinaldi J. Sex is an important variable affecting spontaneous micronucleus frequency in cytokinesis-blocked lymphocytes. Mutation Research. 1994; 313: 203–7.
22. Bolognesi C, Abbondandolo A, Barale R, et al. Age-related increase of baseline frequencies of sister chromatid exchanges, chromosome aberrations, and micronuclei in human lymphocytes. Cancer Epidemiology. 1997; 6 (4): 249–56.
23. Jones KH, York TP, Juusola J, et al. Genetic and environmental influences on spontaneous micronuclei frequencies in children and adults: a twin study. Mutagenesis. 2011; 26 (6): 745–52.
24. Akhmadullina YuR. Sostav mikroyader v T-limfotsitakh u zhenshchin, podvergshikhsya khronicheskomu radiatsionnomu vozdeystviyu. Radiation Biology. Radioecology. 2022; 62 (6): 591–601. Russian.
25. Vozilova AV, Krivoshchapova YaV. Investigation of the Frequency of Inversions and Complex Translocations in T-Lymphocytes in Irradiated Residents of the Southern Urals. Radiation Biology. Radioecology. 2022; 62 (4): 408–15. Russian.
26. Ning Y, Xu JF, Li Y, et al. Telomere length and the expression of natural telomeric genes in human fibroblasts. Human Molecular Genetics. 2003; 12 (11): 1329–36.
27. Ferrucci L, Gonzalez-Freire M, Fabbri E, et al. Measuring biological aging in humans: A quest. Aging Cell. 2020; 19 (2): e13080.
28. Shaffer LG, Tommerup N, editors. An International System for Human Cytogenetic Nomenclature (2005) («ISCN 2005»). Recommendations of the International Standing Committee on Human Cytogenetic Nomenclature. Basel: S. Karger, 2005; p. 132.
29. Ilyenko I, Lyaskivska O, Bazyka D. Analysis of relative telomere length and apoptosis in humans exposed to ionising radiation. Exp Oncol. 2011; 33 (4): 235–8.
30. Lustig A, Shterev I, Geyer S, et al. Long term effects of radiation exposure on telomere lengths of leukocytes and its associated biomarkers among atomic-bomb survivors. Oncotarget. 2016; 7 (26): 38988.
31. Reste J, Zvigule G, Zvagule T, et al. Telomere length in Chernobyl accident recovery workers in the late period after the disaster. Journal of Radiation Research. 2014; 55 (6): 1–12. DOI: 10.1093/jrr/rru060.
32. Berardinelli F, Nieriab D, et al. Telomere loss, not average telomere length, confers radiosensitivity to TK6-irradiated cells. Mutation Research. 2012; 740: 13–20.
33. Vozilova AV. Assessment of the effect of chronic exposure on premature aging of human T-lymphocytes based on unstable chromosome aberrations. Extreme medicine. 2023; 2: 85–90. Russian.

Литература

1. Аклеев А. В., редактор. Последствия радиоактивного загрязнения реки Теча. Челябинск: Книга, 2016; 400 c.
2. Aunan J, Watson MM, Hagland HR, et al. Molecular and biological hallmarks of ageing. British Journal of Surgery. 2016; 103 (2): 29–46.
3. Richardson R. Ionizing radiation and aging: rejuvenating an old idea. Aging. 2009; 1 (11): 887–902.
4. Little MP, Brenner AV, Grant E J, et al. Age effects on radiation response: summary of a recent symposium and future perspectives. International Journal of Radiation Biology. 2022; 2: 1–11.
5. López-Otín C, Blasco MA, Partridge L. The hallmarks of aging. Cell. 2013; 153 (6); 1194–217.

6. Bauchinger M. Quantification of low-level radiation exposure by conventional chromosome aberration analysis. Mutation Research. 1995; 339: 177–89.

7. Любимова Н. Е., Воробцова И. Е. Влияние возраста и низкодозового облучения на частоту хромосомных аберраций в лимфоцитах человека. Радиационная биология. Радиоэкология. 2007; 47 (1): 80–5.

8. Севанькаев А. В., Хвостунов И. К., Снигирёва Г. П. и др. Сравнительный анализ результатов цитогенетических обследований контрольных групп лиц в различных отечественных лабораториях. Радиационная биология. Радиоэкология. 2013; 53 (1): 5–24.

9. Sigurdson A, Hauptmann M, Bhatti P, et al. International study of factors affecting human chromosome translocations. Mutation Research. 2008; 652 (2): 112–21.

10. Fenech M, Bonassi S. The effect of age, gender, diet and lifestyle on DNA damage measured using micronucleus frequency in human peripheral blood lymphocytes. Mutagenesis. 2011; 26 (1): 43–9.

11. Оловников А. М. Старение есть результат укорочения «дифферотены» в теломере из-за концевой недорепликации и недорепарации ДНК. Известия АН СССР, Сер. биол. 1992; 4: 641–3.

12. Aubert G, Lansdorp PM. Telomeres and aging. Physiological Reviews. 2008; 88 (2): 557–79.

13. Degteva MO, Napier BA, Tolstykh EI, et al. Enhancements in the Techa River Dosimetry System: TRDS-2016 D code for reconstruction of deterministic estimates of dose from environmental exposures. Health Physics. 2019; 117 (4): 378–87.

14. IAEA. Cytogenetic dosimetry: applications in preparedness for and response to radiation emergencies. Vienna, Austria: IAEA, 2011; p. 229.

15. Fenech M. Cytokinesis-block micronucleus cytome assay. Nat Protoc. 2007; 2 (5): 1084–104.

16. Кривощапова Я. В., Возилова А. В. Исследование длины теломерных районов хромосом в Т-лимфоцитах облученных лиц. Вопросы радиационной безопасности. 2022; 3 (107): 71–9.

17. King RC, Stansfield WD, Mulligan PK. A Dictionary of genetics. 7th ed. Oxford University Press, 2006; p. 608.

18. Пилинская М. А. Цитогенетические эффекты в соматических клетках лиц, пострадавших вследствие Чернобыльской катастрофы, как биомаркер действия ионизирующих излучений в малых дозах. Международный журнал радиационной медицины. 1999; 2: 60–6.

19. Fenech M, Kirsch-Volders M, Natarajan A, et al. Molecular mechanisms of micronucleus, nucleoplasmic bridge and nuclear bud formation in mammalian and human cells. Mutagenesis. 2011; 26 (1): 125–32.

20. Ахмадуллина Ю. Р. Изучение возрастной зависимости спонтанной частоты лимфоцитов с микроядрами у жителей Южного Урала. Социально-экологические технологии. 2021; 11 (2): 230–45.

21. Fenech M, Neville S, Rinaldi J. Sex is an important variable affecting spontaneous micronucleus frequency in cytokinesis-blocked lymphocytes. Mutation Research. 1994; 313: 203–7.

22. Bolognesi C, Abbondandolo A, Barale R, et al. Age-related increase of baseline frequencies of sister chromatid exchanges, chromosome aberrations, and micronuclei in human lymphocytes. Cancer Epidemiology. 1997; 6 (4): 249–56.

23. Jones KH, York TP, Juusola J, et al. Genetic and environmental influences on spontaneous micronuclei frequencies in children and adults: a twin study. Mutagenesis. 2011; 26 (6): 745–52.

24. Ахмадуллина Ю. Р. Состав микроядер в Т-лимфоцитах у женщин, подвергшихся хроническому радиационному воздействию. Радиационная биология. Радиоэкология. 2022; 62 (6): 591–601.

25. Возилова А. В., Кривощапова Я. В. Исследование частоты инверсий и комплексных транслокаций в Т-лимфоцитах у облученных жителей Южного Урала. Радиационная биология. Радиоэкология. 2022; 62 (4): 408–15.

26. Ning Y, Xu JF, Li Y, et al. Telomere length and the expression of natural telomeric genes in human fibroblasts. Human Molecular Genetics. 2003; 12 (11): 1329–36.

27. Ferrucci L, Gonzalez-Freire M, Fabbri E, et al. Measuring biological aging in humans: A quest. Aging Cell. 2020; 19 (2): e13080.

28. Shaffer LG, Tommerup N, editors. An International System for Human Cytogenetic Nomenclature (2005) («ISCN 2005»). Recommendations of the International Standing Committee on Human Cytogenetic Nomenclature. Basel: S. Karger, 2005; p. 132.

29. Ilyenko I, Lyaskivska O, Bazyka D. Analysis of relative telomere length and apoptosis in humans exposed to ionising radiation. Exp Oncol. 2011; 33 (4): 235–8.

30. Lustig A, Shterev I, Geyer S, et al. Long term effects of radiation exposure on telomere lengths of leukocytes and its associated biomarkers among atomic-bomb survivors. Oncotarget. 2016; 7 (26): 38988.

31. Reste J, Zvigule G, Zvagule T, et al. Telomere length in Chernobyl accident recovery workers in the late period after the disaster. Journal of Radiation Research. 2014; 55 (6): 1–12. DOI: 10.1093/jrr/rru060.

32. Berardinelli F, Nieriab D, et al. Telomere loss, not average telomere length, confers radiosensitivity to TK6-irradiated cells. Mutation Research. 2012; 740: 13–20.

33. Возилова А. В. Оценка влияния хронического облучения на преждевременное старение Т-лимфоцитов человека на основе нестабильных хромосомных аберраций. Медицина экстремальных ситуаций. 2023; 2: 85–90.

EVALUATION OF ANTI-RADIATION EFFICACY OF THE *STAPHYLOCOCCUS AUREUS*-DERIVED THERAPEUTIC AGENT

Gaynutdinov TR[1,2,3]✉, Ryzhkin SA[2,3,4,6], Shavaliev RF[4,5], Vagin KN[1,2], Kurbangaleev YaM[1], Kalimullin FH[1], Plotnikova EM[1], Idrisov AM[1], Ohrimenko SE[3], Mayorova EN[1]

[1] Federal Center for Toxicological, Radiation, and Biological Safety, Kazan, Russia
[2] Kazan Federal University, Kazan, Russia
[3] Russian Medical Academy of Continuing Professional Education of the Ministry of Health of the Russian Federation, Moscow, Russia
[4] Kazan State Medical University of the Ministry of Health of the Russian Federation, Kazan, Russia
[5] Republican Clinical Hospital of the Ministry of Health of the Republic of Tatarstan, Kazan, Russia
[6] Academy of Sciences of the Republic of Tatarstan, Kazan, Russia

The study is relevant due to the fact that the decrease in microbial toxicity observed during the radio-inactivation of microorganisms is accompanied by synthesis of radioprotective substances and exertion of the radioprotective effects associated with administration of such microbial agents to exposed animals. The study was aimed to assess radioprotective efficacy of the exposed *Staphylococcus aureus* variants. The study showed that the *Staphylococcus aureus* culture treated with a single dose of gamma radiation (30–40 kGy) ensured protection of 55–66% of the lethally irradiated animals. Multiple exposures of the test microorganism to the gradually increasing doses of gamma radiation induced an even larger increase in radioresistance resulting from the synthesis of endogenic radioprotectors, particularly peroxidase, the antioxidant enzyme, and IL1β cytokine, ensuring interception of the radiation-induced toxic radicals and thereby preventing post-exposure pancytopenia in the bone marrow. The experiments involving white mice exposed to the absolutely lethal gamma radiation doses (7.9 Gy, $LD_{100/30}$) showed that a single subcutaneous administration of the *St. aureus* radioresistant variant (strain $209R_{70}$) in a dose of 2×10^8 bacterial cells per animal 3 days after the exposure ensured the 77.7% survival rate, while 100% of untreated animals died. Based on the findings it was concluded that inclusion of the exposed agents of microbial origin would make it possible to increase the efficacy of the combination radioprotectors.

Keywords: *Staphylococcus aureus*, gamma rays, radio inactivation, radio modification, laboratory animals, anti-radiation effectiveness

✉ **Correspondence should be addressed:** Timur R. Gaynutdinov
Nauchnyj Gorodok, 2, Kazan, 420075, Russia; gtr_timur@mail.ru

ОЦЕНКА ПРОТИВОРАДИАЦИОННОЙ ЭФФЕКТИВНОСТИ ЛЕЧЕБНОГО СРЕДСТВА НА ОСНОВЕ *STAPHYLOCOCCUS AUREUS*

Т. Р. Гайнутдинов[1,2,3] ✉, С. А. Рыжкин[2,3,4,6], Р. Ф. Шавалиев[4,5], К. Н. Вагин[1,2], Я. М. Курбангалеев[1], Ф. Х. Калимуллин[1], Э. М. Плотникова[1], А. М. Идрисов[1], С. Е. Охрименко[3], Е. Н. Майорова[1]

[1] Федеральный центр токсикологической, радиационной и биологической безопасности, Казань, Россия
[2] Казанский (Приволжский) федеральный университет, Казань, Россия
[3] Российская медицинская академия непрерывного профессионального образования Министерства здравоохранения Российской Федерации, Москва, Россия
[4] Казанский государственный медицинский университет Министерства здравоохранения Российской Федерации, Казань, Россия
[5] Республиканская клиническая больница Министерства здравоохранения Республики Татарстан, Казань, Россия
[6] Академия наук Республики Татарстан, Казань, Россия

Актуальность проведенных исследований заключается в том, что снижение токсичности микроорганизмов в процессе их радиоинактивации сопровождается синтезом радиопротекторных субстанций и проявлением радиозащитного действия при введении этих микробных препаратов в организм облученных животных. Целью исследования было изучить радиозащитную эффективность облученных вариантов золотистого стафилококка. В работе установлено, что культура *Staphylococcus aureus*, подвергнутая однократному гамма-облучению в диапазоне доз от 30 до 40 кГр, обеспечивает защиту от 55 до 66% летально облученных животных. Многократное облучение тест-микроба постепенно возрастающими дозами гамма-лучей индуцировало еще большее возрастание радиорезистентности, обусловленное синтезом эндогенных радиопротекторов, в частности антиоксидантного фермента пероксидазы и цитокина IL1β, обеспечивающих перехват радиоиндуцированных токсических радикалов, предотвращая тем самым пострадиационную панцитопению в костном мозге. В опытах на белых мышах, облученных гамма-лучами в абсолютно летальных дозах (7,9 Гр, $ЛД_{100/30}$), показано, что однократное подкожное введение радиорезистентного варианта *St. aureus* штамм $209R_{70}$ в дозе 2×10^8 микробных клеток на особь через 3 суток после облучения обеспечивало 77,7% выживаемость при 100% гибели нелеченых животных. На основании полученных результатов сделано предположение, что включение облученных препаратов микробного происхождения позволит повысить эффективность комплексных радиозащитных средств.

Ключевые слова: золотистый стафилококк, гамма-лучи, радиоинактивация, радиомодификация, лабораторные животные, противорадиационная эффективность

✉ **Для корреспонденции:** Тимур Рафкатович Гайнутдинов
ул Научный городок, д. 2, г. Казань, 420075, Россия, gtr_timur@mail.ru

The principal bases of today's radiation microbiology are widely used in medicine and veterinary medicine (sterilization of the substances of microbial origin, antibiotics, blood, serums, vaccines, culture media, estimation of the irradiated feed and food biosafety) [1, 2]. The radio-inactivated bacteria and viruses, as well as antigens (radio-vaccines, radio-antigens) are widely used in infectious diseases as preventive and diagnostic options. The determined antibacterial effects of ionizing radiation have made it possible to postulate the provisions most important for radiation microbiology and virology that provide the basis for modern radiation biology and radiation genetics of microorganisms and are used to obtain or construct radio-vaccines and radio-antigens [3–6]. Furthermore, the important role is played by the information that radio-inactivation of microorganisms is accompanied by the rapid decrease in microbial toxicity and the changes in microbial metabolism with induction of the synthesis of substances having radioprotective properties [7–10].

Reduction of microorganisms' toxicity with simultaneous induction of the radioprotective substance synthesis during attenuation or radio-inactivation provided the basis for assessment of the exposed microorganisms' capability of exerting radioprotective activity in cases of body's exposure to ionizing radiation [11, 12]. Furthermore, it was found that the use of both corpuscular Gram-negative bacteria vaccines (*Salmonella*, *Escherichia*, *Klebsiella*, etc.) and cellular components of microbial metabolits (endo-, exotoxins, polysaccharides, DNA) contributed to the significant increase in the exposed animals' survival rate, when the microbial products (MPs) were prescribed several hours or 1–2 days before, or during the first hours or days after the exposure [13–16].

The study was aimed to assess the effects of gamma rays on *Staphylococcus aureus* and the possibility of using the exposed microbial variants as radioprotective agents.

METHODS

The *Staphylococcus aureus* strain (st.) 209 obtained from the state collection of microorganisms of the Federal Center for Toxicological, Radiation, and Biological Safety, Kazan, Russia, was used as a test strain. Cultures were grown in the Kitt–Tarozzi liquid medium supplemented with 1% normal bovine serum (Federal Center for Toxicological, Radiation, and Biological Safety; Russia), tempered at the temperature of 37 °C for 72 h before the exposure. The 3-day culture grown was poured into glass flasks and pelleted by centrifugation at 3000 rpm for 40 min. Supernatant was drained, and the centrifugation pellet was diluted with sterile distilled water to the concentration of 1×10^9 microbial cells (m. c.) per cm^3. The resulting suspension of the *St. aureus* culture was packed in vials, 10 cm^3 per vial; these were secured with rubber stoppers and rolled in with aluminum caps. After that the vials containing the test culture were irradiated using the Researcher gamma device (Baltiets factory; Estonia) with the ^{60}Co radiation source, exposure dose rate of 2.652×10^{-2} A/kg, absorbed doses of 20, 25, 30, 35, 40, 45, 50, 55, 60, 65, and 70 kGy. The degree of the gamma-irradiated St. aureus suspension inactivation was determined by plating suspensions on the Kitt–Tarozzi medium with subsequent 7-day thermostating and daily registration of the presence or absence of microorganism growth.

To select radioresistant mutants, the single subcultures grown were repeatedly plated on the Kitt–Tarozzi medium containing normal bovine serum until confluence was achieved. The resulting subcultures were further exposed to the above steadily growing doses of gamma radiation in case of confluence.

The exposed cultures were subjected to microbiological analysis, for which serial dilutions in the sterile phosphate buffer were prepared and analyzed using the colony forming unit (CFU) assay by conducting standard procedures involving reinoculation of Petri dishes with the meat peptone agar (MPA). The latter were incubated for 24 h at a temperature of 3 °C. CFU were enumerated in three Petri dishes with 30–300 colonies using the New Brunswick Scientific Rietran II R automatic colony counter (New Brunswick Scientific; USA), the arithmetic mean was determined for each sample. Cell viability was expressed as the mean log10 ± SD for three iterations.

Smears of the cultures grown were made, Gram stained, and examined by microscopy using immersion and 90x magnification.

Anti-radiation activity of the exposed *St. aureus* variants and radioresistant *St. aureus* st. 209R variant was tested using the lethally irradiated outbred white mice with the body weight of 18–20 g. Acute radiation syndrome (ARS) was simulated using the stationary Puma gamma device (Isotope JSC; Russia) with the ^{137}Cs radiation source at a dose of 7.9 Gy ($LD_{100/30}$), dose rate of 2.5×10^{-5} A/kg, gamma field non-uniformity not exceeding 10%.

The experiments involved 117 white mice divided into 13 groups, 9 animals per group. Animals of 12 groups were exposed to the lethal gamma radiation dose (7.9 Gy), three days later they were once subcutaneously administered 0.2 cm^3 (2×10^8 m. c./animal) of the original non-exposed *St. aureus* st. 209 culture (group 1), St. aureus st. 209 culture exposed to the dose of 30 kGy (group 2), *St. aureus* st. 209 culture exposed to the dose of 35 kGy (group 3), *St. aureus* st. 209 culture exposed to the dose of 40 kGy (group 4), *St. aureus* st. 209 culture exposed to the dose of 45 kGy (group 5), *St. aureus* st. 209 culture exposed to the dose of 50 kGy (group 6), *St. aureus* st. 209 culture exposed to the dose of 55 kGy (group 7), *St. aureus* st. 209 culture exposed to the dose of 60 kGy (group 8), *St. aureus* st. 209 culture exposed to the dose of 65 kGy (group 9), *St. aureus* st. 209 culture exposed to the dose of 70 kGy (group 10), radioresistant *St. aureus* st. 209R$_{70}$ culture (group 11). Exposed animals of the control group (group 12) were administered 0.2 cm^3 of saline under the same conditions. Animals of group 13 remained non-exposed and untreated; they were used as biological controls.

The exposed, control and experimental animals were monitored for 30 days, dead animals and survivors were registered. The effects of the test substances of microbial origin were assessed based on survival rate and lifespan (ALS), blood morphology and biochemistry by the methods widely accepted in radiation hematology, as well as based on the antioxidant defense status (based on the malondialdehyde synthesis level).

Considering the fact that irradiation of animals, plants and microorganisms is associated with formation of toxic radiolytic products (radiotoxins), the experiments were conducted based on indication of these metabolites in the original and exposed staphylococcal cultures. The indirect hemagglutination assay (IHA) was used for indication of radiotoxins in the studied samples. For that the indirect hemagglutination reaction (IHR) was conducted using the anti-radiation antibody erythrocyte diagnosticum (ARAED) represented by the formalinized and tanned sheep erythrocytes sensitized with the anti-radiotoxic hyperimmune serum we had developed.

Immunochemical analysis of the disintegrants of the exposed *St. aureus* st. 209 variants was performed by conducting IHR with ARAED. For that serial two-fold (1:2, 1:4, 1:8, etc.) dilutions of the antigen in saline were prepared, each dilution was added one drop (330 µL) of the formalinized and tanned

sheep erythrocytes sensitized with the anti-radiotoxic serum (ARAED). The mixture of the test antigen and the diagnosticum was mixed thoroughly to obtain a homogenous suspension and left in the thermostat for 2–2.5 h at a temperature of 37 °C.

The reaction results were assessed using the method widely accepted in immunology. Quantitative estimates of the reaction were expressed as the radiotoxin titers (1:2, 1:4, 1:8, etc.) or logarithms to the base 2 (1:2 = 1$\log_2$; 1:4 = 2$\log_2$, etc.).

The reaction was supported by appropriate controls. The standard quinoid radiotoxin obtained from the lethally irradiated *St. aureus* st. 209 was used as a positive control in IHR, while the non-exposed variant of the culture was used as a negative control.

In the next phase of the study, peroxidase activity was determined in the cell suspension and the culture fluid of the radioresistant *St. aureus* st. 209R$_{70}$ variant [17]. Furthermore, pyrogallol, which was oxidized to purpurogallin with maximum absorbance, was used as the oxidizable substrate. Optical density was measured in the SF-46 spectrophotometer (LOMO LLC; Russia). The cell suspension culture fluid of the original and radioresistant *St. aureus* variants were obtained by the generally accepted method through centrifugation of broth culture; centrifugation pellet was diluted to the concentration of 1×10^3 m. c./cm^3, and supernatant was used as the culture fluid.

The test solution contained 0.8 mg of the 0.006 M sodium phosphate buffer, pH 6.8; 0.12 cm^3 of the enzyme extract (suspension, centrifuge liquid); 0.5 cm^3 of the 0.15% H$_2$O$_2$; 1.1 cm^3 of H$_2$O and 0.5 cm^3 of the 0.003 M pyrogallol. In controls, 0.5 cm^3 of H$_2$O were added instead of H$_2$O$_2$.

The enzyme activity was determined using the following formula:

$$A = D_{t2} - D_{t1} / (t2 - t1) \times c,$$

where A — enzyme activity, D — optical density, t — time, c — concentration.

Measurement was performed for 2.5–3 min.

In the next series of experiments, we assessed the mechanism underlying the anti-radiation effects of *St. aureus* st. 209R70 on the irradiated body. For that, the experiments were performed involving 30 white mice with the body weight of 15–20 g, divided into three groups, 10 animals per group. Animals of groups 1 and 2 were exposed to the lethal dose of gamma radiation (7.9 Gy, LD$_{100/30}$) using the Puma device. Animals of group 1 received a single subcutaneous injection of 0.2 cm^3 of the radioresistant *St. aureus* st. 209R$_{70}$ variant with a titer of 1×10^8 m. c./animal 3 days after the exposure. Animals of group 2 exposed to the specified gamma radiation dose were administered 0.2 cm^3 of sterile injection solution (exposure control). The non-exposed animals of group 3 received nothing and were used as biological controls.

The exposed animals were monitored throughout 30 days; clinical features and the ARS course were assessed. Anti-radiation activity of the agent was estimated based on survival rate, ALS, as well as blood morphology, antioxidant defense system status, cytokine synthesis, and response of the cell renewal system (depletion and restoration of hematopoietic cells in the bone marrow).

The cytokine-inducing activity of the radioresistant *St. aureus* st. 209R$_{70}$ variant was assessed by determining interleukin 1β (IL1β) concentrations in blood serum and bone marrow suspension by enzyme-linked immunoassay (ELISA) 24, 48, 72 h after the exposure and administration of the therapeutic agent. The Mouse IL1β ELISA kit (Biosourse, R&D, and Eudogen; USA) had an IL1β detection limit of 50 ng/cm^3 [18].

To estimate the levels of IL1β secretion by the red bone marrow cells, the femur was dissected in aseptic environment, crushed thoroughly in 0.5 cm^3 of saline supplemented with heparin. The resulting suspension was incubated for 5 h at 37 °C, and then centrifuged for 10 min at 800 g. The levels of cytokines in supernatant were determined per million bone marrow cells and the total number of myelokaryocytes in the femur.

The 30-day survival was used as an integral indicator of the test agent anti-radiation effect. Hemoprotective effect of the agent was estimated by enumeration of peripheral blood cells in the MINOS STO automatic analyzer (Horiba ABX Diagnostics; France). The antioxidant defense system functional competence was determined by measuring serum concentrations of the lipid peroxidation (LPO) stable aldehyde products reacting with thiobarbituric acid [19].

Statistical data processing was performed by parametric methods. Significance of differences between the indicators compared was determined using the Bonferroni adjusted Student's t-test.

RESULTS

Assessment of the *St. aureus* 209 test strain sensitivity to gamma radiation showed that the microorganism was highly radioresistant. Our findings showed that the lack of growth was observed in the sample exposed to the dose of 70 kGy only, while slow growth was reported in the dose range of 45–65 kGy [20].

After being exposed to the doses of 40–70 kGy, no culture growth was observed throughout 4 days after inoculation; sporadic colonies grew up in cases of prolonged cultivation (120 h). That is why we continued the experiments aimed to study the development of resistance to gamma radiation by the original culture during sequential exposure of the surviving colonies to the increasing radiation doses. Furthermore, sporadic colonies that grew up after the lethal exposure (40 kGy) were subjected to the prolonged passage on the Kitt–Tarozzi, MPA and MPB media until confluence was reached in order to obtain the radioresistant *St. aureus* variant. Such procedures were repeated many times using the increasing gamma radiation doses of 45, 50, 55, 60, 65, and 70 kGy.

When performing microscopic examination of the smears obtained from the exposed and Gram stained culture, Gram-positive single and paired cocci in the form of asymmetric grape bunches typical for this culture were clearly visible in the field of view.

The results of the study showed that the radioresistant *St. aureus* st. 209R$_{70}$ variant, the resistance of which to gamma radiation twice exceeded that of the original strain, was obtained from the original *St. aureus* st. 209 culture by selection of single surviving colonies after the exposure to each radiation dose and prolonged passage on the appropriate culture media during passage 10 following the exposure to the dose of 70 kGy.

In the next phase of the study, St. aureus 209 exposed to the specified doses of 30–70 kGy (30, 35, 40, 45, 50, 55, 60, 65, 70) and the radioresistant variant (*St. aureus* st. 209R$_{70}$) were tested for radioprotective properties in the lethally exposed white mice.

A slight swelling at the injection site that resolved within 24 h was reported in some animals after subcutaneous administration of the exposed *St. aureus* st. 209 cultures. Swelling, local hyperemia, pain at the injection site were observed in the control group in animals administered *St. aureus* st. 209 (original non-exposed culture).

Anti-radiation activity of the tested non-exposed and exposed *St. aureus* 209 variants assessed in the lethally exposed white mice is provided in Table 1.

Table 1. Survival of the lethally exposed white mice against the background of using the test *St. aureus* st. 209 variants 3 days after the single subcutaneous injection of the therapeutic agent, *n* = 9

Group number	*Staphylococcus aureus* st. 209 variant native and exp. to various doses	Agent administration method and volume, cm^3	ALS, days	Survival rate, %
1	Original st. *St. aureus* 209	subcutaneous, 0.2	8	22.2
2	*St. aureus* st. 209, exp. to the dose of 30 kGy	subcutaneous, 0.2	12.7	66.6
3	*St. aureus* st. 209, exp. to the dose of 35 kGy	subcutaneous, 0.2	13.7	66.6
4	*St. aureus* st. 209, exp. to the dose of 40 kGy	subcutaneous, 0.2	11.5	55.5
5	*St. aureus* st. 209, exp. to the dose of 45 kGy	subcutaneous, 0.2	11.2	44.4
6	*St. aureus* st. 209, exp. to the dose of 50 kGy	subcutaneous, 0.2	11	44.4
7	*St. aureus* st. 209, exp. to the dose of 55 kGy	subcutaneous, 0.2	9	44.4
8	*St. aureus* st. 209, exp. to the dose of 60 kGy	subcutaneous, 0.2	8.7	22.2
9	*St. aureus* st. 209, exp. to the dose of 65 kGy	subcutaneous, 0.2	8.4	22.2
10	*St. aureus* st. 209, exp. to the dose of 70 kGy	subcutaneous, 0.2	7.8	22.2
11	*St. aureus* st. 209R$_{70}$ (radioresistant variant)	subcutaneous, 0.2	17.5	77.7
12	Exposure control	–	6.8	0
13	Biological control	–	–	–

Note: m. c. — microbial cells; st. — strain; exp. — exposed.

Table 1 shows that the Staphylococcus exposure to the gamma radiation doses of 30–40 kGy leads to modification of the test microorganisms associated with the increase in anti-radiation activity, ensuring 55–66.6% of the lethally exposed animals' survival rate, which 2–3 times exceeds the baseline anti-radiation activity level in group 1. The further increase in the exposure dose of the original culture has a negative effect on the microorganisms: the anti-radiation activity level of animals exposed to the doses of 45–70 kGy drops from 44.4 to 22.2%, respectively.

In contrast to the original culture single exposure to the doses of 30–70 kGy, multiple exposure of the original culture obtained during the experiments from the *Staphylococcus* subcultures using the gradually increasing doses had a modifying effect on the test microorganisms. Anti-radiation activity of the radioresistant *St. aureus* st. 209R$_{70}$ variant 3.5 times exceeded that of the original strain and accounted for 77.7%. Furthermore, it was noted that the increase in another important radioprotection indicator, the average lifespan of dead animals (ALS), was reported along with the increase in survival rate of the lethally exposed animals when using the exposed *St. aureus* variants as radioprotective agents.

According to the data provided, ALS of the animals suffering from ARS after using the non-exposed *St. aureus* st. 209 variant was 8.0. The use of cultures exposed to the doses of 30–50 kGy resulted in the increase of this indicator to 11.0–13.7 days (variants 6, 5, 4, 3, 2). The use of the radioresistant *St. aureus* st. 209R$_{70}$ variant as a radioprotective agent ensured the increase in the average lifespan of dead animals to 17.5 days vs. 8.0 days reported for the original *Staphylococcus* strain, which 2.19 times exceeded the value of the original strain.

The above experiments repeated using the other laboratory animal species, white rats exposed to the lethal doses (9.5 Gy, LD$_{100/30}$) and treated with the radio-modified *St. aureus* st. 209 variants (30, 35, 40, 45, 50, 55, 60, 65, 70) and the radioresistant variant (St. aureus st. 209R$_{70}$), yielded similar results.

Analysis of the data provided in Table 1 shows that the exposure of the original *St. aureus* st. 209 culture to the gamma radiation doses of 30–70 kGy has a multidirectional effect on the exposed cultures' capability of inducing various degrees of body's radioresistance to lethal irradiation. Furthermore, it was found that the *St. aureus* st. 209 cultures exposed to the doses of 30–40 kGy increased the anti-radiation activity level to 66.6%, while the exposure of the original culture to the

Table 2. Results of the radiotoxin indication in the *Staphylococcus aureus* st. 209 variants exposed to various gamma radiation doses

Staphylococcus aureus culture and its exp. variants	Radiation dose, kGy	Radiotoxin concentration, log$_2$	Survival rate of the lethally exp. animals against the background of using the exp. *St. aureus* variants
Original *St. aureus* st. 209 (non-exposed)	–	0.7 ± 0.01	22.2
St. aureus st. 209 (30)	30	2.0 ± 0.3	66.6
St. aureus st. 209 (35)	35	3.0 ± 0.5	66.6
St. aureus st. 209 (40)	40	4.0 ± 0.7	55.5
St. aureus st. 209 (45)	45	6.0 ± 0.9	44.4
St. aureus st. 209 (50)	50	7.0 ± 1.2	44.4
St. aureus st. 209 (55)	55	7.5 ± 0.9	44.4
St. aureus st. 209 (60)	60	8.0 ± 1.5	22.2
St. aureus st. 209 (65)	65	9.0 ± 1.7	22.2
St. aureus st. 209 (70)	70	10.0 ± 2.1	22.2
St. aureus st. 209R$_{70}$ (radioresistant variant)	70	2.4 ± 1.6	77.7

Note: st. — strain; exp. — exposed.

Table 3. Peroxidase activity of the cells of the original and radioresistant *St. aureus* st. 209 cultures

Bacterial strain	Peroxidase activity (c^{-1} mg^{-1})	
	Cell suspension	Culture fluid
St. aureus st. 209 (original culture)	$0.123 \times 10^{-3} \pm 0.01$	$0.031 \times 10^{-3} \pm 0.01$
St. aureus st. 209 R_{70} (radioresistant culture)	$0.267 \times 10^{-3} \pm 0.03$ ××	$0.09 \times 10^{-3} \pm 0.009$ ×××

Note: ×× — $p < 0.01$; ××× — $p < 0.001$; st. — strain.

doses of 45 kGy and above had an opposite effect, reducing radioprotective activity of the exposed *Staphylococcus* variants to 22.2%.

The results of the quinoid radiotoxin indication in the disintegrators of the *St. aureus* exposed to various gamma radiation doses in IHA with the antibody erythrocyte diagnosticum are provided in Table 2.

Table 2 shows that the *Staphylococcus* exposure to gamma radiation induces the increased synthesis of toxic radiolytic products (radiotoxins), the low doses of which (2.0–4.0 $\log_2$) have a stimulant effect on the body. The survival rate of the lethally irradiated animals increases to 66.6%, while excess production of toxic products (6.0–10.0 $\log_2$) decreases the exposed animals' survival rate; the anti-radiation level is between 44.4 and 22.2%. Therefore, the optimal gamma radiation exposure for the Staphylococcus culture is 30–35 kGy, and the exposure dose increase results in the increased synthesis of radiotoxin by the microorganism, i.e. is associated with reduction of the exposed *St. aureus* variants' anti-radiation factors.

In this regard, the increase in the anti-radiation effect of the radioresistant *St. aureus* st. 209R_{70} achieved by the repeated exposure of the original culture and its subcultures to the gradually increasing doses of 30–70 kGy is of interest. It is well known that the radioresistance development is accompanied by synthesis of antioxidant enzymes (catalase, superoxide dismutase). We conducted experiments on determining peroxidase, the antioxidant enzyme. This enzyme was selected for the study due to the fact that peroxidase represents the antioxidant enzyme, the major function of which is to disrupt peroxides, toxic radiolytic products that are dangerous for cell functioning.

The peroxidase activity measurement results for the *St. aureus* st. 209 and *St. aureus* st. 209R_{70} variants are provided in Table 3.

Table 3 shows that both test *St. aureus* variants exert peroxidase activity. However, that of radioresistant variant is 2.17 times higher ($p < 0.01$) compared to the original variant of microorganism. Similar upward trend of peroxidase activity was observed in the culture fluid, where the test microorganisms were grown. Furthermore, peroxidase concentration in the

culture fluid obtained when growing *St. aureus* st. 209R_{70} was 3 times higher ($p < 0.001$), than that in the original culture.

The data on the peroxidase antioxidant enzyme concentration increase in the culture fluid during incubation of *St. aureus* st. 209R_{70} obtained in this experiment show that the test culture can synthesize and express this enzyme *in vivo*, i.e. in the bodies of intact and exposed animals, exerting the antioxidant and, as a result, anti-radiation effect.

Considering the above, we conducted a series of experiments on exploring the mechanism underlying body's radioprotection in the context of using the radioresistant *St. aureus* st. 209R_{70} variants as potential anti-radiation agents.

The dynamic monitoring of the experimental animals showed that the single subcutaneous injection of the radioresistant *St. aureus* st. 209R_{70} variant had a radio-modifying effect, modifying both the ARS course and the exposed animals' survival rate and increasing the lifespan of dead animals. Furthermore, it was found that the control (exposed) animals had severe ARS and ALS of 6.8 days. In contrast to the controls, animals of the experimental group receiving *St. aureus* st. 209R_{70} as an anti-radiation agent had milder ARS. The animals' survival rate was 77.7%, and ALS of dead animals was 17.5 vs. 6.8 days in the control (exposed) group.

The increase in the lethally exposed animals' survival rate associated with using the test agent was accompanied by adjustment of radiation-induced pancytopenia (Table 4).

Table 4 shows that lethal irradiation of white mice causes a hemotoxic effect associated with the bone marrow depletion (myelokaryocyte death) and hematopoiesis suppression (significant leucopenia and lymphopenia). The use of the test agent had hemoprotective and myeloprotective effects, preventing severe pancytopenia, preserving the myelocyte and granulocyte pool in the bone marrow and peripheral blood.

Hemoprotective effect of the test agent was realized via inhibition of the toxic radiolytic product (malondialdehyde) synthesis and the more intense synthesis of cytokines, the immunohematopoiesis mediators (Table 5).

Table 5 shows that lethal irradiation of animals with gamma rays is associated with the rapid increase in serum MDA levels (5.85-fold, $p < 0.001$), along with the decrease in the IL1β immunoregulatory cytokine synthesis.

Table 4. Blood indicators of white mice on day 10 after the exposure and single subcutaneous injection of *St. aureus* st. 209R_{70}, $n = 10$

Indicators	Group of animals		
	Control	Exposure	Exposure + treatment *St. aureus* st. 209 R_{70}
Peripheral blood leukocyte counts ×10^9/L	5.4 ± 0.7	1.95 ± 0.1 ×××	4.98 ± 0.5
Peripheral blood neutrophil counts ×10^9/L	2.17 ± 0.3	1.03 ± 0.5 ××	1.95 ± 0.2
Peripheral blood lymphocyte counts ×10^9/L	4.39 ± 0.4	1.63 ± 0.3 ×××	3.98 ± 0.9
Myelokaryocyte counts in the hip bone marrow ×10^6/L	27.1 ± 1.3	15.7 ± 0.5 ××	26.3 ± 0.7

Note: ×× — $p < 0.01$; ××× — $p < 0.001$; st. — strain.

Table 5. Concentrations of malondialdehyde (MDA) and interleukin 1β in blood serum and bone marrow of the lethally irradiated white mice treated with *St. aureus* 209R$_{70}$ 8 days after the exposure and treatment, *n* = 10

Indicator	Group of animals		
	Control	Exposure	Exposure + treatment *St. aureus* 209R$_{70}$
MDA concentration in blood serum, µmol/g of protein	0.87 ± 0.05	5.09 ± 0.37***	1.05 ± 0.15
IL1β concentration in blood serum, ng/mL	55.1 ± 3.7	41.1 ± 5.9	87.1 ± 2.5
IL1β concentration in bone marrow of the femur, ng per 1 million cells	1.93 ± 0.31	1.05 ± 0.17**	1.78 ± 0.25

Note: ** — $p < 0.01$; *** — $p < 0.001$.

In this context, the use of substances of microbial origin (radioresistant *St. aureus* st. 209R$_{70}$ variant) has an antioxidant effect, inhibiting free radical oxidation and peroxidation of lipids and decreasing synthesis of the LPO aldehyde product, malondialdehyde.

At the same time, the agent of microbial origin used showed itself as the enhancer of the interleukin IL1β synthesis in peripheral blood and bone marrow of the exposed animals.

The reported biochemical alterations in the immunohematopoietic organs associated with the effects of the agent of microbial origin ensure the 70% survival rate in the lethally irradiated animals.

DISCUSSION

In recent years, domestic and foreign researchers have accumulated experimental data suggesting that substances of microbial origin (endotoxins, polysaccharides, toxoids, etc.) can increase body's resistance to ionizing radiation when studying various aspects of the mechanism underlying the anti-radiation effect [4, 11, 13–16]. Considering the above, we have carried out this study focused on assessing radioprotective properties of the radio-modified *St. aureus* variant.

The experiments conducted have shown conclusively that the Staphylococcus exposure to the gamma radiation doses of 30–40 kGy has a modifying effect on the microorganisms, it increases their anti-radiation activity by 22.2% compared to the original culture. Such results are well consistent with all the literature data on the issue. Many authors have shown that corpuscular bacteria, microbial polysaccharides, exo-, endotoxins, and toxoids increase survival rate of the experimental animals exposed to the ionizing radiation doses of about LD$_{80-90/30}$ by 20–30% [21]. There is no doubt that staphylococcal lipopolysaccharides contained in vaccines and other bacterial formulations have the same properties [22].

Staphylococcus was selected as a model to construct the microbial radioprotector due to the following facts: first, these microorganisms produce potent exo- and endotoxins, which convert to toxoids having radioprotective properties under exposure to physical and chemical factors (UV, ionizing radiation, formaldehyde, etc.) [23]; second, *St. aureus* has a powerful antioxidant system and is capable of inducing antioxidant enzymes [24] and cytokines [25]; third, highly effective medicines with the broad-spectrum biological activity are derived from phagolysates of pathogenic Staphylococcus strains.

When conducting this study, we proceeded from the premise that the role of microorganisms in protection against the effects of ionizing radiation is well understood. The animal body's defense mechanisms in the form of enhanced proliferation of the granular and lymphoid hematopoietic cells directly involved in the immune response are activated under exposure to the substances of microbial origin; platelet,

granulocyte counts and hemoglobin levels are increased, along with the activity of the endogenous and exogenous cells of the lymphoid system of the spleen, lymph nodes [26]. Furthermore, it was also considered that irradiation of microorganisms with the doses, insufficient to disrupt their DNA molecules, but quite enough for DNA rearrangement involving alteration of the DNA chain fragments, can lead to formation of the mutant bacteria with different cultural and morphological properties and some acquired useful qualities, specifically the ability to produce certain substances that are useful in terms of human practice [27].

Considering the need to develop new safe and effective anti-radiation agents for treatment of ARS, we conducted this study focused on assessing anti-radiation effects of the substances of microbial origin represented by medicines derived from *Staphylococcus*. When conducting the study, we used the data on the fact that physical effects on microorganisms induced the increase in the exposed organism's radioresistance through induction of Toll-like receptors (TLR) by microorganisms as a working hypothesis [4].

To test this hypothesis for eligibility, we exposed *Staphylococcus* to gamma radiation in the dose range of 30–70 kGy. The experiments showed that the *Staphylococcus* gamma exposure had a multidirectional effect on the microorganism, it increased or decreased the *St. aureus* radioprotecitive efficacy, depending on the dose. It was found that the *Staphylococcus* cultures exposed to gamma radiation doses of 30, 35 and 40 kGy exerted radioprotective activity, protecting 55.5–66.6% of the lethally exposed white mice from radiation-induced death. However, further increase in radiation dose (45–70 kGy) had an opposite effect, it decreased the level of animal's protection against ARS. The decrease in radioprotective activity of the *St. aureus* variants exposed to high doses is explained by the increased production of radiotoxins in the irradiated cultures, which results in the increased mortality among exposed animals due to summation (potentiation) of toxic effects of the irradiated bacteria and the macroorganism [20].

The repeated exposure of microorganisms to the gradually increasing ionizing radiation doses results in the stepwise radioresistance increase [27] accompanied by changes in cell metabolism together with induction of endogenous radioprotectors [21]; we conducted the study involving obtaining the radioprotective *St. aureus* variant. We obtained the radioresistant *St. aureus* 209R$_{70}$ variant that survived under exposure to the supraletal radiation dose (70 kGy) through repeated exposure of the test microorganism to the gradually increasing gamma radiation doses in the range of 30–70 kGy. When studying the mechanism of targeted acquisition of extreme radioresistance by *St. aureus*, it was found that the process of adaptation to the supraletal gamma radiation dose was accompanied by changes in bacterial cell metabolism with the increase in the levels of peroxidase, the antioxidant enzyme

playing one of the key roles in the context of body's exposure to stress factors, including ionizing radiation [17]. Our findings are consistent with the data of other authors, who revealed increased production of antioxidant enzymes (superoxide dismutase, hydroperoxidase), ubiquinone, enhanced recombination DNA repair in the radio-thermo-resistant *St. aureus* mutants [7, 28].

The ability of the radioresistant *St. aureus* variant to synthesize antioxidant enzymes during radio-adaptation ensured the increase in its anti-radiation properties in case of being used as an anti-radiation agent *in vivo*. The experiments involving white mice exposed to the absolutely lethal gamma radiation doses (7.9 Gy, $LD_{100/30}$) showed that the single subcutaneous injection of the radioresistant *St. aures* $209R_{70}$ variant in a dose of 2×10^8 m. c./animal 3 days after the exposure ensured the 77% survival rate, against 100% mortality among untreated animals. The increase in survival rate of the animals exposed and treated with *St. aureus* $209R_{70}$ was accompanied by transition from acute ARS to mild ARS, which resulted from prevention of pancytopenia and depopulation of the bone marrow. The mechanism underlying the hemo- and myeloprotective effect of the gamma-exposed microorganism (*St. aureus* $209R_{70}$) was realized as follows: first, through interception and neutralization by anti-radical enzymes (peroxidase and superoxide dismutase) of the radio-induced toxic radiolytic products ((malondialdehyde), the main

target of which is represented by the immunohematopoietic system cells (lymphocytes, monocytes, bone marrow stem cells); second, through induction of the cytokines (IL1β in our study) initiating post-radiation restoration of hematopoiesis via induction by the test microorganism, which is in line with the data reported by other researchers [29, 30].

CONCLUSIONS

The findings suggest that the therapeutic agents derived from *St. aureus* that have been exposed to radiation in the dose range of 30–40 kGy, demonstrate anti-radiation efficacy ensuring 66.6% survival of the lethally irradiated animals, while the radioresistant *St. aureus* st. $209R_{70}$ variant is superior to these agents, since it increases survival of animals exposed to $LD_{100/30}$ to 77.7% and prevents radiation-induced death. Substances of microbial origin are promising and feasible, since agents of this class are harmless and, which is more important, have polyfunctional (immunotropic, antioxidant, hemo- and myeloprotective) properties. Given the above, we believe that it is important to continue the search for measures increasing the efficacy of substances of microbial origin, since inclusion of agents of this class in the range of medications for radiation-induced injury might increase the efficacy of combined anti-radiation treatment.

References

1. de Cassan D, Hoheisel AL, Glasmacher B. Impact of sterilization by electron beam, gamma radiation and X-rays on electrospun poly-(ε-caprolactone) fiber mats. J Mater Sci: Mater Med. 2019; 30: 42. DOI: 10.1007/s10856-019-6245-7.
2. Tapia-Guerrero YS, Del Prado-Audelo ML, Borbolla-Jiménez FV, Gomez D, García-Aguirre l, Colín-Castro CA, et al. Effect of UV and Gamma Irradiation Sterilization Processes in the Properties of Different Polymeric Nanoparticles for Biomedical Applications. Materials (Basel, Switzerland). 2020; 13 (5): 1090. DOI: 10.3390/ma13051090.
3. Shehata MM, Gomaa FA, Helal Z. Effects of gamma and electron beam irradiation on viability and DNA elimination of Staphylococcus aureus. Archives of Clinical Microbiology. 2011; 121: 44–55. DOI: 10:3823/244.
4. Xu Y, Chen Y, Liu H, Lei X, Guo J, Cao K, et al. Heat-killed salmonella typhimurium (HKST) protects mice against radiation in TLR4-dependent manner. Oncotarget. 2017; 40 (8): 67082–93. DOI: 10.18632/oncotarget.17859.
5. Tobin GJ, Tobin JK, Gaidamakova EK, Wiggins TJ, Bushnell RV, Lee WM, et al. A novel gamma radiation-inactivated sabin-based polio vaccine. PloS one. 2020; 15 (1): e0228006. DOI: 10.1371/journal.pone.0228006.
6. Mullbacher A, Pardo J, Furuya Y. SARS-CoV-2 Vaccines: Inactivation by Gamma Irradiation for T and B Cell Immunity. Pathogens (Basel, Switzerland). 2020; 9 (11): 928. DOI: 10.3390/pathogens9110928.
7. Bruno-Barcena JM, Azcárate-Peril AM, Hassan HM. Role of antioxidant enzymes in bacterial resistance to organic acids. Applied and Euvironuental Microbiology. 2010: 76 (9): 2747–50. DOI: 10.1128/AEM.02718-09.
8. Mun GI, Kim S, Choi E, Kim CS, Lee YS. Pharmacology of natural radioprotectors. Archives of pharmacal research. 2018; 41 (11): 1033–50. DOI: 10.1007/s12272-018-1083-6.
9. Montoro A. Radioprotection and Radiomitigation: From the Bench to Clinical Practice. Biomedicines. 2020; 8 (11): 461. DOI: 10.3390/biomedicines8110461.
10. Gaynutdinov TR. Evaluation of the anti-radiation effectiveness of drugs derived from substances of microbial origin. Veterinarny Vrach. 2024; 1: 52–7. DOI: 10.33632/1998-698X_2024_1_52. Russian.
11. Riehl TE, Alvarado D, Ee X, Zuckerman A, Foster L, Kapoor V, et al. Lactobacillus rhamnosus GG protects the intestinal epithelium from radiation injury through release of lipoteichoic acid, macrophage activation and the migration of mesenchymal stem cells. Gut. 2019; 68 (6): 1003–13. DOI: 10.1136/gutjnl-2018-316226.
12. Gaynutdinov TR, Nizamov RN, Idrisov AM, Rakhmatullina GI, Guryanova VA. Obtaining radioactivated strains of microorganisms and studying their antiradiation efficiency IOP Conf. Series: Earth and Environmental Science. 2021; 723: 042008. DOI: 10.1088/1755-1315/723/4/042008.
13. Ivanov AA, Simbircev AS, Maltsev VN, Petrov LN, Andrianova IE, Stavrakova NM, et al. Lowering risk of being a carrier of opportunistic infections in case of radiation damage by using probiotic vitaflor and antibiotics. Extreme medicine. 2013; 1 (43): 76–81. Russian.
14. Kobatov AI, Verbitskaya NB, Polotsky AE, Savin II, Grebenyuk AN. Development of a technology for producing a fermented milk product on space shipboard and evaluation of its probiotic and potential radioprotective properties. Extreme medicine. 2019; 21 (4): 517–26. Russian.
15. Kobatov AI, Polyntsev DG, Savin II, Popova EV, Kutnik IV. The «Probiovit» Space Experiment: Outputs and Outlook (Part 1). Manned Spaceflight. 2023; 1 (46): 74–87. Russian.
16. Kobatov AI, Polyntsev DG, Savin II, Popova EV, Kutnik IV. The «Probiovit» Space Experiment: Outputs and Outlook (Part 2). Manned Spaceflight. 2023; 2 (47): 87–98. Russian.
17. Chance B, Sies H, Boveris A. Hydroperoxide methabolism in mammalian organs. Physiol Rev. 1979; 59 (3): 527–605. DOI: 10.1152/physrev.1979.59.3.527.
18. Mathialagan N, Roberts RM. A role for cytokines in early pregnancy. Indian J. Physiol Pharmacol. 1994; 38: 153–62. PubMed PMID: 7814074.
19. Guryanova VA, Tarasova NB. Lipid peroxygenation at liver injury by ionizing radiation. Academic notes of Kazan state academy of veterinary medicine named after N. Bauman. 2013; 213: 76–80. Russian.
20. Gaynutdinov TR. Experimental selection of doses of ionizing radiation causing growth inhibition and full inactivation of golden stafilokok. Veterinarny Vrach. 2020; 4: 4–8. DOI: 10.33632/1998-698X.2020-4-4-8. Russian.

21. Smith WW, Alderman IM, Gillespie RE. Increased survival in irradiated animals treated with bacterial endotoxins. Am J Physiol. 1957; 191 (1): 124–30. DOI: 10.1152/ajplegacy.1957.191.1.124.
22. Pluznik DY. Benefecial effect on endotoxins. Immunobiology and Immunopharmacology of Bacterial Endotoxins. 1986; 7: 124–8. DOI: 10.1007/978-1-4613-2253-5.
23. Ledney GD, Wilson R. Protection induced by bacterial endotoxin against whole body X-irradiation germfree and conventional mice. Proc Soc Exptl Biol Med. 1996; 118 (4): 1062–5. DOI: 10.3181/00379727-118-30046.
24. Almagambetov KKh. Molecular biology of Staphylococcus aureus. Meditsinskiy zhurnal Astana. 2021; 1 (107): 61–8. Russian.
25. Neta R. Role of cytokines in radioprotection. Pharmacology end Therapeutics. 1988; 39 (1–3): 261–6. DOI: 10.1016/0163-7258(88)90070-8.
26. Grebenyuk AN, Strelova OYu, Legeza TI, Stepanova EN. Osnovy radiobiologii i radiatsionnoy meditsiny: uchebnoe posobie. SPb.: OOO «Izd-vo FOLIANT», 2012; p. 232. Russian.
27. Gallyamova MYu, Vagin KN, Gaynutdinov TR, Rakhmatullina GI, Ryzhkin SA. The effect of multiple ionizing radiation on the activity of antioxidant enzymes of Escherichia coli "PL-6" cells. Radiation and risk. 2024; 33 (1): 68–76. DOI: 10.21870/0131-3878-2024-33-1-68-76. Russian.
28. Gaupp R, Lei S, Reed JM, Peisker H, Boyle-Vavra S, Bayer AS, et al. Staphylococcus aureus metabolic adaptations during the transition from a daptomycin susceptibility phenotype to a daptomycin nonsusceptibility phenotype. Antimicrobial agents and chemotherapy. 2015; 59 (7): 4226–38. DOI: 10.1128/AAC.00160-15.
29. Linder H, Holler E, Ertl B, Multhoff G, Schreglmann M, Klauke I, et al. Peripheral blood mononuclear cells induce programmed cell death in human endothelial call and may prevent repair: role of cytokines. Blood. 1997; 29 (6): 1931–8. PubMed PMID: 9058713.
30. Neta R, Oppenheim J. The role of cytokines in immunoregulation. Cancer call. 1991; 3 (10): 391–6. DOI: 10.1016/0163-7258(88)90070-8.

Литература

1. de Cassan D, Hoheisel AL, Glasmacher B. Impact of sterilization by electron beam, gamma radiation and X-rays on electrospun poly-(ε-caprolactone) fiber mats. J Mater Sci: Mater Med. 2019; 30: 42. DOI: 10.1007/s10856-019-6245-7.
2. Tapia-Guerrero YS, Del Prado-Audelo ML, Borbolla-Jiménez FV, Gomez D, García-Aguirre I, Colín-Castro CA, et al. Effect of UV and Gamma Irradiation Sterilization Processes in the Properties of Different Polymeric Nanoparticles for Biomedical Applications. Materials (Basel, Switzerland). 2020; 13 (5): 1090. DOI: 10.3390/ma13051090.
3. Shehata MM, Gomaa FA, Helal Z. Effects of gamma and electron beam irradiation on viability and DNA elimination of Staphylococcus aureus. Archives of Clinical Microbiology. 2011; 121: 44–55. DOI: 10:3823/244.
4. Xu Y, Chen Y, Liu H, Lei X, Guo J, Cao K, et al. Heat-killed salmonella typhimurium (HKST) protects mice against radiation in TLR4-dependent manner. Oncotarget. 2017; 40 (8): 67082–93. DOI: 10.18632/oncotarget.17859.
5. Tobin GJ, Tobin JK, Gaidamakova EK, Wiggins TJ, Bushnell RV, Lee WM, et al. A novel gamma radiation-inactivated sabin-based polio vaccine. PloS one. 2020; 15 (1): e0228006. DOI: 10.1371/journal.pone.0228006.
6. Mullbacher A, Pardo J, Furuya Y. SARS-CoV-2 Vaccines: Inactivation by Gamma Irradiation for T and B Cell Immunity. Pathogens (Basel, Switzerland). 2020; 9 (11): 928. DOI: 10.3390/pathogens9110928.
7. Bruno-Barcena JM, Azcárate-Peril AM, Hassan HM. Role of antioxidant enzymes in bacterial resistance to organic acids. Applied and Euvironuental Microbiology. 2010: 76 (9): 2747–50. DOI: 10.1128/AEM.02718-09.
8. Mun GI, Kim S, Choi E, Kim CS, Lee YS. Pharmacology of natural radioprotectors. Archives of pharmacal research. 2018; 41 (11): 1033–50. DOI: 10.1007/s12272-018-1083-6.
9. Montoro A. Radioprotection and Radiomitigation: From the Bench to Clinical Practice. Biomedicines. 2020; 8 (11): 461. DOI: 10.3390/biomedicines8110461.
10. Гайнутдинов Т. Р. Оценка противорадиационной эффективности препаратов, полученных на основе веществ микробного происхождения. Ветеринарный врач. 2024; 1: 52–7. DOI: 10.33632/1998-698X_2024_1_52.
11. Riehl TE, Alvarado D, Ee X, Zuckerman A, Foster L, Kapoor V, et al. Lactobacillus rhamnosus GG protects the intestinal epithelium from radiation injury through release of lipoteichoic acid, macrophage activation and the migration of mesenchymal stem cells. Gut. 2019; 68 (6): 1003–13. DOI: 10.1136/gutjnl-2018-316226.
12. Gaynutdinov TR, Nizamov RN, Idrisov AM, Rakhmatullina GI, Guryanova VA. Obtaining radioactivated strains of microorganisms and studying their antiradiation efficiency IOP Conf. Series: Earth and Environmental Science. 2021; 723: 042008. DOI: 10.1088/1755-1315/723/4/042008.
13. Иванов А. А., Симбирцев А. С., Мальцев В. Н., Петров Л. Н., Андрианова И. Е., Ставракова Н. М. и др. Снижение опасности носительства условно-патогенной микрофлоры при радиационном поражении с помощью пробиотика «Витафлор» и антибиотиков. Медицина экстремальных ситуаций. 2013; 1 (43): 76–81.
14. Кобатов А. И., Вербицкая Н. Б., Полоцкий А. Е., Савин И. И., Гребенюк А. Н. Разработка технологии получения кисломолочного продукта на борту космического корабля и оценка его пробиотических и потенциальных радиозащитных свойств. Медицина экстремальных ситуаций. 2019; 21 (4): 517–26.
15. Кобатов А. И., Полынцев Д. Г., Савин И. И, Попова Е. В., Кутник И. В. Космический эксперимент «Пробиовит»: итоги и перспективы (Часть 1). Пилотируемые полеты в космос. 2023; 1 (46): 74–87.
16. Кобатов А. И., Полынцев Д. Г., Савин И. И., Попова Е. В., Кутник И. В. Космический эксперимент «Пробиовит»: итоги и перспективы (Часть 2). Пилотируемые полеты в космос. 2023; 2 (47): 87–98.
17. Chance B, Sies H, Boveris A. Hydroperoxide methabolism in mammalian organs. Physiol Rev. 1979; 59 (3): 527–605. DOI: 10.1152/physrev.1979.59.3.527.
18. Mathialagan N, Roberts RM. A role for cytokines in early pregnancy. Indian J Physiol Pharmacol. 1994; 38: 153–62. PubMed PMID: 7814074.
19. Гурьянова В. А., Тарасова Н. Б. Перекисное окисление липидов при поражении печени ионизирующей радиацией. Ученые записки Казанской государственной академии ветеринарной медицины им. Н. Э. Баумана. 2013; 213: 76–80.
20. Гайнутдинов Т. Р. Экспериментальный подбор доз ионизирующего излучения, вызывающих ингибирование роста и полную инактивацию золотистого стафилококка. Ветеринарный врач. 2020; 4: 4–8. DOI: 10.33632/1998-698X.2020-4-4-8.
21. Smith WW, Alderman IM, Gillespie RE. Increased survival in irradiated animals treated with bacterial endotoxins. Am J Physiol. 1957; 191 (1): 124–30. DOI: 10.1152/ajplegacy.1957.191.1.124.
22. Pluznik DY. Benefecial effect on endotoxins. Immunobiology and Immunopharmacology of Bacterial Endotoxins. 1986; 7: 124–8. DOI: 10.1007/978-1-4613-2253-5.
23. Ledney GD, Wilson R. Protection induced by bacterial endotoxin against whole body X-irradiation germfree and conventional mice. Proc Soc Exptl Biol Med. 1996; 118 (4): 1062–5. DOI: 10.3181/00379727-118-30046.
24. Алмагамбетов К. Х. Молекулярная биология Staphylococcus aureus. Медицинский журнал Астана. 2021; 1 (107): 61–8.
25. Neta R. Role of cytokines in radioprotection. Pharmacology end Therapeutics. 1988; 39 (1–3): 261–6. DOI: 10.1016/0163-7258(88)90070-8.
26. Гребенюк А. Н., Стрелова О. Ю., Легеза Т. И., Степанова Е. Н. Основы радиобиологии и радиационной медицины: учебное пособие. СПб.: ООО «Изд-во ФОЛИАНТ», 2012; 232 с.

27. Галлямова М. Ю., Вагин К. Н., Гайнутдинов Т. Р., Рахматуллина Г. И., Рыжкин С. А. Влияние ионизирующего излучения на активность антиоксидантных ферментов штамма Escherichia coli «ПЛ-6» при многократном облучении. Радиация и риск (Бюллетень Национального радиационно-эпидемиологического регистра). 2024; 33 (1): 68–76. DOI: 10.21870/0131-3878-2024-33-1-68-76.

28. Gaupp R, Lei S, Reed JM, Peisker H, Boyle-Vavra S, Bayer AS, et al. Staphylococcus aureus metabolic adaptations during the transition from a daptomycin susceptibility phenotype to a daptomycin nonsusceptibility phenotype. Antimicrobial agents and chemotherapy. 2015; 59 (7): 4226–38. DOI: 10.1128/AAC.00160-15.

29. Linder H, Holler E, Ertl B, Multhoff G, Schreglmann M, Klauke I, et al. Peripheral blood mononuclear cells induce programmed cell death in human endothelial call and may prevent repair: role of cytokines. Blood. 1997; 29 (6): 1931–8. PubMed PMID: 9058713.

30. Neta R, Oppenheim J. The role of cytokines in immunoregulation. Cancer call. 1991; 3 (10): 391–6. DOI: 10.1016/0163-7258(88)90070-8.

SECONDARY HYPERPARATHYROIDISM ASSOCIATED WITH VITAMIN D DEFICIENCY IN YOUNG HIGHLY TRAINED ATHLETES

Isaeva EP[1,3,4] ✉, Okorokov PL[1,2], Zyabkin IV[1,3]

[1] Federal Research and Clinical Center for Children and Adolescents of the Federal Medial Biological Agency, Moscow, Russia

[2] National Endocrinology Research Center, Moscow, Russia

[3] Medical and Biological University of Innovation and Continuing Education, Burnazyan Federal Medical Biophysical Center of the Federal Medial Biological Agency, Moscow, Russia

[4] Russian University of Medicine, Moscow, Russia

Vitamin D deficiency that remains non-compensated for a long time is associated with high risk of rickets in children and osteomalacia in adults, myopathies and low-energy fractures, as well as secondary hyperparathyroidism (SHPT). SHPT represents one of the main mechanisms, through which vitamin D deficiency can contribute to pathogenesis of low-energy fractures. The study was aimed to assess the calcium and phosphorus metabolism state and the bone tissue metabolism markers in highly trained athletes with SHPT, as well as the prevalence of SHPT in elite sports. The study involved 527 young athletes aged 12–18 years (average age 15.2 years) doing 32 sports. The group with SHPT included 16 children (11 girls and 5 boys) with the average age of 15.0 years. The control group with normal levels of parathyroid hormone consisted of 511 children (254 boys and 273 girls) with the average age of 15.2 years. The studied subgroups were matched by age (p = 0.678). Girls predominated in the group with SHPT (p = 0.02). SHPT associated with vitamin D deficiency was revealed in 3% of young highly trained athletes, it was more prevalent among girls. The SHPT development does not result in alteration of the calcium and phosphorus metabolism indicators, however, it is accompanied by the increase in bone resorption markers, β-CrossLaps and total alkaline phosphatase. Many aspects related to vitamin D deficiency in SHPT are currently poorly understood, and there are no clinical guidelines on the cholecalciferol replacement therapy. Large-scale clinical trials are required to determine the optimal threshold values of 25(OH)D3 and the powerful and effective treatment regimens for young athletes having SHPT associated with vitamin D deficiency.

Keywords: children, young athletes, sports medicine, secondary hyperparathyroidism, vitamin D deficiency

ВТОРИЧНЫЙ ГИПЕРПАРАТИРЕОЗ НА ФОНЕ ДЕФИЦИТА ВИТАМИНА D У ЮНЫХ ВЫСОКОКВАЛИФИЦИРОВАННЫХ СПОРТСМЕНОВ

Е. П. Исаева[1,3,4] ✉, П. Л. Окороков[1,2], И. В. Зябкин[1,3]

[1] Федеральный научно-клинический центр детей и подростков Федерального медико-биологического агентства, Москва, Россия

[2] Национальный медицинский исследовательский центр эндокринологии, Москва, Россия

[3] Медико-биологический университет инноваций и непрерывного образования Федерального государственного бюджетного учреждения «Государственный научный центр Российской Федерации — Федеральный медицинский биофизический центр имени А. И. Бурназяна» Федерального медико-биологического агентства, Москва, Россия

[4] Российский университет медицины Минздрава России, Москва, Россия

Длительно некомпенсированный дефицит витамина D сопряжен с высокими рисками развития рахита у детей и остеомаляции у взрослых, миопатий и низкоэнергетических переломов, а также вторичного гиперпаратиреоза (ВГПТ). ВГПТ — один из основных механизмов, посредством которых дефицит витамина D может вносить вклад в патогенез фосфорно-кальциевого обмена и значения маркеров метаболизма костной ткани у высококвалифицированных спортсменов с ВГПТ, а также его распространенность в спорте высших достижений. Целью работы было изучить состояние фосфорно-кальциевого обмена и значения маркеров метаболизма костной ткани у высококвалифицированных спортсменов с ВГПТ, а также его распространенность в спорте высших достижений. В исследование включено 527 юных спортсменов в возрасте 12–18 лет (средний возраст 15,2 лет), занимающихся 32 видами спорта. В группу с ВГПТ вошло 16 детей (11 девочек и 5 мальчиков); средний возраст 15,0 лет. Контрольную группу с нормальным уровнем паратиреоидного гормона составили 511 детей (254 мальчика и 273 девочки); средний возраст 15,2. Исследуемые подгруппы не различались по возрасту (p = 0,678). В группе ВГПТ преобладали девочки (p = 0,02). ВГПТ на фоне гиповитаминоза D у юных высококвалифицированных спортсменов был выявлен в 3% случаев и чаще встречался у девочек. Развитие ВГПТ не приводит к изменению показателей фосфорно-кальциевого обмена, однако сопровождается повышением маркеров костной резорбции — β-CrossLaps и общей щелочной фосфатазы. Многие аспекты, связанные с дефицитом витамина D при ВГПТ, в настоящее время не изучены, а клинические рекомендации по заместительной терапии колекальциферолом у юных спортсменов отсутствуют. Необходимо проведение крупных клинических исследований для определения «оптимальных «пороговых» уровней 25(OH)D3 и действенных, эффективных схем лечения у юных спортсменов с ВГПТ на фоне гиповитаминоза D.

Ключевые слова: дети, юные спортсмены, спортивная медицина, вторичный гиперпаратиреоз, дефицит витамина D

The population-based studies suggest high prevalence of low vitamin D status both in pediatric population and among young elite athletes [1–3]. Vitamin D supply is fundamentally important to maintain children's health. This is due to the fact that viramin D is used not only for treatment of rickets, but also to maintain lipid metabolism, prevent obesity, cardiovascular disorders, maintain anti-infection immunity; vitamin D deficiency is also associated with high risk of secondary hyperparathyroidism (SHPT). SHPT represents one of the main mechanisms, through which vitamin D deficiency can contribute to pathogenesis of low-energy fractures [4, 5].

Today, there are no statistical data on the state of calcium and phosphorus metabolism and the values of bone tissue metabolism markers in young elite athletes with SHPT in the Russian Federation; the prevalence of SHPT is still poorly understood.

The study was aimed to assess the state of calcium and phosphorus metabolism and bone tissue metabolism in SHPT and determine the prevalence of SHPT in young highly trained athletes.

METHODS

A cross-sectional single center study involving young athletes, members of national teams of the Russian Federation, who underwent in-depth medical assessment at the Federal Research and Clinical Center for Children and Adolescents between March and June 2022, was conducted.

Inclusuion criteria: elite atletes – members of national teams of the Russian Federation aged 12–18 years.

Exclusion criteria: history of acute respiratory viral infection or other disease resulting in missing three or more training sessions within 30 days before assessment.

Serum levels of 25-hydroxycalciferol (25(OH) D3), parathyroid hormone (PTH), C-telopeptide (β-CrossLaps), total alkaline phosphatase (ALP), total calcium, phosphorus, and magnesium were measured in all young athletes. The 25(OH) D3 and PTH levels were measured by the Chemiluminescent Microparticle Immuno Assay (CMIA) using the specialized kits (Abbott Laboratories; USA). The concentration of 25(OH)D3 ≥ 30 ng/mL was considered to be normal, vitamin D insufficiency was diagnosed when the concentration was 20–29.9 ng/mL, deficiency was diagnosed at 10–19.9 ng/mL [6]. The PTH reference range for children aged 9–18 years was 2.32–9.28 pmol/L. Assessment of β-Cross laps and total ALP was performed by the electrochemiluminescence assay using the Cobas e 411 analyzer (Roche Diagnostics; Germany). The value < 0.584 ng/mL was considered to be the upper end of the β-CrossLaps reference range for the general population. The total calcium, phosphorus, and magnesium levels were measured using the Indiko Plus automatic analyzer (Thermo Fisher Scientific;

USA). Sexual development was estimated using the Tanner classification.

The following parameters were considered to be the major endpoints of the study: SHPT rate, serum levels of PTH, β-CrossLaps, total ALP, 25(OH)D3, and total calcium in the young highly trained athletes.

All study participants were divided into two subgroups according to the presence of SHPT.

SHPT was diagnosed in cases of the parathyroid hormone (PTH) levels exceeding > 9.28 pmol/L in combination with the decreased 25(OH)D3 levels.

Statistical processing of the results was performed using the Statistica version 10.0 software package (StatSoft Inc.; USA).

Since the distribution of the studied quantitative indicators was non-normal (based on the Kolmogorov–Smirnov test), all data are presented as the median (Me) and 1st and 3rd quartiles [Q_1; Q_3]. The Mann–Whitney U test and Kruskal–Wallis test were used to assess significance of differences in quantitative traits. Qualitative traits are presented as the percentage (%) with an absolute value. Contingency tables were compiled to assess the differences between qualitative traits, which was followed by assessment based on the Pearson's chi-squared test (χ^2). The differences were considered significant at $p \leq 0.05$.

RESULTS

A total of 527 young athletes aged 12–18 years engaged in 32 sports were included in the study. The group with SHPT included 16 children (11 girls and 5 boys); average age 15.0 [14.1; 16.2] years. The comparison group with normal PTH levels consisted of 511 children (254 boys and 273 girls); average age 15.2 [14.2; 16.5] years. The studied subgroups were matched by age ($p = 0.678$), body height ($p = 0.124$), and body weight ($p = 0.632$), however, their sexual development stages were different. Girls with incomplete sexual development prevailed in the group with SHPT, while 86% of the comparison group had compete puberty. The clinical characteristics of the studied subgroups are provided in Table 1.

Elevated PTH levels were revealed in 16 young athletes, which accounted for 3% of surveyed individuals. SHPT was twice more often detected in girls, than in boys (11 vs. 5; $p = 0.034$). The average PTH levels of athletes with SHPT were 10.2 pmol/L, with individual fluctuations within the range of 9.3–11.4 pmol/L. The average PTH levels of athletes engaged in certain sports turned out to be comparable ($p = 0.14$; Fig. 1)

Elevated PTH levels were revealed in the athletes engaged in such sports, as rhythmic gymnastics (4 individuals), boxing (3 individuals), wrestling, synchronized swimming, figure skating, softball (2 individuals), and volleyball (1 individual).

Then we assessed the indicators that characterized the state of calcium and phosphorus metabolism and bone tissue metabolism.

Table 1. Clinical characteristics of the studied subgroups

	SHPT group	Comparison group (normal PTH levels)	p
Number, n	16	511	–
Sex: m/f	5/11	254/273	0.021
Age	15.0 [14.1;16.2]	15.2 [14.2;16.5]	0.678
Body height, m	1.66 [1.61; 1.7]	1.72 [1.65; 1.79]	0.124
Body weight, kg	57 [48.0; 69.0]	52 [45; 65]	0.632
Sexual development: Tanner stage 1 Tanner stage 2–3 Tanner stage 4–5	– 7 (43%) 9 (57%)	6 (1%) 67 (13) 438 (86%)	– 0.001 0.001

The serum levels of total calcium (p = 0.351), phosphorus (p = 0.692), and magnesium (p = 0.751) of young athletes with SHPT and their peers with normal PTH levels turned out to be comparable (Table 1).

A significant decrease in the 25(OH)D3 levels relative to the control group was revealed in young athletes with SHPT (p = 0.0002; Table. 1). The prevalence of vitamin D deficiency turned out to be significantly higher in the group of young athletes with SHPT, than in their peers with normal PTH levels (p = 0.021; Fig. 2). No normal vitamin D levels were revealed in young athletes with SHPT. Vitamin D insufficiency was reported in the group with SHPT and the control group in 19 and 42.2% of cases, respectively (p = 0.072).

When assessing markers of bone metabolism, we found that athletes with SHPT had the increased levels of bone resorption markers relative to the comparison group (Table 2). The median β-CrossLaps value of young athletes with SHPT was 1.71 ng/mL, and the maximum values reached 2.6 ng/mL. The increase in ALP activity was also revealed in the group with SHPT (208.1 vs. 155.1 U/L; p = 0.037).

DISCUSSION

In our study, the prevalence of SHPT among young athletes was 3%. Furthermore, 81% of young athletes having elevated PTH levels were diagnosed with vitamin D deficiency. We have found no similar studies focused on assessing the rate of SHPT in elite sports in the available literature. However, considering high prevalence of hypovitaminosis D among athletes engaged in various sports demonstrated in many studies [2–4], it can be assumed that the problem of SHPT in professional sports is systemic.

It is well known that SHPT results from abnormal stimulation of excess PTH production by the parathyroid glands. Uremic

and non-uremic etiological variants of SHPT are distinguished. Uremic SHPT represents PTH hypersecretion developing against the background of chronic kidney disease [7]. This SHPT variant is not typical for highly trained athletes. The subgroup of non-uremic causes includes primarily vitamin D deficiency or vitamin D metabolism disorder (decreased activity of the calcium-sensing (CaSR) and vitamin D-sensing (VDR) receptors in the parathyroid glands; bone tissue resistance to the PTH calcemic effect or fibroblast growth factor 23 (FGF-23)) [7].

Hypovitaminosis D results in the reduced intestinal calcium absorption and, therefore, paves the way for hypocalcemia. In response to this, the PTH-associated mechanisms aimed to stimulate osteoclastic bone resorption with the release of calcium and phosphate that increase calcium reabsorption in the kidney distal tubules are activated [8]. The increase in bone tissue resorption associated with SHPT is inter alia mediated by the effect of 1.25(OH)2D3, an active vitamin D metabolite capable of inducing expression of the RANKL TNFα-like factor (activator receptor of the NF-kB ligand) activating osteoclasts, from chondrocytes, osteoblasts and osteocytes. Furthemore, 1.25(OH)2D3 modulates expression of the factors regulating mineralization, such as Spp1 (osteopontin), MGP (matrix Gla protein), ENPP1 (ectonucleotide pyrophosphatase/ phosphodiesterase 1), and ENPP2, as well as ANK (progressive ankylosis protein) and ALPL (intestinal alkaline phosphatase) [9].

Thus, vitamin D deficiency leads to the increased PTH secretion to maintain calcium homeostasis, which is due to the increased intensity of resorptive processes in the bone tissue. The above mechanisms lead to the decrease in the bone mineral density (BMD), including in children and adolescents. According to the data provided by the group of Korean authors, who have analyzed bone tissue condition in 1063 adolescents, the increase in the 25(OH)D3 levels is associated with the
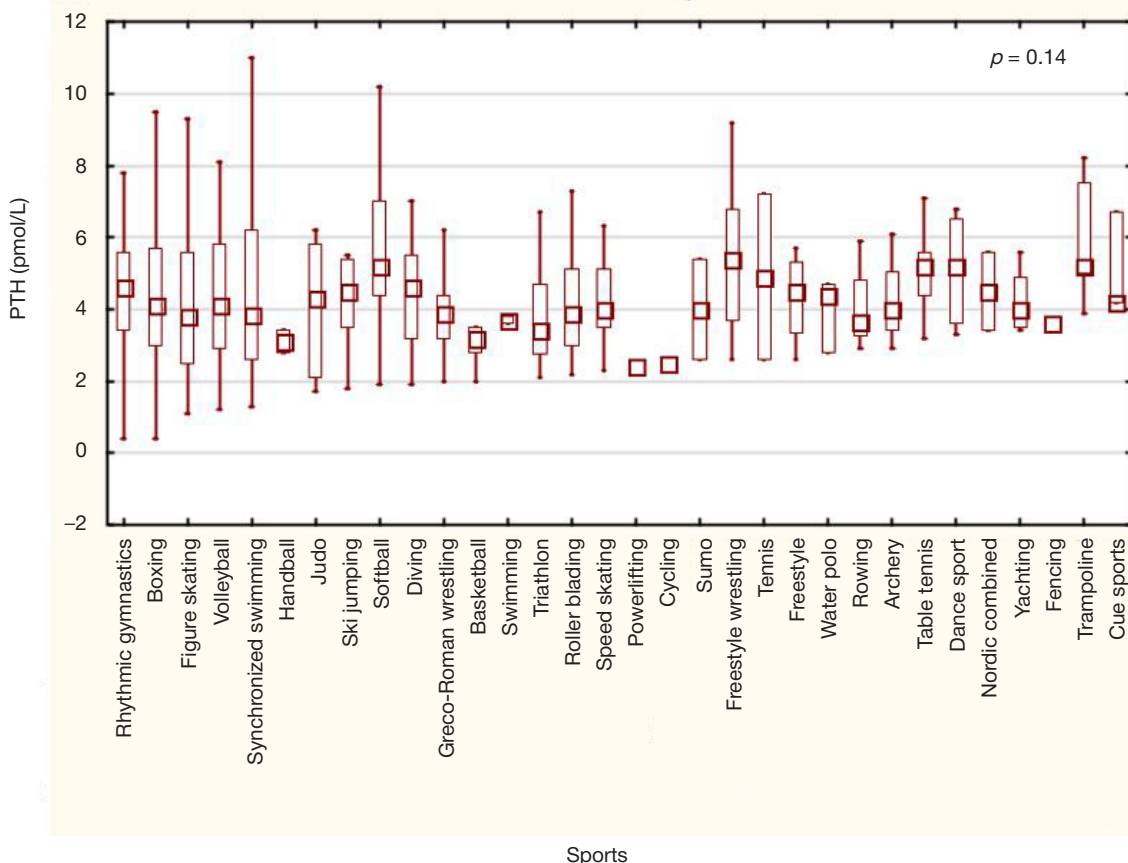
Fig. 1. Parathyroid hormone levels in young athletes engaged in certain sports

Table 2. Parameters of calcium and phosphorus metabolism and markers of bone tissue metabolism in young elite athletes depending on secondary hyperparathyroidism

	SHPT group $n = 16$	Comparison group (normal PTH levels) $n = 511$	p
Total calcium, mmol/L	2.48 [2.43; 2.58]	2.52 [2.46; 2.58]	0.351
Phosphorus, mmol/L	1.47 [1.45; 1.54]	1.42 [1.28; 1.58]	0.692
Magnesium, mmol/L	0.80 [0.77; 0.84]	0.80 [0.77; 0.85]	0.751
Total alkaline phosphatase, U/L	208.1 [147.0; 270.0]	155.1 [103.4; 227.9]	0.037
β-CrossLaps, ng/mL	1.71 [1.17; 2.36]	1.34 [0.92; 1.99]	0.042
PTH, pmol/L	10.2 [9.3; 11.1]	4.1 [3.2; 5.4]	<0.0001
25(OH)D3, ng/mL	15.6 [12.3; 19.3]	21.5 [17.0; 26.7]	0.0002

significant increase in the BMD Z-score in the lumbar spine and femoral head [10].

The meta-analysis including more than 7500 children from 23 studies has shown that the drop of 25(OH)D3 levels below 20 ng/mL is associated with the increased risk of fractures [11].

SHPT is one of the main mechanisms, through which vitamin D deficiency may contribute to the pathogenesis of low-energy fractures [4, 5].

However, the 25(OH)D3 threshold (cutoff point), at which PTH clearly begins to increase, remains undefined [12]. High variability of the 25(OH)D3 levels, at which PTH levels decrease, is reported [13]. According to some data, serum PTH concentrations start to decrease, when the 25(OH)D3 levels increase to 15–20 ng/mL, and are maximally depressed at the values of 30–40 ng/mL [14, 15]. According to other data, the threshold serum 25(OH)D3 level of 30 ng/mL is essential for prevention of SHPT and bone mineral density reduction [16]. These data contradict the results showing that PTH levels reach a plateau, when the 25(OH)D3 level is 17 ng/mL [17]. The 25(OH)D3 threshold of 12 ng/mL essential for preservation of bone tissue health in adults was established based on the ROC analysis data [18]. However, all the above studies were conducted in the adult population with the usual amount of physical activity, and these cannot be confidently extrapolated to the cohort of highly trained athletes.

The data on the PTH reference ranges for athletes are controversial. A number of authors report that the athletes' PTH levels are elevated compared to that of their peers with usual

amount of physical activity. However, other studies have shown that PTH concentration remains unchanged or increases during physical activity [19–21].

Normal to low normal calcium levels and decreased phosphorus levels are typical for SHPT associated with vitamin D deficiency [4]. In our study, the development of SHPT in young athletes was not associated with the calcium and phosphorus metabolism disorder.

The study conducted revealed elevated β-CrossLaps and total ALP levels reflecting the activity of bone resorption processes in young athletes with SHPT. However, 43% of young athletes in the group with SHPT had incomplete sexual development characterized by active bone tissue metabolism. Thus, the identified differences in the course of puberty can explain the increase in bone metabolism markers in the group of young athletes with SHPT. When assessing bone metabolism markers in children and adolescents, it is necessary to consider that a pronounced imbalance between osteoresorptive and osteosynthetic processes due to active bone tissue growth is reported in children. The above age-related features explain higher values of bone metabolism markers in children compared to adults.

Assessment of β-CrossLaps levels in young highly trained athletes demonstrated the increase in this indicator in all age groups, especially in the 14–15-year-old athletes (Fig. 1). The average β-CrossLaps levels of athletes 2–3 times exceed the reference values for individuals with usual levels of physical activity [22]. The authors explain the increase in this marker by
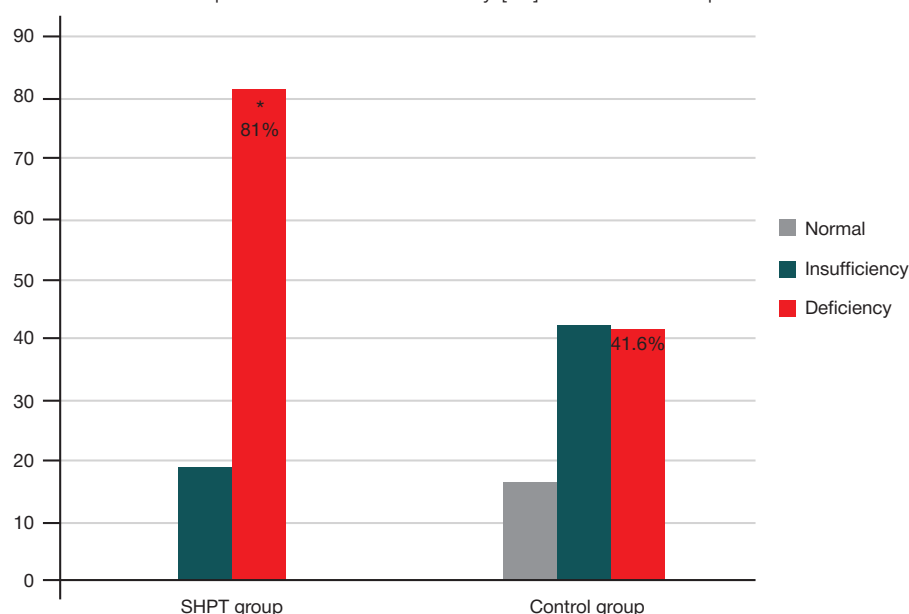
Fig. 2. Vitamin D supply in the studied groups. * — $p = 0.021$

the anabolic orientation of metabolic processes in the young athlete's body. When performing assessment based on the nature of sports activity during our study, it was also shown that the highest β-CrossLaps levels were found in representatives of combat sports and team sports; the average β-CrossLaps levels were higher in males, that in females [22].

ALP levels are widely used in clinical practice to diagnose disorders of bone remodeling. It is advisable to determine acidic ALP when assessing bone metabolism, since it is the only isoenzyme that is invoved in bone matrix mineralization and demonstrates metabolic activity of osteoblasts. According to the literature the concentration of bone ALP correlates with blood levels of ionized calcium, while the dynamic changes in blood ALP levels characterize the changes in bone mineral density [23, 24]. The total ALP increase in nonspecific, it can be found in various conditions, including some tumors and hepatobiliary diseases.

Thus, clinical assessment and interpretation of bone metabolism markers in young highly trained athletes is difficult. Currently, this does not allow to use these as reliable biomarkers of the disorders of bone tissue remodeling.

The season, when blood was collected for 25(OH)D3 testing, is an important limitation of this study. Hypovitaminosis D is most prevalent in spring, which could affect low vitamin D supply in the studied cohort. Furthermore, there are no data on taking cholecalciferol and other dietary supplements by young athletes at the time of blood collection.

The changes in bone tissue metabolism markers (β-CrossLaps and total alkaline phosphatase) revealed in the studied subgroups can result from the children's growth and the features of physical exertion in certain sports, which does not allow us to objectively estimate the contribution of SHPT to variability of these indicators.

CONCLUSIONS

SHPT associated with hypovitaminosis D is found in 3% of young elite athletes and more prevalent among girls, than boys. The development of SHPT does not lead to changes in the indicators of calcium and phosphorus metabolism, however, it is associated with the increase in bone resorption markers (β-CrossLaps and total ALP). Many aspects related to vitamin D deficiency in SHPT are currently poorly understood; there are no clinical guidelines on cholecalciferol replacement therapy in young athletes. It necessary to conduct large-scale clinical trials to determine optimal threshold levels of 25(OH)D3 and effective treatment regimens for young athletes with SHPT associated with hypovitaminosis D.

References

1. Zaharova IN, Malcev SV, Borovik TYe, i dr. Rezul'taty mnogocentrovogo kogortnogo issledovanija «RODNIChOK» po izucheniju nedostatochnosti vitamina D u detej rannego vozrasta v Rossii. Pediatrija. Zhurnal im. G.N. Speranskogo 2015; 94 (1): 62–67. Russian.

2. Stoljarova SA, Okorokov PL, Zjabkin IV, Isaeva EP. Ocenka obespechennosti vitaminom D junyh sportsmenov. Pediatrija. Zhurnal im. G.N. Speranskogo 2023; 102 (5): 116–21. DOI: 10.24110/0031-403X-2023-102-5-116-121. Russian.

3. Melnichenko GA, Namazova-Baranova LS, Gromova OA, i dr. Profilaktika i lechenie deficita vitamina D: vybor optimal'nogo podhoda. Voprosy sovremennoj pediatrii. 2021; 20 (4): 338–45. Dostupno po ssylke: https://doi.org/10.15690/vsp.v20i4.2246. Russian.

4. Dreval AV. Osteoporoz, giperparatireoz i deficit vitamina D. Rukovodstvo. «GJeOTAR-Media», 2019; 160 s. Russian.

5. Owens DJ, Fraser WD, Close GL. Vitamin D and the athlete: emerging insights. Eur J Sport Sci. 2015; 15 (1): 73–84. DOI: 10.1080/17461391.2014.944223.

6. Federal'nye klinicheskie rekomendacii po diagnostike, lecheniju i profilaktike osteoporoza MZ RF. Problemy jendokrinologii. 2018; 63 (6): 392–426. DOI: 10.14341/probl2017636392-426. Russian.

7. Mokrysheva NG, Eremkina AK, Mirnaja SS, i dr. Trudnosti differencial'noj diagnostiki mezhdu pervichnoj i vtorichnoj formami giperparatireoza. Ozhirenie i metabolizm. 2017; 14 (3): 48–53. Dostupno po ssylke: https://doi.org/10.14341/omet2017348-53. Russian.

8. Qing H, Ardeshirpour L, Pajevic PD, et al. Demonstration of osteocytic perilacunar/canalicular remodeling in mice during lactation. J Bone Miner Res. 2012; 27 (5): 1018–29.

9. Global Consensus Recommendations on Prevention and Management of Nutritional Rickets. J Clin Endocrinol Metab. 2016; 101 (2): 394–415.

10. Song K, Kwon A, Chae HW, et al. Vitamin D status is associated with bone mineral density in adolescents: Findings from the Korea National Health and Nutrition Examination Survey. Nutr Res. 2021; 87: 13–21. DOI: 10.1016/j.nutres.2020.12.011.

11. Yang G, Lee WYW, Hung ALH, et al. Association of serum 25(OH)Vit-D levels with risk of pediatric fractures: a systematic review and meta-analysis. Osteoporos Int. 2021 ; 32 (7): 1287–300. DOI:

12. Manson JE, Brannon PM, Rosen CJ, Taylor CL. Vitamin D Deficiency — Is There Really a Pandemic? N Engl J Med. 2016; 375: 1817–20. Available from: https://doi.org/10.1056/nejmp1608005.

13. Sai AJ, Walters RW, Fang X, Gallagher JC. Relationship between Vitamin D, Parathyroid Hormone, and Bone Health. J Clin Endocrinol Metab. 2011; 96 (3): E436–E446. Available from: https://doi.org/10.1210/jc.2010-1886.

14. Ginde AA, Wolfe P, Camargo CA, Schwartz RS. Defining vitamin D status by secondary hyperparathyroidism in the U.S. population. J Endocrinol Invest. 2012; 35: 42–48. Available from: https://doi.org/10.3275/7742.

15. Monk RD, Bushinsky DA. Making Sense of the Latest Advice on Vitamin D Therapy. J Am Soc Nephrol. 2011; 22 (6): 994–8. Available from: https://doi.org/10.1681/ASN.2011030251.

16. Olmos JM, Hernández JL, García-Velasco P, et al. Serum 25-hydroxyvitamin D, parathyroid hormone, calcium intake, and bone mineral density in Spanish adults. Osteoporos Int. 2016; 27 (1): 105–13. Available from: https://doi.org/10.1007/s00198-015-3219-6.

17. Shen M, Li Z, Lv D, et al. Seasonal variation and correlation analysis of vitamin D and parathyroid hormone in Hangzhou, Southeast China. J Cell Mol Med. 2020; 24 (13): 7370–7. Available from: https://doi.org/10.1111/jcmm.15330.

18. Al Quaiz AM, Mujammami M, Kazi A, et al. Vitamin D cutoff point in relation to parathyroid hormone: a population based study in Riyadh city, Saudi Arabia. Arch Osteoporos. 2019; 14 (1): 22. Available from: https://doi.org/10.1007/s11657-019-0565-6.

19. Caroli B, Pasin F, Aloe R, et al. Characterization of skeletal parameters in a cohort of North Italian rugby players. J Endocrinol Invest. 2014; 37 (7): 609–17.

20. Brzeziański M, Migdalska-Sęk M, Stuss M, et al. Effect of physical training on parathyroid hormone and bone turnover marker profile in relation to vitamin D supplementation in soccer players. Biology of Sport. 2022; 39 (4): 921–32. DOI: 10.5114/biolsport.2022.109956.

21. Solarz K, Kopeć A, Pietraszewska J, et al. An evaluation of the levels of 25-hydroxyvitamin D3 and bone turnover markers in professional football players and in physically inactive men. Physiol Res. 2014; 63 (2): 237–43.

22. Kljuchnikov SO, Kravchuk DA, Ogannisjan MG. Osteoporoz u detej i ego aktual'nost' dlja detskoj sportivnoj mediciny.

Ros vestn perinatol i pediatr. 2017; 62 (3): 112–20. DOI: 10.21508/1027–4065–2017–62–3–112–120. Russian.

23. Wyatt PB, Reiter CR, Satalich JR, et al. Effects of Vitamin D Supplementation in Elite Athletes: A Systematic Review. Orthopaedic Journal of Sports Medicine. 2024; 12 (1). DOI:

10.1177/23259671231220371.

24. Thode J, et al. Comparison of serum total calcium, albumin-corrected total calcium, and ionized calcium in 1213 patients with suspected calcium disorders. Scand J Clin. Lab Invest England. 1989; 49 (3): 217–23.

Литература

1. Захарова И. Н., Мальцев С. В., Боровик Т. Э., и др. Результаты многоцентрового когортного исследования «РОДНИЧОК» по изучению недостаточности витамина D у детей раннего возраста в России. Педиатрия. Журнал им. Г.Н. Сперанского 2015; 94 (1): 62–67.

2. Столярова С. А., Окороков П. Л., Зябкин И. В., Исаева Е. П. Оценка обеспеченности витамином D юных спортсменов. Педиатрия. Журнал им. Г.Н. Сперанского 2023; 102 (5): 116–21. DOI: 10.24110/0031-403X-2023-102-5-116-121.

3. Мельниченко Г. А., Намазова-Баранова Л. С., Громова О. А., и др. Профилактика и лечение дефицита витамина D: выбор оптимального подхода. Вопросы современной педиатрии. 2021; 20 (4): 338–45. Доступно по ссылке: https://doi.org/10.15690/vsp.v20i4.2246.

4. Древаль А. В. Остеопороз, гиперпаратиреоз и дефицит витамина D. Руководство. «ГЭОТАР-Медиа», 2019; 160 с.

5. Owens DJ, Fraser WD, Close GL. Vitamin D and the athlete: emerging insights. Eur J Sport Sci. 2015; 15 (1): 73–84. DOI: 10.1080/17461391.2014.944223.

6. Федеральные клинические рекомендации по диагностике, лечению и профилактике остеопороза МЗ РФ. Проблемы эндокринологии. 2018; 63 (6): 392–426. DOI: 10.14341/probl2017636392-426.

7. Мокрышева Н. Г., Еремкина А. К., Мирная С. С., и др. Трудности дифференциальной диагностики между первичной и вторичной формами гиперпаратиреоза. Ожирение и метаболизм. 2017; 14 (3): 48–53. Доступно по ссылке: https://doi.org/10.14341/omet2017348-53.

8. Qing H, Ardeshirpour L, Pajevic PD, et al. Demonstration of osteocytic perilacunar/canalicular remodeling in mice during lactation. J Bone Miner Res. 2012; 27 (5): 1018–29.

9. Global Consensus Recommendations on Prevention and Management of Nutritional Rickets. J Clin Endocrinol Metab. 2016; 101 (2): 394–415.

10. Song K, Kwon A, Chae HW, et al. Vitamin D status is associated with bone mineral density in adolescents: Findings from the Korea National Health and Nutrition Examination Survey. Nutr Res. 2021; 87: 13–21. DOI: 10.1016/j.nutres.2020.12.011.

11. Yang G, Lee WYW, Hung ALH, et al. Association of serum 25(OH) Vit-D levels with risk of pediatric fractures: a systematic review and meta-analysis. Osteoporos Int. 2021 ; 32 (7): 1287–300. DOI: 10.1007/s00198-020-05814-1.

12. Manson JE, Brannon PM, Rosen CJ, Taylor CL. Vitamin D Deficiency — Is There Really a Pandemic? N Engl J Med. 2016; 375: 1817–20. Available from: https://doi.org/10.1056/nejmp1608005.

13. Sai AJ, Walters RW, Fang X, Gallagher JC. Relationship between

Vitamin D, Parathyroid Hormone, and Bone Health. J Clin Endocrinol Metab. 2011; 96 (3): E436–E446. Available from: https://doi.org/10.1210/jc.2010-1886.

14. Ginde AA, Wolfe P, Camargo CA, Schwartz RS. Defining vitamin D status by secondary hyperparathyroidism in the U.S. population. J Endocrinol Invest. 2012; 35: 42–48. Available from: https://doi.org/10.3275/7742.

15. Monk RD, Bushinsky DA. Making Sense of the Latest Advice on Vitamin D Therapy. J Am Soc Nephrol. 2011; 22 (6): 994–8. Available from: https://doi.org/10.1681/ASN.2011030251.

16. Olmos JM, Hernández JL, García-Velasco P, et al. Serum 25-hydroxyvitamin D, parathyroid hormone, calcium intake, and bone mineral density in Spanish adults. Osteoporos Int. 2016; 27 (1): 105–13. Available from: https://doi.org/10.1007/s00198-015-3219-6.

17. Shen M, Li Z, Lv D, et al. Seasonal variation and correlation analysis of vitamin D and parathyroid hormone in Hangzhou, Southeast China. J Cell Mol Med. 2020; 24 (13): 7370–7. Available from: https://doi.org/10.1111/jcmm.15330.

18. Al Quaiz AM, Mujammami M, Kazi A, et al. Vitamin D cutoff point in relation to parathyroid hormone: a population based study in Riyadh city, Saudi Arabia. Arch Osteoporos. 2019; 14 (1): 22. Available from: https://doi.org/10.1007/s11657-019-0565-6.

19. Caroli B, Pasin F, Aloe R, et al. Characterization of skeletal parameters in a cohort of North Italian rugby players. J Endocrinol Invest. 2014; 37 (7): 609–17.

20. Brzeziański M, Migdalska-Sęk M, Stuss M, et al. Effect of physical training on parathyroid hormone and bone turnover marker profile in relation to vitamin D supplementation in soccer players. Biology of Sport. 2022; 39 (4): 921–32. DOI: 10.5114/biolsport.2022.109956.

21. Solarz K, Kopeć A, Pietraszewska J, et al. An evaluation of the levels of 25-hydroxyvitamin D3 and bone turnover markers in professional football players and in physically inactive men. Physiol Res. 2014; 63 (2): 237–43.

22. Ключников С. О., Кравчук Д. А., Оганнисян М. Г. Остеопороз у детей и его актуальность для детской спортивной медицины. Рос вестн перинатол и педиатр. 2017; 62 (3): 112–20. DOI: 10.21508/1027–4065–2017–62–3–112–120.

23. Wyatt PB, Reiter CR, Satalich JR, et al. Effects of Vitamin D Supplementation in Elite Athletes: A Systematic Review. Orthopaedic Journal of Sports Medicine. 2024; 12 (1). DOI: 10.1177/23259671231220371.

24. Thode J, et al. Comparison of serum total calcium, albumin-corrected total calcium, and ionized calcium in 1213 patients with suspected calcium disorders. Scand J Clin. Lab Invest England. 1989; 49 (3): 217–23.

PREVALENCE OF IRON DEFICIENCY IN ADOLESCENT HIGH PERFORMANCE SPORTS

Isaeva EP[1,3,4] ✉, Okorokov PL[1,2], Zyabkin IV[1,3]

[1] Federal Scientific and Clinical Center for Children and Adolescents of the Federal Medical and Biological Agency of Russia, Moscow, Russia

[2] The National Medical Research Center for Endocrinology, Moscow, Russia

[3] Medical and Biological University of Innovation and Continuing Education of the Federal Medical Biophysical Center named after A. I. Burnazyan of the Federal Medical and Biological Agency of Russia

[4] Russian University of Medicine of the Ministry of Health of the Russian Federation, Moscow, Russia

In children, 90% of all anemia cases are due to iron deficiency. Iron is an essential element so iron metabolism disorders have negative consequences for health. Currently, there are no reliable statistical data on the prevalence of iron deficiency in elite young athletes in the Russian Federation (RF). The aim of this study was to evaluate the prevalence of iron deficiency anemia (IDA) and latent iron deficiency (LID) in young elite athletes. We retrospectively analyzed 802 outpatient records of members of the Russian national sport teams aged 13–18 (mean age is 15.4 ± 2.1 years; 434 (54.1%) girls, 368 (45.9%) boys) in 17 sports, who underwent in-depth medical examination including clinical blood tests and serum iron level assays. IDA was diagnosed in 43 young elite athletes (5.4% of all examined athletes). The prevalence of IDA in female adolescents was significantly higher than in male adolescents (8.9% and 1.1%, respectively; p = 0.0001). The prevalence of LID in game sports was significantly higher compared to the other sports. LID was recorded in 186 athletes (23.2%). LID was less common in cyclic sports and was not gender dependent. It can be concluded that young elite athletes have a moderate prevalence of IDA (> 5%). However, since LID was diagnosed in 20% of the athletes, it may be necessary to perform thorough examination for timely screening and correction of iron deficiency in adolescent high performance sports.

Keywords: children, iron deficiency anemia, latent iron deficiency, young athletes, sports medicine

РАСПРОСТРАНЕННОСТЬ ЖЕЛЕЗОДЕФИЦИТНЫХ СОСТОЯНИЙ В ДЕТСКО-ЮНОШЕСКОМ СПОРТЕ ВЫСШИХ ДОСТИЖЕНИЙ

Е. П. Исаева[1,3,4] ✉, П. Л. Окороков[1,2], И. В. Зябкин[1,3]

[1] Федеральный научно-клинический центр детей и подростков Федерального медико-биологического агентства, Москва, Россия

[2] Национальный медицинский исследовательский центр эндокринологии, Москва, Россия

[3] Медико-биологический университет инноваций и непрерывного образования Федерального государственного бюджетного учреждения «Государственный научный центр Российской Федерации — Федеральный медицинский биофизический центр им. А. И. Бурназяна» ФМБА России

[4] ФГБОУ ВО «Российский университет медицины» Минздрава России, Москва, Россия

Железодефицитная анемия (ЖДА) составляет 90% от всех анемий в детском возрасте. Физиологическая значимость железа для организма человека высока, поэтому нарушения его обмена могут иметь негативные последствия. В настоящее время в Российской Федерации (РФ) отсутствуют достоверные статистические данные о распространенности железодефицитных состояний у элитных юных спортсменов. Целью работы было ценить распространенность ЖДА и латентного дефицита железа (ЛДЖ) у юных элитных спортсменов. Проведен ретроспективный анализ 802 амбулаторных карт членов сборных спортивных команд РФ в возрасте 13–18 лет (средний возраст — 15,4 ± 2,1 лет; 434 (54,1%) девочки, 368 (45,9%) — мальчиков) по 17 видам спорта, прошедших углубленное медицинское обследование, в том числе исследование общеклинического анализа крови и уровня сывороточного железа. ЖДА диагностирована у 43 юных элитных спортсменов, что составило 5,4% обследованных. Частота выявления ЖДА у девушек статистически значимо превышает таковую у юношей (8,9% и 1,1% соответственно; p = 0,0001). Распространенность ЖДА в игровых видах спорта статистически значимо выше по сравнению с другими группами спорта. ЛДЖ зафиксирован у 186 спортсменов (23,2%). ЛДЖ реже встречается у представителей циклических видов спорта и не имеет гендерных особенностей. Выводы: у юных элитных спортсменов отмечается умеренная распространенность ЖДА (> 5%). Однако у каждого пятого атлета выявляется ЛДЖ, что ставит вопрос о необходимости тщательного обследования для своевременного скрининга и коррекции железодефицитных состояний в детско-юношеском спорте высших достижений.

Ключевые слова: дети, железодефицитная анемия, латентный дефицит железа, юные спортсмены, спортивная медицина

Iron deficiency remains the most common nutrient deficiency in the world [1]. The occurrence of iron deficiency is associated with impaired intake and absorption or increased loss of iron, and is characterized by microcytosis and hypochromic anemia [2]. Iron is an essential trace element participating in enzymatic systems and providing redox homeostasis of the body, as well as an important component of proteins involved in aerobic metabolism [3]. In athletes, iron metabolism disorders can have negative consequences such as reduced physical performance, limited recovery opportunities, and decreased tone of skeletal muscles [4, 5]. Currently, there are no reliable statistical data on the prevalence of iron deficiency in young elite athletes in the Russian Federation (RF).

The aim of this study was to estimate the prevalence of iron deficiency anemia and latent iron deficiency in young highly qualified athletes in the Russian Federation.

METHODS

A retrospective single-center uncontrolled study included young athletes of sports teams of the Russian Federation who underwent in-depth medical examination at the Federal Scientific and Clinical Center for Children and Adolescents of the Federal Medical and Biological Agency of Russia (Moscow, Russia) within 2019–2022 period.

Inclusion criteria: age up to 18 years; absence of therapy with iron preparations for three months before the study.

Exclusion criteria: presence of chronic blood diseases.

All young athletes were examined once for complete blood count and serum iron level. The complete blood count was performed using a Sysmex XN-350 hematology analyzer (Sysmex Corporaition; Japan) with determination of hemoglobin level. Blood biochemical analysis including serum iron level was performed using Indiko Plus Automatic Clinical Chemistry Analyzer (Thermo Fisher Scientific; USA). Iron deficiency anemia (IDA) was diagnosed when hemoglobin level decreased to values <120 g/L for female adolescents and 130 g/L for male adolescents in combination with a decrease in serum iron level to values <10.7 µmol/L [6]. Latent iron deficiency (LID) was diagnosed when serum iron levels dropped to <10.7 µmol/L [6].

Depending on main patterns of competitive and training activities, all the athlets were divided into six groups: game, cyclic, complex coordination, endurance, combat and multi sports.

RESULTS

A total of 802 young athletes (368 male adolescents (45.9%), 434 female adolescents (54.1%)) aged 13–18 years (mean age 15.4 ± 2.1 years) in 17 sports were included in the study. IDA was diagnosed in 43 young elite athletes (5.4%) (see Table).

In female adolescents, the prevalence of IDA was higher as compared to male adolescents (8.9% and 1.1%, respectively; $p = 0.0001$). The prevalence of IDA in game sports was statistically significantly higher compared to other sports groups (see Table).

LID was diagnosed in 186 athletes (23.1%). LID was observed to be less common in representatives of cyclic sports. No gender differences were found in the prevalence of LID in young highly qualified athletes (20.9% in male adolescents versus 25.2% in female adolescents; $p = 0.237$). No adverse events were recorded during the study.

DISCUSSION

Iron deficiency ranks first among 38 most common human disorders [7]. In children, the main reasons of iron deficiency are nutritional iron deficiency, increased body demand for this trace element due to weight gain and rapid growth, reduced absorption, helminth infections, iron loss exceeding physiological levels (blood loss due to bleeding, etc.) [2]. Appearence of iron deficiency in athletes results from intense physical activity accompanied by increasing iron losses with urine and through the gastrointestinal tract, as well as dietary patterns (vegetarian diets, overall reduction in caloric intake in order to reduce weight, with existing eating disorders) [8].

Iron is a component of certain proteins and enzymes involved in cellular and systemic aerobic metabolism and redox homeostasis of the organism [4]. In particular, iron is involved in transport of cytochromes, iron-seroproteins and oxygen, and is a component of active centers of redox enzymes [9]. In the human body, vital cellular functions and elimination of possible cellular damage is maintained by regulation of iron metabolism including its absorption, transport and deposition in a nontoxic form [10]. As a catalyst of oxygenation and hydroxylation reactions, iron is involved in production and removal of free radicals, in the processes of tissue proliferation and immune defense as well as development and normal functions of the brain. [11]. As part of hemoglobin, iron is involved in oxygen transport; as part of myoglobin it helps to provide oxygen reserves in muscles; as part of the cytochromes of the respiratory chain, iron is invoilved in the processes of aerobic energy formation. Iron metabolism disorders therefore adversely affect the athletes' professional performance. [5].

Iron deficiency develops in two stages: LID characterized by a progressive decrease of storage iron and appearance of iron-deficient erythropoiesis, and IDA characterized by a combination of sideropenic and anemic syndromes.

Currently, there are no reliable statistical data on the prevalence of iron deficiency in elite young athletes in the Russian Federation. According to foreign studies, the prevalence of iron deficiency in female athletes varies from 15 to 35%, with 3 to

Table. Prevalence of iron deficiency anemia (IDA) and latent iron deficiency (LID) in highly skilled athletes depending on the type of sports activity

Sports	LID	IDA
Combat sports ($n = 332$)	22.9% (76)	3.6% (12)
Game sports ($n = 183$)	21.9% (40)	8.2% (15)
Multi-sport athletic events ($n = 14$)	35.7% (5)	–
Endurance sports ($n = 1$)	–	–
Complex coordination sports ($n = 237$)	25.3% (60)	5.9%(14)
Cyclic sports ($n = 35$)	14.3% (5)	5.7%(2)
p	$p_{1-6} = 0.032$ $p_{2-6} = 0.028$ $p_{3-6} = 0.123$ $p_{5-6} = 0.037$	$p_{1-2} = 0.012$ $p_{5-2} = 0.034$ $p_{6-2} = 0.043$
Total:	23.1% (186)	5.4% (43)

11% in male athletes [4]. Based on our results, IDA in young highly qualified athletes is observed in 5.4% of cases, and it is more frequent in female adolescents than in male adolescents. The obtained data well correlate with general population studies demonstrating gender differences in the prevalence of anemic conditions in children [6].

LID is considered to be a functional disorder and accounts for 70% of all cases of iron deficiency [12]. The analysis of epidemiological data revealed that the prevalence of LID in children varies significantly depending on living conditions, age, nutrition, socioeconomic conditions as well as criteria for diagnosing iron deficiency. According to epidemiologic studies, the prevalence of LID in Russia reaches 7.9–31% and is much more common in girls compared to boys. The most significant causes of LID are nutritional disorders and bleeding of various localizations [13]. Our results show that the prevalence of LID in young athletes is the same as in population on the

whole however, without gender differences. Reduced iron in the body may be accompanied by a decrease in physical performance, impaired adaptation to regular increased loads on cardiovascular, respiratory and central nervous system as well as occurrence of immune deficiency in athletes [14]. Such physiological changes severely limit the professional capabilities of athletes and reduce their chances of achieving high performance.

CONCLUSIONS

The study results reveal a high prevalence of latent iron deficiency in young highly qualified athletes regardless of gender. Timely correction of iron deficiency is very important under intense training and competitive pressure. Further research is needed to develop methods for correcting sideropenic states in young athletes.

References

1. UNICEF. Non-communicable diseases. April 2021. In: UNISEF for every child. Available online: https://data.unicef.org/topic/child health/noncommunicable-diseases. Accessed on Marth 30, 2022.
2. Vasileva EV, Aslanjan KS, Piskunova SG. Zhelezodeficitnaja anemija u detej: sovremennyj vzgljad gematologa. Glavnyj vrach Juga Rossii. 2017; 3 (56): 6–10. Russian.
3. Mozgovaja EV. Prokopenko VM, Oparina TI, Novikova TD. Ocenka klinicheskoj jeffektivnosti vitaminno-mineral'nogo kompleksa dlja profilaktiki oslozhnenij beremennosti. Akusherstvo i ginekologija. 2011; 4: 89–94. Russian.
4. Sim M, Garvican-Lewis LA, Cox GR, Govus A, McKay AKA, Stellingwerff T, et al. Iron considerations for the athlete: a narrative review. Eur J Appl Physiol. 2019; 119 (7): 1463–78. DOI: 10.1007/s00421-019-04157-y.
5. Vasilevskij IV. Latentnyj deficit zheleza kak faktor, limitirujushhij vozmozhnosti sportsmena. Materialy 1-j Rossijskoj nauchnoj konferencii. «Obrazovanie, fizicheskaja kul'tura, sport i zdorov'e: analiz problemy». Smolensk, 2012; s. 62–65. Russian.
6. Zhelezodeficitnaja anemija. Klinicheskie rekomendacii. Moskva, 2021 g. https://cr.minzdrav.gov.ru/recomend/669_1. Russian.
7. United Nations Children's Fund, United Nations University, World Health Organization. Iron deficiency anemia: assessment, prevention and control. A guide for programme managers 2011: 114.
8. McCormick R, Sim M, Dawson B, Peeling P. Refining Treatment Strategies for Iron Deficient Athletes. Sports Med. 2020; 50 (12): 2111–23. DOI: 10.1007/s40279-020-01360-2.
9. Stennikova OV, Levchuk LV, Sannikova NE. Profilaktika deficitnyh po vitaminam i mineral'nym veshhestvam sostojanij u detej. Voprosy sovremennoj pediatrii. 2012; 11 (1): 56–60. Russian.
10. Mattiello V, Schmugge M, Hengartner H, von der Weid N, Renella R. SPOG Pediatric Hematology Working Group. Diagnosis and management of iron deficiency in children with or without anemia: consensus recommendations of the SPOG Pediatric Hematology Working Group. Eur J Pediatr. 2020; 179 (4): 527–45. DOI: 10.1007/s00431-020-03597-5.
11. Durmanov ND, Filimonov AS. Diagnostika i korrekcija narushenij obmena zheleza v sporte vysshih dostizhenij: Metodicheskie rekomendacii dlja vrachej klubov. Moskva, 2010. Russian.
12. Tarasova IS, Chernov VM. Latentnyj deficit zheleza u detej i podrostkov: sostojanie problemy i perspektivy razvitija. Pediatricheskij vestnik Juzhnogo Urala. 2020; 2: 24–35. Russian.
13. Zaharova IN, Tarasova IS, Vasileva TM, Borovik TYe, Zvonkova NG, Machneva EB, i dr. Latentnyj deficit zheleza u detej i podrostkov: diagnostika i korrekcija. Lechenie i profilaktika. 2018; 8 (1): 69–75. Russian.
14. Burden RJ, Morton K, Richards T, Whyte GP, Pedlar CR. Is iron treatment beneficial in, iron-deficient but non-anaemic (IDNA) endurance athletes? A systematic review and meta-analysis. Br J Sports Med. 2015; 49 (21): 1389–97. DOI: 10.1136/bjsports-2014-093624.

Литература

1. UNICEF. Non-communicable diseases. April 2021. In: UNISEF for every child. Available online: https://data.unicef.org/topic/child health/noncommunicable-diseases. Accessed on Marth 30, 2022.
2. Васильева Е. В., Асланян К. С., Пискунова С. Г. Железодефицитная анемия у детей: современный взгляд гематолога. Главный врач Юга России. 2017; 3 (56): 6–10.
3. Мозговая Е. В. Прокопенко В. М., Опарина Т. И., Новикова Т. Д. Оценка клинической эффективности витаминно-минерального комплекса для профилактики осложнений беременности. Акушерство и гинекология. 2011; 4: 89–94.
4. Sim M, Garvican-Lewis LA, Cox GR, Govus A, McKay AKA, Stellingwerff T, et al. Iron considerations for the athlete: a narrative review. Eur J Appl Physiol. 2019; 119 (7): 1463–78. DOI: 10.1007/s00421-019-04157-y.
5. Василевский И. В. Латентный дефицит железа как фактор, лимитирующий возможности спортсмена. Материалы 1-й Российской научной конференции. «Образование,

физическая культура, спорт и здоровье: анализ проблемы». Смоленск, 2012; с. 62–65.
6. Железодефицитная анемия. Клинические рекомендации. Москва, 2021 г. https://cr.minzdrav.gov.ru/recomend/669_1.
7. United Nations Children's Fund, United Nations University, World Health Organization. Iron deficiency anemia: assessment, prevention and control. A guide for programme managers 2011: 114.
8. McCormick R, Sim M, Dawson B, Peeling P. Refining Treatment Strategies for Iron Deficient Athletes. Sports Med. 2020; 50 (12): 2111–23. DOI: 10.1007/s40279-020-01360-2.
9. Стенникова О. В., Левчук Л. В., Санникова Н. Е. Профилактика дефицитных по витаминам и минеральным веществам состояний у детей. Вопросы современной педиатрии. 2012; 11 (1): 56–60.
10. Mattiello V, Schmugge M, Hengartner H, von der Weid N, Renella R. SPOG Pediatric Hematology Working Group. Diagnosis and management of iron deficiency in children with or without anemia:

consensus recommendations of the SPOG Pediatric Hematology Working Group. Eur J Pediatr. 2020; 179 (4): 527–45. DOI: 10.1007/s00431-020-03597-5.

11. Дурманов Н. Д., Филимонов А. С. Диагностика и коррекция нарушений обмена железа в спорте высших достижений: Методические рекомендации для врачей клубов. Москва, 2010.

12. Тарасова И. С., Чернов В. М. Латентный дефицит железа у детей и подростков: состояние проблемы и перспективы развития. Педиатрический вестник Южного Урала. 2020; 2: 24–35.

13. Захарова И. Н., Тарасова И. С., Васильева Т. М., Боровик Т. Э., Звонкова Н. Г., Мачнева Е. Б и др. Латентный дефицит железа у детей и подростков: диагностика и коррекция. Лечение и профилактика. 2018; 8 (1): 69–75.

14. Burden RJ, Morton K, Richards T, Whyte GP, Pedlar CR. Is iron treatment beneficial in, iron-deficient but non-anaemic (IDNA) endurance athletes? A systematic review and meta-analysis. Br J Sports Med. 2015; 49 (21): 1389–97. DOI: 10.1136/bjsports-2014-093624.

PLANTAR PRESSURE DISTRIBUTION FEATURES IN ATHLETES WITH PLANTAR FASCIITIS

Karmazin VV[1], Slivin AV[1,2] ✉, Parastaev SA[1,2]

[1] Federal Research and Clinical Center of Sports Medicine and Rehabilitation of the Federal Medical Biological Agency, Moscow, Russia

[2] Pirogov Russian National Research Medical University, Moscow, Russia

Plantar fasciitis (PF) is one of the leading causes of heel pain in athletes. Since the disease etiology and pathogenesis are poorly understood, determination of impaired biomechanical patterns will make it possible to develop effective and safe therapeutic strategies. The study was aimed to reveal biomechanical changes typical for athletes with PF. Analysis of the results of baropodometric examination of 60 athletes, who were assessed and treated at the Federal Research and Clinical Center of Sports Medicine and Rehabilitation of FMBA of Russia due to foot disorders (1–2 degree combined platypodia and PF), was conducted. Athletes were divided into two groups based on the fact of having/not having a verified diagnosis of PF. The study involved 24 males (40%) and 36 females (60%), the athletes' median age was 24 (19; 28) years. During the study we noted a trend towards higher incidence of PF in female athletes ($p = 0.066$). Hammertoe deformity was often found in athletes with PF ($p < 0.05$). Athletes with combined platypodia and PF showed overload or insufficient load in the posterior part of the affected foot, depending on pain severity, in static tests ($r = 0.592$, $p = 0.001$). The dynamic tests revealed deformation of the general pressure vector and changes in the general center of pressure velocity ($p < 0.01$). Baropodometric examination showed that athletes with PF had deficit or excess increase of plantar pressure in the heel of the affected foot, along with deformation of the general pressure vector.

Keywords: plantar fasciitis, sport, biomechanics, baropodometry, heel pain

ОСОБЕННОСТИ РАСПРЕДЕЛЕНИЯ ПОДОШВЕННОГО ДАВЛЕНИЯ СТОП У СПОРТСМЕНОВ С ПЛАНТАРНЫМ ФАСЦИИТОМ

В. В. Кармазин[1], А. В. Сливин[1,2] ✉, С. А. Парастаев[1,2]

[1] Федеральный научно-клинический центр спортивной медицины и реабилитации Федерального медико-биологического агентства, Москва, Россия

[2] Российский национальный исследовательский медицинский университет имени Н. И. Пирогова, Москва, Россия

Плантарный фасциит (ПФ) — одна из ведущих причин болевого синдрома в пяточной области среди спортсменов. Поскольку этиология и патогенез заболевания непонятны, определение нарушенных биомеханических паттернов позволит разработать эффективные и безопасные терапевтические стратегии. Целью работы было выявить биомеханические изменения, характерные для спортсменов с ПФ. Проведен анализ результатов бароподометрического обследования 60 спортсменов, проходивших обследование и лечение на базе Федерального научно-клинического центра спортивной медицины и реабилитации ФМБА России по поводу патологии стоп (комбинированного плоскостопия 1–2 степени и ПФ). Спортсмены были разделены на две группы в зависимости от наличия/отсутствия у них верифицированного диагноза «плантарный фасциит». В исследовании приняли участие 24 мужчины (40%) и 36 женщин (60%), медиана возраста спортсменов составила 24 (19; 28) года. В ходе исследования было отмечено наличие тенденции к более частому развитию ПФ у спортсменок ($p = 0,066$). У спортсменов с ПФ часто встречалась молоткообразная деформация пальцев стопы ($p < 0,05$). У спортсменов с комбинированным плоскостопием и ПФ в статических тестах выявлена перегрузка или недостаточная нагрузка на задний отдел пораженной стопы, в зависимости от степени выраженности болевого синдрома ($r = 0,592$, $p = 0,001$). В динамических тестах определялись деформация общего вектора давления и изменения скорости общего центра давления ($p < 0,01$). У спортсменов с ПФ по результатам бароподометрического обследования наблюдались дефицит или избыточное повышение подошвенного давления в пяточной области на пораженной стопе и деформация общего вектора давления.

Ключевые слова: плантарный фасциит, спорт, биомеханика, бароподометрия, боль в пяточной области

Plantar fasciitis (PF) is one of the leading causes of foot pain in the adult population. According to the data provided by various authors, the prevalence of PF among athletes varies between 4.5 and 10%. Furthermore, PF is slightly less common among men, than among women [1–3]. The severity of pain occurring in case of the plantar fascia overload often hampers and quite often leads to interruption of the training and competitive activity.

At the same time, it is still unclear, which factors underlie the PF development and whether these factors are different in athletic population. The authors of the systematic review emphasize that all the currently distinguished risk factors of PF

Table 1. Sequence of the tests performed and their description

Test	Description
Static test	Feet are standing parallel, the width of the iliac spines of the pelvis apart. The test is conducted for 30 s. The athlete keeps still during testing
Dynamic tests	
Sagittal test	Feet are standing parallel, the width of the iliac spines of the pelvis apart. The test is conducted for 30 s. The athlete makes the physician-commanded low-amplitude forward and backward movements (in ankle joints only)
Frontal test	Feet are standing parallel, the width of the iliac spines of the pelvis apart. The test is conducted for 30 s. The athlete makes the physician-commanded low-amplitude right and left movements (in ankle joints only)
Test involving standing on the forefoot	Feet are standing parallel, the width of the iliac spines of the pelvis apart. The test is conducted for 30 s. The athlete stands on the forefoot, lifting the heels of both feet 3–4 cm above the platform, by the physician's command
Jump test	Feet are standing parallel, the width of the iliac spines of the pelvis apart. The test is conducted for 30 s. The athlete jumps, synchronously and symmetrically lifting both feet off the platform by 3–4 cm and trying not to bend the knees when taking off and landing, by the physician's command. The athlete makes 4–5 jumps with intervals

have no strong evidence base [4], and high body mass index (BMI) that is usually announced as the leading risk factor has absolutely nothing to do with prediction of the risk of the plantar fascia inflammation onset in athletes [5].

The important role of biomechanical problems with the foot in the PF pathogenesis is reported more and more often [4]. The changes in foot biomechanics associated with PF are poorly understood, however, it is their leading role in the development of the plantar fascia aseptic inflammation that seems to be the most logical, especially in athletic population [6, 7]. Identification of disturbed biomechanical patterns will make it possible to not only better understand the PF pathogenesis, but also get closer to understanding the effective methods to adjust the disorder.

The study was aimed to determine biomechanical changes typical for athletes with PF.

METHODS

The analysis of the results of baropodometric examination of 60 athletes conducted in 2021–2023 at the Federal Research and Clinical Center of Sports Medicine and Rehabilitation of FMBA of Russia by the experts of the rehabilitation treatment department was performed. The inclusion criteria were as follows: sports category (Candidate for Master of Sport of Russia or higher), athletes' age 16–40 years, undergoing baropodometric examination at the Center, combined flat foot.

A total of 24 males (40%) and 36 females (60%) were included in the study. The athletes' median age was 24 (19; 28) years. The athletes were divided into two groups based on having/not having a verified diagnosis of PF: group 1 — athletes with 1–2 degree combined flat foot and PF (n = 30), group 2 — athletes with 1–2 degree combined flat foot and no PF, who had subjective symptoms (pain, feeling uncomfortable in the feet) (n = 30). Athletes with unilateral PF only were included in group 1; the cases of bilateral process were extremely rare. The assumption of possible PF was based on the fact of the presence of rather typical clinical manifestations in an athlete

(kickoff heel pain), and the diagnosis was verified based on the MRI data (plantar fascia hypointense lesions and thickening). Patients with the verified diagnoses of the disorders affecting bone tissues of the foot were excluded from the study. Pain severity was estimated using a 10-point visual analogue scale (VAS).

Biomechanical examination was conducted using the WINTRACK baropodometric hardware-software system (Medicapteurs; France). The study was performed in accordance with the algorithm including the series of tests that was substantiated at the rehabilitation treatment department of the Federal Research and Clinical Center of Sports Medicine and Rehabilitation of FMBA of Russia. The details of the tests conducted are provided in Table 1. The static test was assessed based primarily on the changes in plantar pressure of the forefoot and hindfoot, while the dynamic tests were assessed based on the changes in the general center of pressure (GCP) speed on the X and Y axes.

Statistical data processing was performed using the IBM SPSS Statistics 23 software package (IBM; USA). Given small sample size, nonparametric statistical methods were used for data analysis. The quantitative data descriptive statistics were presented as the median and quartiles, while qualitative traits were described using the absolute and relative frequency values. The nonparametric Mann–Whitney U test was used for comparative intergroup analysis, and the Wilcoxon test was used for intragroup analysis. Discrete values were compared using the chi-squared test (χ^2) with the Yates continuity correction. The differences were considered significant at the statistical significance level below 0.05.

RESULTS

Characteristics of the studied groups

The study involved representatives of various sports: handball, skeleton, football, track and field, fencing, basketball, tennis. The more detailed characteristics of the studied groups are provided in Fig. 1 and Table 2.

Table 2. Characteristics of the studied groups with descriptive statistics

Characteristic	Group 1	Group 2	p
Age, years (Me (Q_1; Q_3))	24 (19; 30)	24 (20; 27)	0.781
Female (abs. (%))	22 (77.3%)	14 (46.7%)	0.066
BMI, kg/m² (Me (Q_1; Q_3))	22.69 (21.25; 23.9)	22.72 (20.11; 24.05)	0.843
Hammertoe deformity (abs. (%))	9 (30%)	2 (6.7%)	0.046*

Note: * — significant difference (p < 0.05).
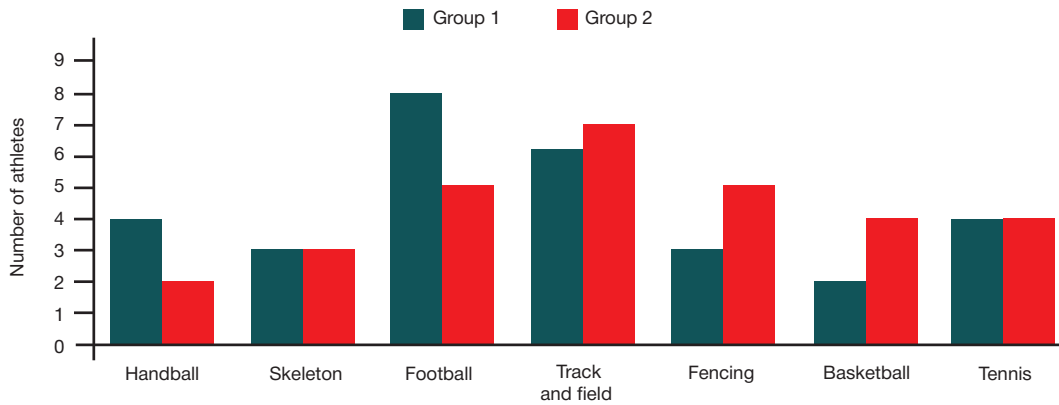
Fig. 1. Distribution of athletes by sports

Despite the fact that statistical significance has not been achieved, the trend towards more frequent development of PF in female athletes can be noted. Hammertoe deformity was significantly more common in male athletes with PF ($p = 0.046$). PF was most common in football players and track and field athletes. BMI did not show any statistical significance as a potential risk factor of PF in athletes ($p > 0.05$).

Results of the baropodometric examination of athletes in the static test

The distribution of plantar pressure in athletes based on the baropodometric examination results is provided in Table 3 and Fig. 2.

Intragroup comparison revealed no significant differences in the groups 1 and 2 ($p > 0.05$). However, the following feature was identified during analysis of the results (Fig. 2): in athletes with PF, the posterior part of the affected foot was either overloaded (plantar pressure exceeding 30%) (Fig. 3A), or insufficiently loaded (plantar pressure below 22%) (Fig. 3B).

Intergroup comparison also revealed no significant differences between the forefoot ($p = 0.637$) and hindfoot ($p = 0.229$).

When assessing the relationship between plantar pressure in the posterior part of the foot with PF and pain severity on VAS, it was found that the degree of the deficit of support on the limb affected with PS in the static test was determined by pain severity ($r = 0.592$, $p = 0.001$) (Fig. 4).

Results of the baropodometric examination of athletes in the dynamic tests

In the study, the most vivid changes of the general pressure vector (GPV) were detected in the sagittal dynamic test. Fig. 5 presents the test results of athletes with PF. The left athlete's foot is affected in Fig. 5A, the right athlete's foot is affected in Fig. 5B.

GPV shift and deformation in the area of pain localization were reported. Furthermore, imbalance of plantar pressure distribution under the affected foot is associated with the plantar pressure decrease in the forefoot.

GPV changes are indirectly reflected in the dynamic changes of GCP speed. The most significant changes in the GCP speed on X axis were reported in the sagittal dynamic test, while that on Y axis were reported in the frontal dynamic test. The analysis showed that changes in GCP speed on X

Table 3. Distribution of plantar pressure in athletes based on the results of baropodometric examination in the static test

Region of the foot	Group 1			Group 2		
	Foot with PF Me (Q$_1$; Q$_3$)	Contralateral foot Me (Q$_1$; Q$_3$)	p	Right foot Me (Q$_1$; Q$_3$)	Left foot Me (Q$_1$; Q$_3$)	p
Forefoot, %	21 (14; 28)	23 (19; 24)	0.992	22 (21; 24)	21 (19.75; 24)	0.539
Hindfoot, %	26.5 (20; 36)	29.5 (27; 31.25)	0.346	28 (25.75; 30)	27.5 (26.75; 30)	0.81
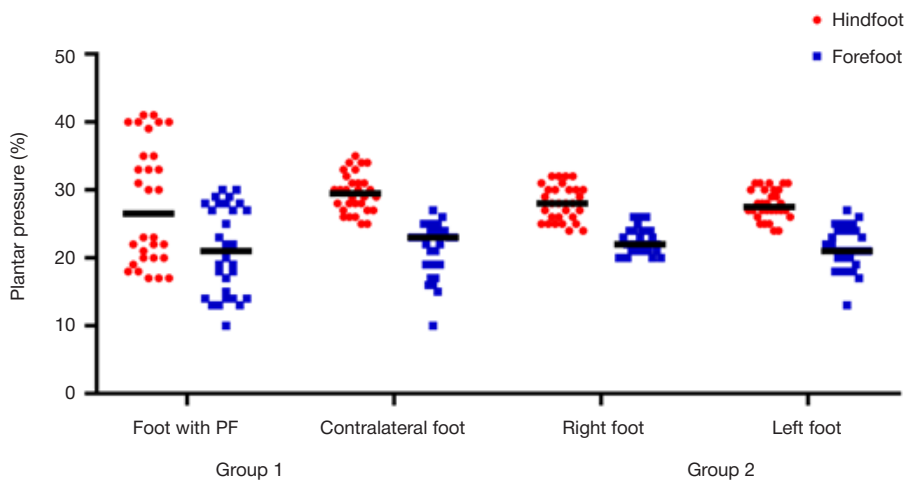
Fig. 2. Plantar pressure distribution in the studied groups based on the results of baropodometric examination in the static test
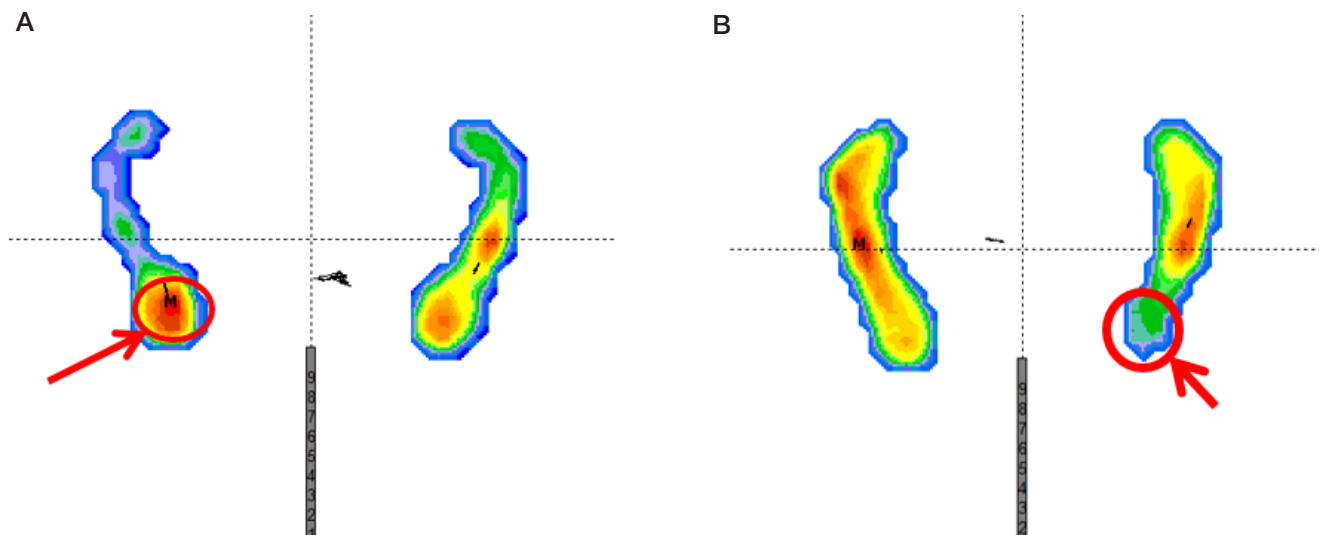
Fig. 3. Plantar pressure distribution in athletes with PF in the static test. The heel of the athlete with PF is highlighted in *red*. **A**. Excess plantar pressure in the affected foot. **B**. Plantar pressure deficit

and Y axes were more significant in group 1, than in group 2 (*p* < 0.01) (Fig. 6).

DISCUSSION

In the study, several baropodometric patterns clearly traceable in athletes with PF were revealed. In static tests, these were represented by deficit of support or overload in the affected area, depending on pain severity; in dynamic tests, these were represented by deformation of GPV in the projection of the most painful area with the reduced pressure in the forefoot. It is likely that degenerative changes of the plantar aponeurosis result from the increased load on the latter that can be associated with the overlying impairment of the lower limb biomechanics in general, which is manifested by the increased plantar pressure in the heel. Further prolongation of excess load on the plantar fascia leads to pain contributing to the emergence of the plantar pressure deficit area in the heel, depending on pain severity. The findings are generally consistent with the data obtained by various authors in the general population of patients. Thus, the group of researchers found that in patients with PF the maximum pressure in the hindfoot and the contact area were significantly lower in the affected foot compared to the contralateral foot [8]. Other researchers obtained similar results and noted that patients with PF showed decreased plantar pressure in the medial part of the forefoot when undergoing dynamic tests, as reported in our study [9]. The plantar pressure deficit in the anteromedial part of the foot wore off in cases of successful therapy [9]. In our study, it was pointed out that plantar pressure in the hindfoot was inversely proportional to pain severity, which had not been previously reported in the literature. Our study revealed GPV deformation in the most painful area in patients with PF when conducting dynamic tests. This is in line with the data, according to which the anteromedial shift of the plantar pressure load is observed in patients with PF [10]. The authors also reported that heel pain occurred in the foot with normal arch in 59% of cases [10]. However, in the above studies, the dynamic test involved plantar pressure estimation during walking, while our study involved the use of a broader range of the dynamic testing methods, which had not been previously reported in the literature. Furthermore, the tests reported in the study are to the greater extent consistent with the essence of the medical and biological support of sports, since these make it possible to detect even minimal functional disorders

impeding intense movement. Similar results were obtained by the researchers, who detected deficit in the initial contact phase only when performing dynamic tests. Furthermore, the reported changes were usually bilateral [11]. We usually observed no imbalance of pressure distribution under the foot on both sides in patients with the confirmed diagnosis of combined flat foot having no PF. Furthermore, no local deformation of the pressure vector under the feet was reported in this group of athletes. It is likely that the GPV changes observed in athletes with PF can be partially explained by postural disorders associated with functional insufficiency of the overlying muscles (particularly, gluteal muscles).

The hypothesis explaining the presence of the zones of excess pressure in the sole we have detected by muscular imbalance seems to be rather logical. Many studies have shown that the decrease in the strength and response time of the plantar flexors is observed in patients with PF [12–14]. It has been assumed that it is these muscles that absorb most of load, and their incorrect functioning can result in the multiple increase of the load on the plantar aponeurosis [15–17]. Furthermore, in 83% of cases PF was associated with the calf muscle shortening [18], which resulted in the ankle dorsiflexion limitation, excess pronation in the rolling phase, and, as a result, the increase in the distance between the heel tubercle and the toes [16, 19]. The reported impossibility of ankle dorsiflexion
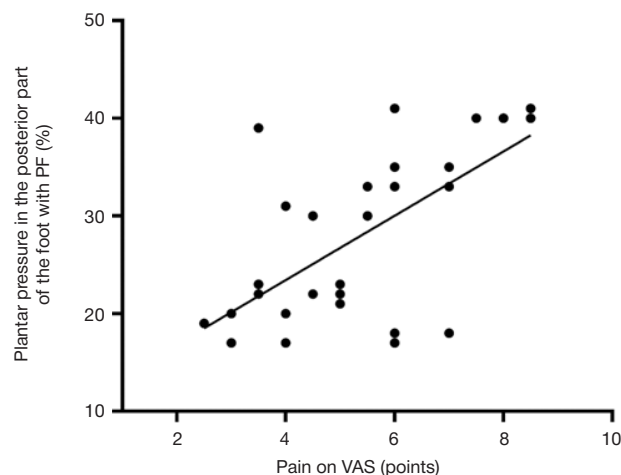
Fig. 4. Relationship between plantar pressure in the posterior part of the foot with PF and pain severity in athletes with PF
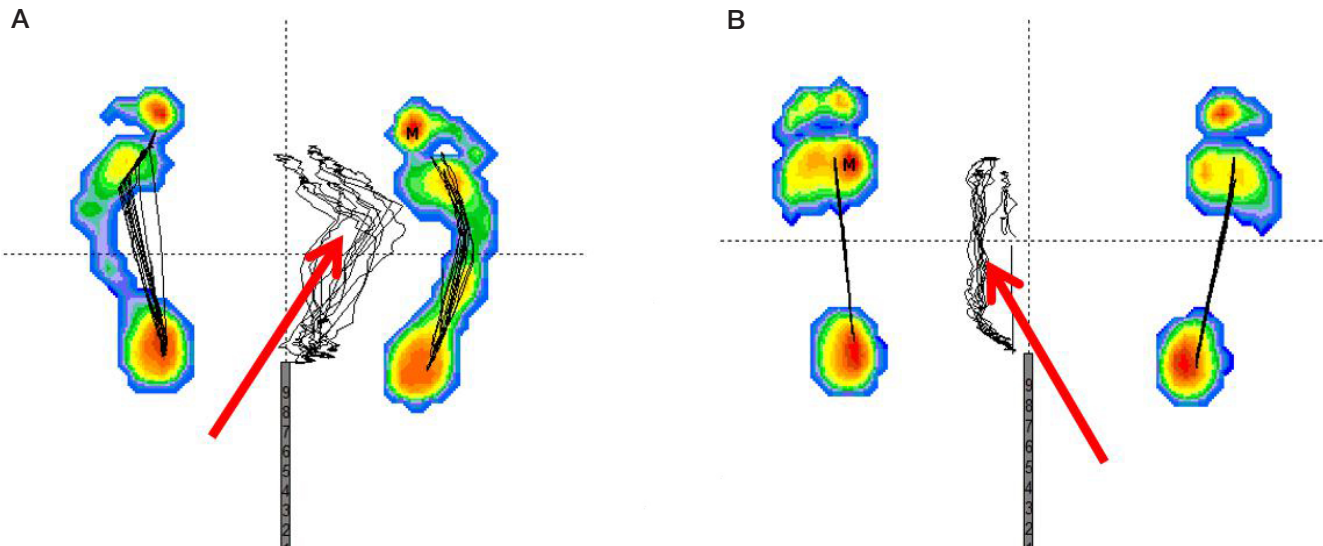
Fig. 5. Plantar pressure distribution in athletes with PF in the sagittal dynamic test. The GPV shift towards healthy side relative to the central axis is marked with *red arrow*. **A**. Left plantar fasciitis. **B**. Right foot is affected

23-fold increases the risk of PF [20]. However, it is still unclear, whether the above changes are primary or secondary relative to other, probably overlying, disorders. Therefore, further research is required.

In this regard, the study reporting a possible relationship between weakness of the hip abductor muscles and the PF development seems to be interesting [21]. The authors described the case of long-term PF refractory to the majority of treatment options. It was inclusion of exercises for the hip abductor muscles that made it possible to achieve clinical improvement and redistribution of the pressure zones in the foot based on the baropodometric data [21]. Similar cases were also reported by other authors [17, 22, 23]. It is likely that PF can be a more complex and multifactorial issue than previously thought.

In our study, PF was slightly more common in females, than in males, which was generally consistent with the literature data [2, 24]. As expected, BMI is not a risk factor of PF in athletes, in accordance with the previously reported data [5]. Higher prevalence of PF among football players and track-and-field athletes is explained by high running load in these sports; impaired biomechanics of running is likely to be the key to understanding the PF pathogenesis in athletes [6, 16]. Furthermore, high prevalence of hammertoe deformity among athletes with plantar aponeurosis inflammation was revealed. Some researchers report that there is a strong correlation between flat foot and the PF development [25]. Previously, the possible contribution of forefoot abnormalities to the PF development was separately reported [26].

Considering the results obtained in our study and the literature data, it seems feasible to include the methods estimating pressure distribution across the sole surface in the PF diagnosis programs. This will make it possible to improve accuracy of the diagnostic measures themselves and the dynamic control of treatment methods for PF in cases of suspected PF and allow us to get closer to understanding biomechanical problems underlying the PF development, especially in the athletic cohort.

CONCLUSIONS

Plantar fasciitis (PF) is an urgent and common issue, including in elite sports, which is still poorly understood. Baropodometric examination of athletes with PF represents an important phase of assessment and detection of pressure distribution abnormalities in the sole that makes it possible to determine impaired biomechanical patterns and, therefore, improve treatment outcomes.

Common baropodometric pattern changes were revealed in athletes with PF during the study. These are deficit of support or overload of the affected area in the static test, depending on pain severity, and deformation of the general pressure vector in projection of the most painful area with the reduced pressure in the forefoot in dynamic tests. It seems important to consider biomechanical changes associated with such baropodometric pattern in order to more adequately select corrective interventions and, as a result, reduce the duration of treatment and rehabilitation of athletes having the discussed disorder.
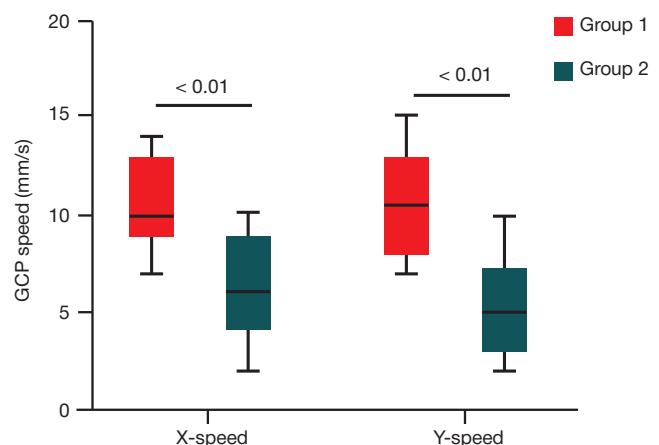
Fig. 6. Comparison of changes in GCP speed in groups 1 and 2

References

1. Sobhani S, Dekker R, Postema K, Dijkstra PU. Epidemiology of ankle and foot overuse injuries in sports: A systematic review. Scand J Med Sci Sports. 2013; 23 (6): 669–86.
2. Taunton JE, Ryan MB, Clement DB, McKenzie DC, Lloyd-Smith DR, Zumbo BD. A retrospective case-control analysis of 2002 running injuries. Br J Sports Med. 2002; 36 (2): 95–101.
3. Lopes AD, Hespanhol Júnior LC, Yeung SS, Costa LO. What are the main running-related musculoskeletal injuries? A systematic review. Sports Med. 2012; 42 (10): 891–905.
4. Petraglia F, Ramazzina I, Costantino C. Plantar fasciitis in athletes: diagnostic and treatment strategies. A systematic review. Muscles Ligaments Tendons J. 2017; 7 (1): 107–18.
5. Butterworth PA, Landorf KB, Smith SE, Menz HB. The association between body mass index and musculoskeletal foot disorders: a systematic review. Obes Rev. 2012; 13 (7): 630–42.
6. Murphy K, Curry EJ, Matzkin EG. Barefoot running: does it prevent injuries? Sports Med. 2013; 43 (11): 1131–8.
7. Ribeiro AP, João SM, Dinato RC, Tessutti VD, Sacco IC. Dynamic patterns of forces and loading rate in runners with unilateral plantar fasciitis: a cross-sectional study. PLoS One. 2015; 10 (9): e0136971.
8. Baris R, Narin S, Elvan A, Erduran M. FRI0638-HPR Investigating plantar pressure during walking in plantar fasciitis. Annals of the Rheumatic Diseases. 2016; (75): 1284–5.
9. Ulusoy A, Cerrahoğlu H, Örgüç Ş. The assessment of plantar pressure distribution in plantar fasciitis and its relationship with treatment success and fascial thickness. Kastamonu Med J. 2023; 3 (3): 139–43.
10. Balaji G, Jagadevan M, Mohanakrishnan B, Murugesan S, Palaniappan P. "Antero-medial load shift" in unilateral plantar heel pain — a cross-sectional exploratory study. J Bodyw Mov Ther. 2024; (37): 151–5.
11. Padrón L, Bayod J, Becerro-de-Bengoa-Vallejo R, Losa-Iglesias M, López-López D, Casado-Hernández I. Influence of the center of pressure on baropodometric gait pattern variations in the adult population with flatfoot: A case-control study. Front Bioeng Biotechnol. 2023; (11): 1147616.
12. Lee JH, Shin KH, Jung TS, Jang WY. Lower extremity muscle performance and foot pressure in patients who have plantar fasciitis with and without flat foot posture. Int J Environ Res Public Health. 2022; 20 (1): 87.
13. Allen RH, Gross MT. Toe flexors strength and passive extension range of motion of the first metatarsophalangeal joint in individuals with plantar fasciitis. J Orthop Sports Phys Ther. 2003; 33 (8): 468–78.
14. McClinton S, Collazo C, Vincent E, Vardaxis V. Impaired foot plantar flexor muscle performance in individuals with plantar heel pain and association with foot orthosis use. J Orthop Sports Phys Ther. 2016; 46 (8): 681–8.
15. Pollack Y, Shashua A, Kalichman L. Manual therapy for plantar heel pain. Foot (Edinb). 2018; (34): 11–6.
16. Bolgla LA, Malone TR. Plantar fasciitis and the windlass mechanism: a biomechanical link to clinical practice. J Athl Train. 2004; 39 (1): 77–82.
17. Kirby KA. Longitudinal arch load-sharing system of the foot. Revista Española de Podología. 2017; 28 (1): e18–e26.
18. Patel A, DiGiovanni B. Association between plantar fasciitis and isolated contracture of the gastrocnemius. Foot Ankle Int. 2011; 32 (1): 5–8.
19. Gutteck N, Schilde S, Delank KS. Pain on the plantar surface of the foot. Dtsch Arztebl Int. 2019; 116 (6): 83–8.
20. Riddle DL, Pulisic M, Pidcoe P, Johnson RE. Risk factors for plantar fasciitis: a matched case-control study. J Bone Joint Surg Am. 2003; 85 (5): 872–7.
21. Lee JH, Park JH, Jang WY. The effects of hip strengthening exercises in a patient with plantar fasciitis: A case report. Medicine (Baltimore). 2019; 98 (26): e16258.
22. Lewis CL, Ferris DP. Walking with increased ankle pushoff decreases hip muscle moments. J Biomech. 2008; 41 (10): 2082–9.
23. Mueller MJ, Sinacore DR, Hoogstrate S, Daly L. Hip and ankle walking strategies: effect on peak plantar pressures and implications for neuropathic ulceration. Arch Phys Med Rehabil. 1994; 75 (11): 1196–200.
24. Orchard J. Plantar fasciitis. BMJ. 2012; (345): e6603.
25. Park SY, Bang HS, Park DJ. Potential for foot dysfunction and plantar fasciitis according to the shape of the foot arch in young adults. J Exerc Rehabil. 2018; 14 (3): 497–502.
26. Noriega DC, Cristo Á, León A, García-Medrano B, Caballero-García A, Córdova-Martinez A. Plantar fasciitis in soccer players — a systemic review. Int J Environ Res Public Health. 2022; 19 (21): 14426.

Литература

1. Sobhani S, Dekker R, Postema K, Dijkstra PU. Epidemiology of ankle and foot overuse injuries in sports: A systematic review. Scand J Med Sci Sports. 2013; 23 (6): 669–86.
2. Taunton JE, Ryan MB, Clement DB, McKenzie DC, Lloyd-Smith DR, Zumbo BD. A retrospective case-control analysis of 2002 running injuries. Br J Sports Med. 2002; 36 (2): 95–101.
3. Lopes AD, Hespanhol Júnior LC, Yeung SS, Costa LO. What are the main running-related musculoskeletal injuries? A systematic review. Sports Med. 2012; 42 (10): 891–905.
4. Petraglia F, Ramazzina I, Costantino C. Plantar fasciitis in athletes: diagnostic and treatment strategies. A systematic review. Muscles Ligaments Tendons J. 2017; 7 (1): 107–18.
5. Butterworth PA, Landorf KB, Smith SE, Menz HB. The association between body mass index and musculoskeletal foot disorders: a systematic review. Obes Rev. 2012; 13 (7): 630–42.
6. Murphy K, Curry EJ, Matzkin EG. Barefoot running: does it prevent injuries? Sports Med. 2013; 43 (11): 1131–8.
7. Ribeiro AP, João SM, Dinato RC, Tessutti VD, Sacco IC. Dynamic patterns of forces and loading rate in runners with unilateral plantar fasciitis: a cross-sectional study. PLoS One. 2015; 10 (9): e0136971.
8. Baris R, Narin S, Elvan A, Erduran M. FRI0638-HPR Investigating plantar pressure during walking in plantar fasciitis. Annals of the Rheumatic Diseases. 2016; (75): 1284–5.
9. Ulusoy A, Cerrahoğlu H, Örgüç Ş. The assessment of plantar pressure distribution in plantar fasciitis and its relationship with treatment success and fascial thickness. Kastamonu Med J. 2023; 3 (3): 139–43.
10. Balaji G, Jagadevan M, Mohanakrishnan B, Murugesan S, Palaniappan P. "Antero-medial load shift" in unilateral plantar heel pain — a cross-sectional exploratory study. J Bodyw Mov Ther. 2024; (37): 151–5.
11. Padrón L, Bayod J, Becerro-de-Bengoa-Vallejo R, Losa-Iglesias M, López-López D, Casado-Hernández I. Influence of the center of pressure on baropodometric gait pattern variations in the adult population with flatfoot: A case-control study. Front Bioeng Biotechnol. 2023; (11): 1147616.
12. Lee JH, Shin KH, Jung TS, Jang WY. Lower extremity muscle performance and foot pressure in patients who have plantar fasciitis with and without flat foot posture. Int J Environ Res Public Health. 2022; 20 (1): 87.
13. Allen RH, Gross MT. Toe flexors strength and passive extension range of motion of the first metatarsophalangeal joint in individuals with plantar fasciitis. J Orthop Sports Phys Ther. 2003; 33 (8): 468–78.
14. McClinton S, Collazo C, Vincent E, Vardaxis V. Impaired foot plantar flexor muscle performance in individuals with plantar heel pain and association with foot orthosis use. J Orthop Sports Phys Ther. 2016; 46 (8): 681–8.
15. Pollack Y, Shashua A, Kalichman L. Manual therapy for plantar

heel pain. Foot (Edinb). 2018; (34): 11–6.

16. Bolgla LA, Malone TR. Plantar fasciitis and the windlass mechanism: a biomechanical link to clinical practice. J Athl Train. 2004; 39 (1): 77–82.

17. Kirby KA. Longitudinal arch load-sharing system of the foot. Revista Española de Podología. 2017; 28 (1): e18–e26.

18. Patel A, DiGiovanni B. Association between plantar fasciitis and isolated contracture of the gastrocnemius. Foot Ankle Int. 2011; 32 (1): 5–8.

19. Gutteck N, Schilde S, Delank KS. Pain on the plantar surface of the foot. Dtsch Arztebl Int. 2019; 116 (6): 83–8.

20. Riddle DL, Pulisic M, Pidcoe P, Johnson RE. Risk factors for plantar fasciitis: a matched case-control study. J Bone Joint Surg Am. 2003; 85 (5): 872–7.

21. Lee JH, Park JH, Jang WY. The effects of hip strengthening exercises in a patient with plantar fasciitis: A case report. Medicine (Baltimore). 2019; 98 (26): e16258.

22. Lewis CL, Ferris DP. Walking with increased ankle pushoff decreases hip muscle moments. J Biomech. 2008; 41 (10): 2082–9.

23. Mueller MJ, Sinacore DR, Hoogstrate S, Daly L. Hip and ankle walking strategies: effect on peak plantar pressures and implications for neuropathic ulceration. Arch Phys Med Rehabil. 1994; 75 (11): 1196–200.

24. Orchard J. Plantar fasciitis. BMJ. 2012; (345): e6603.

25. Park SY, Bang HS, Park DJ. Potential for foot dysfunction and plantar fasciitis according to the shape of the foot arch in young adults. J Exerc Rehabil. 2018; 14 (3): 497–502.

26. Noriega DC, Cristo Á, León A, García-Medrano B, Caballero-García A, Córdova-Martinez A. Plantar fasciitis in soccer players — a systemic review. Int J Environ Res Public Health. 2022; 19 (21): 14426.

VEGETATIVE REGULATION OF BLOOD CIRCULATION AND BIOELECTRIC PROCESSES IN THE HUMAN MYOCARDIUM UNDER SIMULATED HYPOMAGNETIC CONDITIONS

Popova OV ✉, Rusanov VB, Orlov OI

State Scientific Center of the Russian Federation — Institute for Biomedical Problems of the Russian Academy of Sciences, Moscow, Russia

Today, the prospect of long-term interplanetary missions becomes relevant, that is why it is necessary to understand the changes in the cardiovascular system (CVS) that would occur in hypomagnetic environment. The study was aimed to assess the changes in the CVS mechanisms underlying formation of heart rate variability and bioelectric processes in the myocardium under conditions the 350-, 650-, and 1000-fold reduced Earth's magnetic field. The experiment (2023) involved 6 male volunteers aged 26–37 years, in whom electrocardiography was continuously performed throughout 32 h. The data obtained were assessed by cluster analysis and analysis of variance. It was found than male volunteers, who belonged to the group showing predominance of parasympathetic effects, had enough functional reserve for critical values (exposure to the up to 1000-fold reduced magnetic field). In volunteers showing predominance of sympathetic modulatory effects, the adaptive response maintenance was ensured by the metabolic regulatory circuit. In this group, the response to the reduced magnetic field exposure was quite pronounced at the threshold of its 350-fold reduction. Our pilot experiment reflecting the effect of the reduced Earth's magnetic field on the CVS is crucial for development of the concept of further experimental exposures related to magnetic field reduction benefiting space physiology and medicine.

✉ **Correspondence should be addressed:** Olga V. Popova
Khoroshevskoye shosse, 76A, Moscow, 123007, Russia; olya.popovaolga2710@yandex.ru

ВЕГЕТАТИВНАЯ РЕГУЛЯЦИЯ КРОВООБРАЩЕНИЯ И БИОЭЛЕКТРИЧЕСКИЕ ПРОЦЕССЫ В МИОКАРДЕ ЧЕЛОВЕКА В МОДЕЛИРУЕМЫХ ГИПОМАГНИТНЫХ УСЛОВИЯХ

О. В. Попова ✉, В. Б. Русанов, О. И. Орлов

Государственный научный центр Российской Федерации — Институт медико-биологических проблем Российской академии наук, Москва, Россия

На сегодняшний день становится актуальной перспектива длительных межпланетных полетов, поэтому необходимо понимание изменений в сердечно-сосудистой системе (ССС), которые будут происходить в гипомагнитных условиях. Целью исследования было провести анализ изменений механизмов ССС, которые представляют собой основу для формирования вариабельности сердечного ритма и биоэлектрических процессов в миокарде, в условиях сниженного в 350, 650 и 1000 раз магнитного поля Земли. В эксперименте (2023 г.) участвовало 6 мужчин-добровольцев в возрасте 26–37 лет, у которых непрерывно в течение 32 ч регистрировали электрокардиограмму. Анализ полученных данных проводили при помощи кластерного и дисперсионного анализа. Было обнаружено, что у мужчин-добровольцев, относящихся к группе с преобладанием парасимпатических влияний, функционального резерва хватает для критических значений (воздействия сниженного магнитного поля до 1000 раз). У добровольцев с преобладанием симпатических моделирующих влияний поддержание приспособительных реакций осуществляется метаболическим регуляторным контуром. В этой группе реакция на воздействие сниженного магнитного поля достаточно выражена при пороге его снижения от 350 раз. Проведенный нами пилотный эксперимент, отражающий влияние сниженного магнитного поля земли на ССС, имеет определяющее значение для разработки концепции последующих экспериментальных воздействий, связанных с редукцией магнитного поля, для интересов космической физиологии и медицины.

✉ **Для корреспонденции:** Ольга Владимировна Попова
Хорошевское шоссе, 76А, г. Москва, 123007, Россия; olya.popovaolga2710@yandex.ru

The changes in geomagnetic conditions (GMCs) definitely affect the living organisms [1]. Each cell of the biological system incorporated in the magnetic fields MF of the Sun and Earth is continuously exposed to their fluctuations in a broad frequency range [2].

In recent years, the studies were conducted focused on assessing the relationships between magnetic activity and biological systems of various living organisms. These demonstrate the effects of geomagnetic and solar activity on various physiological rhythms, as well as on the possible synchronization of such rhythms, for example the effects of geomagnetic disturbances on the cardiac and vegetative nervous system (VNS) function [3]. Such effects occur, when human physiological systems are affected by various

changes in geomagnetic dynamics. The geomagnetic field line resonances and the Schumann resonances emerging in the space between the Earth's surface and the ionosphere produce the resonant frequency range overlapping frequencies of the human brain, VNS, and cardiovascular system. Rhythms generated by the brain and the heart are more susceptible to the influence of changes in geomagnetic conditions, than other physiological systems investigated so far [4].

Artificial simulation of geomagnetic storm has shown that geomagnetic activity can evoke a pronounced cardiovascular response [5]. Furthermore, there is evidence suggesting the relationship between the short-term geomagnetic disturbances and the number of deaths from cardiovascular disorders and myocardial infarction [6].

At the same time, the geomagnetic field (GMF) changes can modify the cardiovascular system (CVS) functional state related to the physiological process of aging [7].

In the near future, there will be a prospect of flights into deep space, however, the following question remains: how will reduction of the GMF, which is 10^3–10^5 times smaller in space relative to the Earth's magnetic field, affect human physiological systems? Furthermore, hypomagnetic conditions (HMCs) will become an essential part of the complex of factors influencing the austronauts during the long lasting interplanetary missions, outside the Earth's magnetic field, and the human body adaptation to HMCs will interfere with the regulatory processes in various physiological systems.

Animal studies demonstrate the effects of reduced GMF on the mammalian organism. Disorders of lymph and blood flow were revealed in mice after spending 3 h under HMCs (80–120-, 300-, and 1000-fold GMF attenuation). Cardiomyocyte structural alterations were observed after the 6 h-exposure to HMCs. Lysis of the sarcoplasmic reticulum myofibrils, sarcoplasmic matrix, and mitochondrial matrix was activated. Disruption of the mitochondrial cristae and enlargement of vesicles in the smooth and rough endoplasmic reticulum were also observed. The process of protein biosynthesis in cardiomyocytes was impaired or completely suppressed under HMCs. All the above are indicative of the ultrastructural restructuring similar to apoptosis.

The effects of GMF on the blood vessel tone have been repeatedly confirmed in human studies [8–11]. Changes in blood vessel tone modulate the changes in blood pressure (BP) independently of other geomagnetic climatic factors. It has been noticed that geomagnetic storms resulting from solar flares [9] that force the adaptive mechanisms to get out of balance and cause severe adaptive stress responses affect the CVS regulatory mechanisms. This is manifested in the decreased heart rate variability (HRV) and blood flow, increased platelet aggregation activity, blood coagulation and viscosity even in healthy people [11, 12].

Physiological processes following the changes in magnetic and solar activity occur with a lag. This phenomenon is referred to as the "lag phase" lasting from several hours to 2–3 days after the GMF alteration [10, 12, 13]. It is noted that cardiovascular disorders significantly decrease the subjects' sensitivity to GMF changes, which can results in critical health issues [14].

It has been shown that HMCs affect capillary blood flow, blood pressure, and heart rate (HR), increase the activity of the heart rhythm regulation parasympathetic segment [15].

Continuous CVS hemodynamics (HR, blood pressure (BP), Kerdo Vegetative Index) monitoring was performed in eight healthy adult males at rest. The experiment conducted for 8 h consisted of two acquisition series: under HMCs (1000-fold reduction of the Earth's magnetic field induction) and under exposure to the Earth's natural magnetic field. The decrease in HR (on average by 4 bpm) and BP relative to the control group was revealed. Furthermore, systolic BP decreased on average by 16 mm Hg, while diastolic BP decreased by 16 mm Hg. The Kerdo Vegetative Index, in contrast, increased by 20% during the 8 h stay in hypomagnetic environment [16].

Clinical assessment revealed functional changes in the major body systems of the individuals, who had been working under exposure to the 3–10-fold reduced GMF for a long time, such as vegetovascular dystonia syndrome, abnormal myocardial repolarization, essential hypertension, dystonia of the brain with the regulatory interhemispheric asymmetry, significant increase in biological age by 4.2 years relative to chronological age [17].

In this regard, the study was aimed to assess systemic changes in the CVS resulting from the mechanisms underlying HRV and reflecting the regulatory component of this physiological system, as well as bioelectric processes in the myocardium under conditions of n-fold magnetic field reduction.

METHODS

The experimental study was conducted in 2023 using the Arfa stand (State Scientific Center of the Russian Federation — Institute for Biomedical Problems RAS) for simulation of magnetic fields being a part of the unique scientific installation "Medical and technical complex for the development of innovative technologies of space biomedicine in the interests of ensuring orbital and interplanetary flights, as well as the development of practical healthcare" (Fig. 1).

The design and technical characteristics of the Arfa magnetic field simulation system have been reported earlier [18].

The study sequence diagram represented a randomized blind four-series study. The baseline testing was conducted before the beginning of each series. The first session included the subject's 8 h stay in the installation (morning–afternoon) followed by the 3 h controlled break. Second session: the subject stayed in the installation for 8 h (nighttime – sleep), which was also followed by the 3 h controlled break. Third session: the subject was placed in the installation for 8 h (daytime), which was followed by the tests performed within the 3 h period of aftereffect (Fig. 2).

The experimental exposure included four 37 h series that included baseline tests, stay under HMCs, and the periods of aftereffect. Under HMCs, GMF was reduced 350-, 650-, and 1000-fold; there was also a placebo series. The experimental exposure and placebo were randomized. To ensure the subject's adaptation to the unfamiliar condition of stay in the Arfa installation, hypokinesia, and the experimental program methods, a 4 h training series was previously launched for each subject. The volunteer stayed in the Arfa installation in a sitting position with the limited motion (not leaning, not moving his hands in various directions, not standing up).

The experiment with HMCs involved 6 male volunteers aged 26–37 years (body length 178 ± 7 cm, body weight 76.5 ± 15.5 kg, body mass index 24.77 ± 2.99), in whom electrocardiography (ECG) was continuously performed throughout 32 h. Inclusion criteria: all the volunteers underwent medical examination and were allowed to take part in the experimental studies by the expert medical committee of the State Scientific Center of the Russian Federation — Institute for Biomedical Problems RAS. In addition to the medical expert committee examination, medical examination was performed 2 days before the exposure to antiorthostatic hypokinesia,

based on which the subjects were allowed to take part in the experiments by the responsible physician. The Cosmocard ECG monitor (State Scientific Center of the Russian Federation — Institute for Biomedical Problems RAS; Russia) designed for testing at the International Space Station was used. ECG was recorded using four chest leads. The lead II recording was analyzed. The previously recorded ECG was edited by visual inspection and manual adjustment of certain RR intervals. After that the recording was processed using the Iskim-6 software ("Ramena" Institute for Introduction of New Medical Technologies; Russia).

To assess regulatory processes in the CVS, we determined and calculated the HRV values associated with the VNS parasympathetic and sympathetic modulatory effects on the sinoatrial (SA) node. The state of the mechanisms underlying blood circulation regulation was estimated in accordance with the guidelines developed by the European Society of Cardiology and the North American Society of Pacing and Electrophysiology [19]. The ECG dispersion mapping (DM) based on the analysis of microfluctuations characterizing myocardial electrophysiological processes were used to estimate bioelectric processes in the myocardium [20].

Statistical analysis of the acquired dataset was performed using the STATISTICA 13.0 software package (IBM; USA) using cluster analysis and analysis of variance [21].

RESULTS

The Ward's method was used for classification based on the predominant type of the SA node activity autonomic regulation (Fig. 3). The integrated analysis of all the HRV parameters recorded during the experiment was performed. As a result, two groups were allocated:

1) group 1 — volunteers, who took part in the experiment, showing predominance of parasympathetic modulatory effects ($n = 4$, volunteers 1, 2, 4, and 5);

2) group 2 — volunteers, who took part in the experiment, showing predominance of sympathetic modulatory effects ($n = 2$, volunteers 3, 6).

The cluster and discriminant analysis were used to determine the classification functions including the indicators that were most informative under experimental conditions and reflected the balance of autonomic effects, primarily parasympathetic activity and the extent, to which it predominated over sympathetic modulatory autonomic effects: HR (physiologically reflecting the systemic circulation homeostasis), RMSSD (ms, square root of the mean squared difference of successive ECG intervals, indicator of parasympathetic effects on the heart rhythm), pNN50 (%, the number of pairs of successive intervals that differ by more than 50 ms as a percentage of the total number of ECG intervals, reflects the relative extent, to which parasympathetic modulatory autonomic effects in the CVS predominate over sympathetic ones), SDNN (ms, standard deviation of the entire set of ECG intervals, indicator of the overall effect of autonomic blood circulation regulation), HF
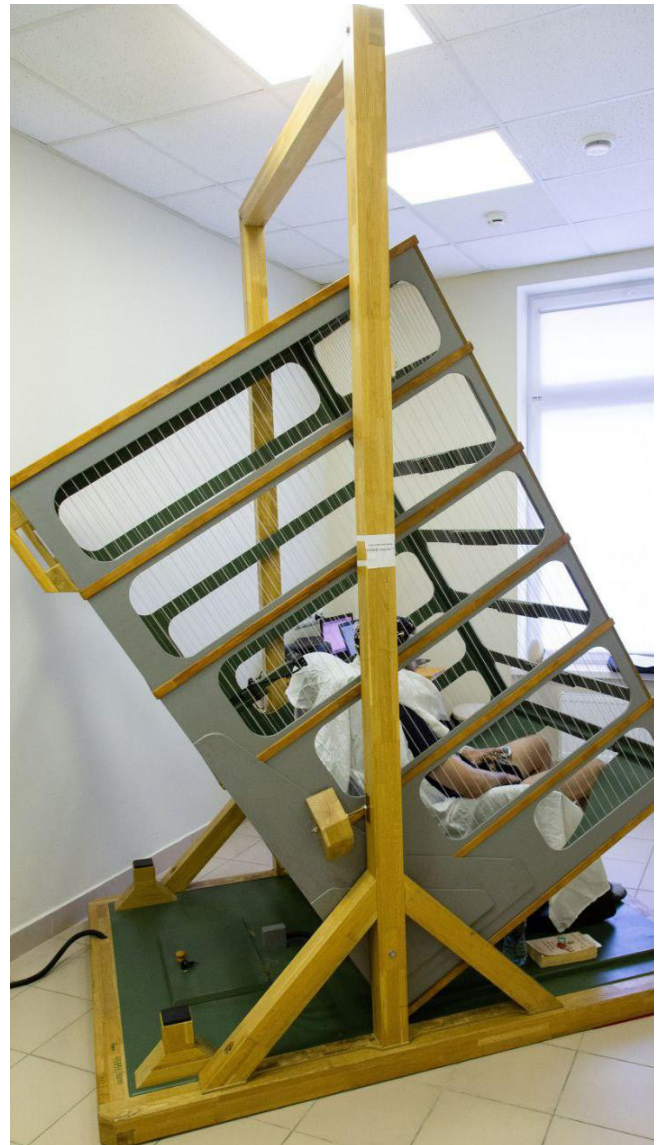
Fig. 1. Arfa magnetic field simulation system and the experimental procedure

(ms2, spectrum power of the HRV high-frequency component from the total oscillation power, characterizes parasympathetic activity and the extent of its predominance over sympathetic activity).

The dynamic changes of these parameters in various phases of the experiment are provided in Fig. 4.

In volunteers showing parasympathetic modulatory effects, the RMSSD and HF parameters significantly decreased compared to the placebo series during the session conducted under exposure to the up to 1000-fold reduced magnetic field; a similar decrease was observed under conditions of up to 650- and 350-fold magnetic field reduction (Fig. 4). In volunteers showing sympathetic modulatory effects, the values
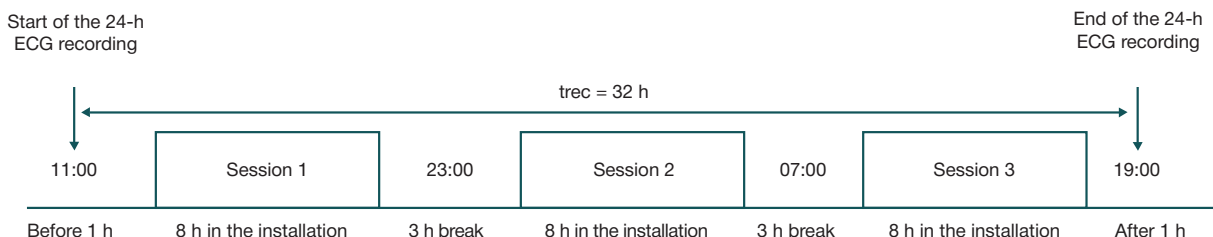
Fig. 2. Sequence diagram of a single experimental session
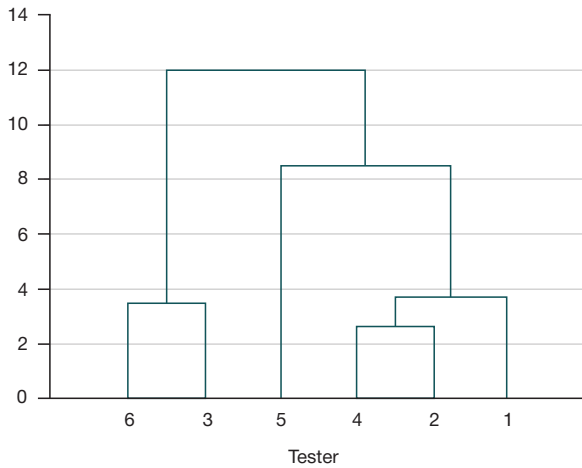
Fig. 3. Dividing volunteers into groups

of these parameters increased after the 24 h stay (session 3) under exposure to the up to 650-fold reduced magnetic field. However, it should be noted that a significant decrease in this indicator relative to placebo was observed during the first 8 h of stay in the installation under exposure to the 1000-fold reduced magnetic field.

The pNN50 and SDNN values decreased in the volunteers showing parasympathetic effects on the heart rhythm compared to placebo during sessions 2 and 3 under conditions of 1000- and 650-fold reduced magnetic field, while in patients showing sympathetic effects a significant decrease in these indicators was observed throughout their stay under exposure to HMCs with the 1000-, 650-, and 350-fold reduced magnetic field.

The dynamics of HR (indicator reflecting the CVS function stability at the systemic level) in the group of volunteers with parasympathetic modulation of the SA node increased throughout the period of experimental exposure without going outside the normal physiological range. In the group with sympathetic modulation, there was a significant increase in this indicator under exposure to the 1000- and 350-fold reduced geomagnetic field during the 8 h (session 1) and 24 h (session 3) stay, respectively (Fig. 5).

The ECG DM analysis showed that the indicator reflecting the right ventricle depolarization (G3) significantly increased throughout the series with the 650-fold reduced magnetic field in the volunteers with parasympathetic effects (Fig. 6). In the group of patients with sympathetic modulation of the heart rhythm, the increase in the indicator under exposure to the 1000- and 350-fold reduced magnetic field was observed.

The G7 (ventricular depolarization symmetry) indicator of the volunteers with parasympathetic effects significantly increased in the series with the 1000- and 659-fold reduced magnetic field; the increase in the indicator was also observed in the series with the 1000-fold reduced magnetic field in the individuals with sympathetic modulation of heart rhythm, however, the indicator also increased under exposure to the 350-fold reduced magnetic field.

As for the emergence of arrhythmias during the experiment, their number increased, which was indicated by the NArr (quantitative parameter characterizing the overall number of arteries) values (%). The indicator values increased in the series with the 1000- and 350-fold reduced magnetic field in the volunteers with parasympathetic regulatory effects. In the group of patients with sympathetic regulatory effects, the NArr
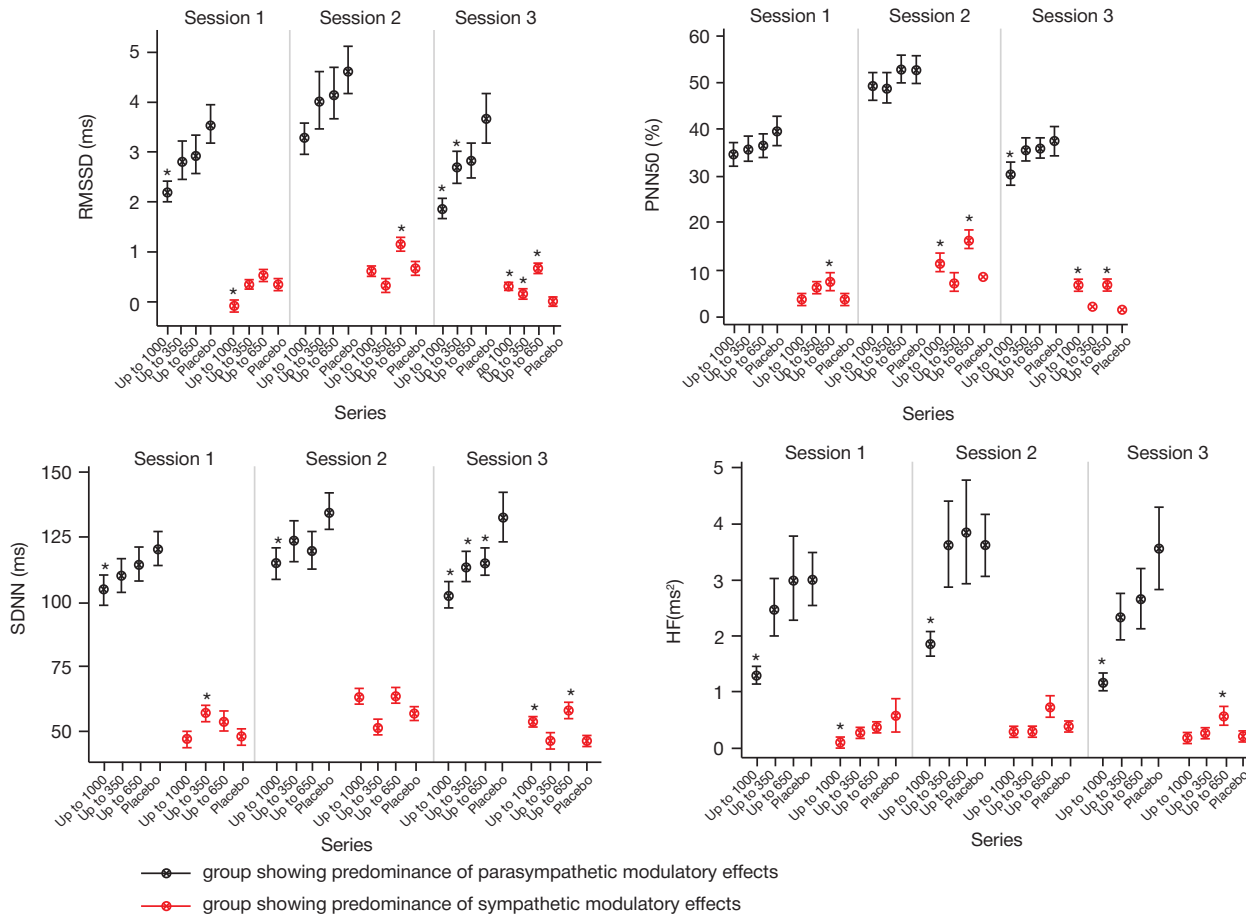
Fig. 4. The most informative parameters characterizing the predominant type of autonomic regulation and their dynamics during the experiment. * — significant difference compared to placebo
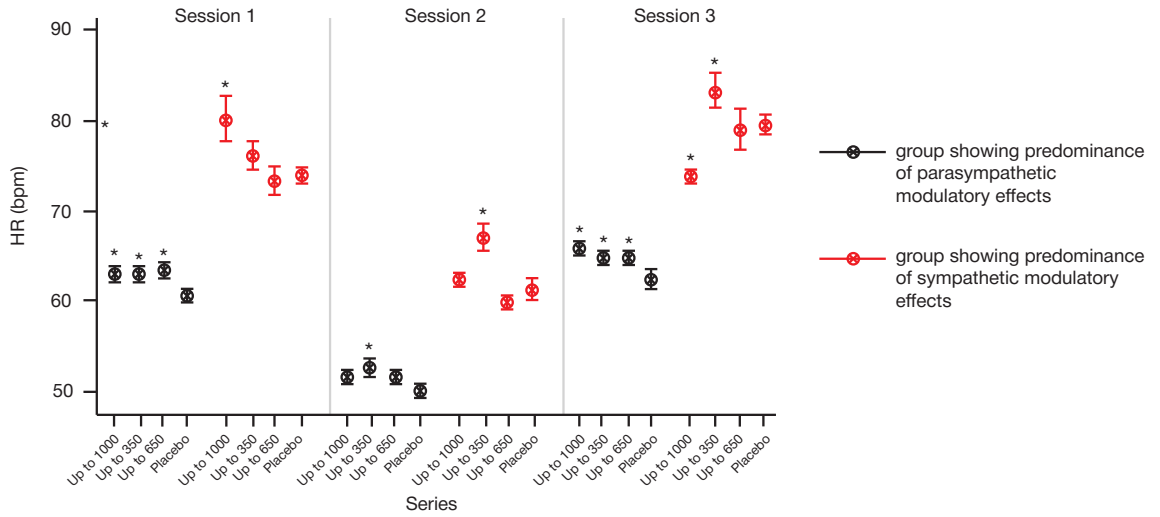
Fig. 5. HR dynamics. * — significant difference compared to placebo

values increased only by the experimental session, in which the magnetic field was reduced 1000-fold (Fig. 7).

DISCUSSION

HRV characterizes the changes of the time windows between the successive heart contractions and serves as an important indicator reflecting the dynamics of the VNS activity and its effects on the circulatory system [22]. The HRV patterns observed show the functional state of the co-dependent regulatory systems that operate at different time scales in order to adapt to the environmental and psychological problems. The lower degrees of the age-adjusted HRV that suggest chronic stress, disorder or functional insufficiency of the regulatory
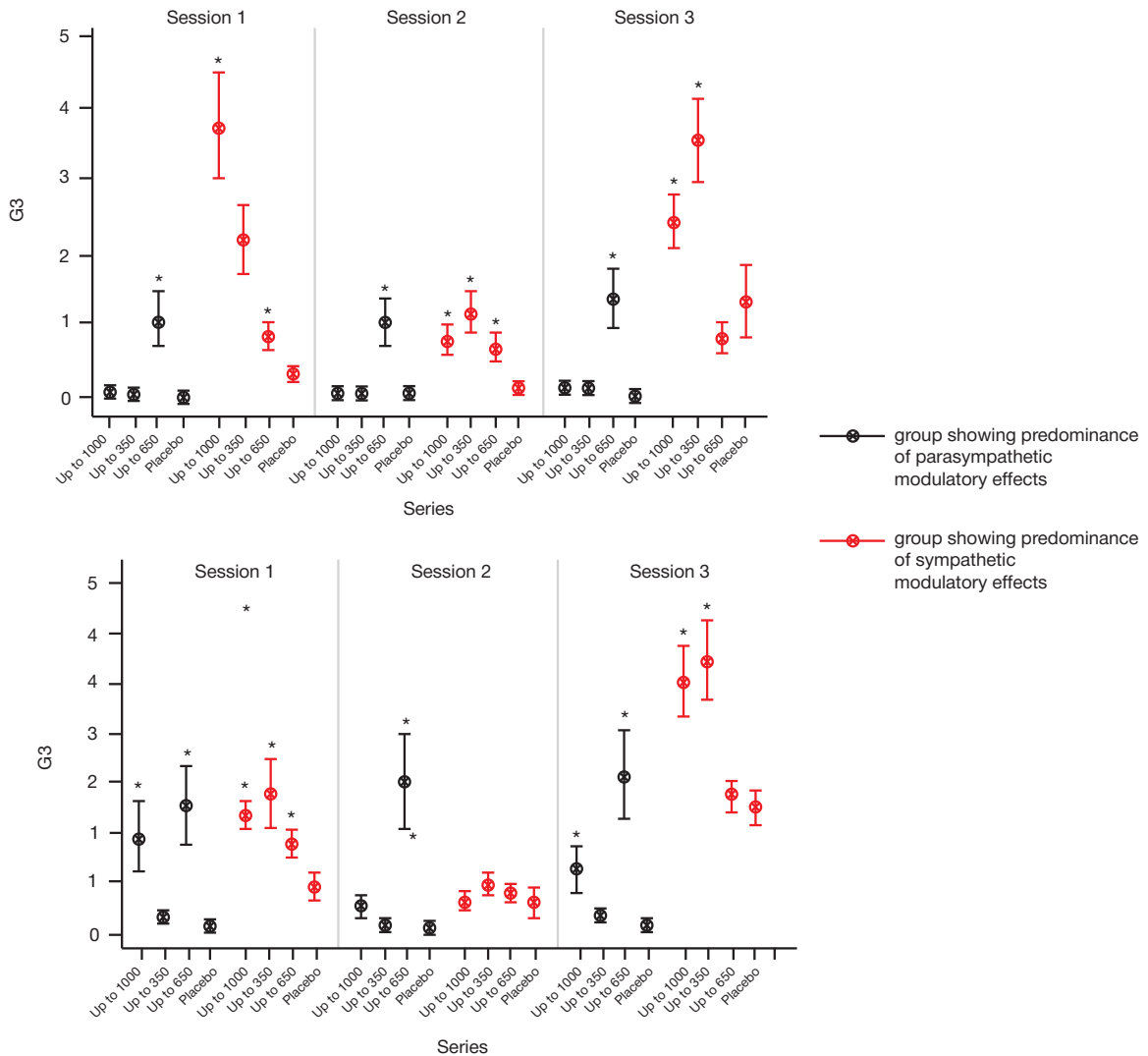
Fig. 6. ECG DM dynamics. * — significant difference compared to placebo
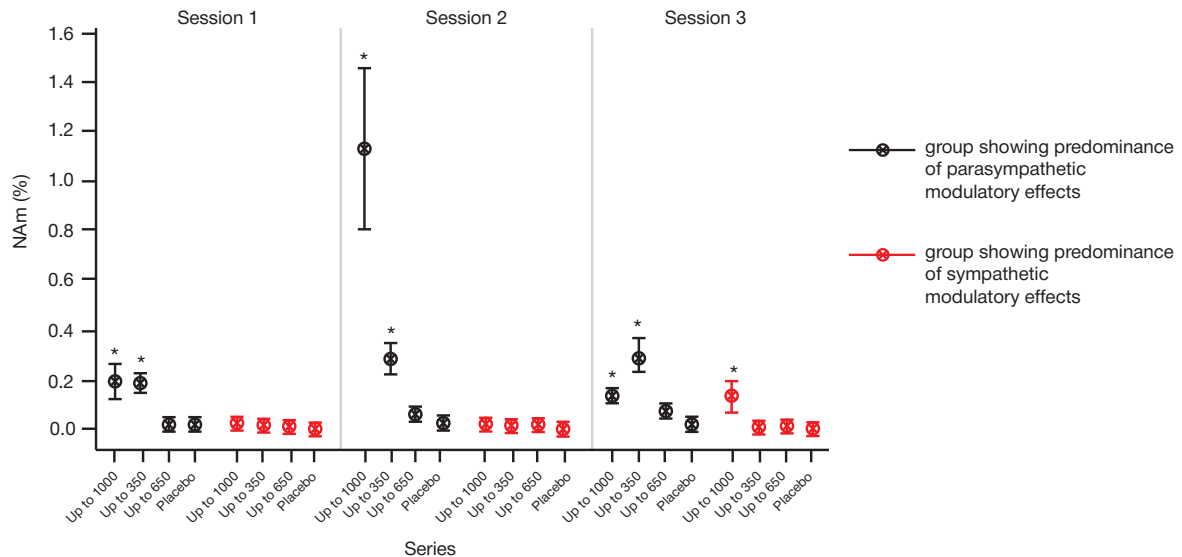
Fig. 7. NArr dynamics. * — significant difference compared to placebo

systems in the nervous system, are associated with all-cause mortality, while higher degrees of variability suggest stability and capacity for self-regulation and adaptation to the changing demands [23].

Since the adaptation processes in volunteers showing predominance of parasympathetic effects are maintained by means of the neural regulatory circuit, the functional reserve is enough for critical values (exposure to the 1000-fold reduced magnetic field). In volunteers showing predominance of sympathetic modulatory effects, the adaptive responses are maintained by the metabolic regulatory circuit. In this group, the response to the reduced magnetic field exposure is rather pronounced at the reduction threshold of 350 times.

The significantly changing ECG DM parameters G3 and G7 constitute parts of the aggregate indicator G3+G4+G7, where G4 represents an indicator reflecting the left ventricular depolarization, which can be indicative of ischemic disorders: probable disturbances of blood flow and myocardial perfusion [20].

The indicator characterizing the number of arrhythmias increased in the group showing predominance of parasympathetic regulation during the nighttime session under the exposure to the 1000-fold decreased magnetic field, however, it was within normal range (1–2%). When reviewing individual recordings, we found ventricular extrasystoles (VEs) in one volunteer; no VEs were reported under placebo conditions.

VE is the most common form of ventricular arrhythmia [24]. It has been reported that VE in patients having no structural heart disease can represent the so-called "arrhythmic" form of the essential hypertension onset, various clinical variants of the onset of coronary heart disease, myocarditis, various forms of cardiomyopathy, stroke and other cerebrovascular disorders. VE can be also an independent predictor of the development of life-threatening ventricular arrhythmias, atrial fibrillation, and sudden death [25].

It is well known that the detection rate of VE increases in organic heart diseases associated with hypoxemia, myocardial damage, and the increase in the VNS sympathoadrenal activity. It was noted that in healthy individuals the number of VEs was higher in the morning, than during the night. Nocturnal VEs were described. Furthermore, it was shown that the emergence of VEs during the night could be associated with the mainly nocturnal type of circadian distribution in patients with sleep apnea syndrome [26].

The GMF strength fluctuations resulting to the decrease in HRV and increase in HR can provoke cardiac arrhythmia [27]. This trend is especially strong in the group of hypertensive patients [28]. It has been found recently that the GMF increased activity in the low-frequency ranges is associated with the higher incidence of acute atrial fibrillation and flutter [29]. Apparently, the higher GMF intensity in the low-frequency ranges is associated with the emergence of arrhythmia, while that in the high-frequency range is associated with the cardiac ischemic events [30].

CONCLUSIONS

Thus, during the experiment involving magnetic field reduction we acquired unique data on the mechanisms underlying autonomic regulation of blood circulation and bioelectric processes in the myocardium. However, the study had an important limitation: relatively low number of participants. Nevertheless, one of the pilot experiments with the GMF effects on the physiological processes in the human body at the systemic level we have conducted is crucial for the development of the concept of further experimental exposures related to magnetic field reduction benefiting space physiology and medicine. The complexity of developing such concept is to the great extent determined by the bioethical issues related to investigation of the effects of poorly understood factors (such as HMCs) on the human body.

References

1. Zhang Z, Xue Y, Yang J, Shang P, Yuan X. Biological effects of hypomagnetic field: Ground-based data for space exploration. Bioelectromagnetics. 2021; 42 (6): 516–31. DOI: 10.1002/bem.22360.
2. Cornélissen G, Halberg F, Schwartzkopff O, Delmore P, Katinas G, Hunter D, et al. Chronomes, time structures, for chronobioengineering for «a full life». Biomed. Instrum. Technol. 1999; 33: 152–87.
3. Kuzmenko NV, Shchegolev BF, Pliss MG, Tsyrlin VA. The Influence of Weak Geomagnetic Disturbances on the Rat Cardiovascular System under Natural and Shielded Geomagnetic Field

Conditions. Biophysics. 2019; 64: 109–16.

4. Otsuka K, Cornelissen G, Norboo T, Takasugi E, Halberg F. Chronomics and «Glocal» (combined Global and Local) assessment of human life. Prog. Theor. Phys. Suppl. 2008; 173: 134–52.

5. Pishchalnikov RY, Gurfinkel YI, Sarimov RM, Vasin AL, Sasonko ML, Matveeva TA, et al. Cardiovascular response as a marker of environmental stress caused by variations in geomagnetic field and local weather. Biomed. Signal Process. Control. 2019; 51: 401–10.

6. Vieira CLZ, Alvares D, Blomberg A, Schwartz J, Coull B, Huang S, et al. Geomagnetic disturbances driven by solar activity enhance total and cardiovascular mortality risk in 263 US cities. Environ. Health. 2019; 18: 83.

7. Otsuka K, Cornelissen G, Kubo Y, Shibata K, Mizuno K, Ohshima H, et al. Anti-aging effects of long-term space missions, estimated by heart rate variability. Sci. Rep. 2019; 9: 1–12.

8. Ozheredov VA, Chibisov SM, Blagonravov ML, Khodorovich NA, Demurov EA, Goryachev VA, et al. Influence of geomagnetic activity and earth weather changes on heart rate and blood pressure in young and healthy population. Int J Biometeorol. 2017; 61: 921–9.

9. Gurfinkel YI, Breus TK, Zenchenko TA, Ozheredov VA. Investigation of the effect of ambient temperature and geomagnetic activity on the vascular parameters of healthy volunteers. Open J Biophys. 2012; 2: 46–55.

10. Zenchenko TA, Skavulyak AN, Khorseva NI, Breus TK. Characteristics of individual reactions of the cardiovascular system of healthy people to changes in meterological factors in a wide temperature range. Izvestiya, Atmos Ocean Phys. 2013; 49: 783–98.

11. Breus TK, Baevskii RM, Chernikova AG. Effects of geomagnetic disturbances on humans functional state in space flight. J Biomed Sci Eng. 2012; 5: 341–55.

12. Vencloviene J, Babarskiene RM, Kiznys D. A possible association between space weather conditions and the risk of acute coronary syndrome in patients with diabetes and the metabolic syndrome. Int J Biometeorol. 2017; 61: 159.

13. Katsavrias C, Preka-Papadema P, Moussas X, Apostolou T, Theodoropoulou A, Papadima T, et al. Helio-geomagnetic influence in cardiological cases. Adv Space Res. 2013; 51: 96–106.

14. Alabdulgader A, McCraty R, Aktinson M, Vainoras I, Berškienė K, Mauricienė V, et al. Human heart rhythm sensitivity to earth local magnetic field fluctuations. JVE International LTD. Journal of Vibroengineering. 2015; 17 (6): 3271–9.

15. Gurfinkel YuI, Vasin AL, Matveeva TA, Sasonko ML. Evaluation of the hypomagnetic environment effects on capillary blood circulation, blood pressure and heart rate. Aviakosmicheskaya i Ekologicheskaya Meditsina. 2014; 48 (2): 24–30. Russian.

16. Demin AV, Suvorov AV, Orlov OI. Osobennosti gemodinamiki u zdorovyh muzhchin v gipomagnitnyh uslovijah. Aviakosmicheskaja i jekologicheskaja medicina. 2021; 55 (2): 63–8. Russian.

17. Pokhodzey L. V. Gipomagnitnye usloviya kak neblagopriyatnyy faktor proizvodstvennoy sredy [dissertation]. M.: 2004. Russian.

18. Kukanov VYu, Vasin AL, Demin AV, Schastlivtseva DV, Bubeev YuA, Suvorov AV, et al. Effect of Simulated Hypomagnetic Conditions on Some Physiological Paremeters under 8-Hour Exposure. Experiment Arfa-19. Hum Physiol. 2023; 49: 138–46.

19. Not author's list. Heart rate variability. Standarts of measurement, physiological interpretation, and clinical use. Task Forse of The European Society of Cardiology and The North American Society of Pacing and Electrophysiology (Membership of the Task Force listed in the Appendix). Eur. Heart J. 1996; 93 (5): 1043–65.

20. Ivanov GG, Sula AS. Dispersionnoe kartirovanie: teoreticheskie osnovy i klinicheskaya praktika. M.: Tekhnosfera, 2009; p. 192. Russian.

21. Nosovsky AM, Popova OV, Smirnov YuI. State-of-the art technologies of medical data statistical analysis and methods of graphic presentation. Aviakosmicheskaya i Ekologicheskaya Meditsina. 2023; 57 (5): 149–54. Russian.

22. Shaffer F, McCraty R, Zerr CL. A healthy heart is not a metronome: an integrative review of the heart's anatomy and heart rate variability. Front. Psychol. 2014; 5: 1040.

23. McCraty R, Shaffer F. Heart rate variability: New perspectives on physiological mechanisms, assessment of self-regulatory capacity, and health risk. Glob. Adv. Health Med. 2015; 4: 46–61.

24. Zipes DP, Libby P, Bonow RO, Mann DL, Tomaselli GF. Braunwald's heart disease: a textbook of cardiovascular medicine. 11th ed. Elsevier Science, 2018; p. 2128.

25. Olesin AI, Konstantinova IV, Zueva YuS, Sokolova MD. Ventricular extrasystoles in patients without cardiac structural changes: mechanisms of development, arrhythmogenic cardiomyopathy predictors, pharmacological and non-pharmacological treatment strategies. International Heart and Vascular Disease Journal. 2020; 8 (26): 28–38. Russian.

26. Lyshova OV, Ivannikova LV, Morgachev VE. Ventricular premature beats during sleep in male patients with syndrome z. Journal of Arrhythmology. 2008; 53: 33–40. Russian.

27. Žiubrytė G, Jaruševičius G, Jurjonaitė J, Landauskas M, McCraty R, Vainoras A. Correlations between acute atrial fibrillation and local earth magnetic field strength. Journal of Complexity of Health Sciences. 2018; 2 (1): 31–4.

28. Liboff AR. A role for the geomagnetic field in cell regulation. Electromagn. Biol. Med. 2010; 29 (3): 105–12.

29. Jaruševičius G, Rugelis T, McCraty R, Landauskas M, Berškienė K, Vainoras A. Correlation between changes in local Earth's magnetic field and cases of acute myocardial infarction. Int J Environ Res Public Health. 2018; 15 (3): 399.

30. Žiubrytė G, Jaruševičius G, Landauskas M, McCraty R, Vainoras A. The local earth magnetic field changes impact on weekly hospitalization due to unstable angina pectoris. Journal of Complexity of Health Sciences. 2018; 1 (1): 16–25.

Литература

1. Zhang Z, Xue Y, Yang J, Shang P, Yuan X. Biological effects of hypomagnetic field: Ground-based data for space exploration. Bioelectromagnetics. 2021; 42 (6): 516–31. DOI: 10.1002/bem.22360.

2. Cornélissen G, Halberg F, Schwartzkopff O, Delmore P, Katinas G, Hunter D, et al. Chronomes, time structures, for chronobioengineering for «a full life». Biomed. Instrum. Technol. 1999; 33: 152–87.

3. Kuzmenko NV, Shchegolev BF, Pliss MG, Tsyrlin VA. The Influence of Weak Geomagnetic Disturbances on the Rat Cardiovascular System under Natural and Shielded Geomagnetic Field Conditions. Biophysics. 2019; 64: 109–16.

4. Otsuka K, Cornelissen G, Norboo T, Takasugi E, Halberg F. Chronomics and «Glocal» (combined Global and Local) assessment of human life. Prog. Theor. Phys. Suppl. 2008; 173: 134–52.

5. Pishchalnikov RY, Gurfinkel YI, Sarimov RM, Vasin AL, Sasonko ML, Matveeva TA, et al. Cardiovascular response as a marker of environmental stress caused by variations in geomagnetic field and local weather. Biomed. Signal Process. Control. 2019; 51: 401–10.

6. Vieira CLZ, Alvares D, Blomberg A, Schwartz J, Coull B, Huang S, et al. Geomagnetic disturbances driven by solar activity enhance total and cardiovascular mortality risk in 263 US cities. Environ. Health. 2019; 18: 83.

7. Otsuka K, Cornelissen G, Kubo Y, Shibata K, Mizuno K, Ohshima H, et al. Anti-aging effects of long-term space missions, estimated by heart rate variability. Sci. Rep. 2019; 9: 1–12.

8. Ozheredov VA, Chibisov SM, Blagonravov ML, Khodorovich NA, Demurov EA, Goryachev VA, et al. Influence of geomagnetic activity and earth weather changes on heart rate and blood pressure in young and healthy population. Int J Biometeorol. 2017; 61: 921–9.

9. Gurfinkel YI, Breus TK, Zenchenko TA, Ozheredov VA. Investigation of the effect of ambient temperature and geomagnetic activity on

the vascular parameters of healthy volunteers. Open J Biophys. 2012; 2: 46–55.

10. Zenchenko TA, Skavulyak AN, Khorseva NI, Breus TK. Characteristics of individual reactions of the cardiovascular system of healthy people to changes in meterological factors in a wide temperature range. Izvestiya, Atmos Ocean Phys. 2013; 49: 783–98.

11. Breus TK, Baevskii RM, Chernikova AG. Effects of geomagnetic disturbances on humans functional state in space flight. J Biomed Sci Eng. 2012; 5: 341–55.

12. Vencloviene J, Babarskiene RM, Kiznys D. A possible association between space weather conditions and the risk of acute coronary syndrome in patients with diabetes and the metabolic syndrome. Int J Biometeorol. 2017; 61: 159.

13. Katsavrias C, Preka-Papadema P, Moussas X, Apostolou T, Theodoropoulou A, Papadima T, et al. Helio-geomagnetic influence in cardiological cases. Adv Space Res. 2013; 51: 96–106.

14. Alabdulgader A, McCraty R, Aktinson M, Vainoras I, Berškienė K, Mauricienė V, et al. Human heart rhythm sensitivity to earth local magnetic field fluctuations. JVE International LTD. Journal of Vibroengineering. 2015; 17 (6): 3271–9.

15. Гурфинкель Ю. И., Васин А. Л., Матвеева Т. А., Сасонко М. Л. Оценка влияния гипомагнитных условий на капиллярный кровоток, артериальное давление и частоту сердечных сокращений. Авиакосмическая и экологическая медицина. 2014; 48 (2): 24–30.

16. Демин А. В., Суворов А. В., Орлов О. И. Особенности гемодинамики у здоровых мужчин в гипомагнитных условиях. Авиакосмическая и экологическая медицина. 2021; 55 (2): 63–8.

17. Походзей Л. В. Гипомагнитные условия как неблагоприятный фактор производственной среды [диссертация]. М.: 2004.

18. Kukanov VYu, Vasin AL, Demin AV, Schastlivtseva DV, Bubeev YuA, Suvorov AV, et al. Effect of Simulated Hypomagnetic Conditions on Some Physiological Paremeters under 8-Hour Exposure. Experiment Arfa-19. Hum Physiol. 2023; 49: 138–46.

19. Not author's list. Heart rate variability. Standarts of measurement, physiological interpretation, and clinical use. Task Forse of The European Society of Cardiology and The North American Society of Pacing and Electrophysiology (Membership of the Task Force listed in the Appendix). Eur. Heart J. 1996; 93 (5):

20. Иванов Г. Г., Сула А. С. Дисперсионное картирование: теоретические основы и клиническая практика. М.: Техносфера, 2009; 192 с.

21. Носовский А. М., Попова О. В., Смирнов Ю. И. Современные технологии статистического анализа медицинских данных и способы их графического представления. Авиакосмическая и экологическая медицина. 2023; 57 (5): 149–54.

22. Shaffer F, McCraty R, Zerr CL. A healthy heart is not a metronome: an integrative review of the heart's anatomy and heart rate variability. Front. Psychol. 2014; 5: 1040.

23. McCraty R, Shaffer F. Heart rate variability: New perspectives on physiological mechanisms, assessment of self-regulatory capacity, and health risk. Glob. Adv. Health Med. 2015; 4: 46–61.

24. Zipes DP, Libby P, Bonow RO, Mann DL, Tomaselli GF. Braunwald's heart disease: a textbook of cardiovascular medicine. 11th ed. Elsevier Science, 2018; p. 2128.

25. Олесин А. И., Константинова И. В., Зуева Ю. С., Соколова М. Д. Желудочковая экстрасистолия у пациентов без структурных изменений сердца: механизмы формирования, предикторы развития аритмогенной кардиомиопатии и принципы фармакологической и немедикаментозной терапии. Международный журнал сердца и сосудистых заболеваний. 2020; 8 (26): 28–38.

26. Лышова О. В., Иванникова Л. В., Моргачев В. Е. Желудочковая экстрасистолия на протяжении сна у мужчин с синдромом z. Вестник аритмологии. 2008; 53: 33–40.

27. Žiubrytė G, Jaruševičius G, Jurjonaitė J, Landauskas M, McCraty R, Vainoras A. Correlations between acute atrial fibrillation and local earth magnetic field strength. Journal of Complexity of Health Sciences. 2018; 2 (1): 31–4.

28. Liboff AR. A role for the geomagnetic field in cell regulation. Electromagn. Biol. Med. 2010; 29 (3): 105–12.

29. Jaruševičius G, Rugelis T, McCraty R, Landauskas M, Berškienė K, Vainoras A. Correlation between changes in local Earth's magnetic field and cases of acute myocardial infarction. Int J Environ Res Public Health. 2018; 15 (3): 399.

30. Žiubrytė G, Jaruševičius G, Landauskas M, McCraty R, Vainoras A. The local earth magnetic field changes impact on weekly hospitalization due to unstable angina pectoris. Journal of Complexity of Health Sciences. 2018; 1 (1): 16–25.

THE EFFECT OF HIGH CONCENTRATIONS OF FENTANYL ON AN ISOLATED HEART OF RAT

Nechaykina OV ✉, Laptev DS, Bobkov DV, Petunov SG, Radilov AS

Research Institute of Hygiene, Occupational Pathology and Human Ecology of the Federal Medical Biological Agency, Leningrad region, Russia

Synthetic short-acting opioids are commonly used in anesthesiology as painkillers because their effect is more pronounced compared to that of natural substances. However, they have a number of side effects that, when fentanyl is used in doses larger than therapeutic, can lead to a lethal outcome. This study aimed to assess the cardiotropic effects of high doses of fentanyl using a rat heart isolated in a Langendorff perfusion system. Parameters of the heart's contractile activity were recorded with the help of PowerLab Data acquisition system 8/30 (ADInstruments, USA) and processed in the LabChartProUpgrade 7.0 program. At the concentration of 3.7×10^{-6} M, which corresponds to the opioid content in blood after administration of a 5 ED_{50} dose, fentanyl caused the QT interval duration to grow by 22%, as registered on an ECG, and a 256% spike of T wave (compared to control; $p < 0.05$). At the concentration of 7.4×10^{-6} M (10 ED_{50}), the drug decreased heart rate by 20.4% ($p < 0.05$) and triggered a coronary constrictor effect that raised the perfusion pressure by 18.6% ($p < 0.05$). Further increase of fentanyl concentration to 1.5×10^{-5} M (20 ED_{50}) was accompanied by an 83.5% growth of the end diastolic pressure ($p < 0.05$). Administration of nalmefene, non-selective opioid receptor blocker, did not cancel the cardiovasotropic action of fentanyl. Thus, fentanyl has a dose-dependent cardiotoxic effect. Despite the drop in the registered values of isolated heart's parameters, the results of this experiment confirm that cardiac activity persists under the influence of high doses of the opioid.

Keywords: opioid analgesics, isolated heart, fentanyl

ДЕЙСТВИЕ ВЫСОКИХ КОНЦЕНТРАЦИЙ ФЕНТАНИЛА НА ИЗОЛИРОВАННОЕ СЕРДЦЕ КРЫСЫ

О. В. Нечайкина ✉, Д. С. Лаптев, Д. В. Бобков, С. Г. Петунов, А. С. Радилов

Научно-исследовательский институт гигиены, профпатологии и экологии человека Федерального медико-биологического агентства, Ленинградская область, Россия

Синтетические опиоиды короткого действия получили широкое распространение в анестезиологии в качестве обезболивающих средств за счет более выраженного эффекта в сравнении с природными веществами. Однако они обладают рядом побочных эффектов, которые при использовании фентанила в дозах, превышающих терапевтические, могут приводить к смертельным исходам. Целью работы было оценить кардиотропные эффекты высоких доз фентанила на модели изолированного по Лангендорфу сердца крысы. Параметры сократительной активности изолированного сердца крысы регистрировали с помощью системы PowerLab Data acquisition system 8/30 (ADInstruments, USA) с последующей обработкой в программе LabChartProUpgrade 7.0. При действии фентанила в концентрации $3,7 \times 10^{-6}$ М, что соответствует содержанию опиоида в крови при его внутривенном введении в дозе 5 ED_{50}, зарегистрировано увеличение продолжительности QT-интервала на ЭКГ на 22% и рост амплитуды зубца T на 256% по сравнению с контролем ($p < 0,05$). При действии фентанила в концентрации $7,4 \times 10^{-6}$ М (10 ED_{50}) зарегистрированы снижение ЧСС на 20,4% ($p < 0,05$) и коронароконстрикторное действие, выражающееся в увеличении давления перфузии на 18,6% ($p < 0,05$) по сравнению с контролем. Увеличение концентрации фентанила до $1,5 \times 10^{-5}$ М (20 ED_{50}) сопровождалось ростом конечного диастолического давления на 83,5% ($p < 0,05$). Использование неселективного блокатора опиоидных рецепторов налмефена не приводило к отмене кардиовазотропных эффектов фентанила. Таким образом, фентанил обладает дозозависимым кардиотоксическим влиянием. Несмотря на снижение регистрируемых показателей изолированного сердца, полученные результаты свидетельствуют о сохранении сердечной деятельности миокарда при влиянии высоких доз опиоида.

Ключевые слова: опиоидные анальгетики, изолированное сердце, фентанил

Synthetic opioids are widely used in medicine as powerful painkillers (opioid analgesics) or as an adjunct to non-narcotic anesthetics. At the same time, abuse of narcotic substances and the associated growth of the number of acute poisoning cases remain a serious social problem. According to the State Antidrug Committee, in 2022, there has been registered 22,000 cases of acute poisoning with narcotic substances and psychodisleptics in Russia, 10,000 of which had a lethal

outcome. Fentanyl, an agonist mainly of the μ-opioid receptors found in the central nervous system, heart, lungs, blood vessels and intestines, is one of the commonly abused drugs [1]. The main side effects of opioid analgesics are well known: respiratory depression and an increased risk of lethal apnea, hemodynamic changes, histamine release, hypersensitivity reactions, and serotonin syndrome [2]. Among the most significant causes of death associated with fentanyl overdose are respiratory depression, pulmonary edema, respiratory arrest, bradycardia, and cardiac arrest.

There is only a limited number of published papers that touch upon the subject of effect of deliberately high doses of fentanyl on the myocardium in the context of an overdose. This study aimed to assess the cardiotropic effects of toxic doses of fentanyl using a rat's heart isolated in a Langendorff perfusion system.

METHODS

An isolated heart model is the most informative and adequate solution for the task of gauging direct effects of opioids on the myocardium: it removes the influence of systemic regulatory factors, provides the most objective information about how xenobiotics affect the functional activity parameters, allows determining the degree of dysfunction caused by xenobiotics at the level of organs, and enables assessment of the possibility of pharmacological adjustment of the identified changes.

For the experiment, we made isolated heart models using the myocardium of male white mongrel rats weighing 300–350 g (branch of the Kurchatov Institute – PNPI – Rappolovo Laboratory Animal Nursery; Leningrad region).

The rooms where the animals were kept had the following parameters: temperature 20 ± 1 °C, relative humidity $60 \pm 5\%$, 12 hours of daylight and 12 hours of night. The animals had unrestricted access to water and food.

The choice of the active substance concentrations for the study was based on the data found in scientific literature, according to which injection of a 5 ED_{50} dose of fentanyl into the rat's tail vein induced a superficial coma with a 100% survival rate [3, 4]. Hot plate test allowed establishing the ED_{50} of fentanyl for white rats: 0.01 mg/kg [5].

For the purpose of evaluating the resistance of myocardium to the effects of high doses of fentanyl, we selected three concentrations: 3.7×10^{-6} M, 7.4×10^{-6} M, and 1.5×10^{-5} M, which, in terms of fentanyl content in blood after an IV injection, are equivalent to doses 5 ED_{50}, 10 ED_{50}, 20 ED_{50}, respectively.

Experimental animals were euthanized by stunning and bilateral transabdominal thoracotomy, the latter performed after securing the bodies in the preparation pans. This method of euthanasia was chosen because of the need to have an intact contracting heart, which disallows narcotization of experimental animals or inducing systemic hypoxia. The heart, once exposed, was taken by the base with thumb and forefinger of the left hand, carefully pulled ventrally and downward, then the great vessels were cut with scissors. Immediately after the heart was removed from the chest cavity, it was placed in Krebs-Henseleit saline solution of the following composition (in mM): NaCl — 118.99; KCl — 4.69; $NaHCO_3$ — 25; KH_2PO_4 — 1.18; $MgSO_4$ x 7 H_2O — 1.17; $CaCl_2$ x 2 H_2O — 2.5; EDTA — 0.03; $C_6H_{12}O_6$ — 5.5. The aorta was fixed to the cannula of the Langendorff System perfusion rig (Panlab; Spain) with a crocodile clamp and then with sutures. The heart was perfused through the cannula, with the perfusate retrogradely delivered to the left ventricle. The perfusate was Krebs-Henseleit solution warmed to 37 °C. To bring its pH to the physiological level (7.39–7.41)

and to ensure adequate oxygenation of the heart, the solution was continuously aerated with carbogen (95% oxygen and 5% carbon dioxide). The feeding rate of the perfusate (delivered by a peristaltic pump) was 10 ml per minute per 1 g of heart wet weight. The adequacy of perfusion was judged by the pressure in the "pump – aortic cannula" circuit (at least 50 mmHg). Contractile activity of the heart stabilized within 30 minutes from its locking in the system; after that, the contractility baseline value was registered [6]. We used a catheter with a polyethylene balloon to measure pressure in the left ventricle. The parameters of cardiac contractile activity were recorded using the PowerLab Data acquisition system 8/30 (ADInstruments; USA) and subsequently processed in the LabChartProUpgrade 7.0 software (ADInstruments; USA). The recorded parameters were perfusion pressure (PerP; reflects coronary flow); pressure in the left ventricle (systolic, diastolic); heart rate (HR; beats/minute); end diastolic pressure (EDP, mmHg; reflects the left ventricle's relaxation capacity). Simultaneously with registration of the parameters of myocardial contractile activity, we recorded ECG.

At the end of stabilization, we added fentanyl to the perfusate in one of the studied concentrations, seeking to identify the dose — effect relationship. For each concentration, the exposure time was 10 minutes. Nalmefene, a non-selective opioid receptor antagonist, was used at a concentration of 1×10^{-6} M to evaluate fentanyl's receptor activation capacity.

After the experiment, we calculated pulse pressure (PP, mmHg), the integral cardiac contractility index per minute (Int_{1min}, c.u.), and the first time derivative of pressure (+dP/dt and –dP/dt, mmHg/s) that describes the rate of left ventricle's contraction and relaxation.

For the analysis part, we compared the dynamics of parameters of the cardiac contractile and electrical activity in treatment and control groups. GraphPad Prism 5.04 software (USA) was used for statistical processing. To establish the significance of differences in the values intragroup, we applied the Wilcoxon T-test for related samples, and for intergroup differences we used the Mann–Whitney U-test. The differences were considered significant at $p \leq 0.05$.

RESULTS

The study has shown that the action of fentanyl on an isolated heart depends on the concentration, and the drug can have opposite effects. Minimal and medium concentrations yielded potentiating effect: left ventricular contraction rate increased by 9.7 and 8.4%, respectively (Table 1).

Medium (7.4×10^{-6} M) and high (1.5×10^{-5} M) concentrations trigger vasoconstriction, wuth perfusion pressure growing by 18.6 and 46.5%, respectively. A negative lusitropic effect, when the heart's diastolic relaxation capability deteriorates, was registered only after administration of the maximum studied concentration, with the said effect confirmed by the growth of end diastolic pressure by 83.5% compared to the values recorded in the control group.

Medium and high concentrations of fentanyl provoked a significant drop in the heart rate: by 20.4 and 28.3%, respectively, compared to the control. The negative chronotropic effect of the drug pushed the integral myocardial contractility index down while the pulse pressure did not change (Table 1).

The vasotropic effects of fentanyl at the concentration of 1.5×10^{-5} M were almost unaffected by nalmefene injected at the concentration of 1×10^{-6} M (Table 1).

The effect of fentanyl at concentrations of 3.7×10^{-6} M, 7.4×10^{-6} M, 1.5×10^{-5} M on the isolated heart's electrical activity manifested in the growth of the QT interval (compared

Table 1. Parameters of contractile activity of the isolated heart of white rats under the action of fentanyl. The data are percentage relative to the background (M ± SE)

Perfusate	n	PerP	Int$_{1min}$	Heart rate	PP	+dP/dt	–dP/dt	EDP
Control (saline solution)	20	99.3 ± 1.8	99.4 ± 2.2	98.7 ± 4.1	103 ± 4.1	100.9 ± 1.5	101.5 ± 2.9	100.1 ± 3.2
Fentanyl 3.7 × 10^{-6} M	6	110.4 ± 7.8	95.1 ± 5.2	100.3 ± 6.0	102.4 ± 7.1	110.6 ± 4.4*	110.2 ± 2.8	78.9 ± 12.3
Fentanyl 7.4 × 10^{-6} M	6	118.6 ± 7.1*	93.3 ± 3.4	78.3 ± 5.5*	105.2 ± 2.4	109.3 ± 1.5*	104.8 ± 2.3	90.3 ± 8.3
Фентанил 1.5 × 10^{-5} M	6	146.5 ± 6.1*	93.9 ± 2.2	70.4 ± 7.1*	94.5 ± 2.6	97.0 ± 0.7	94.0 ± 4.5	183.6 ± 18.8*
Fentanyl 1.5 × 10^{-5} M + nalmefene 1 × 10^{-6} M	6	125.8 ± 13.6*	81.6 ± 4.7*	68.7 ± 15.2*	91.3 ± 6.9	92.9 ± 3.3	90.6 ± 1.7	195.8 ± 23.5*

Note: * — statistically significant difference from the control at $p < 0.05$; n — number of observations; PerP — perfusion pressure; Int$_{1min}$ — integral indicator of heart contractility per minute; PP — pulse pressure; +dP/dt and –dP/dt — first time derivative of pressure; EDP — end diastolic pressure.

to the control) by 22%, 24% and 53%, and T-wave amplitude of 256%, 307% and 245%, respectively (Table 2).

The increase in the rate of myocardial contraction (+dP/dt) associated with administration of fentanyl at the concentrations of 3.7 × 10^{-6} M and 7.4 × 10^{-6} M was accompanied by an increase amplitude of the R-wave.

DISCUSSION

The effects of fentanyl on the cardiovascular system in general and on the myocardium in particular have been investigated for a long period of time. The respective studies yielded large amount of evidence from experiments with models based on objects of various levels of organization. An ex vivo isolated heart model that excludes modulation from the central nervous system allowed documenting the most complete and objective description of the cardiotropic effect of fentanyl, with some points thereof confirmed by numerous works by Russian and foreign authors [7–9].

This study looked into the direct effects fentanyl has on the heart. For the minimal considered concentration of the drug (3.7 × 10^{-6} M), we learned that it raises the rate of contraction of the left ventricle, which is a sensitive marker of its systolic function, and does not affect heart rate and PP. As a trend, we have also registered faster relaxation of the left ventricle and a drop of the end diastolic pressure associated therewith, which signal a positive lusitropic effect of fentanyl on the isolated rat heart. This effect is likely mediated by catecholamines that induce calcium uptake in the sarcoplasmic reticulum and, consequently, trigger a rapid depletion thereof in the cytosol.

A higher concentration of fentanyl in the perfusate (7.4 × 10^{-6} M) raises perfusion pressure by inducing vasoconstriction of the coronary artery and heart rate slowdown (a negative chronotropic effect). The rate of contraction of the left ventricle grows further, but the positive lusitropic effect is offset almost completely.

Addition of fentanyl to the perfusate to the concentration of 1.5 × 10^{-5} M causes heart rate drop and perfusion pressure growth. Coronary vessels narrow significantly, which limits inflow of oxygen and energy substrates and, consequently, disrupts transportation of calcium ions from the cytosol to intracellular depots of cardiomyocytes. The ultimate outcome is the significant increase of EDP, which reflects deterioration of the myocardium's relaxation capacity.

Pretreatment of isolated heart preparations with nalmefene (1 × 10^{-6} M) did not yield cancellation of the cardiovasotropic effects of fentanyl administered at the concentration of 1.5 × 10^{-5} M. Moreover, with nalmefene in the background, we registered a progressive inhibition of the heart's contractile function, which was seen in all its parameters except the perfusion pressure. Continued depression of the myocardium's functional activity under the action of fentanyl when opioid receptors are blocked can indicate that the drug's cardiotropic effects are realized, inter alia, through the activation of non-opioid receptors [10].

Studying the effect of fentanyl on the electrical activity of an isolated rat heart, we registered a dose-dependent elongation of the QT interval, which reflects the longer time of excitation of the ventricles. Such changes are possible when the electrolyte balance is disrupted, or in case of a myocardial ischemia, which are unfavorable prognostic signs. This fact was confirmed by an experimental study that reported a significant increase of duration of action potential of dog's cardiomyocytes under the influence of fentanyl (1.9 × 10^{-7} M) [11]. In addition, the negative effect of the studied concentrations of the drug on the myocardium are evidenced by an increase amplitude T-wave that reflects repolarization of the ventricular myocardium, which may indicate myocardial ischemia caused by increased coronary artery tone and decreased oxygen flow.

CONCLUSIONS

In the course of the study, we analyzed the effect of fentanyl on an isolated rat heart in concentrations significantly higher than

Table 2. Parameters of ECG of the isolated heart of white rats under the action of fentanyl. The data are in absolute values (M ± SE)

Group of animals	RR interval, s	PR interval, s	Duration P, s	QRS interval, s	QT interval, s	Amplitude R, mV	Amplitude T, mV
Control	0.265 ± 0.020	0.061 ± 0.011	0.032 ± 0.010	0.022 ± 0.001	0.078 ± 0.007	4.016 ± 0.570	0.749 ± 0.152
Fentanyl 3,7 × 10^{-6} M	0.309 ± 0.270	0.064 ± 0.003	0.019 ± 0.002	0.024 ± 0.001	0.095 ± 0.004*	11.150 ± 1.852*	2.667 ± 0.942*
Fentanyl 7,4 × 10^{-6} M	0.373 ± 0.047	0.064 ± 0.005	0.019 ± 0.002	0.020 ± 0.002	0.097 ± 0.007*	10.790 ± 1.539*	3.047 ± 0.928*
Fentanyl 1,5 × 10^{-5} M	0.381 ± 0.063	0.069 ± 0.009	0.023 ± 0.002	0.025 ± 0.001	0.119 ± 0.003*	8.167 ± 0.905*	2.883 ± 0.450*

Note: * — statistically significant difference from control at $p < 0.05$.

those achieved when the drug is used for therapeutic purposes. For the minimal studied concentration (3.7×10^{-6} M), the effects were visible mostly on ECG. The parameters describing myocardium's contractile activity practically remained unchanged, with the exception of the rate of contraction of the left ventricle (it increased), which is a sensitive indicator of the cardiotropic effect of the drug. Higher concentrations of fentanyl in the perfusate (7.4×10^{-6} M and 1.5×10^{-5} M) supported changes in the electrical activity and triggered further negative changes: heart rate depression, vasoconstriction and subsequent drop in the coronary flow, disruption of the heart's diastolic function, which indirectly points to hindered energy supply. Thus, fentanyl has a dose-dependent cardiotoxic effect. Our results indicate that under the influence of high (sublethal) doses of the opioid, cardiac activity persists. Fentanyl's cardiotoxic effects are realized through activation of both opioid and non-opioid receptors, which should be factored in when planning pharmacological measures to counter its negative effects.

References

1. LiverTox: Clinical and Research Information on Drug-Induced Liver Injury [Internet]. Bethesda (MD): National Institute of Diabetes and Digestive and Kidney Diseases; 2012-Fentanyl. [Updated 2019 Apr 25].
2. Baldo BA. Toxicities of opioid analgesics: respiratory depression, histamine release, hemodynamic changes, hypersensitivity, serotonin toxicity. Arch Toxicol. 2021; 95 (8): 2627–42. DOI: 10.1007/s00204-021-03068-2. Epub 2021 May 11. PMID: 33974096.
3. Metodicheskie rekomendacii. Modelirovanie intoksikacij deprimirujushhimi agentami i ocenka vyrazhennosti deprimirujushhego jeffekta. M.: MR FMBA Rossii, 2013; 31 s.
4. Gorbunov DV, Jerdniev LP, Nelga IA, Medveckij IV, Mikshta AJu, Andreeva EJu. Jeksperimental'nye issledovanija biohimicheskih sistem organizma belyh krys pri ostroj intoksikacii fentanilom. Toksikologicheskij vestnik. 2018; 6 (153): 25–27. Russian.
5. Loshadkin NA, Kurljandskij BA, Bezhenar GV, Darina LV. Voennaja toksikologija. M: Medicina, 2006; 207 s. Russian.
6. Laptev DS, Petunov SG, Bobkov DV, Radilov AS. Vlijanie b-jendorfina na funkcional'nuju aktivnost' izolirovannogo serdca krysy. Rol' del'ta-opioidnyh receptorov. Regionarnoe krovoobrashhenie i mikrocirkuljacija. 2015; 3 (55): 66–71. Russian.
7. Hanouz JL, Yvon A, Guesne G, Eustratiades C, Babatasi G, Rouet R, et al. The in vitro effects of remifentanil, sufentanil, fentanyl, and alfentanil on isolated human right atria. Anesth Analg. 2001; 93 (3): 543–9. DOI: 10.1097/00000539-200109000-00005. PMID: 11524316.
8. Gürkan A, Birgül Y, Ziya K. Direct cardiac effects in isolated perfused rat hearts of fentanyl and remifentanil. Ann Card Anaesth. 2005; 8 (2): 140–4. PMID: 17762064.
9. Chernikov VS. Deĭstvie fentanila na sokratitelnuiu sposobnost' aérobno perfuzirovannogo izolirovannogo serdtsa krysy [Effect of fentanyl on the contractile capacity of the aerobically perfused isolated rat heart]. Patol Fiziol Eksp Ter. 1994; (4): 8–11. Russian.
10. Hatano Y, Toda N. Influence of fentanyl on the chronotropic response of isolated rabbit atria to cholinergic and adrenergic stimulation. Jpn J Pharmacol. 1978; 28 (1): 105–14. DOI: 10.1254/jjp.28.105. PMID: 651008.
11. Blair JR, Pruett JK, Introna RP, Adams RJ, Balser JS. Cardiac electrophysiologic effects of fentanyl and sufentanil in canine cardiac Purkinje fibers. Anesthesiology. 1989; 71 (4): 565–70. DOI: 10.1097/00000542-198910000-00015. PMID: 2529795.

Литература

1. LiverTox: Clinical and Research Information on Drug-Induced Liver Injury [Internet]. Bethesda (MD): National Institute of Diabetes and Digestive and Kidney Diseases; 2012-Fentanyl. [Updated 2019 Apr 25].
2. Baldo BA. Toxicities of opioid analgesics: respiratory depression, histamine release, hemodynamic changes, hypersensitivity, serotonin toxicity. Arch Toxicol. 2021; 95 (8): 2627–42. DOI: 10.1007/s00204-021-03068-2. Epub 2021 May 11. PMID: 33974096.
3. Методические рекомендации. Моделирование интоксикаций депримирующими агентами и оценка выраженности депримирующего эффекта. М.: МР ФМБА России, 2013; 31 с.
4. Горбунов Д. В., Эрдниев Л. П., Нельга И. А., Медвецкий И. В., Микшта А. Ю., Андреева Е. Ю. Экспериментальные исследования биохимических систем организма белых крыс при острой интоксикации фентанилом. Токсикологический вестник. 2018; 6 (153): 25–27.
5. Лошадкин Н. А., Курляндский Б. А., Беженарь Г. В., Дарьина Л. В. Военная токсикология. М: Медицина, 2006; 207 с.
6. Лаптев Д. С. Петунов С. Г., Бобков Д. В., Радилов А. С. Влияние b-эндорфина на функциональную активность изолированного сердца крысы. Роль дельта-опиоидных рецепторов. Регионарное кровообращение и микроциркуляция. 2015; 3 (55): 66–71.
7. Hanouz JL, Yvon A, Guesne G, Eustratiades C, Babatasi G, Rouet R, et al. The in vitro effects of remifentanil, sufentanil, fentanyl, and alfentanil on isolated human right atria. Anesth Analg. 2001; 93 (3): 543–9. DOI: 10.1097/00000539-200109000-00005. PMID: 11524316.
8. Gürkan A, Birgül Y, Ziya K. Direct cardiac effects in isolated perfused rat hearts of fentanyl and remifentanil. Ann Card Anaesth. 2005; 8 (2): 140–4. PMID: 17762064.
9. Chernikov VS. Deĭstvie fentanila na sokratitelnuiu sposobnost' aérobno perfuzirovannogo izolirovannogo serdtsa krysy [Effect of fentanyl on the contractile capacity of the aerobically perfused isolated rat heart]. Patol Fiziol Eksp Ter. 1994; (4): 8–11. Russian.
10. Hatano Y, Toda N. Influence of fentanyl on the chronotropic response of isolated rabbit atria to cholinergic and adrenergic stimulation. Jpn J Pharmacol. 1978; 28 (1): 105–14. DOI: 10.1254/jjp.28.105. PMID: 651008.
11. Blair JR, Pruett JK, Introna RP, Adams RJ, Balser JS. Cardiac electrophysiologic effects of fentanyl and sufentanil in canine cardiac Purkinje fibers. Anesthesiology. 1989; 71 (4): 565–70. DOI: 10.1097/00000542-198910000-00015. PMID: 2529795.

RESULTS OF TESTING BASIC KNOWLEDGE ABOUT THE ISSUES OF FIRST AID IN DIFFERENT CATEGORIES OF PEOPLE

Ivanov YuV[1], Stankevich VR[1], Kakurin OV[1], Velichko YeA[1] ✉, Smirnov AV[1], Gornov SV[2]

[1] Federal Scientific and Clinical Center for Specialized Types of Medical Care and Medical Technologies of the Federal Medical Biological Agency, Moscow, Russia

[2] Russian Biotechnological University, Moscow, Russia

Timely first aid (FA) for acute conditions makes it possible to improve treatment outcomes and sometimes save human life. Assessing the basic knowledge about FA will help develop a rational system for training and dissemination of knowledge about FA. The study was aimed to perform quantitative and qualitative analysis of mistakes made by residents of Moscow and Moscow Region during assessment of their basic knowledge about FA. The questionnaire consisting of 10 questions (four possible answers, among then one correct) was created. Polling conducted before testing showed that all the respondents had basic knowledge about FA. The total study sample was 946 individuals (aged 15 years and older), it was divided into group based on the fact of having/not having medical education. It was found that the basic knowledge about FA was generally low, mainly due to the respondents having no medical education. Qualitative analysis of the answers revealed a large number of gross mistakes reflecting a high risk of wrong actions leading to deterioration of health of a victim or FA provider. The study confirms the fact of insufficient awareness of various categories of citizens, including healthcare professionals, on the issues of FA, which suggests the need to improve the system for training and dissemination of knowledge about FA across the population.

РЕЗУЛЬТАТЫ ТЕСТИРОВАНИЯ УРОВНЯ БАЗОВЫХ ЗНАНИЙ ПО ВОПРОСАМ ОКАЗАНИЯ ПЕРВОЙ ПОМОЩИ У РАЗНЫХ КАТЕГОРИЙ НАСЕЛЕНИЯ

Ю. В. Иванов[1], В. Р. Станкевич[1], О. В. Какурин[1], Е. А. Величко[1] ✉, А. В. Смирнов[1], С. В. Горнов[2]

[1] Федеральный научно-клинический центр специализированных видов медицинской помощи и медицинских технологий Федерального медико-биологического агентства, Москва, Россия

[2] Медицинский институт непрерывного образования ФГБОУ ВО «Российский биотехнологический университет (РОСБИОТЕХ)», Москва, Россия

Своевременное оказание первой помощи (ПП) при острых состояниях позволяет улучшить результаты лечения и иногда спасти человеческую жизнь. Оценка уровня базовых знаний по ПП поможет сформировать рациональную систему обучения и распространения знаний по ПП. Целью исследования было провести количественный и качественный анализ ошибок, допущенных населением Москвы и Московской области при оценке уровня их базовых знаний по вопросам оказания ПП. Разработана анкета, включающая 10 вопросов (четыре варианта ответа, один — правильный). Перед проведением тестирования методом опроса установлено, что все респонденты имели базовые знания по ПП. Общая выборка исследования составила 946 человек (15 лет и старше) и разделена на группы по наличию медицинского образования. Установлен общий низкий уровень базовых знаний по вопросам оказания ПП, преимущественно за счет респондентов, не имеющих медицинского образования. При качественном анализе ответов выявлено большое число грубых ошибок, отражающих высокий риск совершения ошибочных действий, которые приведут к ухудшению состояния пострадавшего, либо оказывающего ПП. Проведенное исследование подтверждает факт недостаточной информированности различных категорий граждан, в том числе медицинских работников, по вопросам оказания ПП, что свидетельствует о необходимости усовершенствования системы обучения и распространения знаний оказания ПП среди населения.

Because of the recently increase in the rate of emergency situations with the large number of victims, acute conditions and injuries, training of various categories of people to provide first aid (FA) is a very important issue. Statistical research performed in Russia shows that among 70% of those in need of FA for various conditions, only 2% received it [1]. The timely and correct actions of the incident witnesses aimed to provide FA for the conditions associated with human health deterioration make it possible to not only improve treatment outcomes, but often save human life [2].

The people's willingness to provide FA is determined not only by the theoretical and practical training, but also by the fear of legal prosecution in case of possible harm to the victim during or after the FA provision [1, 4, 5].

In our country, people first encounter with the FA training at school, during classes on the basics of life safety. The

international scientific community conducts research on teaching children skills in FA provision. The data show that children can be able to properly provide FA after the FA training [6]. In our opinion, classes on FA in some educational institutions are formal: training involves the use of unapproved programs or obsolete workbooks, there are no simulators or mannequins for students to master practical skills. When organizing practical training, the FA provision algorithms should be worked out to automaticity using specific equipment and considering the category of students (discrete approach) [1, 7]. FA training is part of the complex of measures on shaping the culture of safe behavior and prevention of various risks [3, 12]. knowledge about FA and FA provision skills are in the list of job functions and professional skills of teachers, instructors and trainers [8, 9].

The rate of sudden death during P.E. classes in Russia twice exceeds that reported for other high income countries and constitutes 1.4 cases per 100,000 students or up to 200 cases annually. Injuries during P.E. classes account for 2–5% of the total number of injuries [10].

Teachers working in the Russian educational system are not competent enough in the issues of FA provision; their willingness to provide FA is generally low [3, 11]. Today, when training in a driving school, the course on FA is a mandatory component of the driver training program, while in some other educational institutions it is introduced at the initiative of managers, who understand the importance of this course for the increase in the number of individuals willing to properly provide FA. Some employers concerned conduct classes on FA as part of the occupational safety course not only every three years (in accordance with the regulatory documents), but also additionally, since they appreciate the knowledge about FA provision indicating the levels of competence, willingness, and responsibility [13–15].

Considering the above, it is obvious that at the moment it is necessary to widely disseminate knowledge about the methods and rules of providing FA for injuries, acute disorders, and other conditions. Russian legislation regulates mandatory FA training of some categories of citizens (officers of the internal affairs bodies of the Russian Federation, military personnel and employees of the State Fire Service, rescuers of the emergency rescue teams and emergency services, etc.) [16, 17] However, along with this, there is still no statutory FA training system for other categories of citizens, which stifles dissemination of knowledge on the issue. Assessment of basic knowledge about FA in the population will make it possible to determine the priority directions of the development of FA training system.

The study was aimed to perform quantitative and qualitative analysis of mistakes made by residents of Moscow and Moscow Region during assessment of their basic knowledge about FA.

METHODS

Prior to testing, a questionnaire survey was carried out that showed that all the respondents had been previously taught to provide FA during classes on the basics of life safety at school, in vocational schools, colleges, as well as in higher educational institutions and driving schools, i.e. all of them had basic knowledge about FA.

To perform quantitative and qualitative analysis of mistakes made by residents of Moscow and Moscow Region during assessment of their basic knowledge about FA, we created a special questionnaire consisting of 10 questions (four possible answers, among then one correct). Answers to the questions of the questionnaire allow one to determine potential risk to the FA provider associated with wrong actions in specific situations,

possible deterioration of patient's health associated with the care provider's wrong actions, the use of medicines without the doctor's appointment at the stage of FA, understanding of new FA provision standards and technologies, being familiar with the term "first aid".

The total sample of the study was 946 people (15 years and older), it was divided into groups based on the fact of having/ not having medical education.

Statistical processing of the results was performed in the Microsoft Excel-XP and STATISTICA 7 software packages.

RESULTS

Based on education, the respondents were divided as follows: 741 people (78.3%) had no medical education; 205 people (21.7%) had medical education.

When analyzing the answers to the questions of the test proposed, we performed quantitative and qualitative assessment of the common mistakes made by respondents in order to determine possible consequences for the patient and care provider in case of implementing a faulty algorithm.

It was proposed to provide care to the victim with electric shock in the following question of the test: "*What would you do, if you see a victim lying on the floor, with a broken electrical wire sticking out of the wall, which is in his/her hand, when entering the room (the victim does not respond when spoken to)*?" The right answer ("*Turn off the circuit breaker, try to pull the wire away with an insulating object (for example, with a stick, if do not know, where the circuit breaker is), call the ambulance and proceed to FA provision*" [19, 20]) was given by 505 people (53.4%) (126 medical professionals (61.5%) and 379 respondents having no medical education (51.1%)). The wrong answers were given by 441 people (46.6%), among them 79 were medical professionals (38.5%) and 362 were respondents having no medical education (48.9%). The respondents' willingness to provide care to the victim with electric shock without de-energizing the room could undoubtedly cause electric shock in the respondents.

It was proposed to provide care to the victim with carbon monoxide poisoning in the following question: "*What would you do, if you find an unconscious, breathless adult victim after entering the closed garage filled with smoke?*" The right answer to this question ("*Call the ambulance, remove the victim from the garage, start cardiopulmonary resuscitation*" [18, 20]) was given by 760 people (80.3%), among them 188 were medical professionals (91.7%) and 572 people (77.2%) had no medical education. The wrong answers were given by 186 respondents (19.7%), among them 17 (8.3%) were medical professionals and 169 (22.8%) were respondents having no medical education: they decided that removal of the victim from the room filled with smoke was not a priority, thereby exposing themselves and the victim to probable danger.

When asked about their actions in case of snake bite (the answer options were as follows: suck poison out of the wound; make a deep cross-shaped incision in the bite area and squeeze out poison with blood; cauterize the bite site with a hot metal object; none of the above), the right answer ("*None of the above*", since it is necessary to immobilize the bitten limb and put something cold on the bite site) [18, 20]) was given by 237 respondents (25.1%): 79 medical professionals (38.5%), 158 people having no medical education (21.3%). A total of 709 (74.9%) respondents (126 medical professionals (61.5%) and 583 people having no medical education (78.7%)) were ready to endanger themselves (suck snake poison out of the wound or do more harm to the patient (cauterize the bite site with a hot metal object or make a deep cross-shaped incision).

As for the question about the actions of the witness of epileptic seizure in a male aged 30–35 years ("*You are a witness of epileptic seizure in a male aged 30–35 years. What would you do?*"), the right answer ("*Place a soft cushion under the victim's head and wait until seizure is over, call the ambulance*" [21, 22]) was given by 305 respondents (32.2%), among them 112 had medical education (54.6%), 193 had no medical education (26.0%). A total of 641 (67.8%) respondents (among them 93 medical professionals (45.4%) and 548 people having no medical education (74.0%)) gave wrong answers (immediately unclench the victim's jaws to clear the airways (separately) or in combination with the correct answer, "none of the above"). While it is known that impaired breathing during seizures occurs due to the lack of adequate contraction of the respiratory muscles, and the above intervention can lead to damage to the teeth/prostheses, oral mucosal injury and, as a result, aspiration of blood and/or foreign matter (fragments of teeth) [22].

As for the question "*While in the school laboratory, you witnessed the hydrochloric acid solution getting into the child's eyes. What would you do?*", the right answer ("*Rinse the eyes with running water from nose to temple, call the ambulance*" [23]) was given by 270 respondents (28.5%), among them 44 were medical professionals (21.5%) and 226 had no medical education (30.5%). The wrong answers (immediately rinse the eyes with a weak alkali solution and put a dressing on the eyes, call the ambulance; rinse the eyes with running water from nose to temple, call "03"; none of the above) were given by 676 (71,5%) respondents (161 medical professionals (78.5%) and 515 people having no medical education (69.5): they suggested to rinse the eyes with a weak alkali solution or water from nose to temple or not to do anything of the above. It is forbidden to use neutralizers (alkali in this case) for chemical burns, since the neutralization reaction is exothermic: heat is released that can aggravate the tissue damage [24]. Furthermore, it is necessary to rinse the eyes from nose to temple in order to avoid getting the chemical into the nasolacrimal duct and prevent burn of the nasal mucosa [23].

The right answer to the question "*What would you do if you witnessed your friend choking on foreign body (while eating in the canteen), but you fail to remove foreign body, and your friend falls, loses consciousness, and stops breathing?*" ("*Start artificial respiration and chest compressions*" [18]) was given by 189 respondents (20.0%), among them 56 were medical professionals (27.3%) and 133 were people having no medical education (17.9%). The wrong answers (send someone for help, while trying to open the victim's mouth, find foreign body with the finger and remove it; wait for the arrival of medical professionals, understanding that cardiopulmonary resuscitation is useless; none of the above) were given by 757 respondents (80.0%), among them 149 were medical professionals (72.7%) and 608 were people having no medical education (82.1%). It is strictly forbidden to remove foreign bodies from the airways blindly, and what more, this delays the start of cardiopulmonary resuscitation and increases the probability that the foreign body would travel deeper into the airways.

The right answer to the question "*What would you do if you witnessed the child knocking over a pot of boiling water while visiting, and you see that the damage is extensive but superficial?*" ("*Rinse the damaged surface with cold running water for 10–15 min, call the ambulance, apply a dry sterile dressing*" [18]) was given by 313 respondents (33.1%), among them 77 were medical professionals (37.6%) and 236 were people having no medical education (31.8%). The wrong answers (immediately treat the affected surface with the Olazol or Panthenol anti-burn gel, call the ambulance and apply a dry sterile dressing; call the ambulance and apply a dry sterile dressing; none of the above) were given by 633 respondents (66.9%), among them 128 were medical professionals (62.4%) and 505 were people having no medical education (68.2%).

These questions were about the possible use of the Olazol and Panthenol anti-burn ointments for burns and hydrogen peroxide for wound treatment. According to the regulatory documents, the use of medicines at the stage of FA provision is not regulated [17]. The above medications are not included in the FA kit. It would be inappropriate to use these medications when providing FA in both cases, regardless of the respondents' education.

The question "*What is the ratio of breaths and compressions during cardiopulmonary resuscitation performed by two rescuers in an adult victim?*" assessed the respondents' knowledge about the ratio of compressions and artificial respiration in cardiopulmonary resuscitation. The right answer ("*Two breaths to 30 compressions*" [18, 20]) was given by 225 respondents (23.8%), among them 100 (48.8%) had medical education, 125 (16.9%) had no medical education. The wrong answers (one breath to five compressions; two breaths to 15 compressions; none of the above) were given by 721 respondents (76.2%). Such ratios of compressions and breaths, as 15 : 2 and 5 : 1, are noncompliant with the principles of cardiopulmonary resuscitation.

The right answer to the question "*How long should you perform cardiopulmonary resuscitation in an unconscious victim with no breathing or cardiac function?*" ("*Until medical professionals arrive*" [18, 25]) was given by 641 respondents (67.8%), among them 173 (84.4%) had medical education, 468 (63.2%) had no medical education. The wrong answers ("5 min"; "15 min", "none of the above") were given by 305 respondents (32.2%), among them 32 (15.6%) had medical education, 273 (36.8%) had no medical education.

The right answer to the question "*How to determine, whether someone is conscious?*" ("Ask the victim "*Can you hear me*?" and tap him/her on the shoulder" [18, 25]) was given by 364 respondents (38.5%), among them 144 (70.2%) had medical education, 220 (29.7%) had no medical education. The wrong answers ("based on pupils, carotid artery pulse", "based on the presence of reflexes, pupils", "none of the above") were given by 582 respondents (61.5%), among them 61 (29.8%) had medical education, 521 (70.3%) had no medical education.

DISCUSSION

Mistakes made when answering questions of the test represents the actions that can worsen the victim's condition or do harm to the FA provider, which will result in the increased number of victims at the accident site and difficulty providing skilled professional assistance. The data obtained are consistent with the results reported by Claire Louise Heard et al. (2020) after the study of collective knowledge about FA conducted based on the systematic review of 40 papers on providing FA and emergency care in emergency situations from 22 countries (mostly from Asia, Australia, Europe, and USA) and confirm that the verified collective knowledge about certain FA skills is generally low [26].

CONCLUSIONS

The quantitative and qualitative analysis of mistakes made by the respondents during assessment of their basic knowledge about FA showed that their basic knowledge was generally low;

the alarming rate of gross mistakes made when answering the questions about the respondents' potential actions during FA provision was reported. All the above demonstrates high risk of the respondents' erroneous actions resulting in the significant worsening of victim's condition and causing harm to care provider. The study conducted confirm the fact that various categories of citizens (including medical professionals) are insufficiently aware of the issues of FA provision, as well as the fact that it is necessary to improve the system for dissemination of knowledge about FA provision in the population.

References

1. Bolotova IA, Zadorozhnaja NA, Dubkova NV, Merkushev IA, Makoeva FK. Normativno-pravovaja baza obuchenija prepodavatelej fizicheskoj kul'tury i sporta navykam okazanija pervoj pomoshhi pri neotlozhnyh sostojanijah. Teorija i praktika fizicheskoj kul'tury. 2023; (5): 75–77. Russian.

2. Gigal A. Obuchenie naselenija pravilam okazanija pervoj pomoshhi i volonterskoe dvizhenie. V sbornike: Pervaja pomoshh' 2020: Sbornik tezisov Vserossijskoj nauchno-prakticheskoj konferencii (v sootvetstvii s planom nauchno-prakticheskih meroprijatij MZ RF); 9–10 oktjabrja 2020 g.; Moskva: FGBU «CNIIOIZ» Minzdrava Rossii, 2020; s. 54–58. Russian.

3. Piskunova VV. Obuchenie pervoj pomoshhi v VUZe kak komponent pedagogiki bezopasnosti. Vestnik Prikamskogo social'nogo instituta. 2023; 3 (96): 90–93. Russian.

4. Jakovleva EV, Frolov AS. Rassmotrenie sovremennyh metodov obuchenija okazanija pervoj pomoshhi postradavshim, na primere ispol'zovanija programmnogo obespechenija — «SPJeK. Pervaja pomoshh'». Vestnik sel'skogo razvitija i social'noj politiki. 2020; 3 (27): 38–43. Russian.

5. Birkun AA, Dezhurnyj LI. Normativno-pravovoe regulirovanie okazanija pervoj pomoshhi i obuchenija okazaniju pervoj pomoshhi pri vnegospital'noj ostanovke serdca. Zhurnal im. N.V. Sklifosovskogo Neotlozhnaja medicinskaja pomoshh'. 2021; 10 (1): 141–52. https://doi.org/10.23934/2223-9022-2021-10-1-141-152. Russian.

6. Perkins GD, Graesner JT, Semeraro F, et al. European resuscitation council guidelines 2021 — executive summary. Resuscitation. 2021; 161 r.

7. Gajazetdinova AJe, Meljakova OA. Organizacija obuchenija okazanija pervoj pomoshhi. Agrarnoe obrazovanie i nauka. 2022; 4: 9–14. Russian.

8. Bolotova IA, Zadorozhnaja NA, Dubkova NV. Innovacionnyj podhod k izucheniju discipliny «Osnovy medicinskih znanij» s otrabotkoj professional'nyh kompetencij po rezul'tatam provedennoj voenno-patrioticheskoj igry «Po sledam partizanskih otrjadov». Uchenye zapiski universiteta im. P. F. Lesgafta. 2022; 8 (210): 34–36. Russian.

9. Ob obrazovanii v Rossijskoj Federacii: Federal'nyj zakon Rossijskoj Federacii ot 29.12.2012 # 273-FZ [prinjat Gos. Dumoj 21.12.2012] (s izmenenijami na 6 fevralja 2023 goda). Jelektronnyj fond «Kodeks». Dostupno po ssylke: https://docs.cntd.ru/document/902389617 (data obrashhenija: 24.02.2023). Russian.

10. Solodovnik EM. Travmatizm na urokah fizicheskoj kul'tury: osobennost', prichiny i profilaktika. Mezhdunarodnyj zhurnal gumanitarnyh i estestvennyh nauk. 2019; 1–2: 165–68. Russian.

11. Kolodkin AA, Kolodkina VI, Vladimirova OV, Muraveva AA. Obuchenie pedagogicheskih rabotnikov obrazovatel'nyh uchrezhdenij navykam okazanija pervoj pomoshhi. Medicina katastrof. 2017; 3 (99): 56–59. Russian.

12. Dezhurnyj LI, Zakurdaeva AJu, Gumenjuk SA, Kolodkin AA. Opyt profil'noj komissii Minzdrava Rossii po napravleniju «pervaja pomoshh'» po sovershenstvovaniju perechnja meroprijatij po okazaniju pervoj pomoshhi: organizacionno-pravovoj aspekt. Sovremennye problemy zdravoohranenija i medicinskoj statistiki. 2024; 1: 667–82. https://doi.org/10.24412/2312-2935-2024-1-667-682.

13. Podberezina SG. Novyj porjadok obuchenija po ohrane truda: organizacija i provedenie obuchenija po okazaniju pervoj pomoshhi postradavshim. Kadrovye reshenija. 2022; 8: 83–92. Russian.

14. Ob obuchenii rabotnikov okazaniju pervoj pomoshhi postradavshim: Pis'mo Ministerstva truda i social'noj zashhity ot 11 aprelja 2017 goda #15-2/V-950. Jelektronnyj fond «Kodeks». Dostupno po ssylke: https://docs.cntd.ru/document/456060729 (data obrashhenija: 24.02.2023). Russian.

15. Diamant II. Romanov DS. Innovacionnye podhody k obucheniju starshih shkol'nikov okazaniju pervoj pomoshhi. Vestnik Tomskogo gosudarstvennogo pedagogicheskogo universiteta. Tomsk, 2013; 4 (132): 136–38. Russian.

16. Federalnyj zakon ot 14.04.2023 N 135-FZ (red. ot 25.12.2023) «O vnesenii izmenenij v stat'ju 31 Federal'nogo zakona «Ob osnovah ohrany zdorov'ja grazhdan v Rossijskoj Federacii». Russian.

17. Ob osnovah ohrany zdorov'ja grazhdan v Rossijskoj Federacii: Federal'nyj zakon ot 21 nojabrja 2011 goda # 323 [prinjat Gos. Dumoj 01.11.2011] (redakcija, dejstvujushhaja s 11 janvarja 2023 goda). Jelektronnyj fond «Kodeks». Dostupno po ssylke: https://docs.cntd.ru/document/902312609 (data obrashhenija: 24.02.2023). Russian.

18. Dezhurnyj LI, Shojgu JuS, Gumenjuk SA, Neudahin GV, Zakurdaeva AJu, Kolodkin AA, i dr. Pervaja pomoshh': uchebnoe posobie dlja lic, objazannyh i (ili) imejushhih pravo okazyvat' pervuju pomoshh'. M.: FGBU «CNIIOIZ» Minzdrava Rossii, 2018; 68 s. Dostupno po ssylke: https://allfirstaid.ru/system/files/umk/Ucha-n-L.pdf. Russian.

19. Tulupov AN, Lapshin VN, Mihajlov JuM. Klinicheskie rekomendacii (protokol) po okazaniju skoroj medicinskoj pomoshhi pri porazhenii jelektrotokom i molniej. 2014; 10 s. Russian.

20. Mezhdunarodnoe rukovodstvo po pervoj pomoshhi i reanimacii. Zheneva, 2016; 192 s. Russian.

21. International Federation of Red Cross and Red Crescent Societies. Red Cross Red Crescent Networks. International first aid resuscitation and education guidelines 2020. Available from: https://www.globalfirstaidcentre.org/wp-content/uploads/2021/02/EN_GFARC_GUIDELINES_2020.pdf (data obrashhenija 27.12.2022).

22. Birkun AA, Dezhurnyj LI. Okazanie pervoj pomoshhi pri generalizovannyh sudorogah: sovremennye podhody i vozmozhnosti sovershenstvovanija. Jepilepsija i paroksizmal'nye sostojanija. 2023; 15 (2): 115–24. Dostupno po ssylke: https://doi.org/10.17749/2077-8333/epi.par.con.2023.142 Russian.

23. Ozhogi glaz. Klinicheskie rekomendacii MZ RF. 2020; 44 s. Russian.

24. Sobolev AE, redaktor. Uchebnaja kniga po himii: posobie dlja uchashhihsja 8 klassa obshheobrazovatel'nyh uchrezhdenij. Tver': SFK-ofis, 2021; 368 s. Russian.

25. Dezhurnyj LI, Shojgu JuS, Gumenjuk SA, Neudahin GV, Zakurdaeva AJu, Kolodkin AA, i dr. Atlas pervoj pomoshhi: uchebnoe posobie dlja sotrudnikov Gosavtoinspekcii. Moskva: Izdatel'stvo «Nacional'nyj mediko-hirurgicheskij Centr im. N.I. Pirogova», 2022; 72 s. Russian.

26. Heard C, Pearce J, Rogers B. Mapping the public first-aid training landscape: a scoping review. Disasters. 2020; 44 (1): 205–28. DOI: 10.1111/disa.12406.

Литература

1. Болотова И. А., Задорожная Н. А., Дубкова Н. В., Меркушев И. А., Макоева Ф. К. Нормативно-правовая база обучения преподавателей физической культуры и спорта навыкам оказания первой помощи при неотложных состояниях. Теория и практика физической культуры. 2023; (5): 75–77.
2. Гигаль А. Обучение населения правилам оказания первой помощи и волонтерское движение. В сборнике: Первая помощь 2020: Сборник тезисов Всероссийской научно-практической конференции (в соответствии с планом научно-практических мероприятий МЗ РФ); 9–10 октября 2020 г.; Москва: ФГБУ «ЦНИИОИЗ» Минздрава России, 2020; с. 54–58.
3. Пискунова В. В. Обучение первой помощи в ВУЗе как компонент педагогики безопасности. Вестник Прикамского социального института. 2023; 3 (96): 90–93.
4. Яковлева Е. В., Фролов А. С. Рассмотрение современных методов обучения оказания первой помощи пострадавшим, на примере использования программного обеспечения — «СПЭК. Первая помощь». Вестник сельского развития и социальной политики. 2020; 3 (27): 38–43.
5. Биркун А. А., Дежурный Л. И. Нормативно-правовое регулирование оказания первой помощи и обучения оказанию первой помощи при внегоспитальной остановке сердца. Журнал им. Н.В. Склифосовского Неотложная медицинская помощь. 2021; 10 (1): 141–52. https://doi.org/10.23934/2223-9022-2021-10-1-141-152.
6. Perkins GD, Graesner JT, Semeraro F, et al. European resuscitation council guidelines 2021– executive summary. Resuscitation. 2021; 161 p.
7. Гаязетдинова А. Э., Мелякова О. А. Организация обучения оказания первой помощи. Аграрное образование и наука. 2022; 4: 9–14.
8. Болотова И. А., Задорожная Н. А., Дубкова Н. В. Инновационный подход к изучению дисциплины «Основы медицинских знаний» с отработкой профессиональных компетенций по результатам проведенной военно-патриотической игры «По следам партизанских отрядов». Ученые записки университета им. П. Ф. Лесгафта. 2022; 8 (210): 34–36.
9. Об образовании в Российской Федерации: Федеральный закон Российской Федерации от 29.12.2012 № 273-ФЗ [принят Гос. Думой 21.12.2012] (с изменениями на 6 февраля 2023 года). Электронный фонд «Кодекс». Доступно по ссылке: https://docs.cntd.ru/document/902389617 (дата обращения: 24.02.2023).
10. Солодовник Е. М. Травматизм на уроках физической культуры: особенность, причины и профилактика. Международный журнал гуманитарных и естественных наук. 2019; 1–2: 165–68.
11. Колодкин А. А., Колодкина В. И., Владимирова О. В., Муравьева А. А. Обучение педагогических работников образовательных учреждений навыкам оказания первой помощи. Медицина катастроф. 2017; 3 (99): 56–59.
12. Дежурный Л. И., Закурдаева А. Ю., Гуменюк С. А., Колодкин А. А. Опыт профильной комиссии Минздрава России по направлению «первая помощь» по совершенствованию перечня мероприятий по оказанию первой помощи: организационно-правовой аспект. Современные проблемы здравоохранения и медицинской статистики. 2024; 1: 667–82. https://doi.org/10.24412/2312-2935-2024-1-667-682.
13. Подберезина С. Г. Новый порядок обучения по охране труда: организация и проведение обучения по оказанию первой помощи пострадавшим. Кадровые решения. 2022; 8: 83–92.
14. Об обучении работников оказанию первой помощи пострадавшим: Письмо Министерства труда и социальной защиты от 11 апреля 2017 года №15-2/В-950. Электронный фонд «Кодекс». Доступно по ссылке: https://docs.cntd.ru/document/456060729 (дата обращения: 24.02.2023).
15. Диамант И. И. Романов Д. С. Инновационные подходы к обучению старших школьников оказанию первой помощи. Вестник Томского государственного педагогического университета. Томск, 2013; 4 (132): 136–38.
16. Федеральный закон от 14.04.2023 N 135-ФЗ (ред. от 25.12.2023) «О внесении изменений в статью 31 Федерального закона «Об основах охраны здоровья граждан в Российской Федерации».
17. Об основах охраны здоровья граждан в Российской Федерации: Федеральный закон от 21 ноября 2011 года № 323 [принят Гос. Думой 01.11.2011] (редакция, действующая с 11 января 2023 года). Электронный фонд «Кодекс». Доступно по ссылке: https://docs.cntd.ru/document/902312609 (дата обращения: 24.02.2023).
18. Дежурный Л. И., Шойгу Ю. С., Гуменюк С. А., Неудахин Г. В., Закурдаева А. Ю., Колодкин А. А., и др. Первая помощь: учебное пособие для лиц, обязанных и (или) имеющих право оказывать первую помощь. М.: ФГБУ «ЦНИИОИЗ» Минздрава России, 2018; 68 с. Доступно по ссылке: https://allfirstaid.ru/system/files/umk/Ucha-n-L.pdf;
19. Тулупов А. Н., Лапшин В. Н., Михайлов Ю. М. Клинические рекомендации (протокол) по оказанию скорой медицинской помощи при поражении электротоком и молнией. 2014; 10 с.
20. Международное руководство по первой помощи и реанимации. Женева. 2016; 192 с.
21. International Federation of Red Cross and Red Crescent Societies. Red Cross Red Crescent Networks. International first aid resuscitation and education guidelines 2020. Available from: https://www.globalfirstaidcentre.org/wp-content/uploads/2021/02/EN_GFARC_GUIDELINES_2020.pdf (дата обращения 27.12.2022).
22. Биркун А. А., Дежурный Л. И. Оказание первой помощи при генерализованных судорогах: современные подходы и возможности совершенствования. Эпилепсия и пароксизмальные состояния. 2023; 15 (2): 115–24. Доступно по ссылке: https://doi.org/10.17749/2077-8333/epi.par.con.2023.142.
23. Ожоги глаз. Клинические рекомендации МЗ РФ. 2020; 44 с.
24. Соболев А. Е., редактор. Учебная книга по химии: пособие для учащихся 8 класса общеобразовательных учреждений. Тверь: СФК-офис, 2021; 368 с.
25. Дежурный Л. И., Шойгу Ю. С., Гуменюк С. А., Неудахин Г. В., Закурдаева А. Ю., Колодкин А. А., и др. Атлас первой помощи: учебное пособие для сотрудников Госавтоинспекции. Москва: Издательство «Национальный медико-хирургический Центр им. Н.И. Пирогова», 2022; 72 с.
26. Heard C, Pearce J, Rogers B. Mapping the public first-aid training landscape: a scoping review. Disasters. 2020; 44 (1): 205–28. DOI: 10.1111/disa.12406.

ASSESSMENT OF MICRONUTRIENT LEVELS IN THE MILITARY PERSONNEL SERVING IN VARIOUS CLIMATIC ZONES OF RUSSIA

Narutdinov DA[1], Rakhmanov RS[2] ✉, Bogomolova ES[2], Razgulin SA[2], Istomin AV[3], Shurkin DA[1]

[1] Professor V.F. Voino-Yasenetsky Krasnoyarsk State Medical University, Krasnoyarsk, Russia

[2] Privolzhsky Research Medical University, Nizhny Novgorod, Russia

[3] Erisman Federal Scientific Center of Hygiene, Mytishchi, Russia

The lack of vitamins and minerals in the body contributes to the development of acquired deficient conditions. The study was aimed to assess micronutrient levels in the military personnel serving in various climatic zones of Russia. Plasma levels of vitamins (D based on 25(OH)D, B_{12}, B_9) and minerals (K, Na, total and ionized Ca, P, Mg, Fe), working and nutritional conditions were determined in servicemen in the Arctic (n = 54), Subarctic (n = 57), and temporary climate (n = 58) zones. The 25(OH)D levels were 24.06 ± 6.95, 21.5 ± 12.1(p_{1-2} = 0.003), and 27.2 ± 15.2 (p_{1-2} = 0.423, p_{1-3} = 0.032) ng/ml; deficiency and insufficiency were revealed in 82.3, 86.5, and 63.8% of military personnel. The cobalamin levels were 96.46 ± 20.6, 111.7 ± 59.4 (p_{1-2} = 0.046), and 125.7 ± 63.2 (p_{1-2} = 0.002, p_{1-3} = 0.334) pmol/L; the values below 148 pg/mL were reported for 100.0, 73.6, and 67.2% of surveyed individuals. The folate levels were 3.4 ± 0.4, 3.52 ± 1.54 (p_{1-2} = 0.657), and 6.49 ± 6.21 (p_{1-2} = 0.001, p_{1-3} = 0.009) ng/mL; the decreased levels were reported for 89.8, 81.3, and 44.8% of military personnel. The ionized calcium levels were decreased in 29.4, 50.0, and 67.2% of surveyed individuals, while the iron levels were decreased in 2.0, 1.9, and 3.4%. Elevated potassium (23.5, 29.6, and 8.6%), sodium (32.7 and 27.6% of individuals serving in the Subarctic and temporary climate zones) and total calcium (42.6% of individuals serving in the Subarctic zone) levels were reported. In the Arctic zone, the servicemen worked indoors and outdoors (heavy labour), while in the Subarctic and temporary climate zones they worked indoors (hard labour). In the Arctic zone, meals were organized consisting of the delivered canned foods (general military ration, 4466.7 ± 230.7 kcal/day), while in other zones it was homemade food with the disturbed eating pattern, inadequate consumption of fresh vegetables and fruits. The study updates the directions for prevention of health problems in the military personnel serving in the extreme habitat and working conditions: estimation of body's vitamin and mineral balance; optimization of the diet with the vegetable protein food products; raising awareness about the issues of individual diet and the use of vitamin and mineral supplements; developing formulations of multicomponent food products for adjustment of body's vitamin and mineral balance.

Keywords: Arctic, Subarctic, temperate climate zone, male military personnel, vitamins, minerals

ОЦЕНКА СОДЕРЖАНИЯ МИКРОНУТРИЕНТОВ В ОРГАНИЗМЕ ВОЕННОСЛУЖАЩИХ, ПРОХОДЯЩИХ СЛУЖБУ В РАЗЛИЧНЫХ КЛИМАТИЧЕСКИХ ПОЯСАХ РОССИИ

Д. А. Нарутдинов[1], Р. С. Рахманов[2] ✉, Е. С. Богомолова[2], С. А. Разгулин[2], А. В. Истомин[3], Д. А. Шуркин[1]

[1] Красноярский государственный медицинский университет имени профессора В. Ф. Войно-Ясенецкого, Красноярск, Россия

[2] Приволжский исследовательский медицинский университет, Нижний Новгород, Россия

[3] Федеральный научный центр гигиены имени Ф. Ф. Эрисмана, Мытищи, Россия

Недостаток витаминов и минералов в организме способствует развитию приобретенных дефицитных состояний. Цель исследования — оценка содержания микронутриентов в организме военнослужащих, проходящих службу в различных климатических поясах России. У военнослужащих в арктическом (n = 54), субарктическом (n = 57) и умеренном (n = 58) поясах в плазме крови определяли витамины (D по 25 OH витамина D, B_{12}, B_9), минеральные вещества (K, Na, Ca общий и ионизированный, P, Mg, Fe), оценивали условия работ и питания. Значения 25 OH витамина D составили 24,06 ± 6,95, 21,5 ± 12,1(p_{1-2} = 0,003) и 27,2 ± 15,2 (p_{1-2} = 0,423, p_{1-3} = 0,032) нг/мл; дефицит и недостаточность выявлены у 82,3, 86,5 и 63,8% военнослужащих. Уровни кобаламина составляли 96,46 ± 20,6, 111,7 ± 59,4 (p_{1-2} = 0,046) и 125,7 ± 63,2 (p_{1-2} = 0,002, p_{1-3} = 0,334) пмоль/л; значения ниже 148 пмоль/л были определены у 100,0, 73,6 и у 67,2% обследованных. Фолаты составляли 3,4 ± 0,4, 3,52 ± 1,54 (p_{1-2} = 0,657) и 6,49 ± 6,21 (p_{1-2} = 0,001, p_{1-3} = 0,009) нг/мл; снижение их уровня имело место у 89,8, 81,3 и 44,8% военнослужащих. Уровень ионизированного кальция был снижен у 29,4, 50,0 и 67,2% обследованных, железа — у 2,0, 1,9 и 3,4%. Повышался уровень уровень калия (у 23,5, 29,6 и 8,6%), натрия (у 32,7 и 27,6% проходящих службу в Субарктике и умеренном поясе) и общего кальция (у 42,6% проходящих службу в Субарктике). В Арктике военнослужащие выполняли работы в помещениях и на открытой территории (тяжелый труд), в Субарктике и умеренном поясе — в помещениях (напряженный труд). В Арктике организовано питание завозными консервированными продуктами (общевойсковой паек, 4466,7 ± 230,7 ккал/сутки), в иных условиях — домашнее с нарушениями режима, недостаточным потреблением свежих овощей и фруктов. Исследование актуализирует направления профилактики нарушений здоровья у военнослужащих, проходящих службу в экстремальных условиях обитания и труда: оценка витаминно-минерального баланса организма; оптимизация питания продуктами белково-растительного происхождения; повышение осведомленности по вопросам индивидуального питания и приема витаминно-минеральных препаратов; разработка рецептур многокомпонентных продуктов питания для коррекции витаминно-минерального баланса организма.

Ключевые слова: Арктика, Субарктика, умеренный климатический пояс, военнослужащие-мужчины, витамины, минеральные вещества

The need to ensure national security in the Arctic zone (Arctic and Subarctic) of the Russian Federation (RF) determines the permanent presence of military personnel being part of the strategic deterrence forces aimed to prevent aggression against the RF and its allies. The presence of military personnel is also related to the increase of conflict potential in the Arctic, the need to develop the Northern Sea Route as a globally competitive national transport communication system [1, 2]. The Arctic zone is characterized by extreme weather and climatic conditions, underdeveloped infrastructure, both transport and social [3, 4].

The human body's need for micronutrients (vitamins and minerals) increases when working in such conditions [5–7]. Insufficient intake of vitamins and minerals contributes to the development of acquired deficient conditions, such as B_{12} and/or folate deficiency, iron deficiency anemia [8–10]. Vitamin D deficiency manifests itself in the negative impact on the human calcium, magnesium, and phosphate metabolism, immune status, and mental health [11–14]

The study was aimed to estimate micronutrient levels in the military personnel serving in various climatic zones of Russia.

METHODS

The study was carried out in three climatic zones in the Krasnoyarsk Territory: Arctic (group 1), Subarctic (group 2), and temporary climate (continental climate) (group 3) zones. Inclusion criteria: submitted informed consent, no contraindications for serving in the regions of Far North (for the Arctic and Subarctic zones), health group 1 or 2, similar duties performed by military personnel residing in all climatic zones. Exclusion criteria: acute disorder or exacerbation of chronic disease, self-administration of vitamin and mineral supplements within a month before inclusion in the study or during the period of monitoring.

The study involved male military personnel. The samples were large: 54 (group 1), 57 (group 2), and 58 (group 3) individuals. The age of military personnel serving in the Arctic was 35.7 ± 0.57 years, in the Subarctic it was 34.2 ± 0.9 years (p_{1-2} = 0.156), and in the temporary climate zone it was 35.6 ± 0.79 years (p_{1-3} = 0.452, p_{2-3} = 0.241).

When conducting a routine check-up in summer, plasma levels of vitamin D, B_{12} (cobalamin), B_9 (folic acid), and minerals (potassium, sodium, total and ionized calcium, inorganic phosphorus, magnesium, iron) were determined in the military personnel.

The body's vitamin D status was characterized by 25(OH) D, the intermediate product of its transformation, the levels of which were determined using the AB SCIEX QTRAP 5500 mass spectrometer (SCIEX; Germany). Assessment criteria: < 10 ng/mL — severe deficiency, 10–20 ng/mL — deficiency, 20–30 ng/mL — insufficiency, 30–100 ng/mL — optimal levels [15, 16].

The cobalamin levels were determined using the ARCHITECT i2000 automated immunoassay analyzer (Abbott; USA). The normal range was 25–165 pmol/L. Furthermore, the total serum cobalamin levels < 148 pmol/L were considered as vitamin B_{12} deficiency: with this value the B_{12} deficiency diagnosis sensitivity was 97% [17].

The folic acid levels were determined by tandem mass spectrometry using the AD SCIEX QTRAP 5500 system (SCIEX; Germany). The reference range was 5.0–9.0 ng/mL [9].

The total calcium, inorganic phosphorus, magnesium, iron levels were assessed using the AU 5800 analyzer (Beckman Coulter; USA). The potassium, sodium, ionized calcium levels were determined with the AVL9180 electrolyte analyzer (Roche; USA).

The working regime was assessed.

In the Arctic, catering was provided in accordance with the standard No. 1 (general military ration) with provision of addition food supplies in the regions of Far North [18]. Food was brought during the navigation season for the whole year. Vegetables and fruit were canned or dried. Meltwater obtained from snow was used for cooking. The eating pattern and the rate of food consumption were assessed in the Subarctic and temporary climate zones (questionnaire survey).

Primary data were entered in the MS Excel spreadsheet (Microsoft; USA). The spreadsheet was processed using the Statistica 6.1 software package (StatSoft; USA). The sample distributions were tested for normality: the distributions for vitamins, potassium, ionized calcium, and iron were non-normal, while the distributions for total calcium, phosphorus, magnesium, and sodium were normal. We determined mean (M) and standard deviation (σ) for parametric, median (Me) and interquartile range (Q_{25}–Q_{75}) for nonparametric data. Significance of differences between various groups of servicemen was determined using the Student's t-test for independent parametric (normally distributed) data and the Mann–Whitney U test for nonparametric (non-normally distributed) data for the probability $p \leq 0.05$.

RESULTS

The average 25(OH)D levels were within the range considered to indicate insufficiency. Furthermore, the lowest value was reported for individuals of group 2: it was significantly lower compared to the values of groups 1 and 3 (by 11.9 and 26.5%, respectively). The differences between the values of groups 1 and 3 were non-significant.

The average vitamin B_{12} levels were within the reference range. The lowest values that were significantly different from the data obtained for groups 2 and 3 were reported in group 1: these were 15.8 and 30.3% lower, respectively. The differences in the indicators determined in the individuals serving in the Subarctic and temporary climate zones were non-significant.

The average B_9 levels were within normal only in members of group 3. This indicator was significantly higher (by 90.9 and 84.4%, respectively), than in groups 1 and 2. In individuals of groups 1 and 2, the average values were below the reference range and showed no significant differences. However, the upper limit of the deviation from the mean in group 1 indicated the absence of individuals with optimal levels of this vitamin, while in group 2 it indicated the presence of such individuals (Table 1).

Plasma levels of potassium were within normal in members of all three groups. Furthermore, the differences between the values of groups 1 and 3 were non-significant, and the highest value that significantly differed (by 6.1 and 4.3%, respectively) was reported for members of group 2.

The sodium levels of group 1 were within the reference range, while the values of groups 2 and 3 were above the upper end of normal range (146.86 and 146.95 mmol/L). The average levels of groups 2 and 3 were significantly higher than that of group 1 (by 2.6 and 2.0%).

Based on the deviation from the mean, the magnesium levels were slightly above the upper end of normal range only in group 2, the levels of other groups were within normal. The average magnesium level of group 2 was the highest: it was significantly higher compared to the values reported for groups 1 (by 9.6%) and 2 (by 7.1%). The value of group 3 was also 2.4% higher than that of group 1.

The ionized calcium levels were the same in groups 2 and 3, however, these significantly differed from the level of group 1

Table 1. Plasma levels of vitamins in the military personnel serving in various climatic zones (M ± σ)

Vitamins, reference ranges	Groups monitored, abs.		
	1	2	3
25(OH)D, 30.0–100 ng/mL	24.06 ± 6.95	21.5 ± 12.1 0.003*	27.2 ± 15.2 0.423**/0.032***
Cobalamin 25.0–165.0 pmol/L	96.46 ± 20.6	111.7 ± 59.4 0.046*	125.7 ± 63.2 0.002**/0.334***
Folic acid, 5.0–9.0 ng/mL	3.4 ± 0.4	3.52 ± 1.54 0.657*	6.49 ± 6.21 0.001**/0.009***

Note: * — significance of differences between values of groups 1 and 2; ** — significance of differences between values of groups 1 and 3; *** — significance of differences between values of groups 2 and 3.

(were 2.6% lower). The deviations from the mean indicated the presence of individuals with the decreased body's levels of ionized calcium in each group.

The lowest total calcium level was reported for group 1: it was significantly lower, than in groups 2 and 3 (by 16.8 and 7.3%, respectively). The value of group 3 was higher, than the value of group 1, but significantly lower, than the value of group 2. The upper end of the deviation from the mean of group 2 indicated the presence of individuals with the blood total calcium levels higher than normal.

The average inorganic phosphorus levels were within normal in all the studied groups. Furthermore, the lowest value was reported for group 1, group 3 ranked second. The value of group 2 was 45.0% higher, than the value of group 1 (p = 0.001), and 11.5% higher, than the value of group 3 (p = 0.001).

The iron levels were within normal in all the groups; the lowest value was reported for members of group 1: significant differences from the values of groups 2 and 3 were 25.7 and 12.0%, respectively. The value of group 2 was higher, than the value of group 3 (Table 2).

It was found out that there were individuals with severe vitamin D deficiency in groups 2 and 3. In general, the proportions of individuals with optimal levels of this vitamin among military personnel serving in the Arctic and Subarctic zones showed minor differences, but were 1.9–2.4 lower than that among those serving in the continental climate. As for cobalamin and folic acid levels, members of group 3 seemed to be the most prosperous: the proportion of individuals with the B$_{12}$ levels below 148 pg/mL was lower (by 32.8 and 6.4%, respectively), and the values for B$_9$ were 45.0 and 36.5% lower, than in other groups.

In groups 1 and 2, individuals were found with the potassium levels higher than normal. As for excess sodium, groups 2 and 3 stood out. The differences in the proportions of individuals with various magnesium levels turned out to be interesting. Thus, it was lower than normal in almost a fifth of group 1, individuals with the magnesium levels higher than normal were found in group 2, while in group 3 there were individuals with the magnesium levels on the lower end of normal. Significant differences were revealed, when assessing individual ionized calcium levels: the proportions of individuals with low ionized calcium levels in the Subarctic and temporary climate zones were 1.7 and 1.5 times higher than the proportion in the Arctic zone. Given the fact that the ionized calcium level was on the lower end of normal range in a fifth of group 3 (1.15 mmol/L), the greatest imbalance was found in this group. Excess total calcium levels were reported for group 2; there were minor proportions of individuals with low iron levels in each group, while individuals with low phosphorus levels were found in group 3 only (Table 3).

The work order of male military personnel serving in the Arctic zone envisaged the indoor day duty with a 2-day interval (hard labour). During intervals between the indoor tasks they were engaged in activities in an open area for 4–5 h (hard labour). The work order in the Subarctic and temporary climate zones represented the 5–6-day (unofficially) indoor work with the unregulated timing; Sunday was a day off. Sometimes, Saturday was made a day off.

In the Arctic, meals were organized in accordance with the standard established for such conditions [18], no vitamin supplementation was provided. In the Subarctic and temporary climate zones, individual homemade meals and meals at public

Table 2. Plasma levels of minerals in the military personnel serving in various climatic zones (M ± σ for parametric and Me (Q25–Q75) for nonparametric data)

Minerals, reference ranges	Groups monitored, abs.		
	1	2	3
Potassium, 3.5–5.1 mmol/L	4.6 (4.1–5.1)	4.8 (4.55–5.15) 0.015*	4.7 (4.6–4.8) 0.415**/0.023***
Sodium, 136–145 mmol/L	140.5 ± 2.59	144.1 ± 2.76 0.001*	143.3 ± 3.65 0.001**/0.246***
Magnesium, 0.66–1.03 mmol/L	0.83±0.07	0.91 ± 0.13 0.001*	0.85 ± 0.1 0.001**/0.004
Ionized calcium, 1.15–1.35 mmol/L	1.18 (1.14–1.2)	1.16 (1.12–1.2) 0.043*	1.15 ((1.1–1.8) 0.033**/0.339***
Total calcium, 2.02–2.6 mmol/L	2.2 ± 0.06	2.57 ± 0.21 0.001*	2.36 ± 0.14 0.001**/0.001
Inorganic phosphorus, 0.7–1.8 mmol/L	0.8 ± 0.04	1.16 ± 0.21 0.001*	1.04 ± 0.17 0.001**/0.01***
Iron, 9.5–30 µmol/L	17.4 (14.56–19.26)	20.05 (16.35–25.92) 0.001*	18.4 (13.8–22.7) 0.035**/0.011***

Note: * — significance of differences between values of groups 1 and 2; ** — significance of differences between values of groups 1 and 3; *** — significance of differences between values of groups 2 and 3.

Table 3. Characteristics of the vitamin and mineral levels being outside the normal range in the comparison groups (%)

Indicators	Groups monitored		
	1	2	3
Vitamins			
25(OH)D: Severe deficiency Deficiency Insufficiency Optimal levels	0 29.4 52.9 17.7	5.8 46.1 34.6 13.5	3.4 39.7 24.1 32.8
Cobalamin, < 148 pg/mL	100	73.6	67.2
Folic acid, lower than normal	89.8	81.3	44.8
Minerals			
Potassium, higher than normal	23.5	29.6	8.6
Sodium, higher than normal	0	32.7	27.6
Magnesium	19.6 (lower than normal)	7.4 (higher than normal)	6.9 (low end of normal range)
Ionized calcium, lower than normal	29.4	50	44.8 and 22.4 (low end of normal range)
Total calcium	0	42.6% (higher than normal)	0
Phosphorus, lower than normal	0	0	1.7
Iron, lower than normal	2	1.9	3.4

catering enterprises were organized (96.0% had lunch). The frequency of meals was as follows: lunch and dinner in 52.7%, breakfast, lunch, and dinner in 47.3%. Fresh vegetables, greens, fruits were consumed no more than three times per week. Some respondents noted that they sometimes used vitamin supplements on their own, and preference was given to the vitamin D-containing formulations.

DISCUSSION

It is well known that the changes in blood composition and erythrocyte characteristics occur under conditions of the Far North: erythrocyte counts increase, hemoglobin levels decrease, and iron deficiency anemia develop in response to cold exposure and hypoxia that disturb pulmonary ventilation [19, 20]. Furthermore, an important role in hematopoiesis is played by vitamins B_{12} and B_9 (interrelated vitamins), as well as iron [21–23]. It should be noted that all the earlier reported studies were performed under extreme cold exposure. Our study was conducted in summer, which ruled out the effects of extremely low temperatures. Furthermore, the available literature provides no comparative analysis of the indicators we have assessed in individuals performing activities in three climatic zones, as well as in individuals engaged in outdoor and indoor activities, who have different eating patterns.

In our study, plasma cobalamin levels of males of three groups were within the reference range. However, according to the literature data, the cobalamin levels were decreased in a significant proportion of individuals, with predominance in the Arctic [17]. Furthermore, low folic acid levels were revealed in the significant proportion of individuals, with predominance in the Far North.

The findings suggest that nutrition plays a role in supplying the body with the above vitamins. Thus, the energy value of the general military ration used by military personnel in the Arctic is 4466.7 ± 230.7 kcal/day. Vegetables are represented by canned potatoes, carrots, cabbage (including sauerkraut), beets, onions, pickled tomatoes, and cucumbers. The ration includes fruit and berry juices (apple, grape, plum), canned vegetables (green peas, squash caviar), dried fruits (apples, plums, grapes, apricots). However, some authors note that the possible deficit of vitamins in the described rations is among

pressing issues of food supply. According to the research data, even the short-term physical exertion combined with low temperature of the environment and sub-caloric diet can result in body's vitamin C deficiency. Disturbances of the vitamin C, vitamin B and mineral complex metabolism can occur under exposure to low temperatures [6, 7]. Our study revealed vitamin B_9 and B_{12} deficiency in all groups of military personnel. The data on vitamin B_9 insufficiency in the military personnel serving in the Subarctic and temporary climate zones suggest inadequate consumption of fresh plant foods.

Iron, plasma levels of which were within normal in all surveyed individuals, is also required for normal hematopoiesis. However, individuals with low iron levels were found in each group, which suggested the increased body's demand for this mineral.

Thus, the causes of erythropoiesis disorders occurring under conditions of the Far North can include cobalamin and folic acid insufficiency, as well as probable high demand for iron.

The climatic factors of the Far North are characterized by low ultraviolet solar radiation that contributes to body's vitamin D insufficiency [24, 25]. In our study, vitamin D deficiency and insufficiency were found in 82.3 and 86.5% of individuals serving under such conditions, respectively. It is interesting that the proportion in the Subarctic was larger, than in the Arctic. Furthermore, the proportion of individuals with vitamin D severe deficiency and deficiency was 1.8 times higher in the Subarctic. Apparently, this was associated with working environment: in the Arctic military personnel spent much time outdoors, while in the Subarctic they were engaged in indoor activities.

In the temporary climate zone 67.2% of surveyed individuals also had insufficient vitamin D, which was probably due to indoor activities.

The fact attracted attention that vitamin D deficiency was detected in summer in all three climatic zones.

It is well-known that vitamin D status of the body is strongly associated with the phosphate, calcium, and magnesium metabolism [26, 27]. Magnesium contributes to activation of vitamin D that regulates calcium and phosphate homeostasis. All the enzymes that metabolize vitamin D need magnesium engaged in the enzymatic reactions occurring in the liver and kidney as a co-factor [14]. Our findings suggest low magnesium levels in a fifth of individuals serving in the Arctic, as well as low

ionized calcium levels in a third; low ionized calcium levels or the levels on the lower end of the normal range were determined in a half of assessed individuals serving in the Subarctic and temporary climate zones. Furthermore, imbalance of blood potassium and sodium levels was revealed in the Subarctic and temporary climate zones, while imbalance of potassium levels was revealed in the Arctic. Perhaps, magnesium deficiency contributed to the potassium level imbalance, and the decreased magnesium levels were associated with severe emotional stress [28]. The possible causes of such deficiency include the low mineral content drinking water obtained from melt snow. The water contained minimal amounts of iron, zinc, copper, molybdenum essential for human body functioning and engaged in biological processes [29].

Thus, our study updates the directions for prevention of health problems in the military personnel serving in the extreme working conditions:

– the need to estimate body's vitamin and mineral balance in both extreme habitat conditions (Arctic, Subarctic zones) and the temporary climate zone;

– optimization of the diet with the vegetable protein/plant food products with high content of bioactive substances (for catering organized in the Arctic) and raising the military personnel awareness about the issues of individual diet (to increase body's vitamin content) and the use of vitamin and mineral supplements containing cobalamin, folic acid, vitamin D;

– developing formulations of multicomponent food products for adjustment of body's vitamin and mineral balance in extreme habitat conditions.

CONCLUSIONS

1. In the Arctic and Subarctic, vitamin D deficiency and insufficiency in summer were diagnosed in 82.3 and 86.5% of male military personnel. The indoor working conditions determined the vitamin D deficiency severity in both Subarctic and temporary climate zones (vitamin D severe deficiency and deficiency were revealed in 51.9 and 43.1% vs. 29.4% among individuals in the Arctic working in the open areas). 2. In the Far North, the body's demand for vitamins B_9 and B_{12} is increased, which is indicated by cobalamin deficiency found in 100.0% of military personnel in the Arctic and 73.6% in the Subartic zone, as well as by folic acid deficiency (in 89.8 and 81.3%, respectively, vs. 67.2 and 44.8% in the temporary climate zone). This represents the risk factor of erythropoiesis disorder. 3. Imbalance of minerals in the military personnel serving in three studied climatic zones is characterized by low ionized calcium levels (in 29.4, 50.0, and 67.2%, respectively), decreased iron levels (in 2.0, 1.9, and 3.4%), increased potassium levels (in 23.5, 29.6, and 8.6%), excess sodium in the Subarctic and temporary climate zones, excess total calcium in the Subarctic.

References

1. Ukaz Prezidenta RF ot 27 fevralja 2023 g. No. 126 "O vnesenii izmenenij v Strategiju razvitija Arkticheskoj zony Rossijskoj Federacii i obespechenija nacional'noj bezopasnosti na period do 2035 goda, utverzhdennuju Ukazom Prezidenta Rossijskoj Federacii ot 26 oktjabrja 2020 g. No. 645". Russian.
2. Ukaz Prezidenta RF ot 31 ijulja 2022 g. No. 512 "Ob utverzhdenii Morskoj doktriny Rossijskoj Federacii". Russian.
3. Ukaz Prezidenta RF ot 26 oktjabrja 2020 g. No. 645 "O Strategii razvitija Arkticheskoj zony Rossijskoj Federacii i obespechenija nacional'noj bezopasnosti na period do 2035 goda" (s izmenenijami i dopolnenijami). Russian.
4. Ukaz Prezidenta RF ot 5 marta 2020 g. No. 164 "Ob Osnovah gosudarstvennoj politiki Rossijskoj Federacii v Arktike na period do 2035 goda".
5. Metodicheskie rekomendacii MP 2.3.1.0253-21 "Normy fiziologicheskih potrebnostej v jenergii i pishhevyh veshhestvah dlja razlichnyh grupp naselenija Rossijskoj Federacii". M., 2021; 72 p. Russian.
6. Krivcov AV, Kirichenko NN, Ivchenko EV, Smetanin AL, Andrijanov AI, Sorokoletova EF, et al. Fiziologo-gigienicheskaja harakteristika pitanija i vodosnabzhenija voinskogo garnizona v Arktike. Vestnik Rossijskoj voenno-medicinskoj akademii. 2015; 4 (52): 165–8. Russian.
7. Makov VA. Osobennosti prodovol'stvennogo obespechenija voennosluzhashhih, pro-hodjashhih voennuju sluzhbu v arkticheskoj zone Rossijskoj Federacii. Rossijskaja Arktika. 2018; (3): 51. DOI: 10.24411/2658-4255-2018-00011. Russian.
8. Vitamin B12 deficitnaja anemija. Klinicheskie rekomendacii. Minzdrav RF. 2021-2022-2023. Available from: http://disuria.ru/_ld/10/1065_kr21D51MZ.pdf?ysclid=lsvh29b7gt686236909. Russian.
9. Folievodeficitnaja anemija. Klinicheskie rekomendacii. Minzdrav RF. 2021. Available from: https://кр-рф-2021/17023?ysclid=lsvgxmqsxv153502174. Russian.
10. Zhelezodeficitnaja anemija. Klinicheskie rekomendacii. Minzdrav RF. 2021. Available from: https://webmed.irkutsk.ru/doc/pdf/kr669.pdf. Russian.
11. Lanec IE, Gostinishheva EV. Sovremennye vzgljady na rol' vitamina D v organizme cheloveka. Nauchnoe obozrenie. Medicinskie nauki. 2022; (5): 39–45. Russian.
12. Kostromin AV, Panova LD, Malievskij VA, Kryvkina NN, Jarukova EV, Akulshina AV, et al. Sovremennye dannye o vlijanii vitamina D na immunitet i rol' v profilaktike ostryh respiratornyh infekcij. Sovremennye problemy nauki i obrazovanija. 2019; (5). Available from: https://science-education.ru/ru/article/view?id=29186. Russian.
13. Kikuta J, Ishii M. The effects of vitamin D on immune system and inflammatory diseases. Biomolecules. 2021; 11 (11): 1624. DOI: 10.3390/biom11111624.
14. Uwitonze AM, Razzaque MS. Role of magnesium in vitamin D activation and function. J Am Osteopath Assoc. 2018; 118 (3): 181–9. DOI: 10.7556/jaoa.2018.037.
15. Pigareva EA, Rozhinskaja LJa, Belaja ZhE, Dzeranova LK, Karonova TL, Ilin AV, et al. Klinicheskie rekomendacii Rossijskoj associacii jendokrinologov po diagnostike, lecheniju i profilaktike deficita vitamina D vzroslyh. Problemy jendokrinologii. 2016; (4): 60–84. DOI: 10.14341/probl201662460-84. Russian.
16. Maganeva IS, Pigarova EA, Shulpekova NV, Dzeranova LK, Eremkina AK, Miljutina AP, et al. Ocenka fosforno-kal'cievogo obmena i metabolitov vitamina D u pacientov s pervichnym giperparatireozom na fone boljusnoj terapii kolekal'ciferolom. Problemy jendokrinologii. 2021; 67 (6): 68–79. DOI: 10.14341/probl12851. Russian.
17. Krasnovskij AL, Grigorev SP, Alehina RM, Ezhova IS, Zolkina IV, Loshkareva EO. Sovremennye vozmozhnosti diagnostiki i lechenija deficita vitamina B12. Klinicist. 2016; 10 (3): 15–25. DOI: 10.17 650/1818-8338-2016-10-3-15-25. Russian.
18. Postanovlenie Pravitel'stva RF ot 29 dekabrja 2007 g. No. 946 "O prodovol'stvennom obespechenii voennosluzhashhih i nekotoryh drugih kategorij lic, a takzhe ob obespechenii kormami (produktami) shtatnyh zhivotnyh voinskih chastej i organizacij v mirnoe vremja" (v redakcii ot 18 sentjabrja 2020 g., No. 1484). Russian.
19. Balashova SN, Samodova AV, Dobrodeeva LK, Belisheva NK. Hematological reactions in the inhabitants of the Arctic on a polar night and a polar day. Immun Inflamm Dis. 2020; 8 (3): 415–22. DOI: 10.1002/iid3.323.
20. Nagibovich OA, Uhovskij DM, Zhekalov AN, Tkachuk NA, Arzhavkina LG, Bogdanova EG, et al. Mehanizmy gipoksii v Arkticheskoj zone Rossijskoj Federacii, Vestnik Rossijskoj Voenno-medicinskoj akademii. 2016; 2 (54): 202–5. Russian.

21. Costanzo G, Sambugaro G, Giulia Mandis G, Sofia Vassallo S, Scuteri A. Pancytopenia secondary to vitamin B12 deficiency in older subjects. J Clin Med. 2023; 12 (5): 2059. DOI: 10.3390/jcm12052059.

22. Torrez M, Chabot-Richards D, Babu D, Lockhart E, Foucar K. How I investigate acquired megaloblastic anemia. Int J Lab Hematol. 2022; 44 (2): 236–47. DOI: 10.1111/ijlh.13789.

23. De Almeida JG, Gudgin E, Besser M, Dunn WG, Cooper J, Haferlach T, et al. Computational analysis of peripheral blood smears detects disease-associated cytomorphologies. Nat Commun. 2023; 14 (1): 4378. DOI: 10.1038/s41467-023-39676-y.

24. Kostrova GN, Maljavskaja SI, Lebedev AV. Obespechennost' vitaminom D zhitelej g. Arhangel'ska v raznye sezony goda. Zhurnal mediko-biologicheskih issledovanij. 2022; 10 (1): 5–14. DOI: 10.37482/2687-1491-Z085. Russian.

25. Korobicyna RD, Sorokina TJu. Status vitamina D naselenija Rossii reproduktivnogo vozrasta za poslednie 10 let. Rossijskaja Arktika. 2022; (18): 44–55. DOI: 10.24412/2658-4255-2022-3-44-55. Russian.

26. Jureva JeA, Osmanov IM, Vozdvizhenskaja ES, Shabelnikova EI. Obmen kal'cija i fosfatov v norme i pri patologii u detej. Praktika pediatra. 2021; (4): 24–30. Russian.

27. Berkovskaja MA, Kushhanashhova DA, Sych JuP, Fadeev VV. Sostojanie fosforno-kal'cievogo obmena u pacientov posle bariatricheskih operacij i rol' vospolnenija deficita vitamina D v profilaktike i lechenii posleoperacionnyh kostno-metabolicheskih narushenij. Ozhirenie i metabolizm. 2020; 17 (1): 73–81. DOI: 10.14341/omet12306. Russian.

28. Skalnyj AV. Mikrojelementozy: bodrost', zdorov'e, dolgoletie. 4-e izd., pererab. i dop. M.: Pero, 2019; 295 p. Russian.

29. Rahmanov RS, Narutdinov DA, Bogomolova ES, Razgulin SA, Alikberov MH, Neprjahin DV. Ocenka reakcii organizma voennosluzhashhih v Arktike po pokazateljam krovi v uslovijah vodopol'zovanija mestnymi resursami. Zdorov'e naselenija i sreda obitanija. 2023; 31 (7): 48–54. DOI: 10.35627/2219-5238/2023-31-7-48-54. Russian.

Литература

1. Указ Президента РФ от 27 февраля 2023 г. № 126 «О внесении изменений в Стратегию развития Арктической зоны Российской Федерации и обеспечения национальной безопасности на период до 2035 года, утвержденную Указом Президента Российской Федерации от 26 октября 2020 г. № 645».

2. Указ Президента РФ от 31 июля 2022 г. № 512 «Об утверждении Морской доктрины Российской Федерации».

3. Указ Президента РФ от 26 октября 2020 г. № 645 «О Стратегии развития Арктической зоны Российской Федерации и обеспечения национальной безопасности на период до 2035 года» (с изменениями и дополнениями).

4. Указ Президента РФ от 5 марта 2020 г. № 164 «Об Основах государственной политики Российской Федерации в Арктике на период до 2035 года».

5. Методические рекомендации МР 2.3.1.0253-21 «Нормы физиологических потребностей в энергии и пищевых веществах для различных групп населения Российской Федерации». М., 2021; 72 с.

6. Кривцов А. В., Кириченко Н. Н., Ивченко Е. В., Сметанин А. Л., Андриянов А. И., Сороколетова Е. Ф. и Физиолого-гигиеническая характеристика питания и водоснабжения воинского гарнизона в Арктике. Вестник Российской военно-медицинской академии. 2015; 4 (52): 165–8.

7. Маков В. А. Особенности продовольственного обеспечения военнослужащих, проходящих военную службу в арктической зоне Российской Федерации. Российская Арктика. 2018; (3): 51. DOI: 10.24411/2658-4255-2018-00011.

8. Витамин В12 дефицитная анемия. Клинические рекомендации. Минздрав РФ. 2021-2022-2023. URL: http://disuria.ru/_ld/10/1065_kr21D51MZ.pdf?ysclid=lsvh29b7gt686236909.

9. Фолиеводефицитная анемия. Клинические рекомендации. Минздрав РФ. 2021. URL: https://кр-рф-2021/17023?ysclid=lsvgxmqsxv153502174.

10. Железодефицитная анемия. Клинические рекомендации. Минздрав РФ. 2021. URL: https://webmed.irkutsk.ru/doc/pdf/kr669.pdf.

11. Ланец И. Е., Гостинищева Е. В. Современные взгляды на роль витамина D в организме человека. Научное обозрение. Медицинские науки. 2022; (5): 39–45.

12. Костромин А. В., Панова Л. Д., Малиевский В. А., Крывкина Н. Н., Ярукова Е. В., Акульшина А. В. и др. Современные данные о влиянии витамина D на иммунитет и роль в профилактике острых респираторных инфекций. Современные проблемы науки и образования. 2019; (5). URL: https://science-education.ru/ru/article/view?id=29186.

13. Kikuta J, Ishii M. The effects of vitamin D on immune system and inflammatory diseases. Biomolecules. 2021; 11 (11): 1624. DOI: 10.3390/biom11111624.

14. Uwitonze AM, Razzaque MS. Role of magnesium in vitamin D activation and function. J Am Osteopath Assoc. 2018; 118 (3): 181–9. DOI: 10.7556/jaoa.2018.037.

15. Пигарева Е. А., Рожинская Л. Я., Белая Ж. Е., Дзеранова Л. К., Каронова Т. Л., Ильин А. В. и др. Клинические рекомендации Российской ассоциации эндокринологов по диагностике, лечению и профилактике дефицита витамина D взрослых. Проблемы эндокринологии. 2016; (4): 60–84. DOI: 10.14341/probl201662460-84.

16. Маганева И. С., Пигарова Е. А., Шульпекова Н. В., Дзеранова Л. К., Еремкина А. К., Милютина А. П. и др. Оценка фосфорно-кальциевого обмена и метаболитов витамина D у пациентов с первичным гиперпаратиреозом на фоне болюсной терапии колекальциферолом. Проблемы эндокринологии. 2021; 67 (6): 68–79. DOI: 10.14341/probl12851.

17. Красновский А. Л., Григорьев С. П., Алехина Р. М., Ежова И. С., Золкина И. В., Лошкарева Е. О. Современные возможности диагностики и лечения дефицита витамина В12. Клиницист. 2016; 10 (3): 15–25. DOI: 10.17 650/1818-8338-2016-10-3-15-25.

18. Постановление Правительства РФ от 29 декабря 2007 г. № 946 «О продовольственном обеспечении военнослужащих и некоторых других категорий лиц, а также об обеспечении кормами (продуктами) штатных животных воинских частей и организаций в мирное время» (в редакции от 18 сентября 2020 г., № 1484).

19. Balashova SN, Samodova AV, Dobrodeeva LK, Belisheva NK. Hematological reactions in the inhabitants of the Arctic on a polar night and a polar day. Immun Inflamm Dis. 2020; 8 (3): 415–22. DOI: 10.1002/iid3.323.

20. Нагибович О. А., Уховский Д. М., Жекалов А. Н., Ткачук Н. А., Аржавкина Л. Г., Богданова Е. Г. и др. Механизмы гипоксии в Арктической зоне Российской Федерации, Вестник Российской Военно-медицинской академии. 2016; 2 (54): 202–5.

21. Costanzo G, Sambugaro G, Giulia Mandis G, Sofia Vassallo S, Scuteri A. Pancytopenia secondary to vitamin B12 deficiency in older subjects. J Clin Med. 2023; 12 (5): 2059. DOI: 10.3390/jcm12052059.

22. Torrez M, Chabot-Richards D, Babu D, Lockhart E, Foucar K. How I investigate acquired megaloblastic anemia. Int J Lab Hematol. 2022; 44 (2): 236–47. DOI: 10.1111/ijlh.13789.

23. De Almeida JG, Gudgin E, Besser M, Dunn WG, Cooper J, Haferlach T, et al. Computational analysis of peripheral blood smears detects disease-associated cytomorphologies. Nat Commun. 2023; 14 (1): 4378. DOI: 10.1038/s41467-023-39676-y.

24. Кострова Г. Н., Малявская С. И., Лебедев А. В. Обеспеченность витамином D жителей г. Архангельска в разные сезоны года. Журнал медико-биологических исследований. 2022; 10 (1): 5–14. DOI: 10.37482/2687-1491-Z085.

25. Коробицына Р. Д., Сорокина Т. Ю. Статус витамина D населения России репродуктивного возраста за последние 10 лет. Российская Арктика. 2022; (18): 44–55. DOI: 10.24412/2658-4255-2022-3-44-55.

26. Юрьева Э. А., Османов И. М., Воздвиженская Е. С., Шабельникова Е. И. Обмен кальция и фосфатов в норме и при патологии у детей. Практика педиатра. 2021; (4): 24–30.

27. Берковская М. А., Кушханашхова Д. А., Сыч Ю. П., Фадеев В. В. Состояние фосфорно-кальциевого обмена у пациентов после бариатрических операций и роль восполнения дефицита витамина D в профилактике и лечении послеоперационных

костно-метаболических нарушений. Ожирение и метаболизм. 2020; 17 (1): 73–81. DOI: 10.14341/omet12306.

28. Скальный А. В. Микроэлементозы: бодрость, здоровье, долголетие. 4-е изд., перераб. и доп. М.: Перо, 2019; 295 с.

29. Рахманов Р. С., Нарутдинов Д. А., Богомолова Е. С., Разгулин С. А., Аликберов М. Х., Непряхин Д. В. Оценка реакции организма военнослужащих в Арктике по показателям крови в условиях водопользования местными ресурсами. Здоровье населения и среда обитания. 2023; 31 (7): 48–54. DOI: 10.35627/2219-5238/2023-31-7-48-54.

METHOD TO ASSESS THE EFFECTS OF BIOACTIVE COMPOUNDS SOLUTIONS ON BLOOD CLOTTING

Manuvera VA[1,2] ✉, Brovina KA[1,2], Bobrovsky PA[1,2], Grafskaia EN[1], Kharlampieva DD[1], Lazarev VN[1,2]

[1] Lopukhin Federal Research and Clinical Center of Physical-Chemical Medicine of the Federal Medical Biological Agency, Moscow, Russia

[2] Moscow Institute of Physics and Technology (National Research University), Dolgoprudny, Moscow Region, Russia

The search for new anticoagulants requires simple and affordable methods for primary determination of their activity. Clotting tests are widely used for laboratory evaluation of the hemostatic system. These are model studies that assess the state of the hemostatic system from a clinical point of view based on the fibrin clot formation time. Reagents and instruments for such tests are produced in Russia, they have low manufacturing cost and are easy to use. However, it is necessary to make a few modifications to the measurement methods to assess the anticoagulant activity. The study was aimed to demonstrate performance of the protocol for testing the solution anticoagulant activity using the modified standard clinical tests involving measurement of the activated partial thromboplastin time (aPTT), prothrombin time (PT), and thrombin time (TT). Reagents for measurement of aPTT, PT, and TT were used, along with the domestically produced heparin and two recombinant anticoagulant proteins from the medicinal leech obtained in our laboratory. Clotting tests were performed with the addition of anticoagulants to the reaction mixture were performed; performance and applicability limits of the methods used were determined. When studying hirudin, heparin, and cysteine-rich anticoagulant of medical leech using measurement of aPTT, TT, and PT, a dose-dependent increase in clotting time was demonstrated. The methods' compatibility with the use of various common components of buffer solutions used in biochemical tests was determined. It was shown that the slightly modified standard blood clotting tests for determination of hemostatic parameters could be used to test new potential anticoagulants.

МЕТОДИКА ОЦЕНКИ ВЛИЯНИЯ РАСТВОРОВ БИОЛОГИЧЕСКИ АКТИВНЫХ ВЕЩЕСТВ НА КОАГУЛЯЦИЮ

В. А. Манувера[1,2] ✉, К. А. Бровина[1,2], П. А. Бобровский[1,2], Е. Н. Графская[1], Д. Д. Харлампиева[1], В. Н. Лазарев[1,2]

[1] Федеральный научно-клинический центр физико-химической медицины имени Ю. М. Лопухина Федерального медико-биологического агентства, Москва, Россия

[2] Московский физико-технический институт (национальный исследовательский университет), г. Долгопрудный, Московская обл., Россия

Поиск новых антикоагулянтов требует простых и недорогих методов первичного определения их активности. Для лабораторной оценки состояния системы гемостаза широко используют клоттинговые тесты, т. е. модельные исследования, оценивающие с клинической точки зрения состояние системы гемостаза по скорости образования фибринового сгустка. Реактивы и приборы для их выполнения производят в России, они имеют низкую себестоимость и просты в применении, однако для исследования активности антикоагулянтов в методики измерения необходимо внести некоторые изменения. Целью работы было показать работоспособность протокола тестирования антикоагуляционной активности растворов с помощью модифицированных стандартных клинических тестов на измерение активированного частичного тромбопластинового времени (АЧТВ), протромбинового времени (ПВ) и тромбинового времени (ТВ). Использовали реактивы для измерения АЧТВ, ТВ и ПВ, а также гепарин отечественного производства и два рекомбинантных белка-антикоагулянта медицинской пиявки, полученные в нашей лаборатории. Проводили клоттинговые тесты с добавлением в реакционную смесь антикоагулянтов, определяли работоспособность и границы применимости использованных методов. При исследовании гирудина, гепарина и цистеин-богатого антикоагулянта медицинской пиявки с помощью измерения АЧТВ, ТВ и ПВ продемонстрировано дозо-зависимое увеличение времени образования сгустков. Определена совместимость методов с использованием некоторых распространенных компонентов буферных растворов, используемых в биохимических исследованиях. Показано, что после небольших модификаций стандартных клоттинговых методов определения параметров гемостаза можно использовать их для тестирования растворов новых потенциальных антикоагулянтов.

Simple, cheap, and well mastered blood clotting tests (activated partial thromboplastin time (aPTT), prothrombin time (PT), and thrombin time (TT)) are used in clinical practice [1–3]. These tests are developed to determine homeostasis effectiveness in blood plasma of patients. aPTT allows one to estimate functioning of the intrinsic coagulation activation pathway, PT measurement is used to determine coagulation in case of extrinsic pathway activation, while TT demonstrates the effectiveness of thrombin-induced fibrinogen activation and fibrin polymerization. When conducting research focused on finding new anticoagulants, there is a need for rapid and affordable *in vitro* testing of the candidate substances. Furthermore, one has to deal

with various complex protein mixtures, extracts, and similar material. At the initial stage of research, simple and affordable primary screening methods are necessary.

The method to determine the effects of potential anticoagulant proteins derived from the medicinal leech (Hirudo medicinalis) has been developed and is used in our laboratory. We provide the measurement protocols used and demonstrate their effectiveness using three substances inhibiting blood clotting. The first substance, the cysteine-rich anticoagulant from the medicinal leech (CRA), is the recently explored [4] anticoagulant protein related to antistasin [5]. The second research object is the recombinant hirudin protein, a well-known anticoagulant from the medicinal leech [6]. The third anticoagulant tested is heparin, an oligosaccharide very commonly used in clinical practice [2, 7].

The study was aimed to demonstrate the efficacy of the testing protocol for assessing the anticoagulant activity of solutions using modified standard clinical tests involving measurement of aPTT, PT, and TT.

METHODS

Equipment

APG4-03-Ph hemostasis analyzer (EMCO; Russia). Disposable coagulometer cuvettes with balls (EMCO; Russia). Measurement was performed using the analyzer optical channel (Optics mode).

Reagents

PG-7/1 reagent kit for determination of aPTT in blood plasma by the clotting method (aPTT test) (RENAM; Russia).

Thrombin-Reagent PG-9A kit for determination of TT (RENAM; Russia).

MLT-Thromboplastin reagent for determination of PT (EMCO; Russia).

KM-1 control plasma (Plasma-N) (RENAM; Russia).

Anticoagulants

The cysteine-rich anticoagulant (CRA) from the medicinal leech [4] and recombinant hirudin (Hir) from the medicinal leech [4] obtained in our laboratory, as well as the solution of medium molecular weight unfractionated sodium heparin (Hep) in the industrially produced ampoules (Synthesis; Russia) were used as anticoagulants. Serial dilutions of anticoagulants were prepared for the study. Anticoagulants were diluted with the 10 mM TrisCl solution, pH 7.5.

Blood clotting tests

When working with anticoagulants, each sample was measured in four replicates in parallel using four coagulometer measurement cells. The mean and standard deviation were calculated for the values obtained. Curves of clot formation time versus anticoagulant concentration were plotted based on the data acquired (see Figure). To determine the effects of various solutions on the measurement results, each sample was measured in two replicates in parallel using two coagulometer measurement cells of one pair. The mean was calculated for the values obtained and entered in the table (see Table).

Activated partial thromboplastin time

The 2X aPTT reagent was prepared for aPTT measurement. For that 2 mL of water were added to the vial with the lyophilized aPTT reagent, which constituted half of the volume recommended for clinical aPTT test. One milliliter of water was added to the vial with the lyophilized control blood plasma, as recommended by the manufacturer. The vials were kept for 30 min at room temperature with occasional stirring until the precipitate was completely dissolved. The calcium chloride solution was poured in the temperature-controlled coagulometer cell to be heated to 37 °C. A total of 50 μL of control plasma, 25 μL of the test solution, and 25 μL of the 2X aPTT reagent were added to the coagulometer cuvette, then the contents of the cuvette was mixed by triple pipetting. A magnetic ball was put in the cuvette; the cuvette was placed in the temperature-controlled timer coagulometer cell for 3 min. After the incubation was over, cuvettes were transferred to the measurement coagulometer cells; 50 μL of the heated calcium chloride were added in the Autostart mode. Clot formation time was recorded.

Thrombin time

The thrombin reagent with the concentration of 6 U/mL was used to determine TT. To prepare the reagent, 2.7 mL of water and 0.3 mL of the concentrated solvent (buffer solution from the kit) were added to the vial containing the lyophilized thrombin. One milliliter of water was added to the vial with the lyophilized control blood plasma, as recommended by the manufacturer. The vials were kept for 30 min at room temperature with occasional stirring until the precipitate was completely dissolved. The thrombin reagent solution was poured in the temperature-controlled coagulometer cell to be heated to 37 °C. A total of 100 μL of control plasma and 50 μL of the test solution were added to the coagulometer cuvette; the contents of the cuvette was mixed by triple pipetting. After that a magnetic ball was put in the cuvette; the cuvette was placed in the temperature-controlled timer coagulometer cell for 3 min. After the incubation was over, cuvettes were transferred to the measurement coagulometer cells; 50 μL of the heated thrombin reagent were added in the Autostart mode. Clot formation time was recorded.

Prothrombin time

The 2X thromboplastin solution was used to determine PT. To prepare the solution, 3 mL of water were added to the vial containing the lyophilized thromboplastin-calcium mixture, which constituted half of the volume recommended for clinical PT test. One milliliter of water was added to the vial with the lyophilized control blood plasma, as recommended by the manufacturer. The vials were kept for 30 min at room temperature with occasional stirring until the precipitate was completely dissolved. The thromboplastin solution as poured in the temperature-controlled coagulometer cell to be heated to 37 °C. A total of 50 μL of control plasma and 50 μL of the test solution were added to the coagulometer cuvette; the contents of the cuvette was mixed by triple pipetting. After that a magnetic ball was put in the cuvette; the cuvette was placed in the temperature-controlled timer coagulometer cell for 3 min. After the incubation was over, cuvettes were transferred to the measurement coagulometer cells; 50 μL of the heated thromboplastin solution were added in the Autostart mode. Clot formation time was recorded.

Statistical analysis

The nonparametric Mann–Whitney U-test and Python (v. 3.12) (Python Software Foundation; USA) were used for statistical
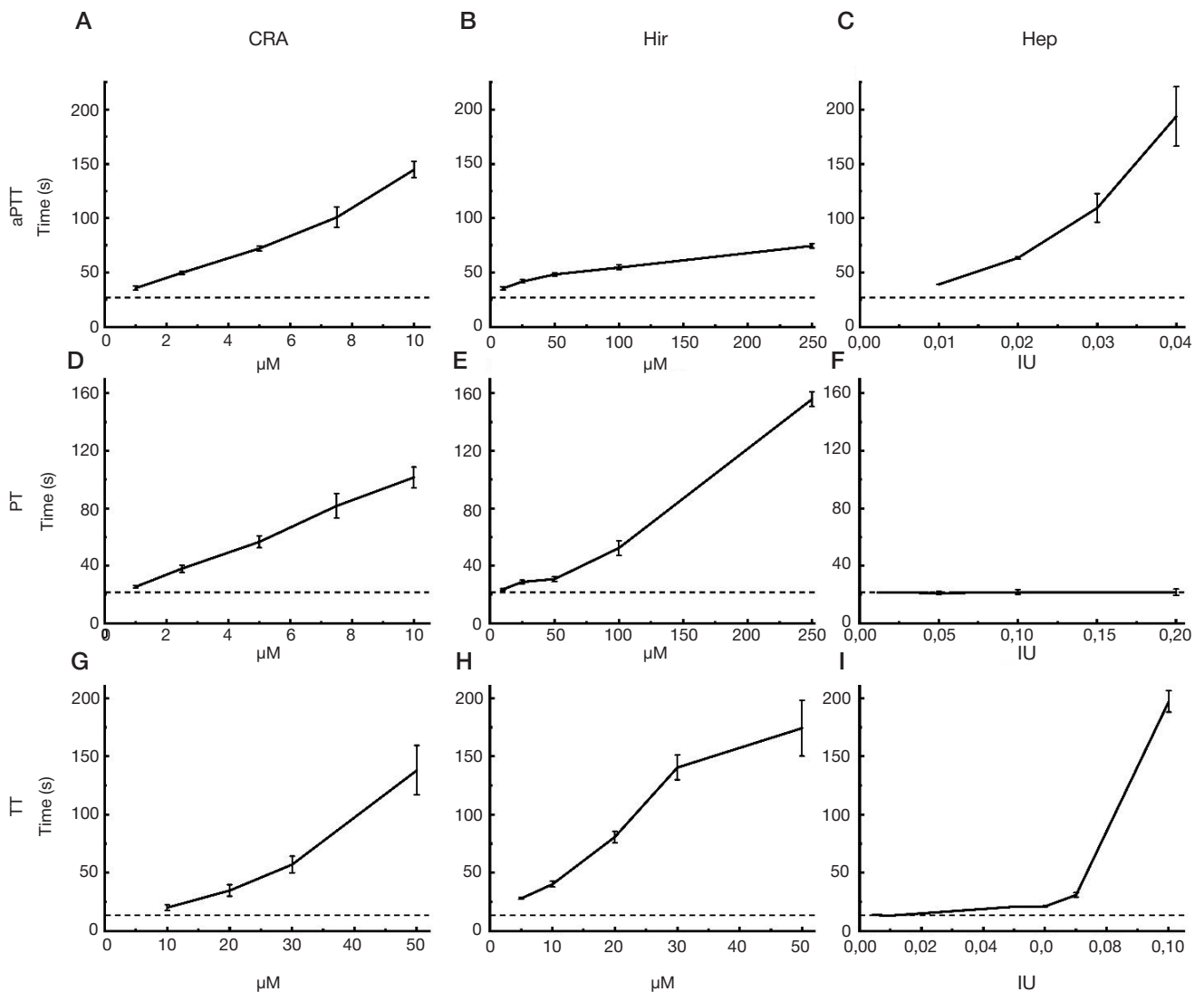
Fig. 1. Results for aPTT, PT, and TT measurements for the solutions of three anticoagulants: cysteine-rich anticoagulant (CRA) derived from the medicinal leech, hirudin (Hir), and heparin (Hep). Concentrations of CRA and Hir are measured in µM of protein in the test solution; the total amount of IU per reaction is provided for Hep. The mean clot formation time for the control sample (10 mM TrisCl, pH = 7.5) is shown as the *dashed line*. The data are provided as the mean values of clot formation time and standard deviations. Four independent measurements per point were performed

analysis when comparing the samples containing test proteins and control plasma.

RESULTS

The aPTT determination results are provided in Fig. 1 A–C. A clear increase in the clot formation time with increasing active substance concentration is reported for all three anticoagulants.

The PT measurement results are provided in Fig. 1D–F. As in case of aPTT measurement, the increase in the reaction mixture coagulation time with increasing concentration is reported for CRA (Fig. 1D) and Hep (Fig. 1E). Heparin that has shown high activity in the aPTT test exerts no activity during TT measurement (Fig. 1F).

The TT measurement results are provided in Fig. 1G–I. All three anticoagulants show a dose-dependent increase in the clot formation time.

To determine compatibility of the reported methods with the common buffer solutions used in biochemical analysis, we examined their effects on the clot formation time for all three tests reported. The results are summarized in the Table. In the majority of cases no effect or negligible effect was observed. However, 1% β-mercaptoethanol prevented coagulation during

aPTT and PT measurement, while the 1M NaCl solution caused a significant increase in the values in all three tests.

DISCUSSION

Boundary applicability conditions are the key parameters for any method. When conducting the experiments, in addition to automatic recording of clot formation time by the device, we performed visual monitoring of the reaction mixture state. When the anticoagulant concentrations in the measurement cuvettes were high, apparent coagulation irregularity, individual clumps and harnesses were observed around the magnetic balls, along with the mobility of balls after the coagulometer sensor activation. In this context the results cannot be considered reliable, so the upper measurement threshold should be limited to a hundred of seconds. Thus, in all three tests the anticoagulant concentrations should be selected so that the clot formation time is about 100 s at the maximum test concentration. If clot formation does not occur within this time during measurement, the sample measured should be further diluted. It should also be noted that reagents and control plasma from different production batches yield slightly different results during measurement of aPTT, TT, and PT. Therefore, it is

Table. Effects of various solutions on the aPTT, TT, and PT determination

Sample/Test	aPTT	TT	PT
Water (K)	28.7 ± 1.0	12.8 ± 0.6	15.9 ± 0.5
PBS[1]	29.7 ± 0.6	18.0 ± 0.4	18.6 ± 0.1
Tris-HCl 100 mM	28.0 ± 1.0	17.4 ± 0.4	17.3 ± 0.3
NaCl 9 g/L	29.1 ± 0.4	17.3 ± 0.3	19.0 ± 1.0
NaCl 1 M	62.0 ± 2.0	114.0 ± 18.0	136.8 ± 0.5
SDS 0.1%	31.0 ± 2.0	13.1 ± 0.7	16.1 ± 0.1
SDS 0.01%	28.5 ± 0.2	12.1 ± 0.8	15.2 ± 0.1
1 M urea	29.0 ± 1.0	33.7 ± 0.1	21.3 ± 0.4
0.1 M urea	28.1 ± 0.7	13.9 ± 0.4	15.7 ± 0.1
β-mercaptoethanol 1%	n. d.[2]	16.0 ± 2.0	n. d.[2]
β-mercaptoethanol 0.1%	33.0 ± 2.0	13.0 ± 2.0	21.8 ± 0.6
Triton X-100 1%	26.0 ± 1.0	13.0 ± 0.1	n. d.[2]
DTT 1 mM	31.0 ± 2.0	14.0 ± 0.4	19.4 ± 0.5

Note: mean clot formation time in seconds ± standard deviation is provided; [1] — phosphate buffer solution (20 mM sodium phosphate, 8 g/L sodium chloride, pH = 7.4); [2] — no clot was formed, no value is available.

strictly necessary to perform all the series of measurements of each sample (or several samples to be compared) and control samples using reagents from the same batch.

Various normalization methods can be used to compare the results obtained at different times using different reagents. For example, the international normalized ratio (INR) is widely used in clinical diagnosis for PT [1–3]. It seems possible to use the relative value (C_S), calculated as a quotient of the clot formation time of the test sample (t_S) to the clot formation time of the control sample (t_C), for screening tests: $CS = t_S/t_C$.

When they suggest to perform three different tests per test sample, the authors assume that the search for substances with unknown characteristics and mechanism of action, the only essential feature of which is the ability to inhibit coagulation, will be conducted. In this regard we believe that it is necessary to use all three tests at once. In such situation the researchers may prefer this or that test, for their own reasons. The differences in the effects of three anticoagulants used in this study are pretty obvious.

An obvious dose-dependent effect is reported for all three test substances in the aPTT test. However, CRA shows the time (Fig. 1A) comparable with that of Hir (Fig. 1B) at the molar concentrations smaller by an order of magnitude. For example, the clot formation time of about 50 s is achieved at the CRA concentration of 2.5 µM in the sample, as for hirudin — only at the concentration of 50 µM. It can be concluded that CRA significantly more effectively inhibits activation of intrinsic blood clotting pathway compared to Hir. Predictably, Hep also effectively inhibits coagulation (Fig. 1C). However, it is impossible to directly compare its specific activity with the activity of the studied proteins, since the concentration of the Hep dosage form is specified in international units (IU) of activity only.

A slightly different pattern is observed for PT measurement (Fig. 1D–F). As for CRA (Fig. 1D) and Hep (Fig. 1E), the increase in the reaction mixture coagulation time with increasing concentration is observed, the same as in the aPTT test. At the same time, heparin that has shown high activity in the aPTT test causes no increase in the clot formation time during TT measurement (Fig. 1F). This is due to the fact that it inhibits

factors Xa and IIa, as well as factors of the intrinsic activation pathway, not directly, but with mediation from antithrombin [7].

When determining TT (Fig. 1G–I), remarkable is that in this case there is a situation opposite to measuring aPTT: Hir (Fig. 1H) shows higher activity, than CRA (Fig. 1G). This may be due to the fact that Hir is a specific inhibitor of thrombin (factor IIa) [6], while CRA inhibits not only thrombin, but also other proteinases of blood clotting cascade [4]. As a result, the CRA activity is more obvious during measurement of aPTT due to cumulative effect. In this case the measurement range of Hep (Fig. 1I) is severely narrowed. When 0.07 IU of Hep are added to the reaction, the coagulation time is 29.3 ± 2.5 s; no full-fledged clot is formed, when 0.1 IU are added to the reaction.

When performing primary search for the substances preventing blood clotting, the researchers often have limited knowledge about their nature and mechanism of action. It is necessary to first detect the active substance and obtain its relatively pure form to thoroughly investigate these aspects. This problem is particularly evident during the study of the complex mixtures of natural origin, such as saliva of blood-sucking animals, secretions, extracts, etc. The researchers can observe manifestations of biological activity, but at this stage do not understand the underlying mechanisms. That is why we think it is reasonable to use three different tests targeting three different parts of blood clotting cascade (intrinsic pathway (aPTT), extrinsic pathway (PT), and terminal phase (TT)) at once. Using three anticoagulants of different nature and properties we have shown that these behave differently in these tests.

During testing the new potential anticoagulants can exist in the form of solutions containing various low molecular weight substances. For example, when studying recombinant anticoagulant proteins, these turn out to be dissolved in buffer solutions, the composition of which depends on the specific extraction method, after the chromatographic purification or refolding. In each specific case, it is strictly necessary to perform control measurements with the buffer solution that is identical to the solution, in which the test substance is dissolved. However, some solutions can be incompatible with the measurement methods used. We tested the effects of some commonly used components of buffer solution used in

biochemical studies on the aPTT, TT, and PT measurement. The results are provided in the Table. In the majority of cases, the impact of the studied solution on the test results was negligible. However, it is impossible to use the solutions with high ionic strength (1M NaCl) in all tests, while strong reducing agents (β-mercaptoethanol) cannot be used when determining aPTT and PT. At the same time, the solutions containing weaker reducing agents (DTT), moderate amounts of detergents (Triton X-100, sodium dodecyl sulfate (SDS)) or 0.1 M urea can be used for measurement.

CONCLUSIONS

The paper provides modifications of methods to determine aPTT, PT, and TT using the common reagents and the domestically produced coagulometer. Modifications include changes in the reagent volume and incubation time and require no additional reagents or equipment for measurement. The methods described can be useful when performing the search for new anticoagulants and studying the effects of various substances on blood clotting.

References

1. Barkagan ZS. Diagnostika i kontroliruemaja terapija narushenij gemostaza. Moskva: OOO "Mediko-tehnologicheskoe predprijatie «N'judiamed», 2008; 292 s. Russian.
2. Winter W, Flax S, Harris N. Coagulation testing in the core laboratory. Laboratory Medicine. 2017; 48 (4): 295–313. Available from: https://doi.org/10.1093/labmed/.
3. Makarov VA, Spasov AA, Plotnikov MB, Belozerskaja GG, Vasileva TM, Drozd NN, i dr. Metodicheskie rekomendacii po izucheniju lekarstvennyh sredstv, vlijajushhih na gemostaz. V knige: Mironov AN, Bunjatjan ND, Vasil'ev AN, Verstakova OL, Zhuravleva MV, Lepahin VK, i dr, redaktory. Rukovodstvo po provedeniju doklinicheskih issledovanij lekarstvennyh sredstv. Chast' pervaja. M.: Grif i K, 2012; s. 453–479. Russian.
4. Manuvera VA, Kharlampieva DD, Bobrovsky PA, Grafskaia EN, Brovina KA, Lazarev VN. New anticoagulant protein from medicinal leech. Biochemical and Biophysical Research Communications. 2024; 696: 149473. Available from: https://doi.org/10.1016/j.bbrc.2024.149473
5. Nutt EM, Jain D, Lenny AB, Schaffer L, Siegl PK, Dunwiddie CT, Purification and characterization of recombinant antistasin: a leech-derived inhibitor of coagulation factor Xa, Arch Biochem Biophys. 1991; 285: 37–44. Available from: https://doi.org/10.1016/0003-9861(91)90325-D.
6. Müller C, Mescke K, Liebig S, et al. More than just one: multiplicity of Hirudins and Hirudin-like Factors in the Medicinal Leech, Hirudo medicinalis. Mol Genet Genomics. 2016; 291: 227–240. Available from: https://doi.org/10.1007/s00438-015-1100-0.
7. Onishi A, St Ange K, Dordick JS, Linhardt RJ. Heparin and anticoagulation. Front Biosci Landmark Ed. 2016; 21 (7): 1372–92. Available from: https://doi.org/10.2741/4462.

Литература

1. Баркаган З. С. Диагностика и контролируемая терапия нарушений гемостаза. Москва: ООО "Медико-технологическое предприятие «Ньюдиамед», 2008; 292 с.
2. Winter W, Flax S, Harris N. Coagulation testing in the core laboratory. Laboratory Medicine. 2017; 48 (4): 295–313. Available from: https://doi.org/10.1093/labmed/.
3. Макаров В. А., Спасов А. А., Плотников М. Б., Белозерская Г. Г., Васильева Т. М., Дрозд Н. Н., и др. Методические рекомендации по изучению лекарственных средств, влияющих на гемостаз. В книге: Миронов А. Н., Бунятян Н. Д., Васильев А. Н., Верстакова О. Л., Журавлева М. В., Лепахин В. К., и др, редакторы. Руководство по проведению доклинических исследований лекарственных средств. Часть первая. М.: Гриф и К, 2012; с. 453–479.
4. Manuvera VA, Kharlampieva DD, Bobrovsky PA, Grafskaia EN, Brovina KA, Lazarev VN. New anticoagulant protein from medicinal leech. Biochemical and Biophysical Research Communications. 2024; 696: 149473. Available from: https://doi.org/10.1016/j.bbrc.2024.149473
5. Nutt EM, Jain D, Lenny AB, Schaffer L, Siegl PK, Dunwiddie CT, Purification and characterization of recombinant antistasin: a leech-derived inhibitor of coagulation factor Xa, Arch Biochem Biophys. 1991; 285: 37–44. Available from: https://doi.org/10.1016/0003-9861(91)90325-D.
6. Müller C, Mescke K, Liebig S, et al. More than just one: multiplicity of Hirudins and Hirudin-like Factors in the Medicinal Leech, Hirudo medicinalis. Mol Genet Genomics. 2016; 291: 227–240. Available from: https://doi.org/10.1007/s00438-015-1100-0.
7. Onishi A, St Ange K, Dordick JS, Linhardt RJ. Heparin and anticoagulation. Front Biosci Landmark Ed. 2016; 21 (7): 1372–92. Available from: https://doi.org/10.2741/4462.

CHANGES IN SOME IMMUNOLOGICAL PARAMETERS AFTER COVID-19: GENERAL TRENDS AND INDIVIDUAL CHARACTERISTICS

Glazanova TV ✉, Shilova ER, Efremova YS, Chubukina JV, Bessmeltsev SS

Russian Hematology and Transfusiology Research Institute of the Federal Medical Biological Agency, St. Petersburg, Russia

The specifics of individual immune reactions after COVID-19 have not been studied sufficiently. This study aimed to describe the changes in indicators of cellular and humoral levels of immunity after COVID-19, and gage general trends and individual characteristics. We sampled blood of 125 unvaccinated COVID-19 patients (29 men and 96 women, median age 53 years) 1 to 4 months after recovery, and determined the relative content of T-lymphocytes (CD3+), B-lymphocytes (CD19+), and cells with late activation markers (CD3+HLA-DR+) in them using flow cytometry. With the help of ELISA, we have registered the level of circulating immune complexes, which can be medium molecular weight (CICmed) and low molecular weight (CIClow), and the content of antibodies to SARS-CoV-2. In the mild course group, significant differences from the normal values ($p < 0.001$) were found for T cells (growth, $74.4 \pm 1.2\%$ vs. $68.6 \pm 1.1\%$) and B cells (decline, $10.2 \pm 0.7\%$ vs. $13.9 \pm 0.9\%$). In the moderately severe course and severe course groups, the level of CD3+HLA–DR+ lymphocytes was increased ($7.7 \pm 0.4\%$ and $15.7 \pm 2.5\%$, respectively, versus $3.9 \pm 0.8\%$ in the control group; $p < 0.01$). All the examined patients had high levels of CIClow (2.6-2.9-fold increase) and CICmed (1.6–1.8-fold increase). The protective level of antibodies to SARS-CoV-2 above 150 BAU/ml was registered in about 50% of the mild group participants, 75% of the moderately severe group members, and 100% of patients who had the disease in a severe form. We detected no connections between immune disorders and clinical features of the course of the disease and the period thereafter, with the exception of abdominal syndrome peculiar to the acute stage of the disease. The article also describes a clinical case of detection in the early post-COVID-19 period of a pathological clone characteristic of B cell chronic lymphocytic leukemia, and its subsequent disappearance and normalization of the immunophenotype as registered during a follow-up 1.5 years after recovery. The persistent immunological shifts should be taken into account when assessing the risks of reinfection and possible complications.

Keywords: COVID-19, T-lymphocytes, B-lymphocytes, circulating immune complexes, individual characteristics

ИЗМЕНЕНИЯ НЕКОТОРЫХ ИММУНОЛОГИЧЕСКИХ ПОКАЗАТЕЛЕЙ ПОСЛЕ ПЕРЕНЕСЕННОЙ ИНФЕКЦИИ COVID-19: ОБЩИЕ ТЕНДЕНЦИИ И ИНДИВИДУАЛЬНЫЕ ОСОБЕННОСТИ

Т. В. Глазанова ✉, Е. Р. Шилова, Ю. С. Ефремова, Ж. В. Чубукина, С. С. Бессмельцев

Российский научно-исследовательский институт гематологии и трансфузиологии Федерального медико-биологического агентства, Санкт-Петербург, Россия

Особенности индивидуальных иммунных реакций после перенесенного COVID-19 недостаточно изучены. Целью работы было охарактеризовать изменения показателей клеточного и гуморального звеньев иммунитета после перенесенного COVID-19 с оценкой общих тенденций и индивидуальных особенностей. У 125 невакцинированных пациентов, перенесших COVID-19 (29 мужчин и 96 женщин, Ме возраста — 53 года), через 1–4 месяца после выздоровления методом проточной цитометрии определяли относительное содержание Т-лимфоцитов (CD3+), В-лимфоцитов (CD19+), клеток с маркерами поздней активации (CD3+HLA-DR+). Исследовали уровень циркулирующих иммунных комплексов — среднемолекулярных (ЦИКср) и низкомолекулярных (ЦИКн) и содержание антител к SARS-CoV-2 методом ИФА. Достоверные отличия от нормы ($p < 0,001$) выявлены для Т-клеток — повышение ($74,4 \pm 1,2\%$ против $68,6 \pm 1,1\%$) и В-клеток — снижение ($10,2 \pm 0,7\%$ против $13,9 \pm 0,9\%$) в группе с легким течением. В группах со среднетяжелым и тяжелым течением COVID-19 повышен уровень CD3+HLA-DR+ лимфоцитов ($7,7 \pm 0,4\%$ и $15,7 \pm 2,5\%$ соответственно, против $3,9 \pm 0,8\%$ в контроле; $p < 0,01$). У всех обследованных повышен уровень ЦИКн (в 2,6–2,9 раз) и ЦИКср (в 1,6–1,8 раз). Защитный уровень антител к SARS-CoV-2 выше 150 BAU/мл отмечен примерно у 50% обследованных с легкой формой инфекции, у 75% — со среднетяжелой формой и у 100% — с тяжелой. Связи между иммунными нарушениями и клиническими особенностями течения COVID-19 и постковидного периода не обнаружено, кроме наличия абдоминального синдрома в остром периоде болезни. Описан клинический случай выявления в раннем постковидном периоде патологического клона, характерного для В-клеточного хронического лимфолейкоза с последующим его исчезновением и нормализацией иммунофенотипа при повторном обследовании через 1,5 года. Сохраняющиеся иммунологические сдвиги необходимо учитывать для оценки рисков повторного заражения и развития возможных осложнений.

Ключевые слова: COVID-19, Т-лимфоциты, В-лимфоциты, иммуноглобулины, циркулирующие иммунные комплексы, индивидуальные особенности

Since the emergence of SARS-CoV-2, there has been accumulated a significant amount of data about risk factors that can make the course of the disease severe, as well as about characteristics of the post-COVID period. The mechanisms of damage to cells and tissues caused by the virus and those behind the development of specific immunity were investigated in sufficient detail. However, several studies suggest that there is an individual immune response to the disease, unrelated to age or gender. The currently unanswered questions pertain to the role of individual immune factors in COVID-19 cases and the specifics of individual reactions in various groups of patients, including in the post-COVID period; the urgency of these questions stems from the fact that the effectiveness of protection against reinfection largely depends on the ability

to preserve immune memory after exposure to the virus. Humoral response has been considered in a sufficient number of publications, unlike the state of T-cell immunity, although it plays an important role in the development of adaptive immunity, and the synthesis of specific immunoglobulins is not a reliable indication of a formed protective immune response [1–4]. Moreover, some papers report that the amount of protective antibodies to SARS-CoV-2 is not a factor that significantly affects the risk of developing the post-COVID syndrome [5].

The term "long COVID" has been widely used since 2020; it unites various symptoms that persist or manifest several weeks or months after SARS-CoV-2 contraction. ICD-10 was extended with a new code, U09.9, post-COVID-19 condition. The symptoms of the post-COVID syndrome may be manifesting for three or more months after the acute stage of COVID-19 [6, 7]. However, persisting immune imbalance can be diagnosed even when there are no clinical signs of the said symptoms. Presence of the anti-infection protection markers for 4–6 months or more after vaccination or a past disease does not always shield against reinfection, especially since even such a significant indicator as the amount of specific antibodies is not the only factor determining the body's neutralizing capacity [8]. In addition, immune response disruptions may predispose people with a history of COVID-19 to secondary bacterial and fungal infections [9].

Papers covering the respective issues note a number of general trends, including altered composition of the circulating immune cells (more activated T lymphocytes, short-lived highly differentiated CD8+T lymphocytes, and proinflammatory T helper cells), which was accompanied by a change in the proportion of anti-inflammatory regulatory T cells and their malfunctioning, along with a growing amount of NK cells (CD16+/CD56+) [10–13]. Another common feature was an increased level of IgA in plasma and the number of circulating immune complexes [2]. At the same time, many researchers note high variability of the immune response to SARS-Cov-2 [2, 12, 13], with attempts to identify patterns thereof and regularities in the development of immune memory associated with the virus remaining largely unsuccessful so far.

Thus, it is necessary to continue studying the state of the immune system after exposure to SARS-CoV-2.

This study aims to describe the changes in some indicators of immunity to COVID-19 (cellular and humoral levels) and assess general trends and individual characteristics.

METHODS

Patients that recovered from COVID-19 1 to 4 months before the start of the study could participate therein. The exclusion criteria were a chronic somatic pathology (including diseases of the respiratory and cardiovascular systems, diabetes mellitus, confirmed immunodeficiency, etc.), and a positive SARS-CoV-2 PCR test result. The study included 125 unvaccinated patients who had had COVID-19 in 2020-2021, including 29 men and 96 women, aged 25-83 years (median — 53 years); on average, they recovered from the disease 2.6 months ago (median — 2 months). Additionally, we re-examined a group of 14 patients (2 men, 12 women) that recovered from COVID-19 6-8 months ago. As for the severity of COVID-19, 61 participant had a mild form of the disease, 55 moderate, and 9 — severe. The degree was determined based on the criteria established by the current revision of the Guidelines for the Prevention, Diagnosis and Treatment of COVID-19, factoring in fever, shortness of breath, blood saturation, serum C-reactive protein levels, and CT data. The respective information was collected from the

medical records provided by the examined individuals. Before taking a blood sample for the study, we asked the participants whether they had clinical symptoms peculiar to the post-COVID period, such as impaired sense of smell and taste, abdominal syndrome, skin syndrome (dryness and peeling of the skin).

To identify lymphocyte subpopulations, we used a Navios EX Flow Cytometer (Beckman Coulter; USA) and the following panel of monoclonal antibodies (Beckman Coulter; USA): CD3-FITC, CD8-PE, CD19-ECD, CD16-Pc5.5, CD56-Pc7, CD4-APC, CD25-A700, HLA-DR-PB, CD45-KO. The lymphocytic region was isolated according to the parameters of direct and lateral light scattering with CD45 gating. The level of total serum G, A and M immunoglobulins was determined by turbidimetry in a Vitalon 400 automatic biochemical analyzer (Human set of reagents; Germany). To establish the content of circulating immune complexes (CIC) of low (CIClow) and medium (CICmed) molecular weight, we measured optical density of the samples after deposition with polyethylene glycol in various concentrations, comparing with the control samples that did not contain the studied sera. The results were expressed in conventional units (CU) [14]. The content of class G antibodies to SARS-CoV-2 was determined by ELISA using the SARS-CoV-2-IgG quantitative IFA-BEST test systems (VECTOR-BEST; Russia); the results were given in BAU (binding antibody units) per 1 ml. The threshold value agreed as providing a full-fledged antiviral protection against COVID-19 is 150 BAU/ml; all samples that reached that figure proved to neutralize the virus in laboratory studies [15].

The control group consisted of 35 donors without a history of COVID-19. For statistical processing of the results, we used the Statistica 10.0 software package (StatSoft Inc.; USA). The intergroup comparison was done with the help of the nonparametric Mann-Whitney test. The differences were considered statistically significant at $p < 0.05$.

RESULTS

After COVID-19, all participants had certain parameters of cellular immunity, the level of class A immunoglobulins, and CIC different from those registered in the control group, which signals an imbalance in the immune system.

As for the specific subpopulations of lymphocytes, the significant deviations were peculiar to T lymphocytes (CD3+) and B lymphocytes (CD19+) only in the mild course group, where their relative content was higher and lower than in the control group, respectively (Table 1). We did not register such differences in the moderate and severe course groups; there, the increased indicator was the relative content of T lymphocytes with markers of late activation (CD3+HLA-DR+).

Overall, in the mild course group, the values fluctuated within a significantly wide range, with the level of CD3+ lymphocytes increased about 4 times more often than decreased, and that of CD19+ lymphocytes, on the contrary, decreased 12 times more often than increased (Table 2). Similar patterns were observed in the moderate course group: elevated CD3+ lymphocyte levels were 1.9 times more common than decreased, and CD19+ lymphocyte levels were 2.2 times more likely to be reduced than elevated. In the severe course group, on the contrary, lower levels of CD3+ lymphocyte were registered 2 times more often than higher, and higher CD19+ levels — 2.2 times more often than lower.

By the level of immunoglobulins G and M, the groups did not differ significantly. In all groups, we registered a drop in the serum concentration of immunoglobulin A, with difference, compared to the control group, significant in the mild and

Table 1. Post-COVID cellular immunity indicators, groups by disease course severity

Indicator / Group	CD3+ (%)	CD3+CD4+ (%)	CD3+CD8+ (%)	CD3+HLA-DR+ (%)	CD3-CD16+/CD56+ (%)	CD19+ (%)
Mild $n = 61$ (I)	74.4 ± 1.2	45.4 ± 1.2	26.3 ± 1.1	4.2 ± 0.2	12.5 ± 0.8	10.2 ± 0.7
Moderate $n = 55$ (II)	69.7 ± 1.7	45.7 ± 1.6	23.1 ± 1.4	7.7 ± 0.4	12.9 ± 1.0	13.3 ± 1.2
Severe $n = 9$ (III)	69.5 ± 4.5	43.8 ± 4.0	23.6 ± 3.9	15.7 ± 2.5	13.3 ± 1.6	13.3 ± 2.8
Control $n = 35$ (IV)	68.6 ± 1.1	42.6 ± 1.1	24.0 ± 0.9	3.9 ± 0.8	12.4 ± 1.0	13.9 ± 0.9
$p_{I–IV}$ $p_{II–IV}$ $p_{III–IV}$	< 0.001 – –	– – –	– – –	– < 0.01 < 0.01	– – –	< 0.001 – –

severe course groups: 2.3 ± 0.1 g/l ($p < 0.01$) and 2.0 ± 0.4 g/l ($p < 0.05$), respectively, versus 2.8 ± 0.1 g/l in the control samples.

In addition, all participants who recovered from COVID-19 had the level of circulating immune complexes increased, which is a noteworthy finding (Table 3).

In 39 individuals (30.5% of all the participants, 30.3% of participating females and 31% of participating males), we have registered an especially significant rise of the level of CIClow: above 400 CU. Many of them (23 persons, 40.4% of the moderate course group) had COVID-19 in a moderately severe form. As for the age, the subgroup of individuals with the highest CIC values did not differ significantly from the entire sample of participants: the median age in the former was 56 years (29 through 83), in the latter — 53.

Level of G class antibodies to SARS-CoV-2: in the mild course group, 51.5% of the patient had it above 150 BAU/ml, in the moderate course group — 75.8%, in the severe course group — 100%.

In the group of 14 people who were re-examined at a later period (6–8 months after recovery), 8 persons (57%) exhibited persistence of pronounced abnormalities. The most common of them was a significantly elevated (>300 CU) level of CIClow, registered in 7 participants, five of whom had COVID-19 in a mild form, and 2 in a moderately severe form. Two individuals had a high content of T cells with markers of late activation (CD3+HLA-DR+): >7% versus normal 3.9 ± 0.8%. In another 2, we registered a significant disruption of the CD4+/CD8+ ratio, and a high amount of CD4+ cells (T helpers). One patient had the IgA level at 4 g/l while the normal value is 2.8 ± 0.1 g/l.

Thus, while we did register immunity abnormalities common for most COVID-19 survivors, some of the examined had rather rare disruptions.

According to the clinical records, during the disease and thereafter, about half of the patients (46.9%) suffered significant smell and taste impairments, a fourth (26.6%) had abdominal symptoms (pain, dyspeptic disorders), and over a third (39.8%) of the entire sample reported skin dryness and peeling. In most participants, the said symptoms were concomitant to each other. Considering the degree of CIClow elevation, it is feasible to distinguish between patients who had the respective

value at above 400 CU and below this figure (Table 4). These cohorts did not differ significantly from in terms of the frequency of manifestation of the abovementioned symptoms, with the exception of the abdominal syndrome, which was registered in patients with the CIClow level above 400 CU twice as often.

As for the changes in cellular immunity, we failed to identify clear patterns and associations with the clinical records. Nevertheless, there were some noteworthy features registered in individual COVID-19 patients. Against the background of reduced relative content of CD3+ lymphocytes and increased content of CD19+ lymphocytes, which was observed in 4 patients, 3 of them (aged 62–65 years) complained of severe skin dryness and peeling, and two had pronounced alopecia. Among younger participants, there was a 44-year-old man with significantly (up to 49.1%) low amount of CD3+ lymphocytes and high levels of CIClmed and CIClow (102 CU and 520 CU, respectively); for a long time, he reported numbness of fingers and legs and headaches along with pronounced weakness and cognitive impairment, which can be interpreted as as post-COVID neurological disorders. Another patient, a female 40 years old, had the low level of CD3+ lymphocytes as the only abnormality; she reported severe abdominal pain and prolonged dyspeptic disorders during the disease and thereafter. The latter case, however, can also be associated with antibiotic therapy and dysbiosis.

Below is the description of a case of detection of a pathological clone in the post-COVID period.

Patient A., 64 years old. No significant chronic diseases in the history. Moderate manifestations of biliary dyskinesia and initial manifestations of hypertension. Survived moderately severe COVID-19 in August 2021. First examination a month after the infection. Features of the post-COVID period: prolonged general weakness, pronounced alopecia, and moderately impaired sense of taste. At the time of examination, key hemogram indicators normal. Amount of leukocytes — 5.5 × 10⁹/l, absolute number of lymphocytes — at the lower limit of the normal range (1.3 × 10⁹/l). At the initial examination, flow cytometry revealed several deviations beyond healthy ranges of the respective indicators. The content of B cells (CD19+) was up to 57.3%, which disturbed the subpopulation

Table 2. Post-COVID abnormalities in the CD3+ and CD19+ counts (peripheral blood), % of the examined

Indicator / Group	CD3+ level			CD19+ level		
	Increased	Decreased	Normal	Increased	v	Normal
Mild	50%	12%	38%	6%	74%	20%
Moderate	38%	20%	42%	22%	49%	29%
Severe	22%	44%	34%	56%	22%	22%

Table 3. Content of CIC in COVID-19 patients, depending on the severity of the disease

	CICmed (CU)	CIClow (CU)
Mild $n = 61$ (I)	53.9 ± 3.1	331.1 ± 12.7
Moderate $n = 55$ (II)	61.8 ± 3.8	362.8 ± 18.0
Severe $n = 9$ (III)	63.6 ± 7.0	325.4 ± 22.5
Control $n = 35$ (IV)	34.1 ± 3.6	122.5 ± 11.9
$p_{\text{I–IV}}$ $p_{\text{II–IV}}$ $p_{\text{III–IV}}$	$p < 0.001$ $p < 0.001$ $p < 0.001$	$p < 0.001$ $p < 0.001$ $p < 0.001$

composition of lymphocytes; the immunophenotype of B cells was pathological, as in a chronic lymphocytic leukemia (CLL): CD19+CD20+lowCD22+lowCD5+CD23+CD43+CD200+ (Figure 1).

At the level of humoral immunity, the changes were similar to those common in the group, with the only noteworthy exception of a higher IgA value, which still remained within the normal range.

Presence of a pathological clone characteristic of B-CLL was confirmed on a fresh sample of peripheral blood, but there were no signs of lymphadenopathy, morphologically altered lymphocytes in clinical blood tests. Nevertheless, accidental detection of chronic lymphocytic leukemia in the initial stage (CLL stage 0) was considered. The plan was to continue monitoring and conduct an additional examination for clonality.

A year after recovery from COVID-19, the patient's general well-being returned to normal. She did not seek medical assistance, nor had any medical interventions, with the exception of a 1.5-month course of multivitamins. A second examination conducted in April 2023 has shown that the relative content of mature T lymphocytes (CD3+), NK cells (CD3–CD16+CD56+) returned to the normal ranges. Higher amount of T helpers (CD3+CD4+) caused an imbalance in the content of the main subpopulations of effector cells. Mature B cells were polyclonal, with a normal CD19+ CD20+ CD22+ CD79b+ IgM+ phenotype, and accounted for about 8.0% of the total pool of lymphocytes (CD45+). No pathological clone of B lymphocytes with a B-CLL phenotype has been identified. To date (April 2024), the patient's condition remains satisfactory, with no pathological symptoms manifesting.

Figure 1 shows the results of the study of individual subpopulations of lymphocytes.

Thus, monitoring of the patient's condition over time yielded no data confirming presence of a chronic lymphoproliferative disease. The disturbance of the subpopulation composition of lymphocytes was regarded as reactive changes against the background of activation of the B-cell immunity in response to COVID-19.

DISCUSSION

Since the emergence of SARS-CoV-2, there has been collected a significant amount of data about the specifics of development of immune response upon exposure thereto. The said data indicate that there are both common trends and individual reactions, as well as dysfunctional immune response in some

patients [12, 13, 16]. The wide range of values of immunological parameters registered in COVID-19 survivors can be attributed to many factors, from innate features of the immune system to dysbiosis and comorbidities [17, 18].

The importance of assessment of persisting immune disorders stems from the need to fully understand the patterns of formation of a full-fledged antiviral immunity, which relies on coordinated cooperation between the cellular and humoral levels of immunity. There is also evidence that COVID-19, triggering dysregulation of the immune system, can promote development of autoimmune diseases [16, 19, 20].

The long recovery of immunity indicators after COVID-19 can be explained by the "squeezed" condition of the immune system after a severe course of the disease, and SARS-CoV-2's ability to suppress development of the adaptive immune response, influence the number and functional activity of lymphocytes, the effectors of cellular immunity, and consequently hinder lymphopoiesis, apoptosis, and causing exhaustion of these cells [1].

As shown by the case reported above, post-COVID, the components of immunity can undergo unusual transformations, including production of cells with characteristics of pathological clones. Such developments necessitate prolonged monitoring of patients after recovery and point to the virus' capability to predispose to hematopoiesis disorders associated the disturbances of the immune system's balance.

It is believed that, post-COVID, a high titer of neutralizing antibodies for a period of 6 months or more and prolonged persistence of SARS-CoV-2 Spike and RBD IgG mean the virus remains in the body/microbiota of the patient, which can naturally affect the state of the immune system. The persistence of viral antigens causing immuno-mediated damage contributes to the polyclonal activation of immunocompetent cells, and the long-term growth of the number of CIC and activated T lymphocytes (described in the literature and noted in our study) is considered a sign of insufficiently effective elimination of the pathogen [20, 21]. Obviously, rehabilitation measures should factor in such a probability.

Thus, the literature data and the results of our study suggest some general trends in post-COVID changes of cellular and humoral components of immunity. At the same time, there are individual patients with unusual abnormalities of immunological parameters. Some of these abnormalities can be associated with the patients' age and severity of the disease, but some remain unclear in terms of their role and meaning. Apparently,

Table 4. Frequency of occurrence of certain symptoms in COVID-19 survivors depending on the level of CIClow

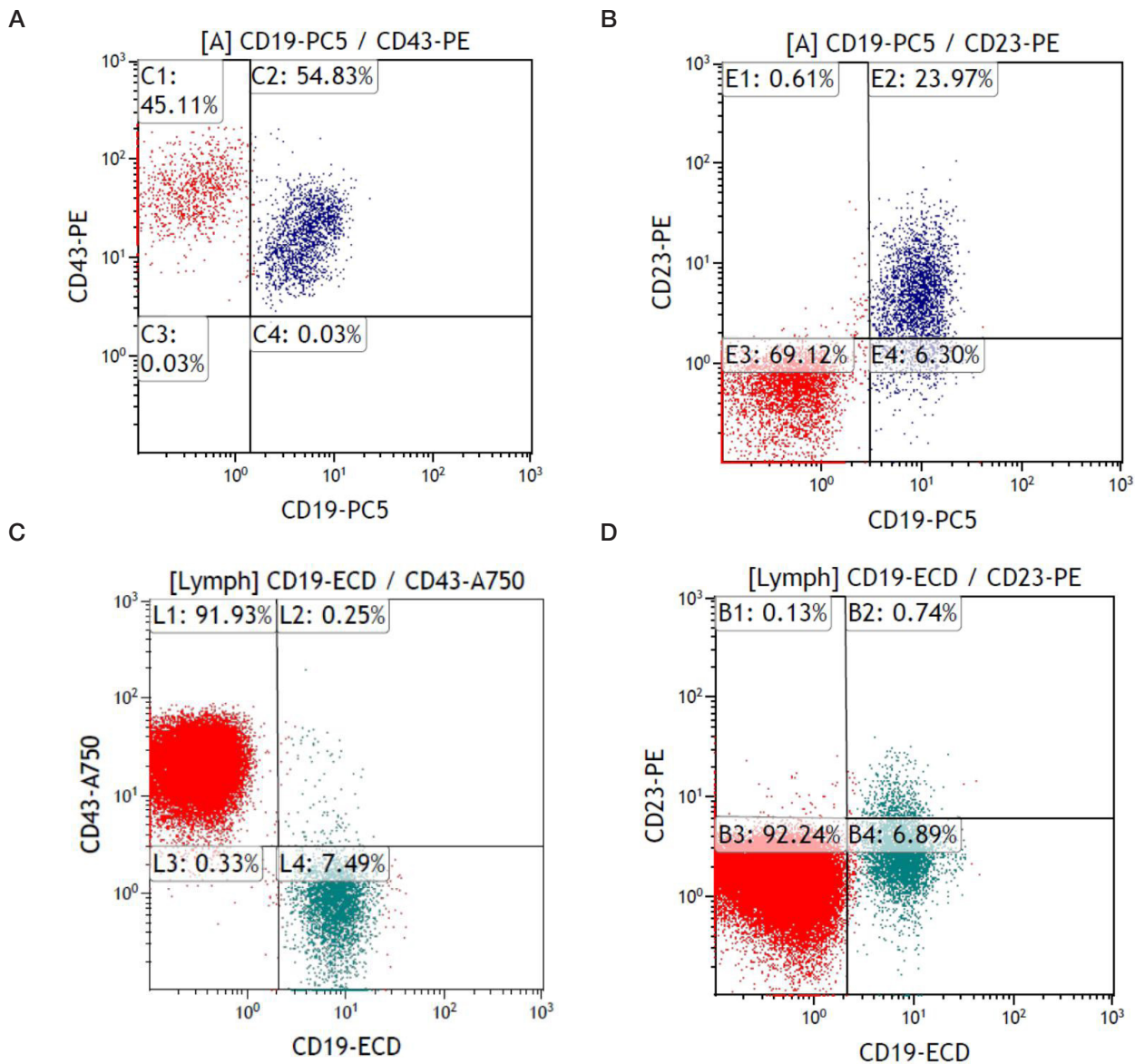| CIClow value	Abdominal syndrome	Impaired taste and sense of smell	Skin disorders
< 400 CU ($n = 89$)	20.20%	46.10%	39.30%
> 400 CU ($n = 39$)	41%	48.70%	41%

Fig. Immunophenotypic study results, patient A. Device used for the study: Navios EX 10 Colors (Beckman Coulter; USA). The lymphocytic pool was isolated by the parameters of direct and lateral light scattering with CD45 gating. A, B. Results of the study of August 2021. For these histograms, a 5 color panel was used: 1) CD20–FITC+CD23–PE+CD45–ECD+CD19–Pc5+CD5–Pc7 and 2) CD22–FITC+CD43-PE+CD19–Pc5+CD45–Pc7. C, D. Results of the study of April 2023. For these histograms, a 10 color panel was used: FMC7–FITC+CD23–PE+CD19–ECD+CD79b–Pc5.5+CD200–Pc7+CD43–A750+CD38–A700+IgM–PB+CD45–KO. X-axis: CD19+ (%), Y-axis: A and C — CD43+ (%), B and D — CD23+ (%). The upper right quadrants of all the histograms (C2 (A), E2 (B), L2(C) and B2 (D)) show the region where the clone of pathological cells characteristic of B-CLL should be located

special long-term monitoring is required for those who have persisting COVID-associated changes of late activation T cells, class A immunoglobulins, and low molecular weight CIC, since they play an essential role in the development of infectious-inflammatory and autoimmune reactions [20, 22].

It is important to take into account the ongoing immunological shifts when assessing the risks of reinfection and considering revaccination. Continued monitoring and examinations are required to better understand the features of changes in the immune profile caused by SARS-CoV-2. In addition, it is necessary to further study the state of the regulatory mechanisms of immunity in patients after COVID-19, and to develop informative prognostic criteria for assessing the post-COVID condition. Currently, it is not possible to fully assess individual risks without conducting a large-scale multifactorial analysis in groups of individuals who are homogeneous in terms of baseline data, age, strain of the pathogen, and severity of the disease. The new data will allow personalization of the revaccination schedules and development of rational immunocorrection programs that will help increase resistance to repeated infections.

CONCLUSIONS

Regardless of the severity of the course, all COVID-19 survivors had their immune systems imbalanced, and this status did not change for a long time in many of them. Those who have the disease in a mild form typically have high relative content of CD3+ T cells and low amount of B cells (CD19+), as well as low level of serum IgA. Almost half of the individuals in this group had a low level of protective antibodies to SARS-CoV-2 (<150 BAU/ml). In the severe course group, compared to other groups, the level of CD19+ cells was often higher, and the drop of the level of IgA most pronounced. Moreover, all members of this group had the amount of antibodies above the protective threshold. In the moderately severe course group, some abnormalities were similar to those registered for the mild form of the disease (high content of CD3+ cells, low amount of

CD19+ cells), but less pronounced; a less common effect was a drop of the level of protective antibodies, and the growth of IgA was unreliable. Along with general trends, some individuals exhibited uncommon immunity deviations, including a patient with a pathological clone characteristic of B-CLL registered a month after recovery, which spontaneously disappeared later

on. The genesis of such disorders is currently not entirely clear, and COVID-19 survivors, obviously, need long-term monitoring and repeated examinations, which would enable not only treatment of the post-COVID syndrome but also further study and comprehensive assessment of the associated immune imbalance.

References

1. Ivanova IA, Omelchenko ND, Filippenko AV, Trufanova AA, Noskov AK. Rol' kletochnogo zvena immuniteta v formirovanii immunnogo otveta pri koronavirusnyh infekcijah. Medicinskaja immunologija. 2021; 23 (6): 1229–38. DOI: 10.15789/1563-0625-ROT-2302. Russian.

2. Semenova EV, Pavljuk VV, Uvarova MA, Ivanov AV. Osobennosti gumoral'nogo immuniteta posle perenesennogo COVID-19. Medicinskaja immunologija. 2022. 24 (2): 337–50. DOI: 10.15789/1563-0625-FOH-2452. Russian.

3. Sette A, Crotty S. Adaptive immunity to SARS-CoV-2 and COVID-19. Cell. 2021; 184 (4): 861–80. DOI: 10.1016/j.cell.2021.01.007.

4. Mohn KG, Bredholt G, Zhou F, et al. Durable T-cellular and humoral responses in SARS-CoV-2 hospitalized and community patients. PloS ONE. 2022; 17 (2): e0261979. DOI: 10.1371/journal.pone.0261979.

5. Asfandijarova NS, Filippov EV, Dashkevich OV, Jakubovskaja AG, Mosejchuk KA, Zhuravleva NS, i dr. Faktory riska razvitija postkovidnogo sindroma. Klinicist. 2022; 16 (4): 19–26. DOI: 10.17650/1818-8338-2022-16-4-K671. Russian.

6. Nalbandian A, Sehgal K, Gupta A, Madhavan MV, McGroder C, Stevens JS, et al. Post-acute COVID-19 syndrome. Nat Med. 2021; 27 (4): 601–15. DOI: 10.1038/s41591-021-01283-z.

7. Su S, Zhao Y, Zeng N, Liu X, Zheng Y, Sun J, et al. Epidemiology, clinical presentation, pathophysiology, and management of long COVID: an update. Molecular Psychiatry. 2023; 28 (10): 4056–69. DOI: 10.1038/s41380-023-02171-3.

8. Generalova LV, Grigoriev IV, Vasina DV, Tkachuk AP, Kruzhkova IS, Kolobukhina LV et al. Properties of RBD specific IgG from COVID-19 patients and Sputnik V vaccinated individuals. Bulletin of RSMU. 2022; 1: 14–22. DOI: 10.24075/brsmu.2022.005.

9. Taraskina AE, Frolova EV, Shadrivova OV, Sekretareva OV, Vasileva NV. Rol' immunnogo gomeostaza u pacientov s novoj koronavirusnoj infekciej (COVID-19) v razvitii invazivnogo aspergilleza legkih. Zhurnal infektologii. 2023; 15 (2): 14–23. DOI: 10.22625/2072-6732-2023-15-2-14-23.

10. Wu J, Tang L, Ma Y, Li Y, Zhang D, Li Q, et al. Immunological Profiling of COVID-19 Patients with Pulmonary Sequelae. mBio. 2021; 12 (5): e0159921. DOI: 10.1128/mBio.01599-21.

11. Orologas-Stavrou N, Politou M, Rousakis P, Kostopoulos IV, Ntanasis-Stathopoulos I, Jahaj E, et al. Peripheral blood immune profiling of convalescent plasma donors reveals alterations in specific immune subpopulations even at 2 months post sars-cov-2

12. infection. Viruses. 2021; 13 (1): 26. DOI: 10.3390/v13010026.

13. Asfandijarova NS, Rubcova MA. Mozhet li disfunkcija kletochnogo immuniteta rassmatrivat'sja kak priznak postkovidnogo sindroma? Rossijskij immunologicheskij zhurnal. 2023; 26 (2): 173–80. DOI: 10.46235/1028-7221-2067-MBD. Russian.

13. Sizjakina LP, Skripkina NA, Antonova EA, Sizjakin DV. Dinamika kliniko-immunologicheskih pokazatelej u pacientov, perenesshih COVID-19 srednejazhelogo techenija i poluchavshih terapiju s vkljucheniem ingibitora janus-kinaz. Immunologija. 2023; 44 (2): 191–201. DOI: 10.33029/0206-4952-2023-44-2-191-201. Russian.

14. Ketlinskij SA., Kalinina NM. Immunologija dlja vracha. SPb.: Gippokrat, 1998; 156 s. Russian.

15. Kazakov SP, Reshetnjak DV, Davydova NV, Efimushkina OA, Putkov SB. Analiz i sravnitel'naja ocenka jeffektivnosti gumoral'nogo immunnogo otveta posle vakcinacii «Sputnik V» s ispol'zovaniem razlichnyh naborov reagentov. Infekcija i immunitet. 2023; 13 (3): 469–80. DOI: 10.15789/2220-7619-VRK-197. Russian.

16. Mather MW, Jardine L, Talks B, Gardner L, Haniffa M. Complexity of immune responses in COVID-19. Seminars in Immunology. 2021; 55: 101545. DOI: 10.1016/j.smim.2021.101545.

17. Han JH, Womack KN, Tenforde MW, et al. Associations between persistent symptoms after mild COVID-19 and long-term health status, quality of life, and psychological distress. Influenza Other Respir Viruses. 2022; 16 (4): 680–9. DOI:10.1111/irv.12980.

18. Battaglini D, Robba C, Fedele A, et al. The Role of Dysbiosis in Critically Ill Patients With COVID-19 and Acute Respiratory Distress Syndrome. Front Med. 2021; 8: 671714. DOI: 10.3389/fmed.2021.671714.

19. Gracia-Ramos A, Martin-Nares E, Hernandez-Molina G. New onset of autoimmune diseases following COVID-19 diagnosis. Cells. 2021; 10: 3592. DOI: 10.3390/cells10123592.

20. Woodruff M, Ramonell R, Haddad N, Anam F, Rudolph M, Walker T et al. Dysregulated naïve B cells and de novo autoreactivity in severe COVID-19. Nature. 2022; 611 (7934): 139–47. DOI: 10.1038/s41586-022-05273-0.

21. Kovtun OP, Olenkova OM, Bejkin JaB. Immunnyj otvet pri novoj koronavirusnoj infekcii Covid-19 u detej i vzroslyh. Ural'skij medicinskij zhurnal. 2021; 20 (4): 12–17. DOI: 10.52420/2071-5943-2021-20-4-12-17. Russian.

22. Zheng HY, Zhang M, Yang CX, et al. Elevated exhaustion levels and reduced functional diversity of T cells in peripheral blood may predict severe progression in COVID-19 patients. Cell Mol. Immunol. 2020; 17(5): 541–43. DOI:10.1038/s41423-020-0401-3.

Литература

1. Иванова И. А., Омельченко Н. Д., Филиппенко А. В., Труфанова А. А., Носков А. К. Роль клеточного звена иммунитета в формировании иммунного ответа при коронавирусных инфекциях. Медицинская иммунология. 2021; 23 (6): 1229–38. DOI: 10.15789/1563-0625-ROT-2302.

2. Семенова Е. В., Павлюк В. В., Уварова М. А, Иванов А. В. Особенности гуморального иммунитета после перенесенного COVID-19. Медицинская иммунология. 2022. 24 (2): 337–50. DOI: 10.15789/1563-0625-FOH-2452.

3. Sette A, Crotty S. Adaptive immunity to SARS-CoV-2 and COVID-19. Cell. 2021; 184 (4): 861–80. DOI: 10.1016/j.cell.2021.01.007.

4. Mohn KG, Bredholt G, Zhou F, et al. Durable T-cellular and humoral responses in SARS-CoV-2 hospitalized and community patients. PloS ONE. 2022; 17 (2): e0261979. DOI:

10.1371/journal.pone.0261979.

5. Асфандиярова Н. С., Филиппов Е. В., Дашкевич О. В., Якубовская А. Г., Мосейчук К. А., Журавлева Н. С. и др. Факторы риска развития постковидного синдрома. Клиницист. 2022; 16 (4): 19–26. DOI: 10.17650/1818-8338-2022-16-4-K671.

6. Nalbandian A, Sehgal K, Gupta A, Madhavan MV, McGroder C, Stevens JS, et al. Post-acute COVID-19 syndrome. Nat Med. 2021; 27 (4): 601–15. DOI: 10.1038/s41591-021-01283-z.

7. Su S, Zhao Y, Zeng N, Liu X, Zheng Y, Sun J, et al. Epidemiology, clinical presentation, pathophysiology, and management of long COVID: an update. Molecular Psychiatry. 2023; 28 (10): 4056–69. DOI: 10.1038/s41380-023-02171-3.

8. Генералова Л. В., Григорьев И. В., Васина Д. В., Ткачук А. П., Кружкова И. С., Колобухина Л. В. и др. Свойства антител

к RBD у переболевших COVID-19 и вакцинированных препаратом «СПУТНИК V». Вестник РГМУ. 2022; 1: 15–22. DOI: 10.24075/vrgmu.2022.005.

9. Тараскина А. Е., Фролова Е. В., Шадривова О. В., Секретарева О. В., Васильева Н. В. Роль иммунного гомеостаза у пациентов с новой коронавирусной инфекцией (COVID-19) в развитии инвазивного аспергиллеза легких. Журнал инфектологии. 2023; 15 (2): 14–23. DOI: 10.22625/2072-6732-2023-15-2-14-23.

10. Wu J, Tang L, Ma Y, Li Y, Zhang D, Li Q, et al. Immunological Profiling of COVID-19 Patients with Pulmonary Sequelae. mBio. 2021; 12 (5): e0159921. DOI: 10.1128/mBio.01599-21.

11. Orologas-Stavrou N, Politou M, Rousakis P, Kostopoulos IV, Ntanasis-Stathopoulos I, Jahaj E, et al. Peripheral blood immune profiling of convalescent plasma donors reveals alterations in specific immune subpopulations even at 2 months post sars-cov-2 infection. Viruses. 2021; 13 (1): 26. DOI: 10.3390/v13010026.

12. Асфандиярова Н. С., Рубцова М. А. Может ли дисфункция клеточного иммунитета рассматриваться как признак постковидного синдрома? Российский иммунологический журнал. 2023; 26 (2): 173–80. DOI: 10.46235/1028-7221-2067-MBD.

13. Сизякина Л. П., Скрипкина Н. А., Антонова Е. А., Сизякин Д. В. Динамика клинико-иммунологических показателей у пациентов, перенесших COVID-19 среднетяжелого течения и получавших терапию с включением ингибитора янус-киназ. Иммунология. 2023; 44 (2): 191–201. DOI: 10.33029/0206-4952-2023-44-2-191-201.

14. Кетлинский С. А., Калинина Н.М. Иммунология для врача. СПб.: Гиппократ, 1998; 156 с.

15. Казаков С. П., Решетняк Д. В., Давыдова Н. В., Ефимушкина О. А., Путков С. Б. Анализ и сравнительная оценка эффективности гуморального иммунного ответа после вакцинации «Спутник V» с использованием различных наборов реагентов. Инфекция и иммунитет. 2023; 13 (3): 469–80. DOI: 10.15789/2220-7619-VRK-197.

16. Mather MW, Jardine L, Talks B, Gardner L, Haniffa M. Complexity of immune responses in COVID-19. Seminars in Immunology. 2021; 55: 101545. DOI: 10.1016/j.smim.2021.101545.

17. Han JH, Womack KN, Tenforde MW, et al. Associations between persistent symptoms after mild COVID-19 and long-term health status, quality of life, and psychological distress. Influenza Other Respir Viruses. 2022; 16 (4): 680–9. DOI:10.1111/irv.12980.

18. Battaglini D, Robba C, Fedele A, et al. The Role of Dysbiosis in Critically Ill Patients With COVID-19 and Acute Respiratory Distress Syndrome. Front Med. 2021; 8: 671714. DOI: 10.3389/fmed.2021.671714.

19. Gracia-Ramos A, Martin-Nares E, Hernandez-Molina G. New onset of autoimmune diseases following COVID-19 diagnosis. Cells. 2021; 10: 3592. DOI: 10.3390/cells10123592.

20. Woodruff M, Ramonell R, Haddad N, Anam F, Rudolph M, Walker T et al. Dysregulated naïve B cells and de novo autoreactivity in severe COVID-19. Nature. 2022; 611 (7934): 139–47. DOI: 10.1038/s41586-022-05273-0.

21. Ковтун О. П., Оленькова О. М., Бейкин Я. Б. Иммунный ответ при новой коронавирусной инфекции Covid-19 у детей и взрослых. Уральский медицинский журнал. 2021; 20 (4): 12–17. DOI: 10.52420/2071-5943-2021-20-4-12-17.

22. Zheng HY, Zhang M, Yang CX, et al. Elevated exhaustion levels and reduced functional diversity of T cells in peripheral blood may predict severe progression in COVID-19 patients. Cell Mol. Immunol. 2020; 17(5): 541–43. DOI:10.1038/s41423-020-0401-3.

ELECTRON MICROSCOPY OF THE *PLASMODIUM FALCIPARUM* TROPHOZOITES AND THE TISSUES THESE HAVE INFECTED IN SEVERE TROPICAL MALARIA

Solovev AI[1], Kapacina VA[2], Sokolova MO[1], Ariukov AR[1]✉, Kovalenko AN[1], Uskov AN[3], Romanenko VA[1]

[1] Kirov Military Medical Academy, Saint-Petersburg, Russia

[2] Botkin Clinical Infectious Diseases Hospital, Saint-Petersburg, Russia

[3] Children's Research and Clinical Center for Infectious Diseases of the Federal Medical Biological Agency, Saint-Petersburg, Russia

The paper provides the results of the comprehensive electron microscopic examination of the venous blood and internal organ tissue samples obtained when studying the imported case of tropical malaria. The study was aimed to assess the fine structure of the erythrocytic stages of *Plasmodium falciparum* and alterations of the affected tissues in severe tropical malaria. The venous blood, cerebral cortical tissue and myocardial samples were examined by light microscopy and electron (scanning and transmission) microscopy. Numerous *Plasmodium falciparum* trophozoites were found in blood. Multiple Maurer's clefts were found in the cytoplasm of the infected erythrocytes. Abnormal intercellular contacts between the infected and unaffected erythrocytes were revealed, which resulted in their adhesion and rosette formation (erythrocyte rosetting/e-rosetting). When studying cortical tissue and myocardial samples, fixation of the affected erythrocytes on the endothelium (erythrocyte adhesion) was noted in the capillary lumen. Rosetting and erythrocyte adhesion lead to capillary thrombosis, disruption of microcirculation and sequestration of tissues in vital organs (parasite sequestration). The identified morphological features of the pathogens causing tropical malaria and the affected tissues determine the parasites' capability of changing properties of the infected erythrocytes' cell membranes, which leads to formation of abnormal intercellular contacts and constitutes one of the main mechanisms underlying the *Plasmodium falciparum* virulence.

Keywords: tropical malaria, *Plasmodium falciparum*, virulence, E-rosetting, erythrocyte adhesion, parasite sequestration, PfEMP1, electron microscopy

ЭЛЕКТРОННАЯ МИКРОСКОПИЯ ТРОФОЗОИТОВ *PLASMODIUM FALCIPARUM* И ИНФИЦИРОВАННЫХ ИМИ ТКАНЕЙ ПРИ ТЯЖЕЛОЙ ФОРМЕ ТРОПИЧЕСКОЙ МАЛЯРИИ

А. И. Соловьев[1], В. А. Капацина[2], М. О. Соколова[1], А. Р. Арюков[1]✉, А. Н. Коваленко[1], А. Н. Усков[3], В. А. Романенко[1]

[1] Военно-медицинская академия имени С. М. Кирова, Санкт-Петербург, Россия

[2] Клиническая инфекционная больница имени С. П. Боткина, Санкт-Петербург, Россия

[3] Детский научно-клинический центр инфекционных болезней Федерального медико-биологического агентства, Санкт-Петербург, Россия

Представлены результаты комплексного электронно-микроскопического исследования образцов венозной крови и тканей внутренних органов, полученных при изучении летального случая завозной тропической малярии. Целью работы было изучить ультраструктуру эритроцитарных стадий развития *Plasmodium falciparum* и изменений пораженных ими тканей при тяжелой форме тропической малярии. Образцы венозной крови, тканей коры головного мозга и миокарда исследовали с помощью световой, а также электронной (сканирующей и трансмиссионной) микроскопии. В крови были выявлены многочисленные трофозоиты *Plasmodium falciparum*. В цитоплазме инфицированных эритроцитов обнаружены множественные расщелины Маурера. Между инфицированными и непораженными эритроцитами выявлены патологические межклеточные контакты, что приводит к их слипанию и формированию розеток (эритроцитарный розеттинг). При исследовании тканей коры головного мозга и миокарда в просвете капилляров отмечена фиксация пораженных эритроцитов на эндотелии (эритроцитарная адгезия). Розеттинг и адгезия эритроцитов приводят к тромбированию капилляров, нарушению микроциркуляции и возникновению секвестров в тканях жизненно важных органов (паразитарная секвестрация). Выявленные морфологические особенности возбудителей тропической малярии и пораженных ими тканей определяют способность паразитов менять свойства клеточных мембран инфицированных эритроцитов, что приводит к формированию патологических межклеточных контактов и служит одним из основных механизмов вирулентности *Plasmodium falciparum*.

Ключевые слова: тропическая малярия, *Plasmodium falciparum*, вирулентность, эритроцитарный розеттинг, эритроцитарная адгезия, паразитарная секвестрация, PfEMP1, электронная микроскопия

Tropical malaria (TM) is a serious problem for tropical and subtropical regions, despite the international community's efforts aimed to decrease the incidence and stop transmission of pathogen causing this infection, *Plasmodium falciparum* (Welch, 1897), by its vector, by female *Anopheles* mosquitoes (Meigen, 1818). The diseases insidiousness often results from the gradual onset followed by the rapid malignant progression, suddenly entering the phase of irreversible fatal complications, even in cases of using antimalarial drugs. Malarial coma, algid, acute renal failure, toxic shock syndrome (TSS), and hemoglobinuric fever can lead to death of non-immune individuals, who have got infected with TM when visiting endemic regions [1].

The severe TM pathogenesis is based on the rosetting process (formation of conglomerates consisting of the infected and uninfected erythrocytes) and erythrocyte adhesion to the capillary endothelium [2]. This leads to small vessel thrombosis and sequestration of the vital organs, especially the brain. The molecular genetic mechanisms underlying the TM pathogenesis are associated with the release of multiple proteins (MAHRP1,2, REX3, HSP40, KAHRP, etc.) by the pathogen. *Pf*EMP1 (erythrocyte membrane protein being the main factor of *P. falciparum* virulence) found on the surface of the infected cell is the most important exported protein family [3, 4]. Transport of parasitic proteins is ensured by the Maurer's clefts defined as the parasitophorous vacuolar membrane protrusions that represent highly mobile structures [5, 6]. During the early phases of parasite development these move quickly, taking part in the PfEMP1 transport to the erythrocyte surface. The main virulence factor of *Plasmodium* has the increased affinity to the major cell receptors, such as ICAM-1 (intercellular adhesion molecule-1), CD36, CR, etc. [7, 8]. The PfEMP1 specific binding to the cell receptors leads to formation of abnormal contacts between the infected erythrocytes and the healthy cells, which results in such phenomena, as rosetting, adhesion, and sequestration [9].

Light microscopy is still the main method of examining parasites in blood and other tissues of the susceptible body. However, this method does not provide the possibility of examining fine structure of microorganisms and cellular mechanisms underlying pathogenesis of malignant malaria. High resolution of the electron microscope significantly expands the possibility of exploring the interplay between the malaria parasite and the cells of blood and other body's tissues. Sample preparation complexity, labor intensity, significant time investment, and high demands on the quality of test samples significantly limit the use of electron microscopy for examination of clinical material [10]. The contributing factors also include rapid development of the *P. falciparum* erythrocytic forms, accumulation of affected erythrocytes in the capillary bed, low parasitemia, and the rapid loss of morphological traits by the parasites and erythrocytes these have infected [11]. In this regard, the samples obtained by artificial cultivation of standard laboratory *Plasmodium* strains that often have low virulence or are non-pathogenic for humans are mostly used for examination by electron microscopy [12]. The data on the ultrastructural morphological alterations in the organism of patients with malaria are sporadic. Thus, we present the results of the comprehensive study of the material obtained from the patient, who died from complications of TM, by electron microscopy.

The study was aimed to assess fine structure of the *P. falciparum* erythrocytic stages of and estimate ultramorphological alterations of the affected tissues when examining the clinical material obtained from the patient with TM.

METHODS

The materials used in the study were represented by the antemortem venous blood samples collected for diagnostic purposes and the material obtained during subsequent postmortem examination of the brain, heart, and kidneys of the patient, who died from complications of TM.

Light microscopy

Blood specimens were prepared in accordance with the generally accepted method and Romanowsky–Giemsa stained [13].

The autopsy material was fixed in the 10% neutral buffered formalin. Then the samples were dehydrated using the increasing alcohol concentrations and embedded in paraffin (Biovitrum LLC; Russia). The tissue slices with the thickness of 5 μm cut from paraffin blocks were stained with hematoxylin and eosin (Biovitrum LLC; Russia). The AxioImager A2 light microscope (Carl Zeiss; Germany) was used for examination.

Scanning electron microscopy

The venous blood samples were fixed in the 2.5% glutaraldehyde in phosphate-buffered saline (PBS), pH 7.2–7.4, for 24 h. Then formed elements of blood were washed from the fixing solution by adding PSB three times, centrifugation, and supernatant removal. The volume of formed elements suspension was brought to 5% of the sample volume, the material obtained was resuspended and applied to the glass slides. After drying the specimens were soaked in the 2% osmium tetroxide (osmium oxide (VIII)) for 30 min, then sequentially dehydrated with the increasing ethanol concentrations (30°, 50°, 70°, 80°, 96°) and air-dried. To ensure the scanning effect, the material was treated with the gold/palladium alloy (Au/Pd (60 : 40). The 5 nm layer sputtering was accomplished using the Q150T ES system (Quorum; Germany). The specimens prepared were examined in the scanning mode using the Merlin electron microscope (Carl Zeiss; Germany) equipped by the SE2 secondary electron detector.

The internal organ tissue sections with the thickness of 5 μm were transferred to the glass slides, deparaffinized by treating with xylene three times (Ecos-1; Russia) throughout 3 days, then soaked in the 2% osmium tetroxide (Serva; Germany). The scanning layer splluttering and examination of the specimens prepared were accomplished using the above method.

Transmission electron microscopy

The venous blood and internal organ tissue samples were prepared by standard methods. The samples prepared were embedded in blocks, the plasticized Araldite resin (EMS; USA) was used as the embedding medium. The 100 nm slices cut from blocks were subjected for double contrasting with lead citrate and 1% aqueous uranyl acetate solution (Serva; Germany). The specimens prepared were examined in the transmission mode with the Merlin microscope (Carl Zeiss; Germany) using the STEM detector. The images of specimens obtained were analyzed using the ImageJ tool for analysis and processing of images (NIH; USA).

RESULTS

Female patient I., 44-years, resident of Saint Petersburg, was infected with the causative agent of TM during the short-term visit to the highly endemic region. She received no
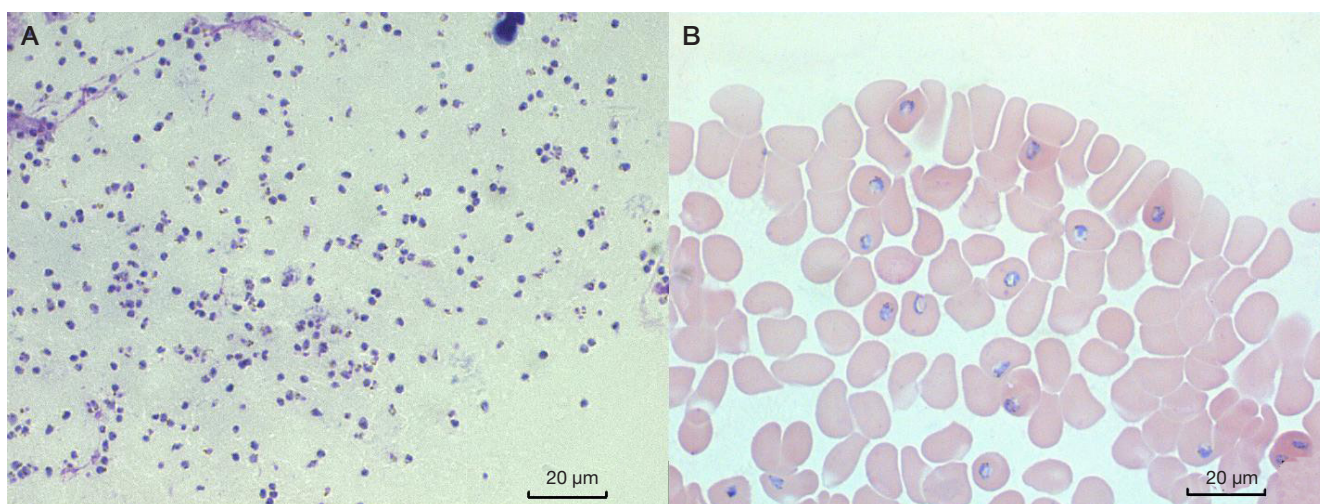
Fig. 1. *P. falciparum* young (ring) trophozoites in the thick blood smear (**A**); thin blood smear (**B**). Romanowsky–Giemsa stain, light microscopy (×1000)

chemotherapy for prevention of malaria. A week after returning from the trip the patient felt unwell, her body temperature increased. Her condition became progressively worse. The patient was admitted to the infectious diseases hospital on day 5 of the disease. Blood testing for parasites was performed in the emergency room due to clinical manifestations and epidemiological history, *P. falciparum* was revealed. Malaria treatment was started immediately. However, the patient died suddenly 13 h later. The immediate causes of death were toxic shock syndrome and edema (swelling of the brain), i.e. well known complications of malignant TM.

Examination of thick and thin blood smears revealed numerous *P. falciparum* young (ring phase) trophozoites in each field of view. Parasitemia exceeded 50,000 cells per 1 μL of blood (Fig. 1).

The images obtained when performing scanning electron microscopy of peripheral blood specimens show a large number of the deformed erythrocytes that had lost their typical biconcave shape. The affected erythrocytes have a bumpy surface repeating the outlines of the parasites developing in the cells. The infected erythrocyte membrane loses elasticity and becomes uneven due to incorporation of parasitic proteins in the membrane. Cell junctions are formed between the affected erythrocytes. This is associated with specific interaction between proteins of the main *P. falciparum* virulence factor incorporated in the membranes of affected erythrocytes and the cell receptors of adjacent cells. The same mechanism

underlies the rosetting phenomenon associated with formation of conglomerates consisting of affected and healthy blood cells. It is assumed that parasites avoid exposure to the cellular immunity factors by surrounding themselves with intact cells (Fig. 2).

According to the literature data, the infected erythrocytes' shape becomes rigid, and the proteins responsible for rigidity are directly related to virulence, which further demonstrates that secretome affects the infection severity [14]. Deformation of erythrocytes results from the emergence of large protrusions over trophozoites. This is where the cytoplasmic membrane areas carrying the *Pf*EMP1 parasite adhesion proteins are located [15].

The fine structure of the parasitic cells and erythrocytes these had affected in blood specimens was assessed by transmission electron microscopy (Fig. 3).

DISCUSSION

The observational random slices of venous blood specimens showed that there were *P. falciparum* trophozoites surrounded by the parasitophorous vacuolar membrane in the erythrocytes. The parasites' nuclei have an amorphous structure, chromatin is not condensed, the nuclear membrane contour is fuzzy, which represent the signs of incipient schizogony accompanied by the asynchronous sequential replication cycles [16]. Specific mechanisms of the *P. falciparum* multiple fission are poorly

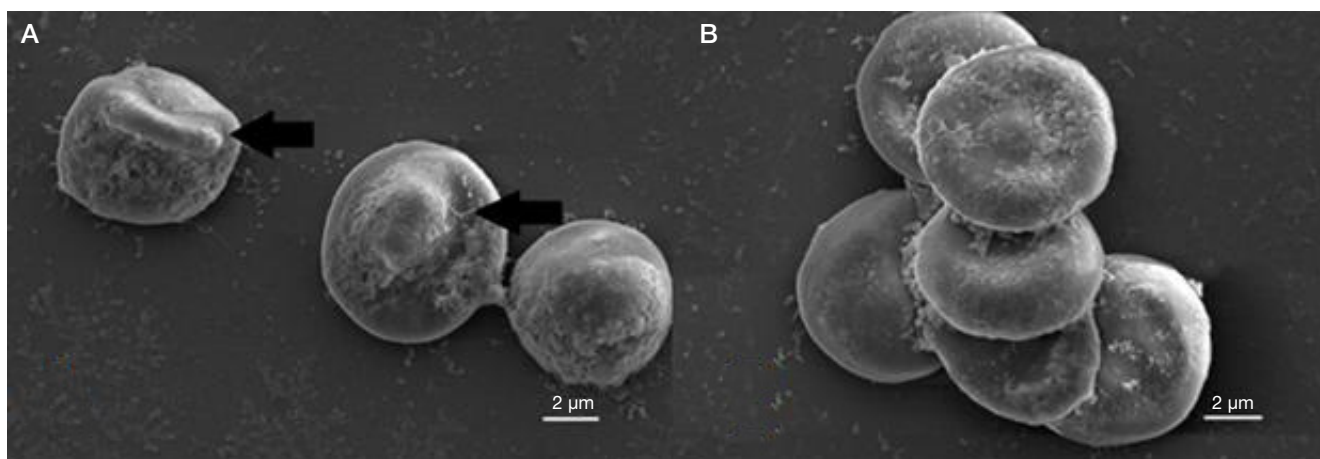**Fig. 2.** Scanning electron microscopy of blood specimens. **A**. Deformation of the erythrocyte cytoplasmic membrane over the trophozoite (*arrow*). **B**. Rosetting — formation of conglomerate consisting of infected and uninfected erythrocytes
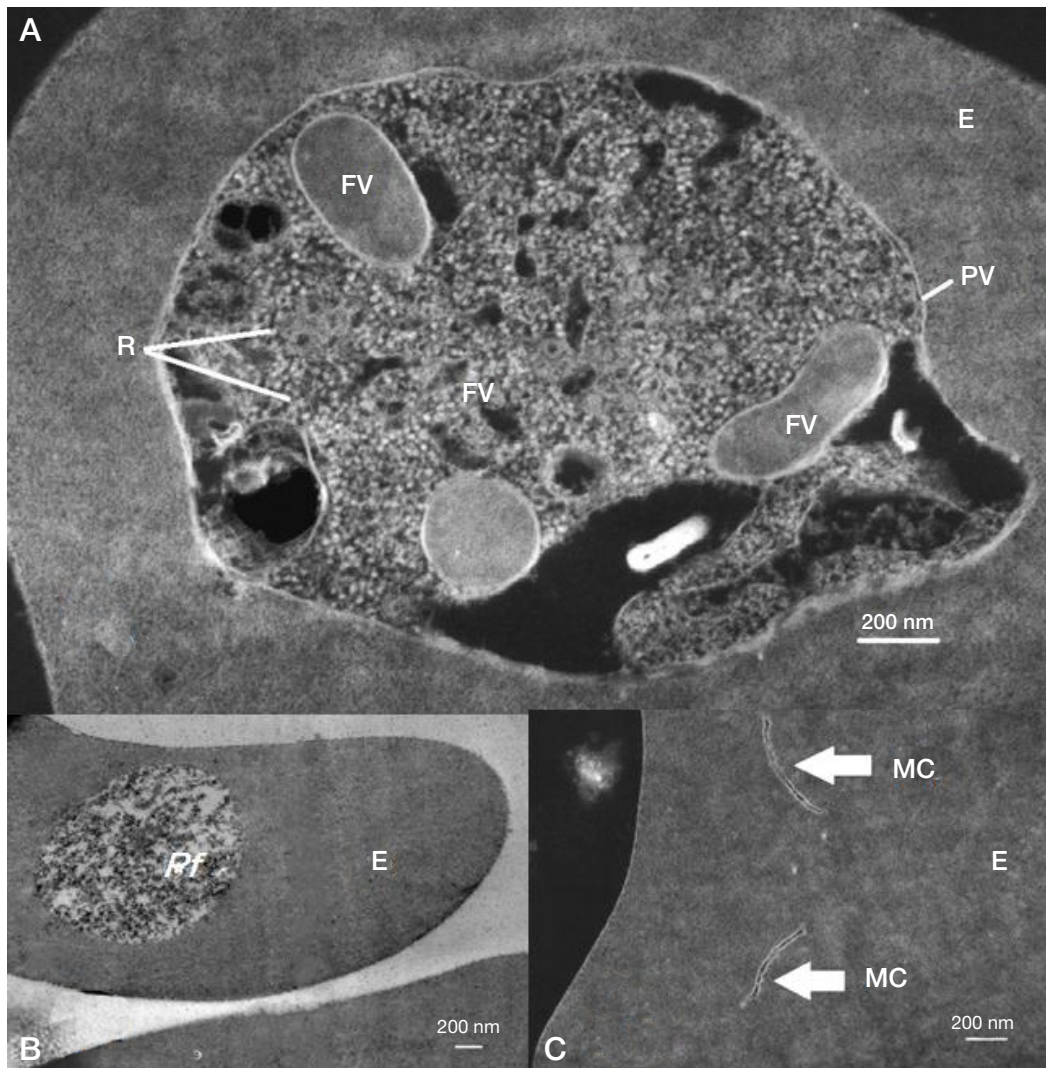
Fig. 3. Transmission electron microscopy: inverted (**A**, **C**), direct (**B**). Random slices of *P. falciparum* trophozoites located in the erythrocytes. E — erythrocyte; *Pf* — *P. falciparum*; FV — food vacuole; PV — parasitophorous vacuole; R — ribosomes; MC — Maurer's clefts in the infected erythrocyte cytoplasm

understood. It has been found that the processes occurring in the *Plasmodium* cells significantly differ from reproduction of other eukaryotes [17]. The food vacuoles are filled with the electron-dense substance similar to hemoglobin. It is well known that hemozoin, the product of the metabolism of hemoglobin ingested by *P. falciparum*, is accumulated in the parasites' food vacuoles (modified lysosomes) [18]. Many unbound ribosomes are found in the trophozoite cytoplasm, which suggests active synthesis of specific proteins essential for its membrane and exomembrane systems by the parasite. The infected erythrocyte's cytoplasm has a loose fine-grained structure; the membrane loses clear contours. Tubulovesicular structures with the electron-dense walls and electronically transparent content, the Maurer's clefts, were clearly visible inside erythrocytes. The Maurer's clefts that emerge at the early stages of parasites' development consist of the processes and whorls extending from the parasitophorous vacuolar membrane; these mature forming the functionally independent structures attached to erythrocyte cytoplasmic membrane [19].

Examination of the myocardium and cortical tissues has revealed the signs of the capillary lumen obliteration with the rosettes of infected erythrocytes attached to the endothelium. Erythrocytes of the rosettes still look as individual cells, their walls are clearly visible (Fig. 4).

Examination of the brain tissue and myocardial slices by scanning electron microscopy has revealed multiple facts of erythrocyte adhesion on the surface of the capillary endothelium. The infected and uninfected erythrocytes are deformed, they form rosettes, there are cells of spherical shape among them. This is probably associated with the changes in the erythrocyte cytoplasmic membrane structure resulting from incorporation of parasitic proteins in the membrane. It is well known that spherocytes can be considered as prehemolytic stage erythrocytes [20]. Apparently, the erythrocyte membrane permeability is impaired, when the membrane structure is changed, however, it remains unclear at which stage of the *P. falciparum* life cycle this occurs (Fig. 5).

In the erythrocytes organized in rosettes on the surface of endothelial cells, the lack of the fibers of fibrin being normally the key contributor to the blood clot formation attracts attention. The lack of fibrin masses observed in the erythrocyte adhesion sites suggests the differences in the mechanism underlying blood clot formation in TM and blood coagulation. It has been proven that conglomeration of erythrocytes into rosettes and their adhesion on the capillary endothelium results from abnormal interaction between parasitic proteins and cell receptors of erythrocytes and endothelial cells [21]. The key role of abnormal cell–cell interaction in the pathogenesis of malignant TM is confirmed by identification of tight junctions between
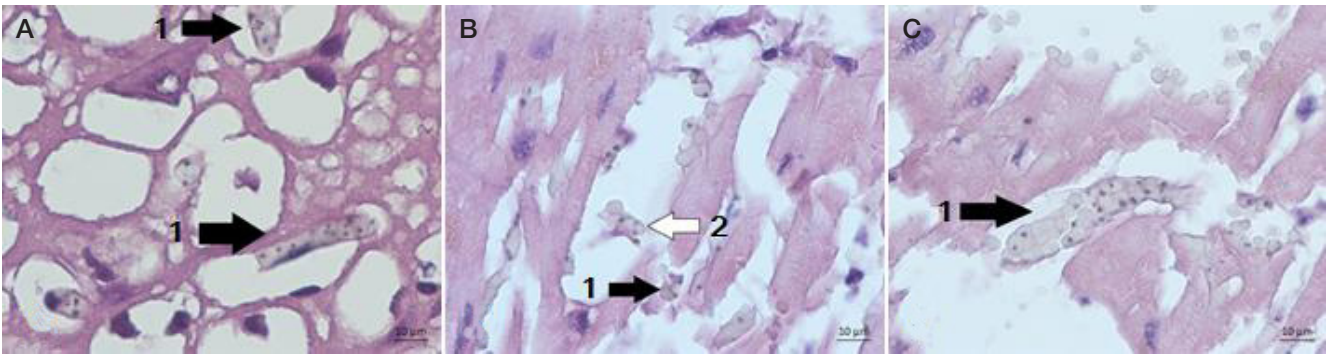
Fig. 4. Light microscopy of the autopsy material (hematoxylin and eosin stain, 1000× magnification): cerebral cortex (**A**); myocardium (**B**, **C**). 1 — rosetting in the small capillary lumen; 2 — adhesion of the rosettes of erythrocytes infected with *P. falciparum* to the capillary wall
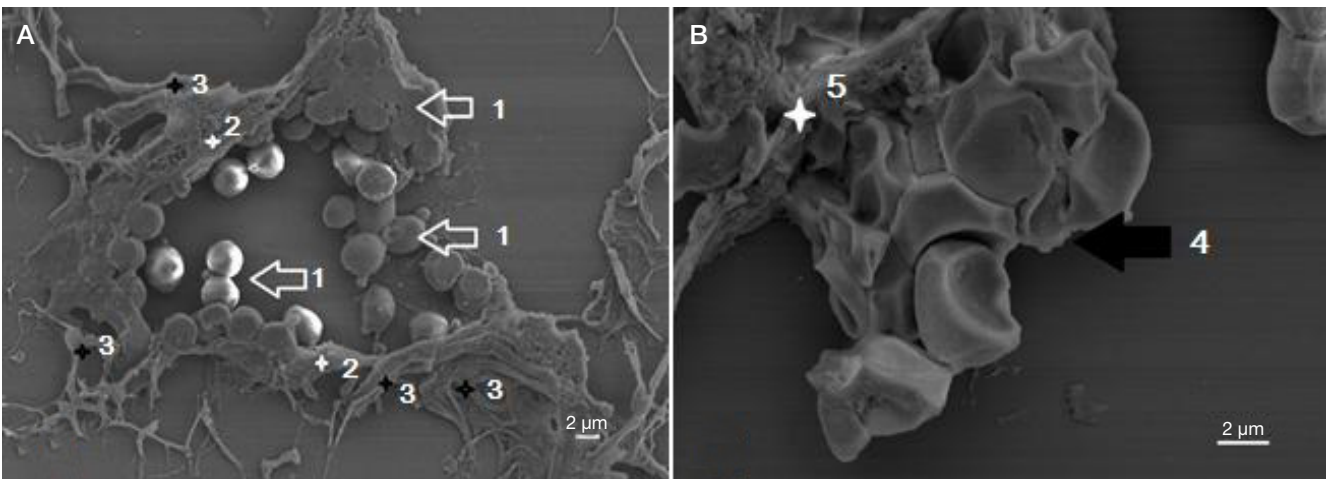
Fig. 5. Scanning electron microscopy of the slices of myocardium (**A**) and cerebral cortex (**B**). 1 — adhesion of spherical erythrocytes to the membranes of endothelial cells; 2 — endothelial cells; 3 — fibers of loose fibrous connective tissue along the periphery of the capillary; 4 — resetting in the capillary lumen; 5 — capillary endothelium

membranes of the erythrocytes forming rosettes in the cerebral capillaries. Of special importance are convoluted channels of the Maurer's clefts located in the area of the parasite adhesion to the membrane of the affected erythrocyte (Fig. 6).

CONCLUSIONS

The paper provides the results of morphological examination of the venous blood erythrocytes, myocardium, and brain tissues in severe tropical malaria. The analysis of the results of assessing ultrastructural changes of *P. falciparum* and erythrocytes during erythrocytic schizogony in *Plasmodium* confirms that there are complex molecular genetic and cellular mechanisms underlying the parasite's adverse effects on the host cells. Such interaction results in the changes of the infected erythrocyte cytoplasmic membrane surface architecture, formation of erythrocyte conglomerates, adhesion of those on the capillary endothelium in the myocardium and cerebral cortex. The changes observed led to microcirculatory
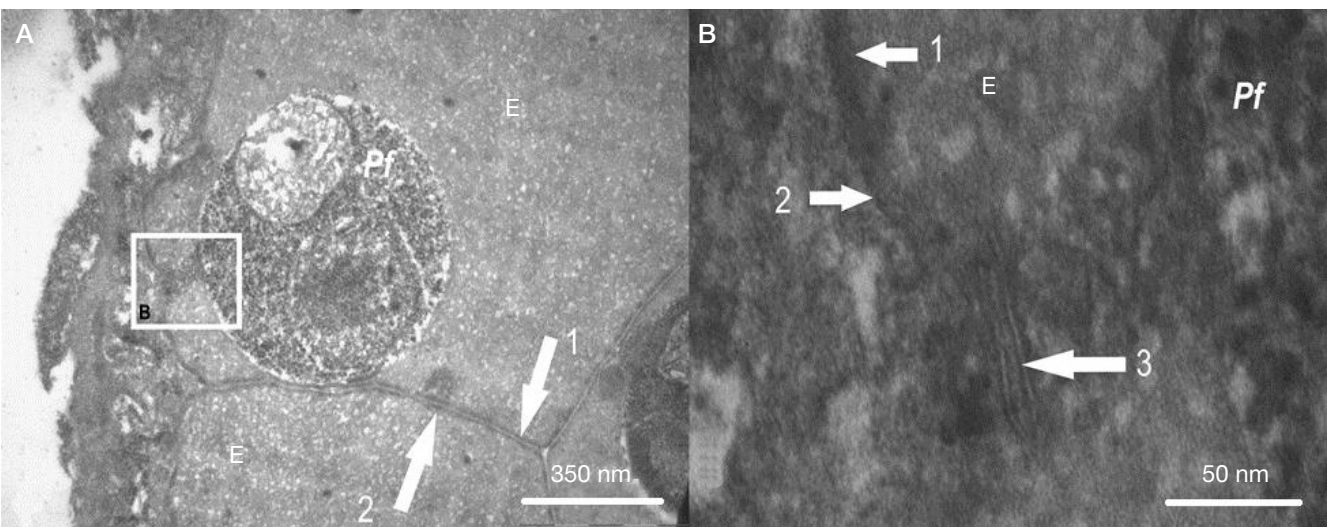
Fig. 6. Transmission electron miscroscopy of brain tissues. **A**. Slice of mature *P. falciparum* (*Pf*) trophozoite inside the erythrocyte (E) fixed on the capillary endothelium surface. **B**. Abnormal endomembrane system of the infected erythrocyte. 1 — cell membrane of the infected erythrocyte; 2 — cell membrane of the adjacent erythrocyte; 3 — channels of the Maurer's cleft located between the parasitophorous vacuolar membrane and the cell membrane of the affected erythrocyte

disturbances in the tissues of vital organs. The ultrastructural changes revealed confirm the parasite's capability of changing properties of cell membranes of the infected erythrocytes, which leads to formation of abnormal cell–cell contacts and serves as one of the main mechanisms of *P. falciparum* virulence determining the malignant course of tropical malaria.

References

1. Venkatesan P. The 2023 WHO World malaria report. The Lancet Microbe. 2024.
2. Lee WC, Russell B, Rénia L. Evolving perspectives on rosetting in malaria. Trends in Parasitology. 2022; 38 (10): 882–9.
3. Abdi A, Yu L, Goulding D, Rono MK, Bejon P, Choudhary J, et al. Proteomic analysis of extracellular vesicles from a Plasmodium falciparum Kenyan clinical isolate defines a core parasite secretome. Wellcome open research. 2017; 2.
4. Heiber A, Kruse F, Pick C, Grüring C, Flemming S, Oberli A, et al. Identification of new PNEPs indicates a substantial non-PEXEL exportome and underpins common features in Plasmodium falciparum protein export. PLoS pathogens. 2013; 9 (8): e1003546.
5. McHugh E, Carmo OM, Blanch A, Looker O, Liu B, Tiash S, et al. Role of Plasmodium falciparum protein GEXP07 in Maurer's cleft morphology, knob architecture, and P. falciparum EMP1 trafficking. MBio. 2020; 11 (2): 10–1128.
6. Yadavalli R, Peterson JW, Drazba JA, Sam-Yellowe TY. Trafficking and Association of Plasmodium falciparum MC-2TM with the Maurer's Clefts. Pathogens. 2021; 10 (4): 431.
7. Ortolan LS, Avril M, Xue J, Seydel KB, Zheng Y, Smith JD. Plasmodium falciparum parasite lines expressing DC8 and Group A PfEMP1 bind to brain, intestinal, and kidney endothelial cells. Frontiers in Cellular and Infection Microbiology. 2022; 12: 813011.
8. Jensen AR, Adams Y, Hviid L. Cerebral Plasmodium falciparum malaria: The role of PfEMP1 in its pathogenesis and immunity, and PfEMP1-based vaccines to prevent it. Immunological reviews. 2020; 293 (1): 230–52.
9. Juillerat A, Lewit-Bentley A, Guillotte M, Gangnard S, Hessel A, Baron B, et al. Structure of a Plasmodium falciparum PfEMP1 rosetting domain reveals a role for the N-terminal segment in heparin-mediated rosette inhibition. Proceedings of the National Academy of Sciences. 2011; 108 (13): 5243–8.
10. Mwenda MC, Fola AA, Ciubotariu II, Mulube C, Mambwe B, Kasaro R, et al. Performance evaluation of RDT, light microscopy, and PET-PCR for detecting Plasmodium falciparum malaria infections in the 2018 Zambia National Malaria Indicator Survey. Malaria Journal. 2021; 20: 1–10.
11. Soulard V, Bosson-Vanga H, Lorthiois A, Roucher C, Franetich JF, Zanghi G, et al. Plasmodium falciparum full life cycle and

12. Plasmodium ovale liver stages in humanized mice. Nature communications. 2015; 6 (1): 1–9.
12. Liffner B, Diaz AKC, Blauwkamp J, Anaguano D, Frolich S, Muralidharan V, et al. Atlas of Plasmodium falciparum intraerythrocytic development using expansion microscopy. Elife. 2023; 12: RP88088.
13. Laboratornaja diagnostika maljarii i babeziozov: Metodicheskie ukazanija. M.: FBUZ «Federal'nyj centr gigieny i jepidemiologii» Rospotrebnadzora, 2015; 43 s. Russian.
14. Borovskaya MK, Kuznecova YeYe, Gorohova VG, Korjakina LB, Kurilskaya TE, Pivovarov YuI. Strukturno-funkcional'naja harakteristika membrany jeritrocita i ee izmenenija pri patologijah raznogo geneza. Acta Biomedica Scientifica. 2010; 3 (73): 334–54. Russian.
15. Melcher M, Muhle RA, Henrich PP, Kraemer SM, Avril M, Vigan-Womas I, et al. Identification of a role for the PfEMP1 semiconserved head structure in protein trafficking to the surface of Plasmodium falciparum infected red blood cells. Cellular microbiology. 2010; 12 (10): 1446–62.
16. Kilian N, Zhang Y, LaMonica L, Hooker G, Toomre D, Mamoun CB, et al. Palmitoylated Proteins in Plasmodium falciparum-Infected Erythrocytes: Investigation with Click Chemistry and Metabolic Labeling. BioEssays. 2020; 42 (6): 1900145.
17. McDonald J, Merrick CJ. DNA replication dynamics during erythrocytic schizogony in the malaria parasites Plasmodium falciparum and Plasmodium knowlesi. PLoS Pathogens. 2022; 18 (6): e1010595.
18. Ostera G, Tokumasu F, Oliveira F, Sa J, Furuya T, Teixeira C, Dvorak J. Plasmodium falciparum: food vacuole localization of nitric oxide-derived species in intraerythrocytic stages of the malaria parasite. Experimental parasitology. 2008; 120 (1): 29–38.
19. Mundwiler-Pachlatko E, Beck HP. Maurer's clefts, the enigma of Plasmodium falciparum. Proceedings of the National Academy of Sciences. 2013; 110 (50): 19987–94.
20. Nigra AD, Casale CH, Santander VS. Human erythrocytes: cytoskeleton and its origin. Cellular and Molecular Life Sciences. 2020; 77: 1681–94.
21. Avril M, Bernabeu M, Benjamin M, Brazier AJ, Smith JD. Interaction between endothelial protein C receptor and intercellular adhesion molecule 1 to mediate binding of Plasmodium falciparum-infected erythrocytes to endothelial cells. MBio. 2016; 7 (4): 10–1128.

Литература

1. Venkatesan P. The 2023 WHO World malaria report. The Lancet Microbe. 2024.
2. Lee WC, Russell B, Rénia L. Evolving perspectives on rosetting in malaria. Trends in Parasitology. 2022; 38 (10): 882–9.
3. Abdi A, Yu L, Goulding D, Rono MK, Bejon P, Choudhary J, et al. Proteomic analysis of extracellular vesicles from a Plasmodium falciparum Kenyan clinical isolate defines a core parasite secretome. Wellcome open research. 2017; 2.
4. Heiber A, Kruse F, Pick C, Grüring C, Flemming S, Oberli A, et al. Identification of new PNEPs indicates a substantial non-PEXEL exportome and underpins common features in Plasmodium falciparum protein export. PLoS pathogens. 2013; 9 (8): e1003546.
5. McHugh E, Carmo OM, Blanch A, Looker O, Liu B, Tiash S, et al. Role of Plasmodium falciparum protein GEXP07 in Maurer's cleft morphology, knob architecture, and P. falciparum EMP1 trafficking. MBio. 2020; 11 (2): 10–1128.
6. Yadavalli R, Peterson JW, Drazba JA, Sam-Yellowe TY. Trafficking and Association of Plasmodium falciparum MC-2TM with the Maurer's Clefts. Pathogens. 2021; 10 (4): 431.

7. Ortolan LS, Avril M, Xue J, Seydel KB, Zheng Y, Smith JD. Plasmodium falciparum parasite lines expressing DC8 and Group A PfEMP1 bind to brain, intestinal, and kidney endothelial cells. Frontiers in Cellular and Infection Microbiology. 2022; 12: 813011.
8. Jensen AR, Adams Y, Hviid L. Cerebral Plasmodium falciparum malaria: The role of PfEMP1 in its pathogenesis and immunity, and PfEMP1-based vaccines to prevent it. Immunological reviews. 2020; 293 (1): 230–52.
9. Juillerat A, Lewit-Bentley A, Guillotte M, Gangnard S, Hessel A, Baron B, et al. Structure of a Plasmodium falciparum PfEMP1 rosetting domain reveals a role for the N-terminal segment in heparin-mediated rosette inhibition. Proceedings of the National Academy of Sciences. 2011; 108 (13): 5243–8.
10. Mwenda MC, Fola AA, Ciubotariu II, Mulube C, Mambwe B, Kasaro R, et al. Performance evaluation of RDT, light microscopy, and PET-PCR for detecting Plasmodium falciparum malaria infections in the 2018 Zambia National Malaria Indicator Survey. Malaria Journal. 2021; 20: 1–10.
11. Soulard V, Bosson-Vanga H, Lorthiois A, Roucher C, Franetich JF, Zanghi G, et al. Plasmodium falciparum full life cycle and

Plasmodium ovale liver stages in humanized mice. Nature communications. 2015; 6 (1): 1–9.

12. Liffner B, Diaz AKC, Blauwkamp J, Anaguano D, Frolich S, Muralidharan V, et al. Atlas of Plasmodium falciparum intraerythrocytic development using expansion microscopy. Elife. 2023; 12: RP88088.

13. Лабораторная диагностика малярии и бабезиозов: Методические указания. М.: ФБУЗ «Федеральный центр гигиены и эпидемиологии» Роспотребнадзора, 2015; 43 с.

14. Боровская М. К., Кузнецова Э. Э., Горохова В. Г., Корякина Л. Б., Курильская Т. Е., Пивоваров Ю. И. Структурно-функциональная характеристика мембраны эритроцита и ее изменения при патологиях разного генеза. Acta Biomedica Scientifica. 2010; 3 (73): 334–54.

15. Melcher M, Muhle RA, Henrich PP, Kraemer SM, Avril M, Vigan-Womas I, et al. Identification of a role for the PfEMP1 semiconserved head structure in protein trafficking to the surface of Plasmodium falciparum infected red blood cells. Cellular microbiology. 2010; 12 (10): 1446–62.

16. Kilian N, Zhang Y, LaMonica L, Hooker G, Toomre D, Mamoun CB, et al. Palmitoylated Proteins in Plasmodium falciparum-Infected Erythrocytes: Investigation with Click Chemistry and Metabolic Labeling. BioEssays. 2020; 42 (6): 1900145.

17. McDonald J, Merrick CJ. DNA replication dynamics during erythrocytic schizogony in the malaria parasites Plasmodium falciparum and Plasmodium knowlesi. PLoS Pathogens. 2022; 18 (6): e1010595.

18. Ostera G, Tokumasu F, Oliveira F, Sa J, Furuya T, Teixeira C, Dvorak J. Plasmodium falciparum: food vacuole localization of nitric oxide-derived species in intraerythrocytic stages of the malaria parasite. Experimental parasitology. 2008; 120 (1): 29–38.

19. Mundwiler-Pachlatko E, Beck HP. Maurer's clefts, the enigma of Plasmodium falciparum. Proceedings of the National Academy of Sciences. 2013; 110 (50): 19987–94.

20. Nigra AD, Casale CH, Santander VS. Human erythrocytes: cytoskeleton and its origin. Cellular and Molecular Life Sciences. 2020; 77: 1681–94.

21. Avril M, Bernabeu M, Benjamin M, Brazier AJ, Smith JD. Interaction between endothelial protein C receptor and intercellular adhesion molecule 1 to mediate binding of Plasmodium falciparum-infected erythrocytes to endothelial cells. MBio. 2016; 7 (4): 10–1128.

THE ISSUE OF PRESERVING INTERICTAL ACTIVITYIN LONG-TERM EEG STUDIES OF EPILEPSY

Gulyaev SA[1,2] ✉, Klimanov SG[1], Germashev GA[1], Khanukhova LM[2], Garmash AA[1]

[1] Engineering and Physical Institute of Biomedicine, National Research Nuclear University MEPhI, Moscow, Russia

[2] La Salute Clinic, Moscow, Russia

Modern application of mathematical methods for analyzing EEG recordings is limited due to the phenomenon of information averaging. In these conditions, it is important to find the most likely method for improving the quality of diagnosis of paroxysmal pathological patterns that have a short "life", such as outbreaks and subclinical paroxysms. The purpose of the study was to evaluate the possibility of excluding interictal activity from a long-term EEG study in order to achieve its information "enrichment" by forming conditional sequences of pathological changes representing its main clinical task. Forty people of different ages and both sexes were examined. The control group included 20 patients aged 12–67 years with direct detection of spike-wave activity on the EEG. The comparison group consisted of 20 patients aged 10–66 years with no spike-wave activity in the recording. It has been shown that interictal data obtained in patients with epileptiform phenomena are not of significant interest for the main group of clinical studies. The exclusion of these data leads to the "enrichment" of information due to the sequential placement of paroxysmal patterns and makes it possible to obtain not only more compact results of examinations of the pathological component, but also to form a basis for developments using technologies for their subsequent mathematical analysis.

ВОПРОС СОХРАНЕНИЯ ИНТЕРИКТАЛЬНОЙ АКТИВНОСТИ В ДЛИТЕЛЬНЫХ ЭЭГ-ИССЛЕДОВАНИЯХ ЭПИЛЕПСИИ

С. А. Гуляев[1,2] ✉, С. Г. Климанов[1], Г. А. Гермашев[1], Л. М. Ханухова[2], А. А. Гармаш[1]

[1] Инженерно-физический институт биомедицины НИЯУ МИФИ, Москва, Россия

[2] Клиника Ла Салюте, Москва, Россия

Современное применение математических методов анализа ЭЭГ-записей ограничено из-за феномена усреднения информации. В этих условиях актуально найти наиболее вероятный метод повышения качества диагностики пароксизмальных патологических паттернов, имеющих малую продолжительность «жизни», таких как вспышки и субклинические пароксизмы. Целью исследования было оценить возможность исключения межприступной интериктальной активности из длительного ЭЭГ-исследования для достижения его информационного «обогащения» путем формирования условной последовательностей патологических изменений, представляющих его главную клиническую задачу. Было обследовано 40 человек разного возраста, обоих полов. В контрольную группу вошли 20 пациентов 12–67 лет с непосредственным выявлением спайк-волновой активности на ЭЭГ. Группу сравнения составили 20 пациентов 10–66 лет с отсутствием спайк-волновой активности в записи. Показано, что интериктальные данные, полученные у пациентов с наличием эпилептиформных феноменов, не представляют значимого интереса для основной группы клинических исследований. Исключение этих данных приводит к «обогащению» информации и за счет последовательного размещения пароксизмальных паттернов позволяет получать не только более компактные результаты обследований патологической составляющей, но и сформировать базу для разработок с использованием технологий их последующего математического анализа.

By the beginning of the current century, video-EEG monitoring had become firmly established in the provision of medical care to patients with epilepsy [1] as the basis for its differential diagnosis and a method that allows prescribing adequate treatment even in the case of drug-resistant forms of the disease [2]. This technology began to develop especially rapidly against the backdrop of the development of electronic systems for storing large amounts of information (big data), which showed its advantage for the differential diagnosis of epileptic seizures over classical routine EEG studies [3–5].

At the same time, the main technology for deciphering EEG recordings is still based on visual phenomenological analysis [6] with the identification of certain types of pathological graph elements, which, in conditions of continued recordings,

significantly increases the visual load on the specialist and can lead to both diagnostic errors and for worker fatigue and the development of occupational vision damage.

According to a survey conducted in Germany at 16 German epilepsy centers between December 2020 and January 2021 [7], EEG performance problems compromised diagnosis in approximately one in 10 patients. Therefore, today one of the most pressing issues in organizing a continued EEG study is the creation of the most comfortable environment for the doctor and, above all, a convenient presentation of the result, the issue of determining the epileptiform graph element can be violated due to visual fatigue, insufficient qualifications or the controversial clinical significance of the phenomenon, or its similarity to a recording artifact [8–10].

This situation has led to the search for ways to reduce the amount of visual information presented to the doctor. It is based on the development of technologies for automatically identifying short-term changes in the spectral density of a signal with their subsequent interpolation onto the conditional surface of the head in a flat or three-dimensional representation [11–16]. However, by the beginning of the 2000s it became clear that this technology is more successful in studying intracranial structural changes that produce unique pathological rhythmic activity [17–19].

At the same time, its use in epilepsy has shown mixed results [20, 21]. According to them, the best results can be achieved in the case of the production of rhythmic epileptiform activity from a focus [22] or when assessing the relationship between different foci of epileptic activity [23], which led to the preservation of routine visualization-phenomenological analysis as the main method for diagnosing epileptic activity.

The next solution was to develop systems for identifying individual epileptic phenomena in recordings [24, 25]. However, this technology required the introduction of pattern recognition systems, since the recorded epileptic phenomenon has a complex shape and it is not always possible to evaluate it using elementary procedures for assessing amplitude and frequency [26–28]. Currently, the analysis of epileptic activity in the context of a continued EEG study requires solving the following issues: 1) identifying pathological paroxysmal activity and excluding artifacts similar to it; 2) its quantitative analysis per unit of time; 3) optimization of the presentation of the result, understandable for both physiologists and clinicians.

Detection of pathological activity can currently be considered both from the position of manual signal extraction from the primary EEG recording, and from the position of complete automation of the process using artificial intelligence (AI) technologies with the development of deep learning systems [29, 30].

Considering the above, the optimal option for presenting continued studies could be the result of automated mathematical post-processing, representing, on the one hand, the selection of all pathological elements [31] when removing interictal activity from the recording. This combination will make it possible to use the entire spectrum of EEG signal processing based on rhythmic activity analysis technology, and not only combine them with two or three-dimensional images obtained during an MRI study in the form of three-dimensional spatial maps, but by solving the inverse EEG problem [32, 33] to determine with great accuracy pathological areas of the cortex that are sources of paroxysmal bioelectrical activity.

To implement this technology, it is necessary to establish how much the information from an EEG study during the interictal period differs from the background (Resting State) EEG activity of people who do not suffer from diseases with increased activity of neural structures, manifested by the appearance of pathological paroxysmal activity during an EEG study, and also how much excluding interictal activity may affect the accuracy of the final result.

Accurate comparative analysis of EEG recordings is usually difficult due to the lack of a single starting point of the event, which leads to a phase shift of the EEG signal and the impossibility of their comparative analysis. This bias does not allow the use of previously widely presented methods of signal correlation and coherence, since the signals studied in different people are absolutely unrelated to each other, and any decision indicating the presence of such a connection will be deliberately false.

However, the answer to this question is provided by the theory of EEG microstates, proposed in the 1990s by D. Lehmann et al. This approach allows one to separate a continuous stream of EEG data through a clustering procedure into individual components. An array is created from individual recording sections that have similar electrophysiological characteristics (microstates) during which the main indicators of the general scalp potential remain relatively stable. Currently, cluster analysis technologies make it possible to identify up to 39 individual EEG microstates. However, maximum representativeness can be achieved only in the first 2–8 classes, which is likely due to the activity of large neural networks responsible for the implementation of basic and most stable brain functions, the violation of which manifests itself in the form of severe changes in the mental sphere [34–36].

Thus, by considering sequences of EEG microstates, the researcher has the opportunity not only to judge the characteristics of the work of large brain networks, but also to compare them with each other.

However, changes in their characteristics are largely associated with structural and anatomical changes in the neural formations that form them, therefore, an isolated analysis of the frequency of representation or lifetime of each of the identified EEG microstates in the absence of an organic substrate that damages interneuron connections may not differ from conventionally normal values. In the structure of neurological diseases caused by increased excitability of neurons in the cerebral cortex, this is observed in patients with genetic forms of epilepsy, when the researcher does not detect organic changes using neuroimaging technologies.

Under these conditions, the disease has a greater impact on the functional sequences of excitation of cortical structures, described as a system of information flows in cortical structures [37, 38].

Each individual EEG microstate represents a relatively stable version of the scalp potential, or a total set of variants of postsynaptic discharges fixed in time, associated with the activity of large neural formations involved in the implementation of a common function, therefore, solving the inverse EEG problem for each individual EEG microstate will allow us to identify several successive points on cortical structures associated with the transition of activity from one neural network to another as part of the information flow model.

As a result, the researcher will be able to determine not only the structural changes in the neural network, but also find out the functional changes associated with changes in the processes of formation of higher nervous functions in the conditions of the development of the disease.

The most widely used solution to this issue was proposed by R. D. Pascual-Marqui in the form of a system for solving the inverse EEG problem based on the technology of combining dipole localization and a layer-by-layer head model, called low-resolution electromagnetic tomography (LORETA) [39].

The technology has now added quantitative neuroanatomy based on templates provided by the Brain Imaging Center of the Montreal Neurological Institute (MNI), allowing spatial localization results at a level comparable to classical functional imaging techniques such as PET and fMRI [40–50].

Thus, the above made it possible to formulate a null theory of the experiment, which consists in the fact that the presence of significant differences in the identified results of studies of interictal recordings of patients suffering from diseases with increased activity of the neural structures of the cerebral cortex and the results of studies of background (Resting State) EEG recordings of healthy people who do not have pathological paroxysmal changes will not allow interictal data to be excluded from the general study, since the information they contain is essential for the researcher and cannot be deliberately lost from the main study record.

The purpose of the study was to evaluate the possibility of excluding interictal interictal activity from a long-term EEG study in order to achieve its information "enrichment" by forming conditional sequences of pathological changes representing its main clinical task.

METHODS

Study Groups

The study involved 40 people of different ages, both sexes, who underwent an EEG examination. The general scenario of the EEG study was carried out according to previously published recommendations [51–53]. The control group included 20 patients aged 12–67 years (average age: 25 years). Criteria for inclusion in the control group: presence of an established diagnosis of epilepsy; direct detection of spike-wave activity on the EEG.

The comparison group consisted of 20 patients aged 10–66 years (average age: 28 years). Criteria for inclusion in the comparison group: absence of an established diagnosis of epilepsy; absence of spike-wave activity in the recording.

For the study, a sample of epochs (on average at least 10 minutes) of the patient's stay in a state of passive, relaxed wakefulness with eyes closed was taken from the general recording. In patients with registration of paroxysmal epileptiform activity, a sample of data was recorded in a state of passive relaxed wakefulness with eyes closed between ictal episodes.

Exclusion criteria: presence of an established diagnosis of epilepsy in the anamnesis; absence of a characteristic ictal pattern in the recording; the presence of specific changes in the EEG recording without a previously established diagnosis of epilepsy; the presence of established epileptic dementia with the development of pronounced cognitive dysfunctions and gross structural changes in the brain substance determined using neuroimaging methods; taking pharmacologically active substances; smoking; drinking strong alcohol less than a week before the study; regular alcohol consumption; pregnancy.

Experimental design

The results were compared in a state of passive relaxed wakefulness with eyes closed in real time using the cluster analysis method (K-means), which makes it possible to calculate individual stable EEG microstates in the frequency range 2–20 Hz. To identify cognitive sequences, a model of eight EEG microstates was used, reflecting the formation of the general scalp potential as a result of the total activity of eight conditional neural networks. The use of this model made it possible to more rationally use the available computing power.

According to the proposed model, for each individual EEG microstate, an inverse EEG problem was solved with the establishment of its connection with individual cortical structures within the Brodmann field system (according to the recommendations of the Montreal Neurosurgical Institute (MNI), Canada).

Technique

The EEG study was carried out on a 52-channel bioamplifier of domestic production (Zelenograd) with a base frequency of the analog-to-digital converter of 500 Hz, which made it possible to confidently obtain data in the range from 1 to 250 Hz without loss of information content. The obtained information was processed on a PC in the software package sLORETA v20210701 Switzerland v20210701 (University of Zurich; Switzerland), as well as by implementing technological prototypes using interpreted software packages EEGLAB and BRAINSTORM, implemented under the control of the MATLAB system (Mathworks ver. 98 (2020); USA).

Statistical analysis

Statistical data processing was carried out using the SPSS Statistics ver.23.0 software package (IBM; USA). The normality of the distribution was checked using the Kolmogorov–Smirnov test, and the statistical significance of the differences was established using the Chi-Square test.

Table 1. Frequency of registration of individual EEG microstates in the control observation group

	I	II	III	IV	V	VI	VII	VIII
Mean	2.28	2.25	2.32	2.2	2.3	2.29	2.31	2.48
Deviation	0.55	0.45	0.46	0.66	0.35	0.54	0.49	0.3
Min	0.414	0.88	1.3	0.3	1.6	0.04	0.38	2.01
Max	3.04	3.03	3.49	2.91	2.95	2.93	3.15	3.16

Table 2. Frequency of registration of individual EEG microstates in the comparative observation group

	I	II	III	IV	V	VI	VII	VIII
Mean	2.28	2.27	2.31	2.38	2.43	2.29	2.48	2.39
Deviation	0.43	0.3	0.36	0.37	0.36	0.31	0.35	0.24
Min	1.55	1.55	1.7	1.87	2	1.64	1.97	1.85
Max	2.78	2.869	2.89	3.2	3.33	2.91	3.07	2.714

Table 3. Lifetime of individual EEG microstates in the control observation group

	I	II	III	IV	V	VI	VII	VIII
Mean	0.05	0.05	0.05	0.05	0.05	0.06	0.05	0.06
Deviation	0	0	0.01	0.01	0	0.02	0.01	0
Min	0.05	0.04	0.04	0.04	0.05	0.05	0.05	0.05
Max	0.06	0.06	0.06	0.06	0.06	0.14	0.07	0.06

Table 4. Lifetime of individual EEG microstates in the comparison group

	I	II	III	IV	V	VI	VII	VIII
Mean	0.05	0.05	0.05	0.05	0.05	0.05	0.05	0.05
Deviation	0	0	0	0	0	0	0	0
Min	0.04	0.04	0.05	0.05	0.05	0.05	0.05	0.05
Max	0.06	0.06	0.06	0.06	0.06	0.06	0.06	0.07

RESULTS

Study of time-frequency characteristics of EEG microstates

The frequency and time characteristics of individual EEG microstates show the preservation of the structural connections of the neural network involved in the implementation of bioelectrical activity, forming a separate EEG microstate.

Therefore, analysis of the frequency of registration of each individual EEG microstate and the time of its existence (life) was necessary to identify a possible violation of the integrity of the structure of brain neural networks in people suffering from epilepsy. If this pathology were detected, the question of excluding information about interictal activity in the recording would not make sense due to the inadequacy of the material being studied. However, the data obtained (Tables 1–4) showed that the time-frequency characteristics of individual EEG microstates did not have statistically significant changes between the study groups (Chi-square test; $p > 0.5$). These observations allow us to reject the null hypothesis of the experiment and justify the possibility of excluding interictal recording from a long-term EEG study for people with epilepsy since its characteristics are quite comparable to the brain activity of a healthy person.

Solution of the inverse EEG problem for the activity of individual EEG microstates

Solving the inverse EEG problem for a selected set of EEG microstates (Fig. 1–3) made it possible to identify the sequence of transition of bioelectrical activity according to the topography of individual fields of K. Brodmann. These data reflected the current activity present in the subjects in a state of passive, relaxed wakefulness with their eyes closed, both in the control group and in the comparison group.

A comparison of these characteristics in representatives of the control group and the comparison group (Fig. 1) showed that the results characterizing the rhythmic activity of Brodmann areas responsible for perception (18, 19) and cognitive processing of data (6, 7) have a low degree of difference (statistical significance according to the Chi-Square test was $p = 0.6$) (Fig. 2).

However, in the projection of fields 22, 27, 30, 31, 39 and 40 (Fig. 3), associated with the centers of sound perception and speech function, as well as the retrosplenial cerebral cortex
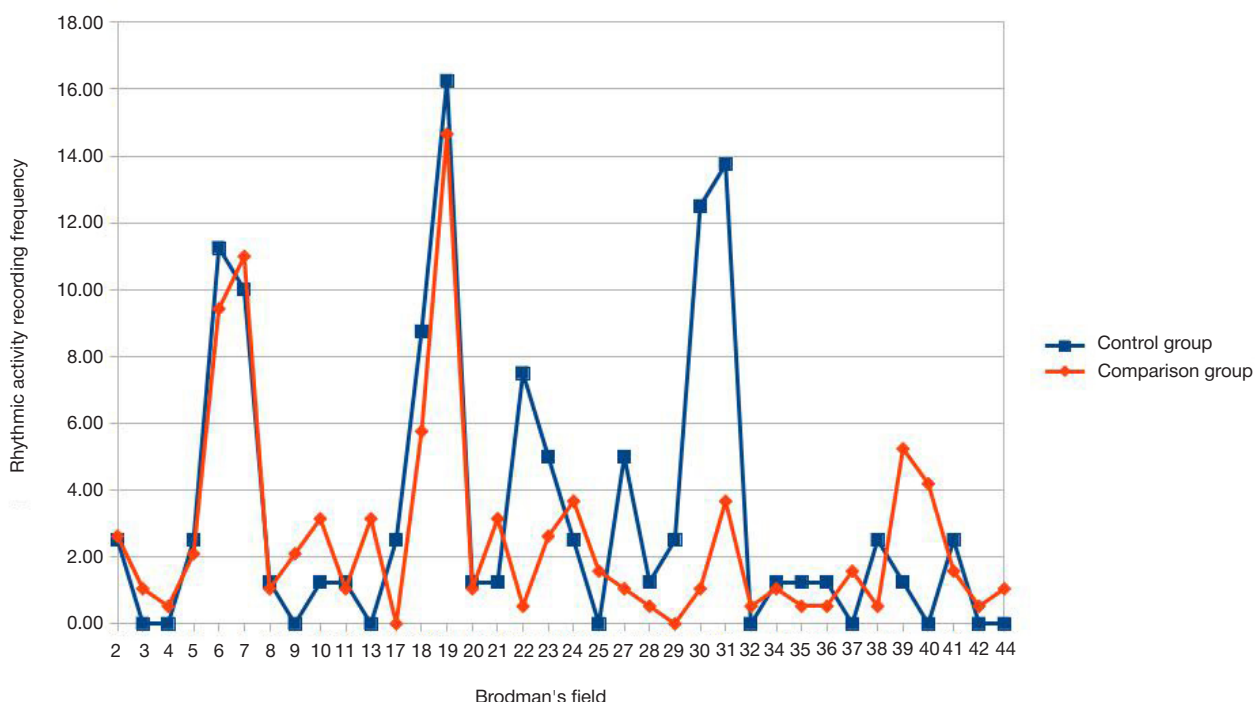

Fig. 1. Percentage of registration of default brain activity when solving an inverse EEG task (Chi-squared test; $p = 0.04$)
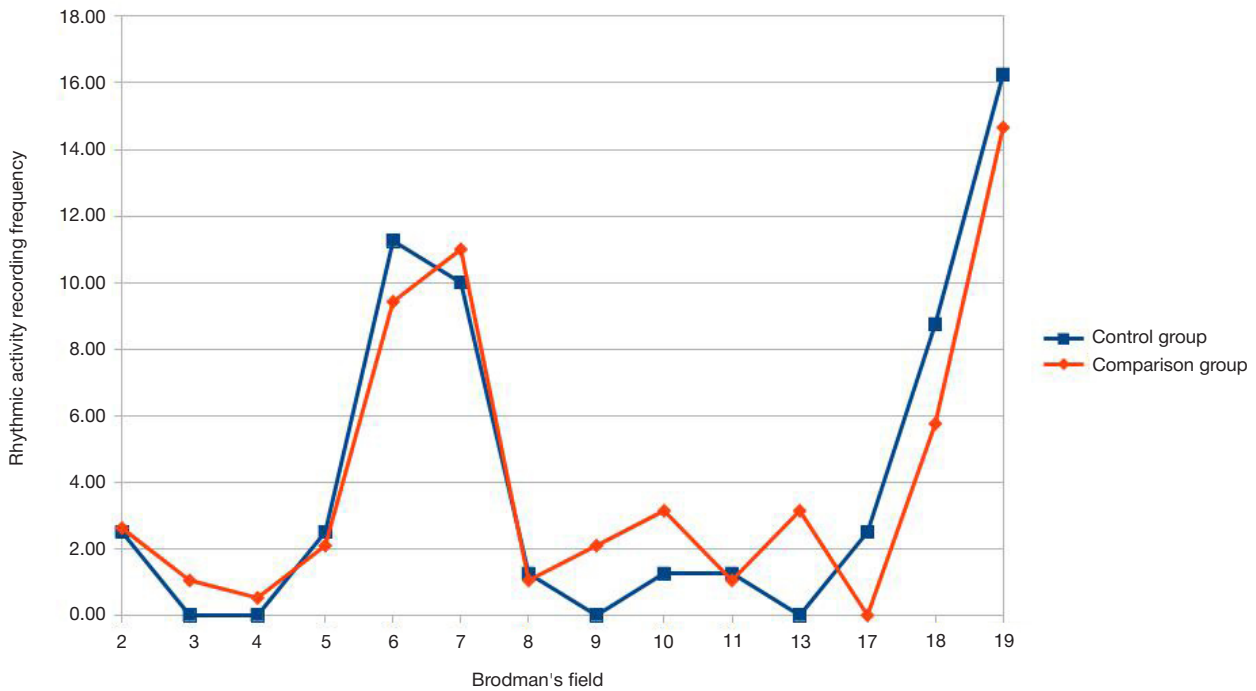
Fig. 2. Default activity in individual Brodmann fields that implement the processes of gnosis and information processing (Chi-squared test; $p = 0.6$)

(spatial orientation), significant changes in characteristics were recorded (Chi-square test; $p = 0.01$).

Thus, by analyzing changes in the sequences of excitation of cortical structures, it is possible to reject the null hypothesis of the experiment, especially if the researcher sets the goal as an analysis of basic cognitive functions, and not a study of their physiological characteristics in the spectrum of the conditional norm, for example, the fact of evidence of epilepsy in the subject or localization epileptic foci in the cortex to justify the possibility of subsequent surgical treatment.

DISCUSSION

Our research showed mixed results. Thus, the lack of data confirming the presence of structural changes in neural

networks in those examined with paroxysmal changes in the electroencephalogram made it possible to reject the null hypothesis of the experiment, especially when studying diseases without organic damage being detected through neuroimaging studies, representing the cause of the disease. These observations correspond to data from previously conducted clinical examinations [43, 54], indicating that in at least 50% of clinical cases of established epilepsy in the interictal period, no significant disorders of higher nervous functions are detected, and patients with such disorders, with properly organized treatment, are quite adequate cope with educational and professional loads.

It is also confirmed that cognitive impairment in patients with epilepsy is either a manifestation of the seizure itself or a consequence of depressive states caused by impaired
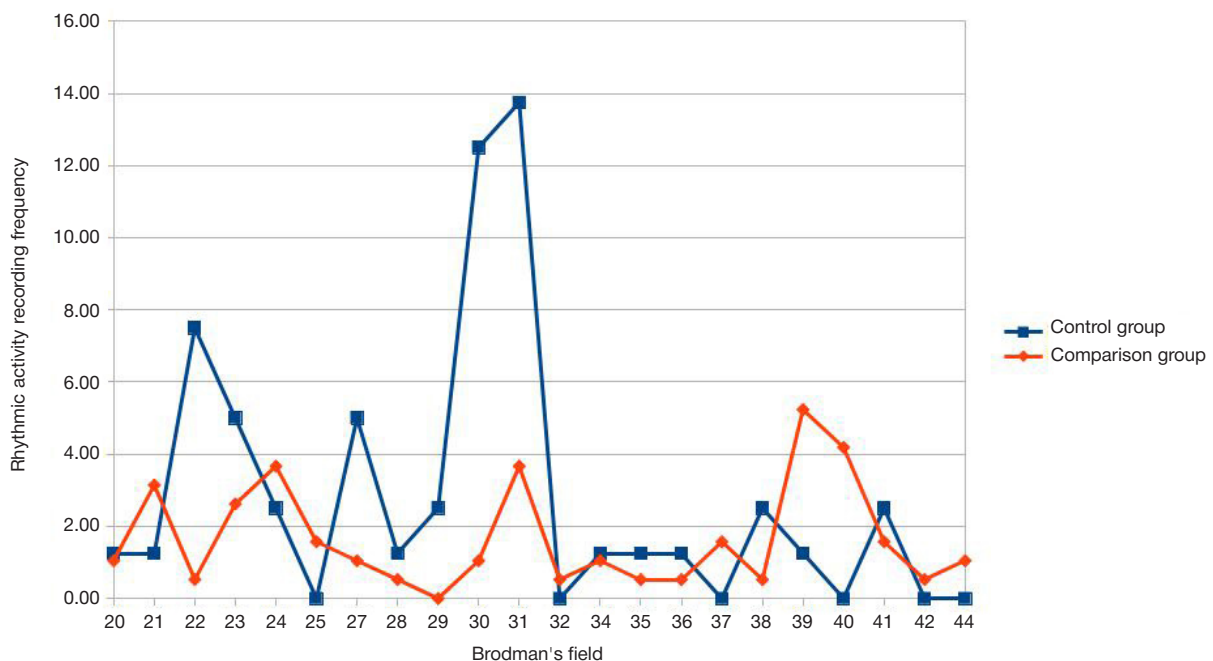

Fig. 3. Default activity in individual Brodmann fields that implement speech function (Chi-squared test; $p = 0.01$)
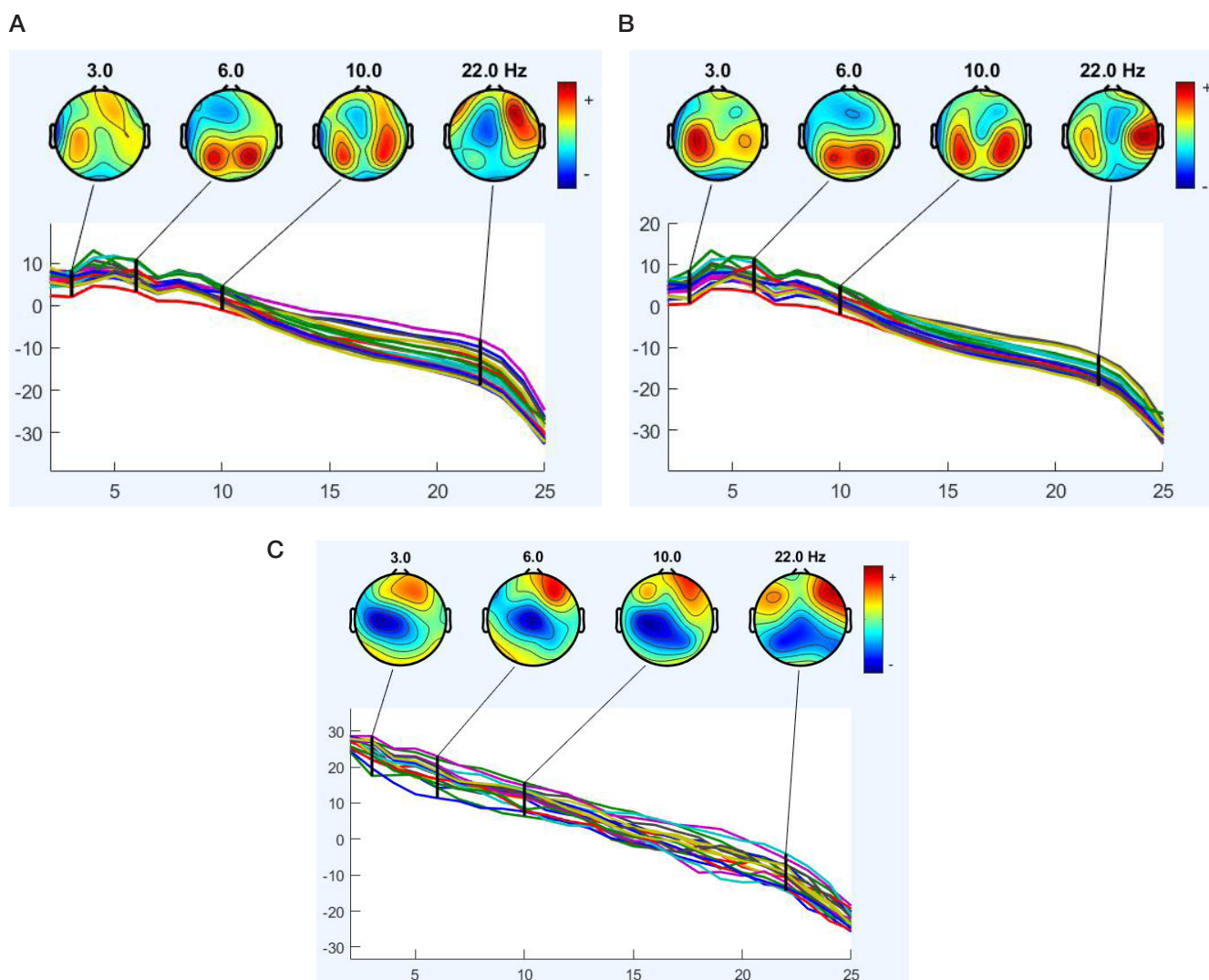
Fig. 4. Two-dimensional EEG mapping of a long-term EEG study performed for the entire volume of data (**A**); for data excluding epileptiform activity (**B**); for epileptiform activity excluding interictal activity (**C**). (EEGLAB program (MATHWORKS). Artifact activity is excluded from the data using independent signal component analysis technology)

perception of the disease, which can be successfully relieved by prescribing adequate drug therapy [55].

However, a study of the functional sequences of transition of bioelectrical activity along cortical structures showed that the activity of speech centers observed in individuals with paroxysmal epileptiform changes in EEG recordings was significantly different from the activity detected in healthy people, which demonstrates the implementation of auditory-speech function in the form of a tono-musical model, typical for children aged from two to five years). These observations make it possible to explain the peculiarities of the occurrence of auditory hallucinations in patients with epilepsy and the changes in the characteristics of bioelectrical activity when listening to certain pieces of music, described previously [56, 57].

This organization of speech function rather represents a developmental option, probably associated with the influence of paroxysmal changes in the bioelectrical activity of the brain on the development and learning of such people, since the human speech function is the youngest of all cognitive functions, the formation of which is observed after birth.

CONCLUSIONS

The results obtained allow us to formulate the main decision of the study that to solve the main clinical problems of continued EEG studies, the use of interictal EEG recordings is not of significant clinical interest. Moreover, its exclusion and, as a consequence, "enrichment" of information due to the sequential placement of ictal patterns allows one to obtain more compact results of examinations of the pathological component using both the existing arsenal of tools for mathematical analysis of electroencephalograms, and new developments using machine learning and artificial intelligence technologies (Fig. 4–5). We hope that this approach will not only reduce the information presented to the specialist, but also improve his working conditions by significantly reducing the amount of visual load.
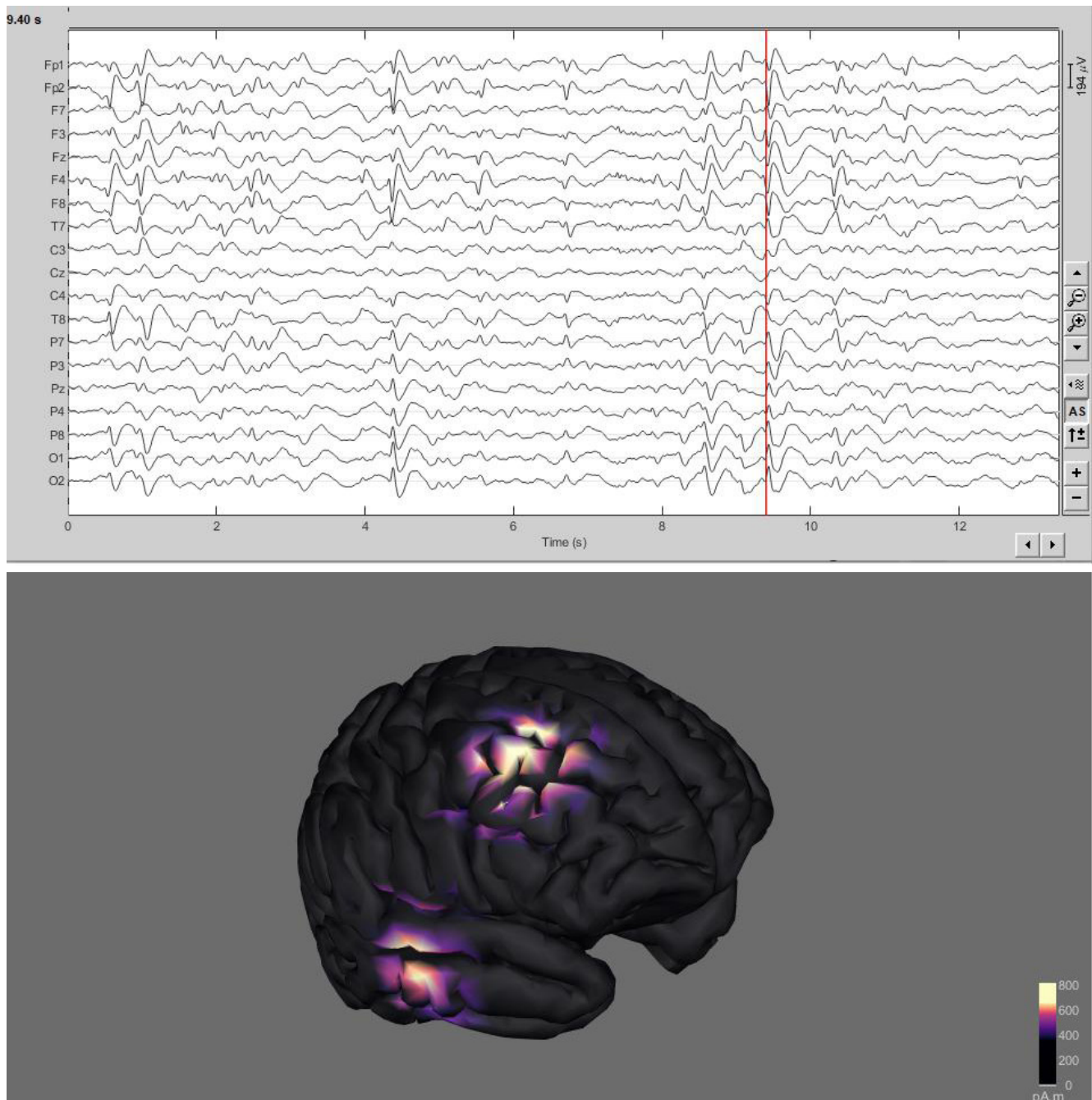
Fig. 5. Implementation of technology (technological prototype) for eliminating interictal activity during a long-term (9 h) EEG study. (BRAINSTORM program (MATHWORKS). Artifact activity is excluded from the data using independent signal component analysis technology)

References

1. Cascino GD. Video-EEG monitoring in adults. Epilepsia. 2002; 43 Suppl 3: 80–93. DOI: 10.1046/j.1528–1157.43.s.3.14.x. PMID: 12060010.
2. Villanueva V, Gutierrez A, Garсна M, Beltran A, Palau J, Conde R, et al. Usefulness of Video-EEG monitoring in patients with drug-resistant epilepsy. Neurologia. 2011; 26 (1): 6–12. English, Spanish. DOI: 10.1016/j.nrl.2010.09.029. Epub 2010 Dec 8. PMID: 21163203.
3. Jamal Omidi S, Hampson JP, Lhatoo SD. Long-term Home Video EEG for recording clinical events. J Clin Neurophysiol. 2021; 38 (2): 92–100. DOI: 10.1097/WNP.0000000000000746. PMID: 33661785.
4. Tatum WO. Editorial: Outcome of ambulatory video-EEG monitoring in a 10,000 patient nationwide cohort. Seizure. 2019; 66: 112–13. DOI: 10.1016/j.seizure.2019.02.016. PMID: 30910236.
5. Fung FW, Abend NS. EEG Monitoring After Convulsive Status Epilepticus. J Clin Neurophysiol. 2020; 37 (5): 406–10. DOI: 10.1097/WNP.0000000000000664. PMID: 32890062.
6. James L. Stone and John R. Hughes. The Gibbs' Boston years: early developments in epilepsy research and electroencephalography at Harvard. Clinical Electroencephalography. 1990; 21 (4): 175–82. DOI: 10.1177/155005949002100404. PMID 2225465. S2CID 143435828.

7. Willems LM, Baier H, Bien CG, Bцsebeck F, Dьmpelmann M, Hamer HM, et al. Satisfaction with and reliability of in-hospital video-EEG monitoring systems in epilepsy diagnosis — A German multicenter experience. Clin Neurophysiol. 2021; 132 (9): 2317–22. DOI: 10.1016/j.clinph.2021.04.020. Epub 2021 Jun 1. PMID: 34154936.

8. Gallotto S, Seeck M. EEG biomarker candidates for the identification of epilepsy. Clin Neurophysiol Pract. 2022; 8: 32–41. DOI: 10.1016/j.cnp.2022.11.004. PMID: 36632368; PMCID: PMC9826889.

9. Kramer MA, Ostrowski LM, Song DY, Thorn EL, Stoyell SM, Parnes M, et al. Scalp recorded spike ripples predict seizure risk in childhood epilepsy better than spikes. Brain. 2019; 142 (5): 1296–309. DOI: 10.1093/brain/awz059. PMID: 30907404; PMCID: PMC6487332.

10. Gotman J. Automatic detection of seizures and spikes. J Clin Neurophysiol. 1999; 16 (2): 130–40. DOI: 10.1097/00004691-199903000-00005. PMID: 10359498.

11. Baumgartner C, Hafner S, Koren JP. Automatische Erkennung von epilepsietypischen Potenzialen und Anfдllen im EEG [Automatic detection of epileptiform potentials and seizures in the EEG]. Fortschr Neurol Psychiatr. 2021; 89 (9): 445–8. German. DOI: 10.1055/a-1370-3058. Epub 2021 Sep 15. PMID: 34525483.

12. Saito M. The significance and the contribution of EEG and other biopotential analysis in clinical psychiatry. Recent adv. EEG and EMG data process. Proc. int. conf., Kanazava, sept. 10—12, 1981, Amsterdam e.a., 1981, p. 279–86.

13. Fedin AI. Compressed spectral EEG analysis in patients with consciousness disorders complicating stroke. Zh Nevropat Psikhiatr Im S S Korsakova. 1981; 81 (9): 1337–42. Russian. PMID: 7324688.

14. Sainio K, Stenberg D, Keskimäki I, Muuronen A, Kaste M. Visual and spectral EEG analysis in the evaluation of the outcome in patients with ischemic brain infarction. Electroencephalogr Clin Neurophysiol. 1983; 56 (2): 117–24. DOI: 10.1016/0013-4694(83)90066-4. PMID: 6191943.

15. Gusev EI, Pokrovskii AV, Volynskii YuD, Pyshkina LI, Erokhin OYu, Goloma VV, et al. Compression spectral analysis of the EEG in patients with occlusive lesions of the carotid and vertebral arteries. Neurosci Behav Physiol. 1989; 19 (1): 51–6. DOI: 10.1007/BF01148411. PMID: 2664551.

16. Tuter NV, Gnezditskiĭ VV. Compressive-spectral analysis of EEG in patients with panic attacks in the context of different psychiatric diseases. Zh Nevrol Psikhiatr Im S S Korsakova. 2008; 108 (3): 58–66. Russian. PMID: 18427541.

17. Frolov AA, Boldyreva GN, Koptelov IuM. Poisk istochnikov patologicheskoĭ al'fa-aktivnosti EEG cheloveka pri porazhenii limbicheskikh struktur [A search for the sources of pathological alpha activity in the human EEG in limbic structure lesions]. Zh Vyssh Nerv Deiat Im I P Pavlova. 1998; 48 (4): 687–96. Russian. PMID: 9778812.

18. Pirlik GP, Gnezditskiĭ VV, Koptelov IuM, Bodykhov MK, Skvortsova VI. Change of bioelectric brain activity registered at the distance from the focus of cerebral tissue injury. Zh Nevrol Psikhiatr Im S S Korsakova. 2001; 101 (5): 24–31. Russian. PMID: 11505911.

19. Grindel OM, Bragina NN, Voronina IA, Masherov EL, Koptelo IuM, Voronov VG, et al. The electroencephalographic correlates of a disorder in higher cortical functions in local lesions of the hypothalamic area. Zh Vyssh Nerv Deiat Im I P Pavlova. 1995; 45 (6): 1101–11. Russian. PMID: 8585300.

20. Zenkov LR, Karlov VA, Ronkin MA, GedekovaA, Kamyshev AN. Possibilities of the diagnosis and the evaluation of epilepsy risk based on the data of EEG spectrum analysis in children and adolescents. Zh Nevropatol Psikhiatr Im S S Korsakova. 1989; 89 (8): 20–2. Russian. PMID: 2588892.

21. Karlov VA, Zenkov LR, Ronkin MA, Gedekova A, Kamyshev AN. Spectrum analysis of the EEG in children and adolescents with epilepsy: general characteristics and pathophysiological interpretation of the data. Zh Nevropatol Psikhiatr Im S S Korsakova. 1989; 89 (8): 15–9. Russian. PMID: 2588891.

22. Pegg EJ, Taylor JR, Mohanraj R. Spectral power of interictal EEG in the diagnosis and prognosis of idiopathic generalized epilepsies. Epilepsy Behav. 2020; 112: 107427. DOI: 10.1016/j.yebeh.2020.107427. Epub 2020 Sep 16. PMID: 32949965.

23. Busonera G, Cogoni M, Puligheddu M, Ferri R, Milioli G, Parrino L, et al. EEG Spectral Coherence Analysis in Nocturnal Epilepsy. IEEE Trans Biomed Eng. 2018; 65 (12): 2713–9. DOI: 10.1109/TBME.2018.2814479. Epub 2018 Mar 9. PMID: 29993423.

24. Wang G, Worrell G, Yang L, Wilke C, He B. Interictal spike analysis of high-density EEG in patients with partial epilepsy. Clin Neurophysiol. 2011; 122 (6): 1098–105. DOI: 10.1016/j.clinph.2010.10.043. Epub 2010 Dec 3. PMID: 21126908; PMCID: PMC3232053.

25. Christou V, Miltiadous A, Tsoulos I, Karvounis E, Tzimourta KD, Tsipouras MG, Anastasopoulos N, Tzallas AT, Giannakeas N. Evaluating the Window Size's Role in Automatic EEG Epilepsy Detection. Sensors (Basel). 2022; 22 (23): 9233. DOI: 10.3390/s22239233. PMID: 36501935; PMCID: PMC9739775.

26. Leal AJ, Passro V, Calado E, Vieira JP, Silva Cunha JP. Interictal spike EEG source analysis in hypothalamic hamartoma epilepsy. Clin Neurophysiol. 2002; 113 (12): 1961–9. DOI: 10.1016/s1388-2457(02)00253-5. PMID: 12464334.

27. Zhu JD, Lin CF, Chang SH, Wang JH, Peng TI, Chien YY. Analysis of spike waves in epilepsy using Hilbert-Huang transform. J Med Syst. 2015; 39 (1): 170. DOI: 10.1007/s10916-014-0170-6. Epub 2014 Dec 4. PMID: 25472728.

28. Aeby A, Santalucia R, Van Hecke A, Nebbioso A, Vermeiren J, Deconinck N, et al. A qualitative awake EEG score for the diagnosis of continuous spike and waves during sleep (CSWS) syndrome in self-limited focal epilepsy (SFE): A case-control study. Seizure. 2021; 84: 34–39. DOI: 10.1016/j.seizure.2020.11.008. Epub 2020 Nov 17. PMID: 33276197.

29. Baumgartner C, Hafner S, Koren JP. Automatische Erkennung von epilepsietypischen Potenzialen und Anfдllen im EEG [Automatic detection of epileptiform potentials and seizures in the EEG]. Fortschr Neurol Psychiatr. 2021; 89 (9): 445–8. German. DOI: 10.1055/a-1370-3058. Epub 2021 Sep 15. PMID: 34525483.

30. Hirano R, Emura T, Nakata O, Nakashima T, Asai M, Kagitani-Shimono K, et al. Fully-automated spike detection and dipole analysis of epileptic MEG using deep learning. IEEE Trans Med Imaging. 2022; 41 (10): 2879–90. DOI: 10.1109/TMI.2022.3173743. Epub 2022 Sep 30. PMID: 35536808.

31. Delorme A, Sejnowski T, Makeig S. Enhanced detection of artifacts in EEG data using higher-order statistics and independent component analysis. NeuroImage. 2007; 34 (4). Available from: https://www.doi.org/10.1016/j.neuroimage.2006.11.004.

32. Tadel F, Baillet S, Mosher JC, Pantazis D, Leahy RM. Brainstorm: a user-friendly application for MEG/EEG analysis. Comput Intell Neurosci. 2011; 2011: 879716. Available from: https://www.doi.org/10.1155/2011/879716.

33. Verhoeven T, Coito A, Plomp G, Thomschewski A, Pittau F, Trinka E, et al. Automated diagnosis of temporal lobe epilepsy in the absence of interictal spikes. Neuroimage Clin. 2017; 17: 10–15. DOI: 10.1016/j.nicl.2017.09.021. PMID: 29527470; PMCID: PMC5842753.

34. Michel CM, Koenig T. EEG microstates as a tool for studying the temporal dynamics of whole-brain neuronal networks: A review. Neuroimage. 2018; 180 (Pt B): 577–93. DOI: 10.1016/j.neuroimage.2017.11.062. Epub 2017 Dec 2. PMID: 29196270.

35. Sun Q, Zhou J, Guo H, Gou N, Lin R, Huang Y, et al. EEG microstates and its relationship with clinical symptoms in patients with schizophrenia. Front Psychiatry. 2021; 12: 761203. DOI: 10.3389/fpsyt.2021.761203. PMID: 34777062; PMCID: PMC8581189.

36. de Bock R, Mackintosh AJ, Maier F, Borgwardt S, Riecher-Rössler A, Andreou C. EEG microstates as biomarker for psychosis in ultra-high-risk patients. Transl Psychiatry. 2020; 10 (1): 300. DOI: 10.1038/s41398-020-00963-7. PMID: 32839449; PMCID: PMC7445239.

37. Keator LM, Yourganov G, Faria AV, Hillis AE, Tippett DC. Application of the dual stream model to neurodegenerative disease: Evidence from a multivariate classification tool in primary progressive aphasia. Aphasiology. 2022; 36 (5): 618–47. DOI: 10.1080/02687038.2021.1897079. Epub 2021 Apr 5. PMID: 35493273; PMCID: PMC9053317.

38. Gulyaev SA, Voronkova YA, Abramova TA, Kovrazhkina EA. Neurophysiological assessment of speech function in individuals having a history of mild COVID-19. Extreme Medicine. 2022; (2): 37–43. DOI: 10.47183/mes.2022.016.

39. Abreu R, Jorge J, Leal A, Koenig T, Figueiredo P. EEG microstates predict concurrent fMRI dynamic functional connectivity states. Brain Topogr. 2021; 34 (1): 41–55. DOI: 10.1007/s10548-020-00805-1. Epub 2020 Nov 7. PMID: 33161518.

40. Gulyaev SA, Khanukhova LM, Garmash AA. Neurophysiological method for studying changes in the brain's default mode network activity. Extreme Medicine. 2023; (2): 64–71. DOI: 10.47183/mes.2023.009.

41. Gulyaev SA, Khanukhova LM, Garmash AA. Features of bioelectric activity of the retrosplenial cortex. Extreme Medicine. 2023; (3): 120–7. DOI: 10.47183/mes.2023.028.

42. Michel CM, Koenig T. EEG microstates as a tool for studying the temporal dynamics of whole-brain neuronal networks: A review. Neuroimage. 2018; 180 (Pt B): 577–93. DOI: 10.1016/j.neuroimage.2017.11.062. Epub 2017 Dec 2. PMID: 29196270.

43. Mukhin KYu, Pylaeva OA. Formation of cognitive and mental disorders in epilepsy: the role of various factors associated with the disease and treatment (a review of the literature and description of clinical cases). Russky Zhurnal Detskoi Nevrologii. 2017; 12 (3): 7–33. DOI: 10.17650/2073-8803-2017-12-3-7-33] Russian.

44. Kanner AM, Helmstaedter C, Sadat-Hossieny Z, Meador K. Cognitive disorders in epilepsy I: Clinical experience, real-world evidence and recommendations. Seizure. 2020; 83: 216–22. DOI: 10.1016/j.seizure.2020.10.009. Epub 2020 Oct 14. PMID: 33127274.

45. Pirlik GP, Gnezditskiĭ VV, Koptelov IuM, Bodykhov MK, Skvortsova VI. Change of bioelectric brain activity registered at the distance from the focus of cerebral tissue injury. Zh Nevrol Psikhiatr Im S S Korsakova. 2001; 101 (5): 24–31. Russian. PMID: 11505911.

46. Pascual-Marqui RD, Michel CM, Lehmann D. Low resolution electromagnetic tomography: a new method for localizing electrical activity in the brain. Int J Psychophysiol. 1994; 18 (1): 49–65. DOI: 10.1016/0167-8760(84)90014-x. PMID: 7876038.

47. Pascual-Marqui RD, Faber P, Kinoshita T, Kochi K, Milz P, Keiichiro N, et al. A comparison of bivariate frequency domain measures of electrophysiological connectivity. bioRxiv 459503. DOI: https://doi.org/10.1101/459503.

48. Grech R, Cassar T, Muscat J, Camilleri KP, Fabri SG, Zervakis M, et al. Review on solving the inverse problem in EEG source analysis. J Neuroeng Rehabil. 2008; 5: 25. Available from: https://doi.org/ 10.1186/1743-0003-5-25.

49. Abreu R, Soares JF, Lima AC, Sousa L, Batista S, et al. Optimizing EEG source reconstruction with concurrent fMRI-Derived spatial priors. Brain Topogr. 2022; 35 (3): 282–301. Available from: https://www.doi.org/10.1007/s10548-022-00891-3. Epub 2022 Feb 10.

50. Thatcher RW, North DM, Biver CJ. LORETA EEG phase reset of the default mode network. Front Hum Neurosci. 2014; 8: 529. Available from: https://www.doi.org/10.3389/fnhum.2014.00529.

51. Babiloni C, Barry RJ, Başar E, Blinowska KJ, Cichocki A, Drinkenburg WHIM, et al. International Federation of Clinical Neurophysiology (IFCN) — EEG research workgroup: Recommendations on frequency and topographic analysis of resting state EEG rhythms. Part 1: Applications in clinical research studies. Clin Neurophysiol. 2020; 131 (1): 285–307. DOI: 10.1016/j.clinph.2019.06.234.

52. Guidelines for carrying out of routine eeg of neurophysiology expert board of Russian league against epilepsy. Epilepsy and paroxysmal conditions. 2016; 8 (4): 99–108. Russian.

53. Beniczky S, Aurlien H, Brugger JC, Hirsch LJ, Schomer DL, Trinka E, et al. Standardized computer-based organized reporting of EEG: SCORE – Second version. Clinical Neurophysiology. 2017; 128 (11): 2334–46. Available from: https://doi.org/10.1016/j.clinph.2017.07.418.

54. van Mierlo P, Huller Y, Focke NK, Vulliemoz S. Network Perspectives on Epilepsy Using EEG/MEG Source Connectivity. Front Neurol. 2019; 10: 721. DOI: 10.3389/fneur.2019.00721. PMID: 31379703; PMCID: PMC6651209.

55. Operto FF, Pastorino GMG, Viggiano A, Dell'Isola GB, Dini G, Verrotti A, et al. Epilepsy and cognitive impairment in childhood and adolescence: a mini-review. Curr Neuropharmacol. 2023; 21 (8): 1646–65. DOI: 10.2174/1570159X20666220706102708. PMID: 35794776; PMCID: PMC10514538.

56. Coebergh JAF, Lauw RF, Sommer IEC, Blom JD. Musical hallucinations and their relation with epilepsy. J Neurol. 2019; 266 (6): 1501–15. DOI: 10.1007/s00415-019-09289-x. Epub 2019 Apr 10. PMID: 30972497; PMCID: PMC6517562.

57. Štillová K, Kiska T, Koriťáková E, Strýček O, Mekyska J, Chrastina J, et al. Mozart effect in epilepsy: why is Mozart better than Haydn? Acoustic qualities-based analysis of stereoelectroencephalography. Eur J Neurol. 2021; 28 (5): 1463–9. DOI: 10.1111/ene.14758. Epub 2021 Feb 24. PMID: 33527581.

Литература

1. Cascino GD. Video-EEG monitoring in adults. Epilepsia. 2002; 43 Suppl 3: 80–93. DOI: 10.1046/j.1528–1157.43.s.3.14.x. PMID: 12060010.

2. Villanueva V, Gutierrez A, Garcнa M, Beltran A, Palau J, Conde R, et al. Usefulness of Video-EEG monitoring in patients with drug-resistant epilepsy. Neurologia. 2011; 26 (1): 6–12. English, Spanish. DOI: 10.1016/j.nrl.2010.09.029. Epub 2010 Dec 8. PMID: 21163203.

3. Jamal Omidi S, Hampson JP, Lhatoo SD. Long-term Home Video EEG for recording clinical events. J Clin Neurophysiol. 2021; 38 (2): 92–100. DOI: 10.1097/WNP.0000000000000746. PMID: 33661785.

4. Tatum WO. Editorial: Outcome of ambulatory video-EEG monitoring in a 10,000 patient nationwide cohort. Seizure. 2019; 66: 112–13. DOI: 10.1016/j.seizure.2019.02.016. PMID: 30910236.

5. Fung FW, Abend NS. EEG Monitoring After Convulsive Status Epilepticus. J Clin Neurophysiol. 2020; 37 (5): 406–10. DOI: 10.1097/WNP.0000000000000664. PMID: 32890062.

6. James L. Stone and John R. Hughes. The Gibbs' Boston years: early developments in epilepsy research and electroencephalography at Harvard. Clinical Electroencephalography. 1990; 21 (4): 175–82. DOI: 10.1177/155005949002100404. PMID 2225465. S2CID 143435828.

7. Willems LM, Baier H, Bien CG, Bьsebeck F, Dьmpelmann M, Hamer HM, et al. Satisfaction with and reliability of in-hospital video-EEG monitoring systems in epilepsy diagnosis — A German multicenter experience. Clin Neurophysiol. 2021; 132 (9): 2317–22. DOI: 10.1016/j.clinph.2021.04.020. Epub 2021 Jun 1. PMID: 34154936.

8. Gallotto S, Seeck M. EEG biomarker candidates for the identification of epilepsy. Clin Neurophysiol Pract. 2022; 8: 32–41. DOI: 10.1016/j.cnp.2022.11.004. PMID: 36632368; PMCID: PMC9826889.

9. Kramer MA, Ostrowski LM, Song DY, Thorn EL, Stoyell SM, Parnes M, et al. Scalp recorded spike ripples predict seizure risk in childhood epilepsy better than spikes. Brain. 2019; 142 (5): 1296–309. DOI: 10.1093/brain/awz059. PMID: 30907404; PMCID: PMC6487332.

10. Gotman J. Automatic detection of seizures and spikes. J Clin Neurophysiol. 1999; 16 (2): 130–40. DOI: 10.1097/00004691-199903000-00005. PMID: 10359498.

11. Baumgartner C, Hafner S, Koren JP. Automatische Erkennung von epilepsietypischen Potenzialen und Anfдllen im EEG [Automatic detection of epileptiform potentials and seizures in the EEG]. Fortschr Neurol Psychiatr. 2021; 89 (9): 445–8. German. DOI: 10.1055/a-1370-3058. Epub 2021 Sep 15. PMID: 34525483.

12. Saito M. The significance and the contribution of EEG and other biopotential analysis in clinical psychiatry. Recent adv. EEG and EMG data process. Proc. int. conf., Kanazava, sept. 10—12, 1981, Amsterdam e.a., 1981, p. 279–86.

13. Fedin AI. Compressed spectral EEG analysis in patients with

consciousness disorders complicating stroke. Zh Nevropatol Psikhiatr Im S S Korsakova. 1981; 81 (9): 1337–42. Russian. PMID: 7324688.

14. Sainio K, Stenberg D, Keskimäki I, Muuronen A, Kaste M. Visual and spectral EEG analysis in the evaluation of the outcome in patients with ischemic brain infarction. Electroencephalogr Clin Neurophysiol. 1983; 56 (2): 117–24. DOI: 10.1016/0013-4694(83)90066-4. PMID: 6191943.

15. Gusev EI, Pokrovskii AV, Volynskii YuD, Pyshkina LI, Erokhin OYu, Goloma VV, et al. Compression spectral analysis of the EEG in patients with occlusive lesions of the carotid and vertebral arteries. Neurosci Behav Physiol. 1989; 19 (1): 51–6. DOI: 10.1007/BF01148411. PMID: 2664551.

16. Tuter NV, Gnezditskiĭ VV. Compressive-spectral analysis of EEG in patients with panic attacks in the context of different psychiatric diseases. Zh Nevrol Psikhiatr Im S S Korsakova. 2008; 108 (3): 58–66. Russian. PMID: 18427541.

17. Frolov AA, Boldyreva GN, Koptelov IuM. Poisk istochnikov patologicheskoĭ al'fa-aktivnosti EEG cheloveka pri porazhenii limbicheskikh struktur [A search for the sources of pathological alpha activity in the human EEG in limbic structure lesions]. Zh Vyssh Nerv Deiat Im I P Pavlova. 1998; 48 (4): 687–96. Russian. PMID: 9778812.

18. Pirlik GP, Gnezditskiĭ VV, Koptelov IuM, Bodykhov MK, Skvortsova VI. Change of bioelectric brain activity registered at the distance from the focus of cerebral tissue injury. Zh Nevrol Psikhiatr Im S S Korsakova. 2001; 101 (5): 24–31. Russian. PMID: 11505911.

19. Grindel OM, Bragina NN, Voronina IA, Masherov EL, Koptelo IuM, Voronov VG, et al. The electroencephalographic correlates of a disorder in higher cortical functions in local lesions of the hypothalamic area. Zh Vyssh Nerv Deiat Im I P Pavlova. 1995; 45 (6): 1101–11. Russian. PMID: 8585300.

20. Zenkov LR, Karlov VA, Ronkin MA, GedekovaA, Kamyshev AN. Possibilities of the diagnosis and the evaluation of epilepsy risk based on the data of EEG spectrum analysis in children and adolescents. Zh Nevropatol Psikhiatr Im S S Korsakova. 1989; 89 (8): 20–2. Russian. PMID: 2588892.

21. Karlov VA, Zenkov LR, Ronkin MA, Gedekova A, Kamyshev AN. Spectrum analysis of the EEG in children and adolescents with epilepsy: general characteristics and pathophysiological interpretation of the data. Zh Nevropatol Psikhiatr Im S S Korsakova. 1989; 89 (8): 15–9. Russian. PMID: 2588891.

22. Pegg EJ, Taylor JR, Mohanraj R. Spectral power of interictal EEG in the diagnosis and prognosis of idiopathic generalized epilepsies. Epilepsy Behav. 2020; 112: 107427. DOI: 10.1016/j.yebeh.2020.107427. Epub 2020 Sep 16. PMID: 32949965.

23. Busonera G, Cogoni M, Puligheddu M, Ferri R, Milioli G, Parrino L, et al. EEG Spectral Coherence Analysis in Nocturnal Epilepsy. IEEE Trans Biomed Eng. 2018; 65 (12): 2713–9. DOI: 10.1109/TBME.2018.2814479. Epub 2018 Mar 9. PMID: 29993423.

24. Wang G, Worrell G, Yang L, Wilke C, He B. Interictal spike analysis of high-density EEG in patients with partial epilepsy. Clin Neurophysiol. 2011; 122 (6): 1098–105. DOI: 10.1016/j.clinph.2010.10.043. Epub 2010 Dec 3. PMID: 21126908; PMCID: PMC3232053.

25. Christou V, Miltiadous A, Tsoulos I, Karvounis E, Tzimourta KD, Tsipouras MG, Anastasopoulos N, Tzallas AT, Giannakeas N. Evaluating the Window Size's Role in Automatic EEG Epilepsy Detection. Sensors (Basel). 2022; 22 (23): 9233. DOI: 10.3390/s22239233. PMID: 36501935; PMCID: PMC9739775.

26. Leal AJ, Passro V, Calado E, Vieira JP, Silva Cunha JP. Interictal spike EEG source analysis in hypothalamic hamartoma epilepsy. Clin Neurophysiol. 2002; 113 (12): 1961–9. DOI: 10.1016/s1388-2457(02)00253-5. PMID: 12464334.

27. Zhu JD, Lin CF, Chang SH, Wang JH, Peng TI, Chien YY. Analysis of spike waves in epilepsy using Hilbert-Huang transform. J Med Syst. 2015; 39 (1): 170. DOI: 10.1007/s10916-014-0170-6. Epub 2014 Dec 4. PMID: 25472728.

28. Aeby A, Santalucia R, Van Hecke A, Nebbioso A, Vermeiren J, Deconinck N, et al. A qualitative awake EEG score for the diagnosis of continuous spike and waves during sleep (CSWS) syndrome in self-limited focal epilepsy (SFE):

29. Baumgartner C, Hafner S, Koren JP. Automatische Erkennung von epilepsietypischen Potenzialen und Anfдllen im EEG [Automatic detection of epileptiform potentials and seizures in the EEG]. Fortschr Neurol Psychiatr. 2021; 89 (9): 445–8. German. DOI: 10.1055/a-1370-3058. Epub 2021 Sep 15. PMID: 34525483.

30. Hirano R, Emura T, Nakata O, Nakashima T, Asai M, Kagitani-Shimono K, et al. Fully-automated spike detection and dipole analysis of epileptic MEG using deep learning. IEEE Trans Med Imaging. 2022; 41 (10): 2879–90. DOI: 10.1109/TMI.2022.3173743. Epub 2022 Sep 30. PMID: 35536808.

31. Delorme A, Sejnowski T, Makeig S. Enhanced detection of artifacts in EEG data using higher-order statistics and independent component analysis. NeuroImage. 2007; 34 (4). Available from: https://www.doi.org/10.1016/j.neuroimage.2006.11.004.

32. Tadel F, Baillet S, Mosher JC, Pantazis D, Leahy RM. Brainstorm: a user-friendly application for MEG/EEG analysis. Comput Intell Neurosci. 2011; 2011: 879716. Available from: https://www.doi.org/10.1155/2011/879716.

33. Verhoeven T, Coito A, Plomp G, Thomschewski A, Pittau F, Trinka E, et al. Automated diagnosis of temporal lobe epilepsy in the absence of interictal spikes. Neuroimage Clin. 2017; 17: 10–15. DOI: 10.1016/j.nicl.2017.09.021. PMID: 29527470; PMCID: PMC5842753.

34. Michel CM, Koenig T. EEG microstates as a tool for studying the temporal dynamics of whole-brain neuronal networks: A review. Neuroimage. 2018; 180 (Pt B): 577–93. DOI: 10.1016/j.neuroimage.2017.11.062. Epub 2017 Dec 2. PMID: 29196270.

35. Sun Q, Zhou J, Guo H, Gou N, Lin R, Huang Y, et al. EEG microstates and its relationship with clinical symptoms in patients with schizophrenia. Front Psychiatry. 2021; 12: 761203. DOI: 10.3389/fpsyt.2021.761203. PMID: 34777062; PMCID: PMC8581189.

36. de Bock R, Mackintosh AJ, Maier F, Borgwardt S, Riecher-Rössler A, Andreou C. EEG microstates as biomarker for psychosis in ultra-high-risk patients. Transl Psychiatry. 2020; 10 (1): 300. DOI: 10.1038/s41398-020-00963-7. PMID: 32839449; PMCID: PMC7445239.

37. Keator LM, Yourganov G, Faria AV, Hillis AE, Tippett DC. Application of the dual stream model to neurodegenerative disease: Evidence from a multivariate classification tool in primary progressive aphasia. Aphasiology. 2022; 36 (5): 618–47. DOI: 10.1080/02687038.2021.1897079. Epub 2021 Apr 5. PMID: 35493273; PMCID: PMC9053317.

38. Gulyaev SA, Voronkova YA, Abramova TA, Kovrazhkina EA. Neurophysiological assessment of speech function in individuals having a history of mild COVID-19. Extreme Medicine. 2022; (2): 37–43. DOI: 10.47183/mes.2022.016.

39. Abreu R, Jorge J, Leal A, Koenig T, Figueiredo P. EEG microstates predict concurrent fMRI dynamic functional connectivity states. Brain Topogr. 2021; 34 (1): 41–55. DOI: 10.1007/s10548-020-00805-1. Epub 2020 Nov 7. PMID: 33161518.

40. Gulyaev SA, Khanukhova LM, Garmash AA. Neurophysiological method for studying changes in the brain's default mode network activity. Extreme Medicine. 2023; (2): 64–71. DOI: 10.47183/mes.2023.009.

41. Gulyaev SA, Khanukhova LM, Garmash AA. Features of bioelectric activity of the retrosplenial cortex. Extreme Medicine. 2023; (3): 120–7. DOI: 10.47183/mes.2023.028.

42. Michel CM, Koenig T. EEG microstates as a tool for studying the temporal dynamics of whole-brain neuronal networks: A review. Neuroimage. 2018; 180 (Pt B): 577–93. DOI: 10.1016/j.neuroimage.2017.11.062. Epub 2017 Dec 2. PMID: 29196270.

43. Mukhin KYu, Pylaeva OA. Formation of cognitive and mental disorders in epilepsy: the role of various factors associated with the disease and treatment (a review of the literature and description of clinical cases). Russky Zhurnal Detskoi Nevrologii. 2017; 12 (3): 7–33. DOI: 10.17650/2073-8803-2017-12-3-7-33] Russian.

44. Kanner AM, Helmstaedter C, Sadat-Hossieny Z, Meador K. Cognitive disorders in epilepsy I: Clinical experience, real-world evidence and recommendations. Seizure. 2020; 83: 216–22.

A case-control study. Seizure. 2021; 84: 34–39. DOI: 10.1016/j.seizure.2020.11.008. Epub 2020 Nov 17. PMID: 33276197.

DOI: 10.1016/j.seizure.2020.10.009. Epub 2020 Oct 14. PMID: 33127274.

45. Pirlik GP, Gnezditskiĭ VV, Koptelov IuM, Bodykhov MK, Skvortsova VI. Change of bioelectric brain activity registered at the distance from the focus of cerebral tissue injury. Zh Nevrol Psikhiatr Im S S Korsakova. 2001; 101 (5): 24–31. Russian. PMID: 11505911.

46. Pascual-Marqui RD, Michel CM, Lehmann D. Low resolution electromagnetic tomography: a new method for localizing electrical activity in the brain. Int J Psychophysiol. 1994; 18 (1): 49–65. DOI: 10.1016/0167-8760(84)90014-x. PMID: 7876038.

47. Pascual-Marqui RD, Faber P, Kinoshita T, Kochi K, Milz P, Keiichiro N, et al. A comparison of bivariate frequency domain measures of electrophysiological connectivity. bioRxiv 459503. DOI: https://doi.org/10.1101/459503.

48. Grech R, Cassar T, Muscat J, Camilleri KP, Fabri SG, Zervakis M, et al. Review on solving the inverse problem in EEG source analysis. J Neuroeng Rehabil. 2008; 5: 25. Available from: https://doi.org/ 10.1186/1743-0003-5-25.

49. Abreu R, Soares JF, Lima AC, Sousa L, Batista S, et al. Optimizing EEG source reconstruction with concurrent fMRI-Derived spatial priors. Brain Topogr. 2022; 35 (3): 282–301. Available from: https://www.doi.org/10.1007/s10548-022-00891-3. Epub 2022 Feb 10.

50. Thatcher RW, North DM, Biver CJ. LORETA EEG phase reset of the default mode network. Front Hum Neurosci. 2014; 8: 529. Available from: https://www.doi.org/10.3389/fnhum.2014.00529.

51. Babiloni C, Barry RJ, Başar E, Blinowska KJ, Cichocki A, Drinkenburg WHIM, et al. International Federation of Clinical Neurophysiology (IFCN) — EEG research workgroup: Recommendations on frequency and topographic analysis of resting state EEG rhythms. Part 1: Applications in clinical research studies. Clin Neurophysiol. 2020; 131 (1): 285–307. DOI: 10.1016/j.clinph.2019.06.234.

52. Guidelines for carrying out of routine eeg of neurophysiology expert board of Russian league against epilepsy. Epilepsy and paroxysmal conditions. 2016; 8 (4): 99–108. Russian.

53. Beniczky S, Aurlien H, Brugger JC, Hirsch LJ, Schomer DL, Trinka E, et al. Standardized computer-based organized reporting of EEG: SCORE – Second version. Clinical Neurophysiology. 2017; 128 (11): 2334–46. Available from: https://doi.org/10.1016/j.clinph.2017.07.418.

54. van Mierlo P, Huller Y, Focke NK, Vulliemoz S. Network Perspectives on Epilepsy Using EEG/MEG Source Connectivity. Front Neurol. 2019; 10: 721. DOI: 10.3389/fneur.2019.00721. PMID: 31379703; PMCID: PMC6651209.

55. Operto FF, Pastorino GMG, Viggiano A, Dell'Isola GB, Dini G, Verrotti A, et al. Epilepsy and cognitive impairment in childhood and adolescence: a mini-review. Curr Neuropharmacol. 2023; 21 (8): 1646–65. DOI: 10.2174/1570159X20666220706102708. PMID: 35794776; PMCID: PMC10514538.

56. Coebergh JAF, Lauw RF, Sommer IEC, Blom JD. Musical hallucinations and their relation with epilepsy. J Neurol. 2019; 266 (6): 1501–15. DOI: 10.1007/s00415-019-09289-x. Epub 2019 Apr 10. PMID: 30972497; PMCID: PMC6517562.

57. Štillová K, Kiska T, Koriťáková E, Strýček O, Mekyska J, Chrastina J, et al. Mozart effect in epilepsy: why is Mozart better than Haydn? Acoustic qualities-based analysis of stereoelectroencephalography. Eur J Neurol. 2021; 28 (5): 1463–9. DOI: 10.1111/ene.14758. Epub 2021 Feb 24. PMID: 33527581.